CRPP

CENTRE DE **R**ECHERCHES EN **P**HYSIQUE DES **P**LASMAS
FACULTE DES SCIENCES DE BASE
ASSOCIATION EURATOM - CONFEDERATION SUISSE

ÉPFL
ÉCOLE POLYTECHNIQUE
FÉDÉRALE DE LAUSANNE

ANNUAL REPORT

2005

Table of content

1 Introduction

1.1 The world scene in the field of magnetic fusion in 2005

The negotiations aiming at a decision on the ITER site progressed during 2004-2005. The deadlock between the European Union (EU) (wishing to construct ITER at the European site of Cadarache in Provence) and Japan (wishing to construct ITER at Rokkasho in the north of Japan) was resolved in June 2005 in an agreement in which the European candidate site was selected. The choice of European site of Cadarache as the ITER site was strongly supported by the Swiss government and the Swiss Association and we are convinced that the CRPP is well placed to take advantage of our proximity to the site. The Director General of the ITER Organisation was nominated in November 2005. India has joined the ITER project

The agreement reached with Japan includes an extremely important component, the inclusion of programmatic elements beyond ITER and aiming towards the fast realisation of fusion as an energy source. This programme, known as the "Broader Approach", could for example include a computational centre for ITER data analysis, the construction of large tokamak to optimise the scientifc exploitation of ITER (the satellite tokamak), a centre to develop the step after ITER, namely a demonstration reactor (DEMO) as well as a facility to advance fusion material science and technology (the International Fusion Material Irradiation Facility IFMIF). The details of this Broader Approach are presently under negotiation between the EU and Japan. In the agreement between the EU and Japan, the EU also conceded part of its own procurement packages to Japan..

1.2 The CRPP in 2005

Research in the CRPP is part of the integrated Euratom Fusion Programme. Through its participation in the Euratom programme, the CRPP benefits from collaborations with all the European Fusion Laboratories, referred to as the Associations, and with laboratories outside Europe. The international fusion programme is aimed towards the exploitation of fusion as an energy source. The research into fusion as an energy source covers:

- Physics research aimed at understanding the phenomena in a "burning plasma" (i.e. in a high temperature plasma where fusion reactions generate a large fraction of the heat source).

Among the European fusion research facilities, the CRPP tokamak, TCV remains unique due to:

- its capability of creating plasma with a very large variety of cross sections. This flexibility allows us to explore plasma with different shapes, contributing to the available data base of tokamak properties;
- its additional heating properties. TCV has a 4.5MW electron cyclotron wave (ECW) heating system with 3 MW in the extraordinary second harmonic mode (X2) and 1.5 MW in the extraordinary third harmonic mode (X3). Combined with a launching system, which controls the spatial deposition of the beam,

this system is still the most powerful ECW installed in a tokamak worldwide and will probably always hae the world record in power density.

In conjunction with a state of the art set of diagnostics and tight collaboration with the CRPP Theory Group for data interpretation, significant contributions have been reported in various important fields of tokamak physics, such as heating and current drive by ECW, plasma shaping and control, studies of internal transport barriers, of magnetohydrodynamics (MHD) phenomena and of plasma-wall interaction.

Theory and numerical simulations of hot magnetized plasma is a well-recognised field of expertise of the CRPP. Numerical modelling is possible through the availability to our researchers of modern computing facilities at the EPFL (for example a cluster including about 100 PCs has been operational since 2003 and will be continuously upgraded and "Blue Gene", a cluster of up to 10'000 PCs), in Switzerland and in other Associations.

Our research activities in this field are focused on:

- the simulation of important phenomena (such as ion temperature gradient mode) which influence transport;
- exploration of novel 3D magnetic confinement structures;
- support for TCV and other experiments
- participation in the activities of the European Integrated Tokamak Task Force.

The CRPP theory group collaborates with many other laboratories such as CEA-Cadarache (F), IPP-Greifswald (D), LHD group (J).

Since 2000, the scientific exploitation of JET and the implementation of major improvements to its hardware are under the responsibility of European laboratories. The exploitation is organized in campaign around "JET Task Forces". The CRPP has contributed to all JET activities:

- A member of the CRPP is Task Force Leader in the field of plasma edge.
- The CRPP is responsible for a major diagnostic implemented on JET, an antenna for Alfvén wave excitation (TAE diagnostic).
- Members of the CRPP have been participating in all JET campaigns, in spite of the heavy domestic load associated with the operation of TCV.

In parallel, our TCV team is also engaged in specific projects on ASDEX-Upgrade, AUG, (D), Tore-Supra (F) and FTU (CNR-Milano and ENEA-Frascati (I)).

Scientific and technical contributions during the present phase of ITER are one of the main priorities of the CRPP. During the construction phase, the CRPP intends to take an important share in its fields of expertise, namely the electron cyclotron wave (ECW) system, diagnostics, and plasma control. At the time of writing this request we are still in the transition phase during which the ITER and the related European management structures are being put into place.

In collaboration with other European Associations, the CRPP is currently participating in:

- the development of the 170GHz-2MW-CW gyrotron and of the ITER ECW upper launcher;
- the construction of the European gyrotron test stand. The test stand will be used for the development of the 170GHz-2MW-CW gyrotron and of the RF components of the ECW upper launcher in ITER operating conditions;
- the development of ITER diagnostics. The CRPP has expressed its wish to be responsible for the coordination of the ITER magnetics diagnostics;

In addition to the fusion plasma activities, CRPP continues to be at the forefront of fusion technology in two fields:

- materials research for both novel materials and basic understanding of high dose behaviour of structural components;
- superconductivity research oriented mainly towards ITER magnets, including the unique SULTAN facility which will be required for quality assurance of the ITER superconductors.

The work of the Industrial Plasma group continues to flourish, but still based on a succession of short mandates with industry.

In parallel, members of the CRPP serve as experts in the "International Tokamak Physics Activities" groups.

The CRPP is also pleased to highlight the nomination of Prof. A. Fasoli as Associate Professor of the EPFL. Prof. Fasoli was Professeur Boursier Fonds National and Professeur Assistant Tenure Track of the EPFL. Dr. L. Villard was nominated Professeur Titulaire and Drs. J.B. Lister and A. Pochelon got the title of Maître d'Enseignement et de Recherche of the EPFL. Prof. M.Q. Tran terminated on 31st March 2006 his mandate as EFDA Leader and is now full time as Director of the CRPP.

1   Introduction

1.1   *La fusion magnétique à travers le monde en 2005*

Les négociations en vue d'une décision pour le site d'ITER ont progressé en 2004-2005. Le blocage entre la Communauté Européenne, qui voulait construire ITER à Cadarache en Provence, et le Japon, qui désirait construire ITER à Rokkasho dans le nord du Japon, s'est résorbé en juin 2005 par un accord à travers lequel l'Europe obtenait le site pour ITER. Le choix du site européen de Cadarache comme site pour ITER était très largement soutenu par le Gouvernement Suisse et l'Association Suisse. Nous sommes convaincus que le CRPP est en mesure de profiter des avantages de la proximité du site. Le Directeur Général d'ITER a été nommé en novembre 2005. L'Inde a également rejoint le projet ITER.

L'accord obtenu avec le Japon contient un point extrêmement important, à savoir des éléments programmatiques pour l'étape après ITER, en vue de la réalisation rapide de la fusion comme source d'énergie. Ce programme, connu sous le nom de 'Approche Elargie' (Broader Approach) inclut un centre informatique pour l'analyse des données d'ITER, la construction d'un grand tokamak pour optimiser l'exploitation scientifique d'ITER, un centre pour développer l'étape suivant ITER, un réacteur de démonstration (DEMO) ainsi que les travaux en vue d'une installation pour la science et la technologie des matériaux d'avant garde pour la fusion (IFMIF: International Fusion Material Irradiation Facility). Les détails concernant cette 'Approche Elargie' sont actuellement l'objet de négociations entre la CE et le Japon. Dans l'accord entre la CE et le Japon, la CE a également concédé au Japon une partie des équipements pour ITER.

1.2   *Le CRPP en 2005*

Les recherches effectuées au CRPP font partie du Programme Euratom de la Recherche en Fusion. Par sa participation à ce programme, le CRPP bénéficie des collaborations avec tous les laboratoires européens engagés également dans ce programme par le biais des 'Associations' ainsi qu'avec des laboratoires hors d'Europe. Le programme international de fusion est tourné vers l'exploitation de la fusion comme source d'énergie et couvre notamment les domaines suivants :

- La recherche en physique dédiée à la compréhension des 'plasmas allumés' (burning plasmas), c-à-d des plasmas à haute température où les réactions de fusion fournissent une grande partie de l'énergie nécessaire à maintenir cet état.

Le tokamak du CRPP, le TCV, reste unique, parmi les machines européennes, de par:

- sa capacité à créer des plasmas dont la section peut avoir des formes très variées. Cette flexibilité nous permet d'explorer des plasmas très différents et d'ainsi contribuer utilement aux bases de données internationales regroupant les propriétés des tokamaks et de leurs plasmas.

- son système de chauffage additionnel. TCV possède un système de chauffage par onde cyclotronique électronique (ECH) d'une puissance de 4.5MW dont 3MW dans le mode X à la seconde harmonique (X2) et 1.5MW dans le mode X à la troisième harmonique (X3). Associée avec un système de miroirs

permettant le contrôle spatial de la déposition de l'énergie du faisceau dans le plasma, notre installation est encore la plus puissante, pour des systèmes ECH, en œuvre dans les tokamaks autour du monde et conservera vraisemblablement longtemps le record mondial de densité de puissance.

Avec un ensemble de systèmes de mesures hors pairs ainsi qu'une étroite collaboration avec le groupe de théorie du CRPP pour l'interprétation des résultats, des contributions significatives ont été rapportées dans différents domaines de la physique des tokamaks tels que le chauffage et la génération de courant avec les ondes cyclotroniques électroniques, le contrôle et le façonnage du plasma, les études des barrières de transports et de phénomènes magnétohydrodynamiques (MHD) ainsi que les interactions plasma-parois.

Il est reconnu que la théorie et la simulation numérique des plasmas chauds magnétisés constituent un domaine d'excellence du CRPP. La modélisation numérique est possible par la mise à la disposition de nos chercheurs de moyens informatiques modernes à l'EPFL, en Suisse ou dans d'autres Associations. Pour exemple: une grappe (cluster), composée d'environ 100 PCs, est opérationnelle depuis 2003 et est améliorée régulièrement; 'Blue Gene' une autre grappe composée cette fois d'environ 10'000 PCs.

Nos activités de recherche dans ce domaines sont axées sur:

- la simulation de phénomènes importants, comme le mode de gradient de température ionique (ITG mode) qui influence le transport;
- l'exploration de nouvelles structures magnétiques, 3D, de confinement;
- le soutien à TCV et d'autres expériences;
- la participation aux activités européennes sur le tokamak numérique.

Le groupe de théorie du CRPP collabore avec plusieurs laboratoires comme le CEA-Cadarache (F), l'IPP-Greifswald (A), le groupe LHD (J).

Depuis 2000, l'exploitation scientifique de JET ainsi que la mise en œuvre des améliorations majeures sont assurées par les laboratoires européens. L'exploitation est organisée en campagnes menées par un ensemble de 'task forces'. Le CRPP a contribué à différentes activités de JET:

- Un collaborateur du CRPP dirige la 'task force' étudiant le plasma de bord;
- Le CRPP est responsable de l'installation sur JET d'un nouvel appareil de mesure, une antenne pour la stimulation d'ondes d'Alfvén (TAE diagnostic);
- Des collaborateurs du CRPP ont participé à chacune des campagnes de JET, malgré leurs lourdes charges de travail, en particulier dues à l'opération de TCV.

En parallèle, notre équipe de TCV est également engagée dans des projets spécifiques sur ASDEX-Upgrade, AUG, (A), Tore-Supra (F) et FTU (CNR-Milano et ENEA-Frascati, I).

Des contributions scientifiques et techniques à ITER forment actuellement l'une des principales priorités du CRPP. Durant la phase de construction, le CRPP a l'intention de jouer un rôle important dans ses domaines d'excellence, notamment dans le système de chauffage par onde cyclotronique électronique, certains appareils de mesure et le contrôle du plasma. Au moment d'écrire ces lignes, nous sommes encore dans la phase de transition pendant laquelle les structures organisationnelles d'ITER et celles européennes qui lui sont liées sont mises en place.

En collaboration avec d'autres Associations Européennes, le CRPP participe actuellement:

- au développement du gyrotron 170GHz-2MW-CW et au lanceur supérieur pour les ondes cyclotroniques électroniques;
- à la construction d'un banc d'essais et de développement pour ce gyrotron et pour les parties RF du lanceur supérieur, dans les conditions d'opération d'ITER;
- au développement de certains appareils de mesure pour ITER. Le CRPP a exprimé le désir d'être responsable de la coordination des mesures magnétiques;
- la conception du système de contrôle d'ITER, de communication et de transfert de données (CODAC).

En parallèle, des collaborateurs du CRPP fonctionnent comme experts dans les groupes d' 'Activités Internationales de Physique des Tokamaks' (ITPA: International Tokamak Physics Activities).

En plus des activités dans les plasmas chauds, le CRPP continue d'être au premier rang de la technologie de la fusion, notamment avec:

- la recherche en matériaux, tant pour de nouveaux matériaux que pour la compréhension des effets de l'irradiation intense des éléments de structure;
- la recherche en supraconductivité, orientée principalement vers les bobines magnétiques d'ITER, avec SULTAN, une installation unique qui sera utilisée pour les tests d'assurance qualité des supraconducteurs d'ITER.

Le travail du groupe 'Plasmas Industriels' continue d'être florissant, tout en étant toujours basé sur une succession de courts mandats provenant de l'industrie.

Le CRPP est aussi très heureux de mentionner la nomination du Prof. A. Fasoli comme Professeur Associé de l'EPFL. Prof. A. Fasoli était Professeur Boursier Fonds National et Professeur 'Tenure Track' de l'EPFL. Dr L. Villard a été nommé Professeur Titulaire et Drs J.B. Lister et A. Pochelon ont reçu le titre de Maître d'Enseignement et de Recherche de l'EPFL. Prof. M.Q. Tran a terminé son mandat de directeur EFDA le 31 mars 2006. Il est maintenant de nouveau directeur du CRPP à plein temps.

1   Einleitung

1.1   *Weltweiter Fortschritt im Bereich der magnetischen Kernfusion im Jahr 2005*

Die Verhandlungen zur Entscheidung des ITER Standorts schritten 2005-2006 voran. Die Blockade zwischen der Europäischen Union (EU) (mit dem Ziel ITER am europäischen Standort Cadarache in der Provence zu errichten) und Japan (mit dem Ziel ITER am japanischen Standort Rokkasho im Norden Japans zu errichten) wurde im Juni 2005 mit einer Einigung auf den europäischen Standort durchbrochen. Die Wahl des europäischen Standorts Cadarache als ITER Standort wurde von der Schweizer Regierung und von der Schweizer Assoziation nachhaltig unterstützt. Wir sind davon überzeugt, dass das CRPP eine gute Ausgangslage besitzt, um von der Nähe des Standorts zu profitieren. Der Generaldirektor der ITER Organisation wurde im November 2005 nominiert. Indien trat 2005 dem ITER Projekt bei.

Die Einigung mit Japan beinhaltet eine extrem wichtige Komponente: Den Einschluß programmatischer Elemente über ITER hinaus, mit der Zielsetzung einer schnellen Realisierung der Kernfusion als Energiequelle. Dieses Programm, bekannt als die 'Umfassendere Projektentwicklung' (Broader Approoach') könnte beispielsweise ein Rechenzentrum zur ITER Datenanalyse, die Konstruktion eines großen Tokamaks zur Optimierung des ITER Betriebes, ein Zentrum zur Entwicklung des nächsten Schrittes nach ITER (nämlich einen Demonstrationsreaktor DEMO) oder eine Einrichtung, um den Fortschritt in der Fusionsmaterialforschung und –technologie (die Internationale Einrichtung zur Bestrahlung von Fusionsmaterialien IFMIF) voranzutreiben, beinhalten. Die Details dieser Umfassenderen Projektentwicklung werden zur Zeit zwischen der EU und Japan verhandelt. In der Einigung zwischen EU und Japan räumte die EU Japan Teile ihres eigenen Beschaffungspackets ein.

1.2   *Das CRPP im Jahr 2005*

Die Forschung am CRPP ist Teil eines integrierten europäischen Fusionsprogramms Durch seine Beteiligung am Euratom Programm profitiert das CRPP von der Zusammenarbeit mit allen europäischen Fusionslaboratorien, die Assoziationen genannt werden, und mit Laboratorien ausserhalb Europas. Das internationale Fusionsprogramm zielt auf die Nutzung der Kernfusion als Energiequelle. Die Forschung im Bereich Fusion als Energiequelle beinhaltet:

-      Forschung in der Physik zielt auf das Verständnis der Phänomene in einem 'brennenden Plasma' (d.h. in einem Hochtemperaturplasma, in dem die Fusionsreaktionen einen großen Teil der Wärmequelle generieren).

Aus folgenden Gründen bleibt der CRPP Tokamak TCV einzigartig unter den europäischen Fusionslaboratorien :

-      seiner Fähigkeit wegen, Plasmen mit einer großen Vielzahl an Querschnitten zu kreieren. Diese Flexibilität ermöglicht es uns Plasmen mit unterschiedlichen Formen zu untersuchen und damit einen Beitrag zu der Datenbank von Tokamakeigenschaften zu leisten,
-      seiner Zusatzheizmethoden wegen. TCV besitzt ein 4.5MW Elektron-Zyklotron-Wellen (ECW) Heizsystem in der außerordentlichen zweiten Harmonischen

(X2) und 1.5MW in der außerordentlichen dritten Harmonischen (X3). Zusammen mit einem Einkopplungssystem, welches die räumliche Deposition des Strahls kontrolliert, ist dieses System noch immer das leistungsstärkste ECW Heizsystem, das weltweit in einem Tokamak installiert ist, und wird vermutlich immer den Weltrekord in der Leistungsdichte halten.

Die auf neustem Stand der Technik stehenden Messmethoden und die enge Zusammenarbeit mit der CRPP Theoriegruppe für Dateninterpretation hat zu signifikanten Beiträgen in verschiedenen wichtigen Gebieten der Tokamakphysik geführt; unter anderem sind Beiträge über Heizung und Stromtrieb durch ECW, über Plasmaformveränderungen und Plasmakontrolle, und über Untersuchungen von internen Transportbarrieren, magnetohydrodynamischen (MHD) Phänomenen und von Plasma-Wand Wechselwirkungen.

Theorie und numerische Simulation von heißen magnetischen Plasmen ist ein weit anerkanntes Spezialgebiet des CRPP. Numerische Modellierung wird möglich durch den Zugang unserer Forscher zu modernen Computereinrichtungen der EPFL (Parallelcomputer mit bis zu 8000 Prozessoren), der Schweiz und anderer Assoziationen.

Unsere Forschung in diesem Bereich konzentriert sich auf folgende Themen:

- die Simulation wichtiger Phänomene (wie die Ionen-Temperaturgradient-Mode), die den Transport beeinflussen,
- Untersuchung neuer 3D Strukturen im Bereich des magnetischen Einschlusses;
- Unterstützung von TCV und anderen Experimenten;
- Teilnahme an Aktivitäten der europäischen integrierten Tokamak Projektgruppe (Task Force).

Die CRPP Theoriegruppe arbeitet mit vielen anderen Laboratorien, wie dem CEA-Cadarache (F), dem IPP-Greifswald (D) und der LHD Gruppe (J), zusammen.

Seit 2000 sind die wissenschaftliche Nutzung von JET und die Durchführung bedeutender Verbesserungen seiner Hardware unter der Verantwortung der europäischen Laboratorien. Die Nutzung ist in einer Kampagne um die 'JET Projektgruppen (Task Forces)' organisiert. CRPP hat zu allen JET Aktivitäten beigetragen:

- Ein Mitarbeiter des CRPP ist Projektgruppenleiter (Task Force Leader) im Bereich des Plasmarands.
- Das CRPP ist verantwortlich für den Einbau einer bedeutenden Diagnostik, einer Antenne zur Anregung von Alfvénwellen (TAE Diagnostik).
- Mitarbeiter des CRPP nahmen an allen JET Messkampagnen teil, trotz der großen heimischen Belastung in Zusammenhang mit dem Betrieb TCVs.

Parallel dazu hat sich unser CRPP Team gezielt an weiteren Projekten wie an ASDEX-Upgrade, AUG, (D), Tore-Supra (F) und FTU (CNR-Milano und ENEA-Frascati (I)) beteiligt.

Die Leistung wissenschaftlicher und technischer Beiträge in der gegenwärtigen ITER Phase ist eine der Hauptprioritäten des CRPP. In der Konstruktionsphase beabsichtigt das CRPP in seinen Spezialgebieten, nämlich des Elektron-Zyklotron-Wellen (ECW) Systems, der Diagnostiken und der Plasmakontrolle, erheblich mitzuwirken. Zu diesem Zeitpunkt sind wir noch immer in einer Übergangsphase, in der die ITER und die zugehörigen europäischen Management Strukturen zugeordnet werden.

In Zusammenarbeit mit anderen europäischen Assoziationen beteiligt sich das CRPP an folgenden Aktivitäten:

- der Entwicklung des 170GHz-2MW-CW Gyrotrons und des ITER ECW oberen Einstrahlsystems (upper launcher);
- der Konstruktion des europäischen Gyrotron Teststandes. Der Teststand wird zur Entwicklung des 170GHz-2MW-CW Gyrotrons und von RF (Radiofrequenz) Komponenten des ECW oberen Einstrahlsystems unter ITER Operationskonditionen eingesetzt werden;
- Entwicklung von ITER Diagnostiken. Das CRPP wünscht ausdrücklich verantwortlich für die Koordination der magnetischen Diagnostiken bei ITER zu sein;
- das konzeptuelle CODAC Design.

Parallel dazu stehen die Mitarbeiter des CRPP als Experten in den 'Internationalen Tokamakphysik Aktivitäten' Gruppen zur Verfügung.
Zusätzlich zu den Fusionsaktivitäten bleibt das CRPP in der Fusionstechnologie in zwei Gebieten an vorderster Front:

- Materialforschung sowohl hin zu neuen Materialien und als auch zum Grundlagenverständnis vom Hoch-Dosis-Verhalten von Strukturelementen;
- Supraleitungsforschung hauptsächlich orientiert in Richtung ITER Magnete, einschliesslich der einzigartigen SULTAN Einrichtung, die zur Qualitätssicherung der ITER Supraleiter erforderlich sein wird.

Die Arbeit der Gruppe der Industriellen Plasmen ist weiterhin sehr erfolgreich, hängt aber immer noch von kurzzeitigen Industriemandaten ab.

Das CRPP freut sich zudem die Nominierung von Prof. A. Fasoli als Ausserordentlichen Professor (Associate Professor) der EPFL mitteilen zu können. Prof. Fasoli war zuvor Professeur Boursier Fonds National und Professeur Assistant Tenur Track der EPFL. Dr. L. Villard wurde zum Professeur Titulaire nominiert und die Doktoren J.B. Lister und A. Pochelon erhielten den Titel Maître d'Enseignement et de Recherche der EPFL. Prof. M.Q. Tran hat sein Mandat als EFDA Leiter am 31. März 2006 niedergelegt und ist jetzt wieder Ganzzeit Direktor des CRPP.

1 Introduzione

1.1 Il panorama mondiale nel campo della fusione magnetica nel 2005

I negoziati volti ad una decisione sulla collocazione geografica di ITER hanno progredito durante il 2004-2005. L'impasse tra l'Unione Europea (UE), che auspicava di costruire ITER nel sito europeo di Cadarache in Provenza, e il Giappone, che proponeva invece Rokkasho nel nord del Giappone, è stato infine risolto nel giugno 2005 grazie ad un accordo che ha favorito il candidato europeo. La scelta del sito europeo di Cadarache per ITER è stata vigorosamente sostenuta dal governo svizzero e dall'Associazione svizzera, e siamo persuasi che il CRPP è ottimamente collocato per trarre vantaggio dalla sua vicinanza al sito. Il Direttore Generale dell'Organizzazione ITER è stato nominato nel novembre 2005. Infine, l'India si è associata al progetto ITER nel corso del 2005.

L'accordo raggiunto con il Giappone comprende un fattore di estrema importanza, ossia l'inclusione di elementi programmatici che vanno oltre ITER e puntano alla rapida realizzazione della fusione come sorgente di energia. Questo programma, noto come "Broader Approach", potrebbe ad esempio comprendere un centro di calcolo per l'analisi dei dati di ITER, la costruzione di un ulteriore grande tokamak per ottimizzare l'operazione di ITER, e infine un centro volto alla progettazione dello stadio successivo a ITER, ossia un reattore dimostrativo (DEMO) e un centro dedicato allo studio della scienza e tecnologia dei materiali per la fusione (il Centro Internazionale di Irradiazione dei Materiali per la Fusione, o IFMIF). I dettagli di questo programma esteso sono attualmente oggetto di negoziati tra l'UE e il Giappone. Come parte dell'accordo, l'UE ha inoltre concesso una parte dei propri contratti di forniture per ITER al Giappone.

1.2 Il CRPP nel 2005

La ricerca al CRPP fa parte del programma integrato di fusione dell'Euratom. Attraverso la sua partecipazione nel programma Euratom, il CRPP trae beneficio da collaborazioni con tutti gli altri laboratori di fusione europei – chiamati Associazioni in questo contesto – e con laboratori esterni all'Europa. Il programma internazionale di fusione ha come scopo lo sfruttamento della fusione come fonte di energia. Questa linea di ricerca ricopre le aree descritte di seguito.

- La prima area è la ricerca in fisica, volta alla comprensione della fenomenologia di un "plasma in condizioni di bruciamento" (ossia un plasma ad alta temperatura in cui le reazioni di fusione generano la frazione dominante della fonte di calore).

Tra i centri europei di ricerca sulla fusione, il tokamak TCV del CRPP si distingue per

- la sua capacità di creare plasmi con una grande varietà di forme: questa flessibilità ci permette di contribuire alla banca dati esistente di proprietà dei tokamak;
- il riscaldamento aggiuntivo: TCV possiede un sistema di riscaldamento a onde ciclotroniche elettroniche (ECW) di 4.5 MW, di cui 3 MW nel modo straordinario alla seconda armonica (X2) e 1.5 MW nel modo straordinario alla terza armonica (X3). In congiunzione con un meccanismo di iniezione che

controlla la posizione spaziale della deposizione dell'energia, questo sistema è tuttora il piú potente apparato ECW tra tutti i tokamak del mondo e deterrà sempre, probabilmente, il primato mondiale di densità di potenza.

In congiunzione con un parco di diagnostiche dell'ultima generazione e in stretta collaborazione con il gruppo di teoria del CRPP per l'interpretazione dei dati, contributi importanti sono stati ottenuti e pubblicati in vari campi importanti della fisica del tokamak, come riscaldamento e generazione di corrente per ECW, controllo della forma del plasma e studi di barriere di trasporto interne, di fenomeni magnetoidrodinamici e di interazione plasma-parete.

La teoria e le simulazioni numeriche di plasmi caldi magnetizzati costituiscono un'area di competenza riconosciuta del CRPP. La modellizzazione numerica è resa possibile dalla disponibilità di moderne apparecchiature di calcolo all'EPFL (ad esempio un cluster di circa 100 PC, in operazione dal 2003 e continuamente potenziato, e "Blue Gene", un cluster di oltre 10000 PC), in Svizzera e nelle altre Associazioni.

Le nostre attività di ricerca in questo settore si concentrano sui temi seguenti:

- la simulazione di fenomeni importanti nell'influenzare il trasporto (tra cui l'instabilità di gradiente di temperatura ohmica);
- l'esplorazione di nuove strutture magnetiche tridimensionali di confinamento;
- sostegno a TCV ed altri esperimenti;
- partecipazione ad attività del Gruppo di Lavoro Integrato Europeo sui Tokamak

Il gruppo di teoria del CRPP collabora con molti altri laboratori tra cui CEA-Cadarache (Francia), IPP-Greifswald (Germania), LHD (Giappone).

A partire dal 2000, l'utilizzo scientifico del JET e l'implementazione di miglioramenti consistenti alle sue apparecchiature ricadono sotto la responsabilità dei laboratori europei. Il lavoro scientifico è organizzato in "campagne" strutturate intorno ai Gruppi di Lavoro ("JET Task Forces"). Il CRPP ha contribuito a tutte le attività del JET:

- Un membro del CRPP dirige la Task Force nel campo della fisica del plasma del bordo.
- Il CRPP è responsabile di un'importante diagnostica del JET, un'antenna per l'eccitazione di onde di Alfvén (diagnostica TAE).
- Membri del CRPP hanno preso parte a tutte le campagne del JET, malgrado il pesante carico di lavoro interno legato all'operazione di TCV.

In parallelo, il gruppo TCV è inoltre coinvolto in progetti specifici su ASDEX-Upgrade (AUG, Germania), Tore-Supra (Francia) e FTU (CNR-Milano and ENEA-Frascati, Italia).

I contributi scientifici e tecnici durante la fase attuale di ITER costituiscono una delle priorità principali del CRPP. Durante la fase di costruzione, il CRPP intende assumere importanti responsabilità nei propri campi di competenza, quali il sistema di riscaldamento con onde ciclotroniche elettroniche (ECW), le diagnostiche e il controllo del plasma. Al momento in cui questa richiesta viene redatta, ci troviamo ancora nella fase di transizione durante la quale vengono definiti sia ITER che le relative strutture di gestione europee.

In collaborazione con altre Associazioni europee, il CRPP partecipa attualmente alle attività seguenti:

- lo sviluppo del girotrone a 170 GHz e 2 MW a funzionamento continuo e del sistema di iniezione delle onde ECW per il settore superiore di ITER;
- la costruzione del banco di prova europeo per i girotroni; tale banco di prova verrà usato per sviluppare il girotrone a 170 GHz e 2 MW e le componenti ad alta frequenza del sistema di iniezione ECW in condizioni operative equivalenti a quelle di ITER;
- lo sviluppo di diagnostiche per ITER; il CRPP ha espresso la propria candidatura alla responsabilità della coordinazione delle diagnostiche magnetiche per ITER;
- il progetto concettuale di CODAC.

In parallelo, membri del CRPP operano in qualità di esperti nei "gruppi internazionali di attività di fisica del tokamak".

Oltre alle attività legate alla fisica di plasma da fusione, il CRPP continua a trovarsi all'avanguardia nel settore della tecnologia per la fusione in due settori:

- ricerca sui materiali, sia per nuovi materiali sia per la comprensione di base del comportamento di componenti strutturali sotto bombardamento neutronico intensivo
- ricerca sulla superconduttività, orientata principalmente in direzione dei magneti per ITER e comprendente il centro SULTAN, unico al mondo, che sarà richiesto per l'assicurazione di qualità dei superconduttori per ITER.

Il lavoro del gruppo di Plasmi Industriali continua a prosperare, sempre sulla base di una serie di contratti di breve durata con l'industria.

Il CRPP è infine lieto di sottolineare la nomina del Prof. A. Fasoli come Professore Associato dell'EPFL. Il Prof. Fasoli era stato in precedenza "Professeur Boursier" del Fondo Nazionale e Professore Assistente "Tenure Track" dell'EPFL. Il Dr. L. Villard è stato nominato Professore Titolare e il Dr. J.B. Lister e il Dr. A. Pochelon hanno conseguito il titolo di "Collaboratore scientifico con funzioni direttive" dell'EPFL. Il Prof. M.Q. Tran terminerà il suo mandato di Direttore Generale dell'EFDA il 31 marzo 2006.

2 Research achievements of the CRPP in 2005

2.1 The TCV tokamak

2.1.1 Scenarios with internal transport barriers

Studies of electron internal transport barriers (eITBs) have advanced along two main lines in 2005. The first seeks to enhance the measurement and modelling base of the eITB scenarios previously discovered on TCV, while the second explores new territory for TCV operation. An example of the first is the study of the formation criteria in fully-steady state eITBs and eITBs in which inductive current is added; and the second approach is epitomized by the search for 100% bootstrap current scenarios starting from more conventional fast-current-ramp generated eITBs.

eITB Formation

Experiments during the 2005 campaign have shown that the same stationary state of highly improved confinement can be reached evolving directly from an ohmic discharge with peaked central current as from a pre-existing barrier with reversed shear. A fine scan of the minimum safety factor, q_{min}, was performed by reducing the central current in a pulse to pulse manner and no step in the H factor was seen as a function of surface voltage (Fig. 2.1.1). These results confirm previous lower power experiments using different off-axis ECCD deposition locations and show that on TCV there is no preference in q_{min} for forming an eITB, at least for power levels well above the eITB power threshold expected from multi-machine database.
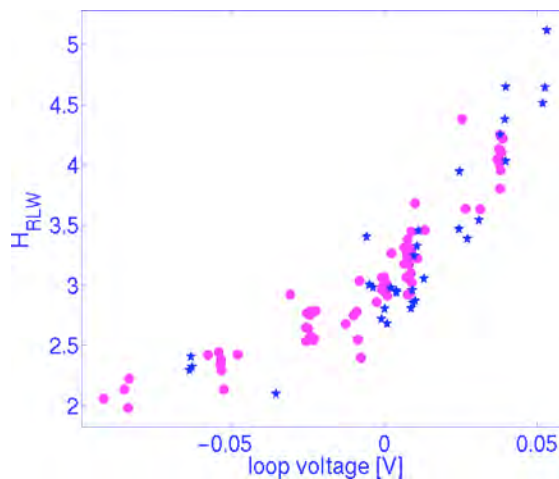
Fig. 2.1.1 *The H factor ($\tau_{exp.}/\tau_{RLW}$) obtained duriing the steady-state portion of the eITB discharges changes smoothly as a function of the loop voltage; increasing with counter, central, inductively driven current. Both 1.35MW (stars) and 2.25MW (circles) ECCD data is shown.*
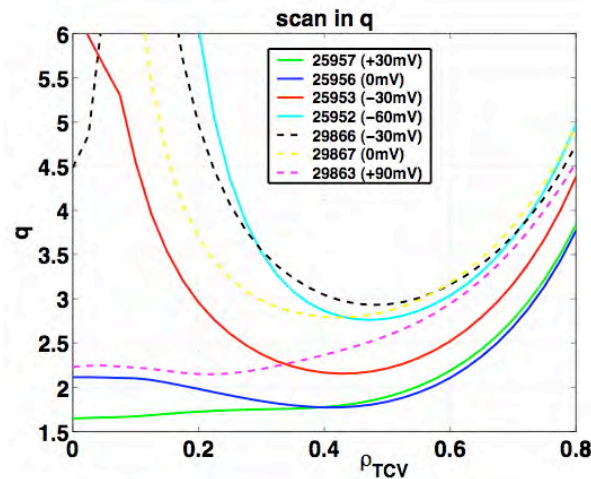
Fig. 2.1.2 *The q-profiles calculated by ASTRA for some pulses of Fig. 2.1.8 (solid at 1.35MW, dashed at 2.25MW) with varying amounts of inductive current. The loop voltages in the legend are reversed from Fig. 2.1.8: here negative values indicate counter central inductive current; hence more reversed shear.*

ASTRA safety factor modelling

The q-profiles are simulated using the ASTRA code, Fig. 2.1.2. The measured electron density and temperature profiles and loop voltages are input to ASTRA, along with the EC driven current profiles. The value of q_{min} varies over at least the $q_{min}=2$ and $q_{min}=5/2$ rational surfaces, though differently in the two scans, due to differences in the EC power and electron density in each. Nevertheless, comparison of these two figures shows that, altough the absolute values of the q-profiles may differ at the same loop voltages, the H factors are the same.

The ECCD profile is determined from Fokker-Planck modelling of the wave-particle interaction in the presence of radial particle diffusion during the stationary portion of the discharge (when the electric field is zero or constant). The particle diffusivity $D(\rho,t)$ is chosen proportional to the electron thermal diffusivity $\chi_e(\rho,t)$, derived from a power balance. The constant of proportionality (e.g. 0.12 in discharge 28873 below) is constrained by forcing the integrated ECCD profile to match $I_{cd}={}_p-I_{bs}$ (for the zero electric field case). This estimated I_{cd} is larger than TORAY-GA linear predictions by a factor that is assumed to be constant for a given shot. The value of $D(\rho,t)$ is adjusted at each time step to provide the same relative variation of driven current in the Fokker-Planck modelling as found from TORAY-GA. Finally, the time evolution of the shear can be simulated by ASTRA. A correspondence is found between both the position and moment of the eITB formation, and the location of q_{min} and the time when it appears off-axis. Note that, while magnetic islands are not always present during barrier formation, when they do occur, they provide a very strong constraint on q-profile simulations and modelling.

Particle transport in eITBs

Particle transport in eITBs is characterised by a strong dependence of the density profile on the degree of reverse shear and on the electron temperature normalised gradient, R/L_T. We observe a strong density peaking (Fig. 2.1.3) and a relation of the type: $R/L_n \sim 0.5 \cdot R/L_T$, despite the large amount of EC power injected into the discharge. The peaking is sometimes stronger than in inductive discharges without auxiliary heating and is contrary to normal Ohmic L-mode plasma behaviour in

which injecting ECH induces a flattening of the density profile by increasing the TEM activity. These results suggest that a thermo-diffusive type of pinch is at work.
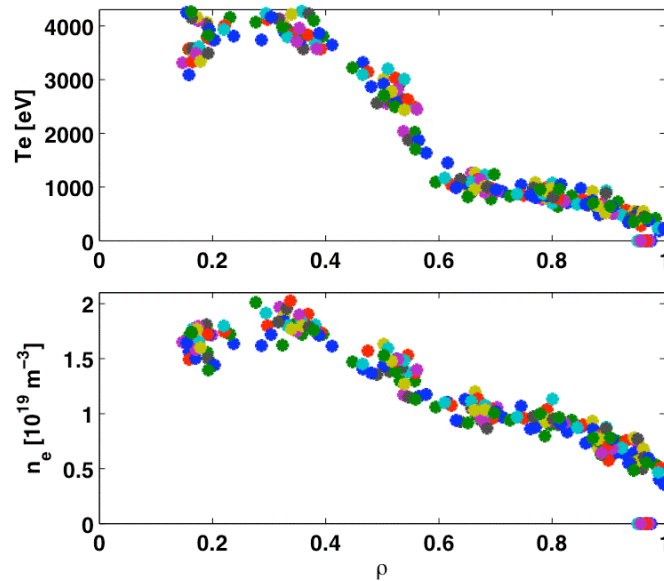
Fig. 2.1.3   *Electron temperature (top) and density (bottom) profiles from repetitive Thomson scattering (20Hz) during vertical movement of the plasma axis (shot 29948). Different colors represent different time slices between 1.1 and 1.95s. The movement corresponds to ~3/4 the distance between measurement points, which provides improved effective spatial resolution: the curve becomes nearly continuous. The ECCD beams have been swept during the plasma shift to maintain the strong barriers in temperature and density peaking seen in the profiles.*

eITBs in current ramps without ECCD

In parallel with our research activities on eITBs in stationary, fully non-inductive conditions using ECCD and the bootstrap current to sustain a hollow current profile, we have recently started an investigation into the possibility of generating internal barriers transiently without the use of ECCD, during plasma current ramps. This method, the most commonly used to create ITBs in tokamaks, relies on strong heating during the current ramp to increase the plasma conductivity and thus slow down the current penetration, resulting in a transiently hollow current profile. In addition to confirming that a negative central magnetic shear is necessary for the appearance of a barrier, the general motivation is to explore the possibility of the entire plasma current being sustained by the neoclassical bootstrap effect, with no external current sources. The experiments have so far been performed at a low plasma current of ~80kA, compatible with the goal of bootstrap sustainment, but causing considerable operational difficulties owing to the short time scales at play, which require that the ECRH power be applied immediately after breakdown. This results in various MHD instabilities as the edge safety factor transits through integer values, and the timing of the power injection had to be optimised empirically in order to avoid disruptions or anomalous current penetration. It nevertheless proved possible to achieve the desired goal, generating eITBs with characteristics similar to their ECCD-sustained counterparts, namely a confinement enhancement factor of four and a bootstrap fraction up to ~85% (see Fig. 2.1.4)
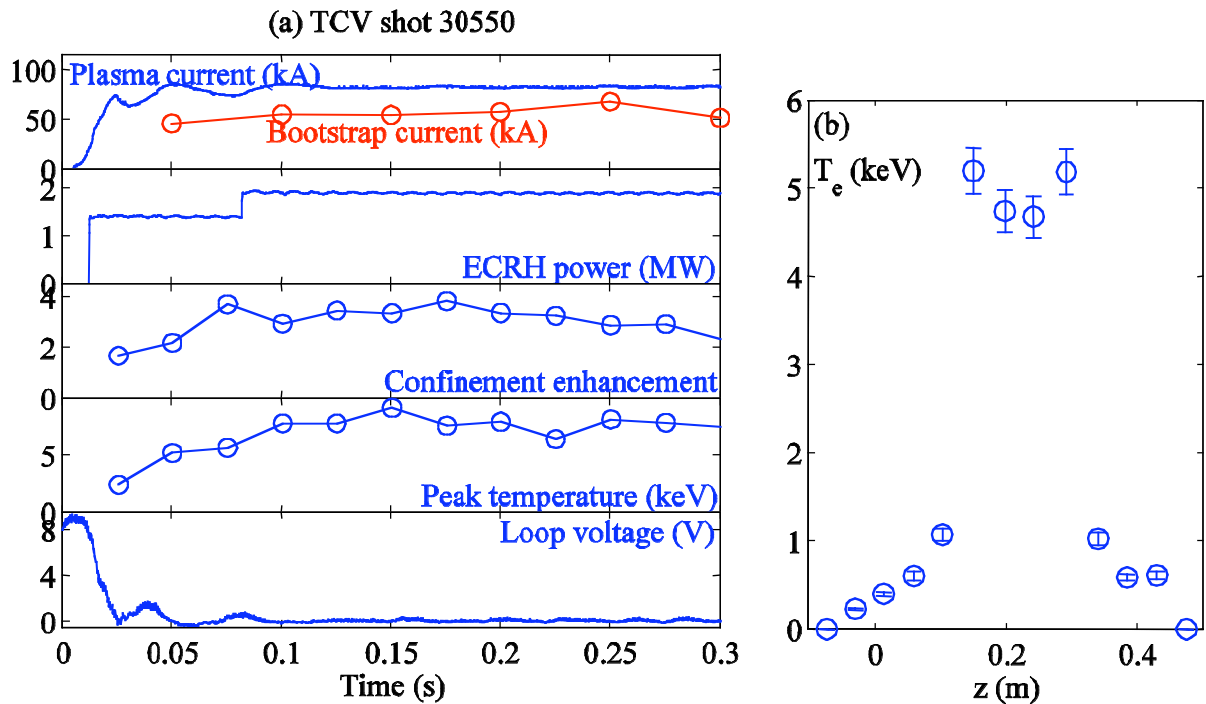
Fig. 2.1.4　　*Creation of an eITB by heating in a current ramp: (a) time history, (b) temperature profile along a vertical chord at 0.05 s.*

2.1.2　　Plasma edge characterisation and modelling

Building on experimental results obtained over the past two years and documented in previous Annual Reports, investigation of electrostatic turbulence in the TCV scrape-off layer (SOL) has turned, to a detailed comparison between measurement and theory. The result constitutes the first quantitative agreement between experimental data and a physics based description of the turbulent fields in the tokamak SOL. This work has been performed in collaboration with the Optics and Plasma Research group of the Risoe National Laboratory, Denmark, who have developed the ESEL code which solves a reduced fluid model describing the evolution of particle density, vorticity and electron temperature in a non-uniform magnetic field. An example is provided in Fig. 2.1.5, which compiles snapshots of the density (a) and vorticity (b) fields from an ESEL code run closely approximating the edge conditions in a high density, deuterium ohmic diverted TCV discharge. The simulation domain is split into three equally sized radial intervals representing the edge (inside the separatrix), main SOL and wall shadow regions in a short poloidal section at the outer midplane. The TCV fast reciprocating Langmuir probe trajectory passes through both the wall shadow and main SOL regions but typically cannot access the confined region without unacceptable perturbation to the plasma.
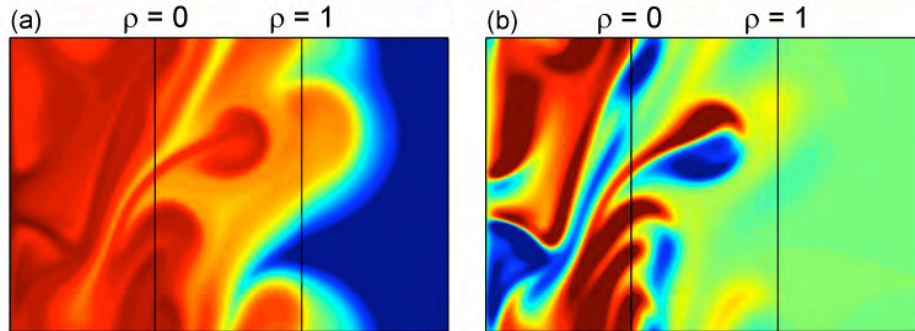
Fig. 2.1.5   *Snapshots of the density (a) and vorticity (b) fields from an ESEL code run with parameters matched to the SOL plasma in the high density TCV discharge #24530. The normalised coordinate, ρ, is defined such that unity distance corresponds to the main SOL width at the outer midplane. In this coordinate, ρ=0 corresponds to the separatrix and ρ=1 to the wall shadow, beyond which magnetic flux surfaces from the outer divertor intersect the outer vessel wall below the midplane. Periodic boundary conditions are assumed in the poloidal direction (the vertical direction in these plots)*

As a consequence of profile relaxations, the edge layer intermittently erupts plasma filaments into the SOL, which may subsequently transport far into the wall shadow. One such structure is seen clearly in the density contour of Fig. 2.1.5a), showing the mushroom-like shape of the blob front associated with a dipolar vorticity field (Fig. 2.1.5b) and thus a large radial velocity component, typically a substantial fraction of the local acoustic speed. This fast radial advection of structures leads to large relative fluctuation levels and contributes significantly to the local time-averaged plasma density profile throughout the SOL. These interchange motions are a strong candidate mechanism for the explanation of the broad radial density profiles (leading to strong main chamber recycling) commonly observed in the SOL of current tokamaks, particularly at high density.

A selection of results from a quantitative comparison between code and experiment for TCV is assembled in Fig. 2.1.13, demonstrating the excellent level of agreement in profile shape and magnitude of the turbulent driven radial outflux, the skewness of the turbulent flux probability density function (PDF) and the conditionally averaged particle density signal and turbulent flux PDF at the wall radius. The strongly intermittent nature of the turbulent particle flux is suggested by the high skewness factor and the sharp front and trailing wake feature observed also in experiments elsewhere. Similarly good agreement is found in the autocorrelation time of the density fluctuations, showing that the simulations match both the typical shape of bursty events and the time correlations. This provides confidence that SOL turbulence is largely governed by interchange motions, and opens the door towards predictive capability for SOL transport levels.
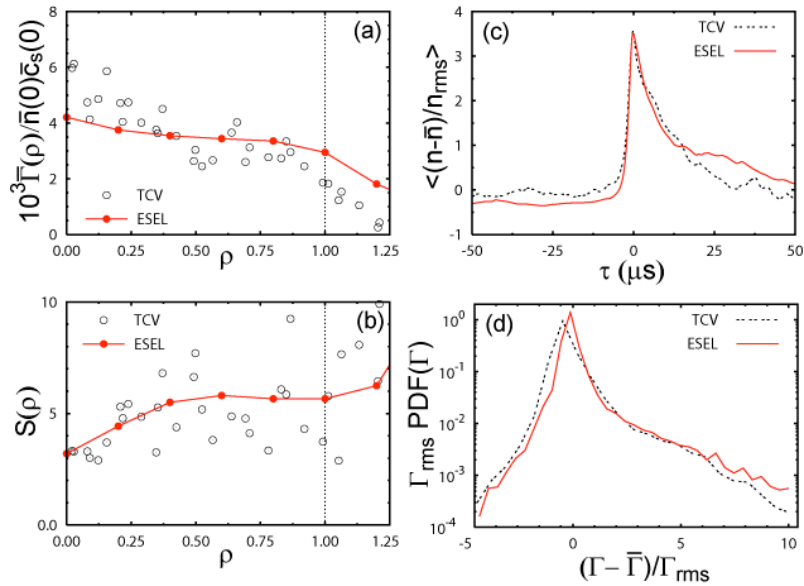
Fig. 2.1.6 *Comparison of experimental electrostatic turbulence data from the TCV SOL with matched ESEL simulations. Radial profiles of (a) turbulent driven fluxes and (b) skewness of the flux PDF. (c) conditionally averaged density for a series of bursts with amplitude exceeding 2.5x the mean density, (d) rescaled turbulent flux PDFs. Note both (c) and (d) are computed at the wall radius, $\rho = 1$, where the most intense plasma surface interaction occurs.*

2.1.3 H-mode physics

ELM control

A magnetic perturbation of the vertical position of the plasma can trigger ELMs in TCV. The question of the cyclic or prompt nature of the interaction between the plasma vertical oscillation and the ELM destabilisation was addressed. Discharges with several perturbation trains were performed. At the first perturbation, the distribution of the delays between perturbation and ELM was already peaked around the usual value for synchronisation. However, the distribution becomes more peaked after a few perturbations. Synchronisation improves with the plasma vertical velocity induced by the perturbation.

Performance improvement through high density operation and X3 heating

Successful attempts have been made to increase the plasma β using X3 heating. By heating an established ELMy H-mode, $\beta \approx 2.2\%$ was reached, below the ideal limit of $\beta \approx 3.4\%$ for these discharges (see Fig. 2.1.7). At the time of the increase in β, the plasma enters a quasi-stationary ELM-free phase that typically lasts many energy confinement times.

At the same time the ion temperature increases from $\approx 500 \text{eV}$ to $\approx 1 \text{keV}$ and the electron temperature increases from $\approx 1 \text{keV}$ to $\approx 3 \text{keV}$. Interestingly, the plasma toroidal rotation increases significantly as the plasma enters the quasi-stationary phase (see Fig. 2.1.8). This new regime is being investigated further with a view to improve the physics understanding and to allow reliable access to it, to provide a basis for routine assessment of high performance ECH-X3 heated discharges in TCV.

The experimental observation that this regime can only be achieved with full available X3-ECH power to avoid the ELM-free phase motivates a future upgrade in the X3 total power capability.
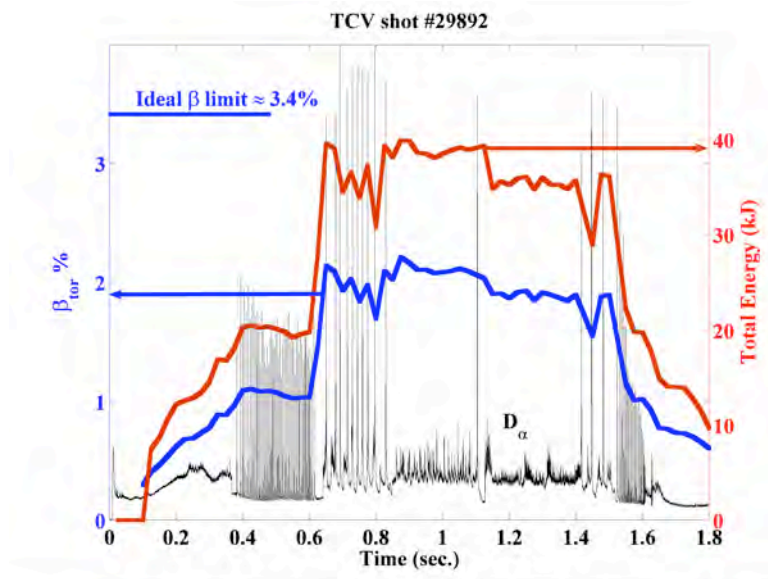
Fig. 2.1.7   *The temporal evolution of an X3 heated H-mode (#29892) that transits to the ELM-free quasi-stationary phase at 0.82sec. The D_{α} signal is shown in black (a.u.) while the toroidal β and total energy as measured using the diamagnetic loop are show in blue and red respectively.*
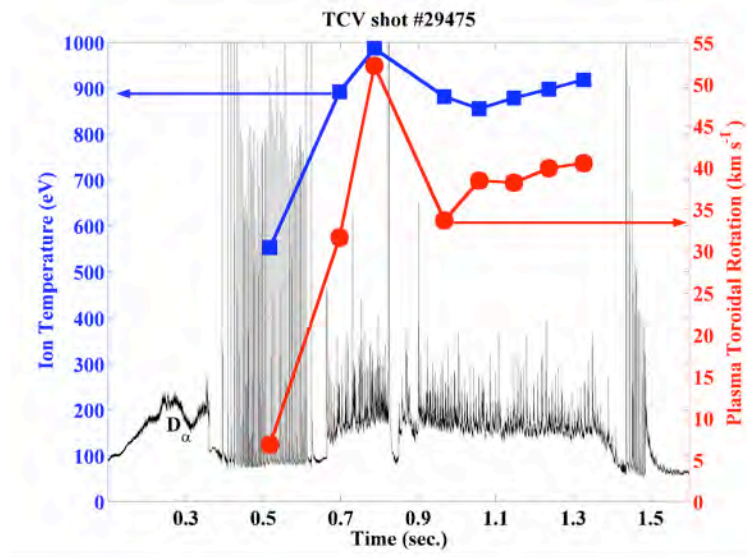
Fig. 2.1.8   *The temporal evolution of an X3 heated H-mode(#29475) that transits to the ELM-free quasi-stationary phase at 0.65sec. The D signal is shown in black (a.u.) while ion temperature (T_i) and toroidal rotation speed, as measured using CXRS, are show in blue and red respectively. T_i increases from 500eV to 1keV at the onset of X3 heating and the transition to quasi-stationary state. At the same time the plasma rotation speed increases from $5kms^{-1}$ to $50kms^{-1}$.*

2.1.4   Plasma rotation, electron energy, particle and impurity transport in shaped plasmas

Plasma rotation

Last year many experiments were undertaken to investigate the link between momentum transport theories and experiments in the basic scenario of L-mode plasmas in limiter configuration. The toroidal velocity profile was measured by the Charge Exchange Recombination Spectroscoy (CXRS) diagnostic, which can provide up to 16 local measurements along the plasma minor radius, with a radial resolution of 2.5cm and a typical sample interval of 90ms. In TCV L-mode plasmas with no external momentum input, toroidal velocities of the order of 10-50km/s are measured, directed in the direction of the plasma current and decreasing towards zero in the edge region.

The influence of MHD perturbations on the toroidal rotation profile has been analysed in experiments where such perturbations naturally develop and lead to plasma disruptions. MHD modes are observed to flatten the ion toroidal rotation profile over the central region, out to the rational surface of the corresponding mode (usually q=2). The central ion rotation decreases to match the mode rotation frequency. Outside the unstable rational surface, MHD modes shift the rotation profile while keeping a fixed gradient. As a consequence, the edge toroidal rotation (negligible in the absence of modes) is observed to reverse direction, showing considerable co-current values. This evolution implies a mechanism that strongly couples the ion fluid with the MHD mode.
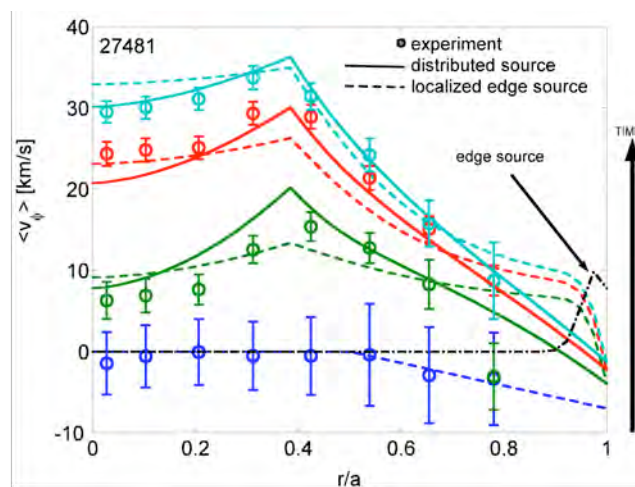
Fig. 2.1.9   *Plasma acceleration following plasma braking due to an MHD event. The points represent the CXRS rotation measurements. The time dependent numerical solutions of the diffusion equation with a source proportional to the ion temperature gradient (full line) are compared with the solutions of the advection-diffusion equation with a Gaussian source at the plasma edge (dashed line).*

The momentum source was investigated by studying the plasma acceleration following global MHD events causing a loss of confinement. After such events the toroidal rotation evolves towards a stationary profile on a slower time scale than the other main plasma parameters (n_e, T_e). The observed evolution of the velocity profiles during plasma spin-up was reproduced using a 1D advection-diffusion-momentum transport model with an ad hoc momentum source (Fig. 2.1.9). The plasma rotation measurements inside ρ=0.8 are equally well simulated using either a source localised at the plasma edge and a strong inward velocity pinch, or a

source distributed along the minor radius, in which case the pinch term is no longer required. In particular, a modified neoclassical source proportional to the ion temperature gradient correctly reproduces both transient and stationary central rotation profiles. The momentum diffusion coefficient was found to range from 10 to 40 times the value calculated from collisional theory, depending on the momentum source model used in the simulation. Hence in this experimental scenario, the momentum transport appears to be dominated by the contribution of plasma micro-instabilities.

For electron densities up to $5 \times 10^{19} m^{-3}$ the absolute value of the toroidal velocity (v_{tor}) was usually found to increase with density (n_e), an indirect effect of the rise of the ionic temperature due to energy equipartition. For higher densities, a new regime was observed in which the value of v_{tor} at the plasma centre is positive. The transition to this regime is reproducible in density ramps, and occurs at a central density $n_{e0} \sim 6 \times 10^{19} m^{-3}$ (Fig. 2.1.10). After the transition, the rotation is positive inside $\rho = 0.7$, while the edge rotation for $\rho > 0.8$ remains unaffected. The transition simultaneously affects all the central part of the plasma, and occurs over a longer timescale, if the fuelling rate is reduced.
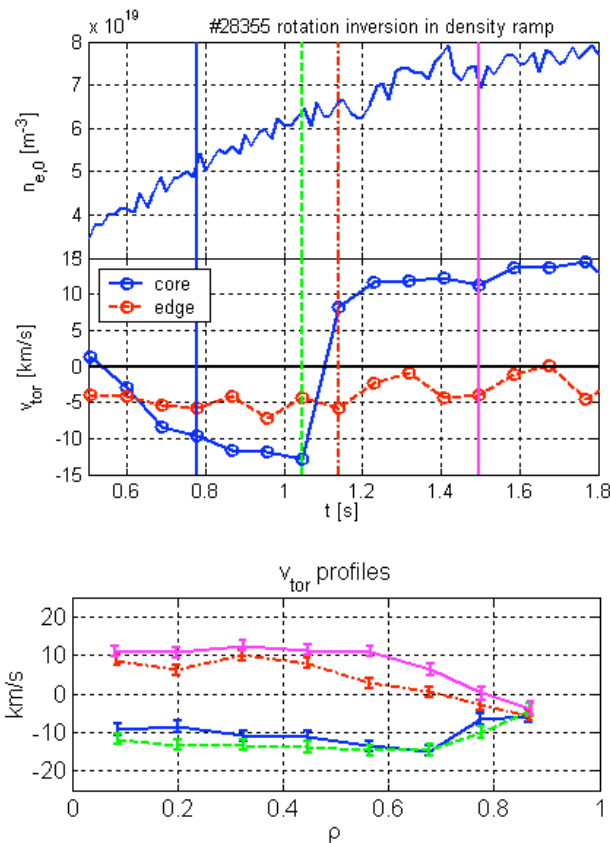
Fig. 2.1.10   *Central electronic density and toroidal velocity evolution during a transition to reversed rotation regime. In the bottom figure, the velocity profiles are plotted for 4 different times.*

In n_e ramp down experiments back transitions have been observed at lower density threshold, indicating hysteresis. The n_e threshold is found to rapidly increase when decreasing the plasma current (I_p): no transition could be attained for $I_p < 270 kA$., and higher (T_e) values correspond to a higher inversion density threshold.

While experiments are still ongoing, the observations to date suggest that the quantity determining the transition can be a combination of n_e and T_e, suggesting a role for collisionality.

Electron heat transport dependence on plasma shape and collisionality

The effect of plasma triangularity on core electron heat transport has been studied in TCV low-density, electron cyclotron (EC) heated L-mode plasmas, to avoid the strong modification of the edge pedestal and stability with triangularity typical of H-mode discharges. In these trapped electron modes (TEM) dominated plasmas, the plasma triangularity was varied from negative to positive values, $\delta=-0.4$ to $\delta=+0.4$, at constant plasma collisionality.

Figure 2.1.11 shows results obtained with EC heating power deposited just outside the q=1 surface, adapted to obtain at negative triangularity $\delta=-0.4$ the same T_e–profile obtained at positive triangularity $\delta=+0.4$. The other parameters, n_e, Z_{eff}, q_{95}, were held constant and less than half of the power was needed, 0.6MW instead of 1.35MW. For negative triangularity the electron energy confinement time and relative enhancement factor are increased compared to the positive triangularity, τ_{Ee}=3.6->7.7ms and H_{RLW}=1.5->1.9. The electron heat diffusivity from power balance estimates is decreased, $\chi_e^{PB}(\rho=0.5)$=8.5->2.6 m^2/s.
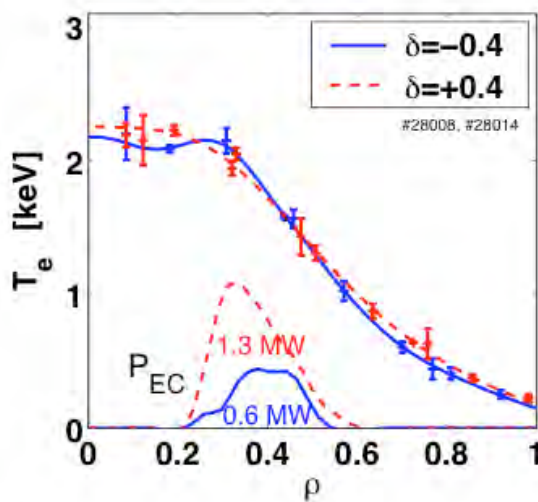
Fig. 2.1.11 *Identical T_e profiles obtained at negative triangularity $\delta=-0.4$, and positive triangularity $\delta=+0.4$, with half the EC power.*
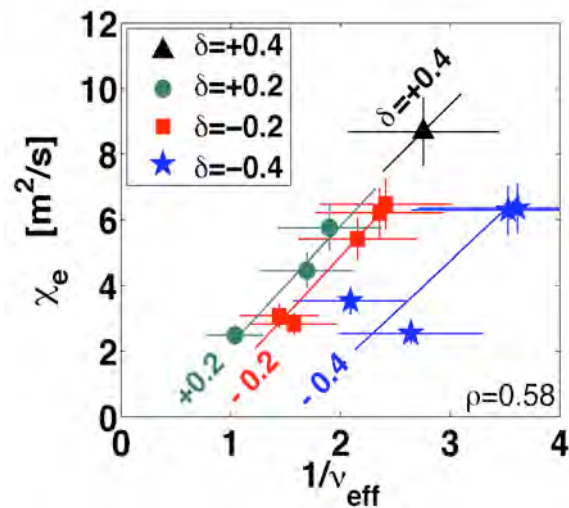
Fig. 2.1.12 *Separation of shape and collisionality effects, both influencing χ_e ($q_{95}=C^{te}$).*

Comparing the data with different values of $n_e Z_{eff}$, it appears that χ_e does not only depend on T_e, but also on $n_e Z_{eff}$ and that the heat diffusivity and the gyro-Bohm normalised heat diffusivity decrease strongly with increasing effective collisionality. The reduction of electron heat transport with ν_{eff} is consistent with ASDEX Upgrade experimental results and with the predicted stabilising effect of ν_{eff} on TEM modes.

The coupled effect of plasma triangularity and collisionality is shown in Fig. 2.1.12. The heat diffusivity does not vary significantly from $\delta=+0.4$ to $\delta=+0.2$. However, with negative triangularity, χ_e clearly decreases with decreasing δ. For the whole range of triangularity, χ_e decreases strongly with increasing ν_{eff}.

Small and negative triangularity, as well as high effective collisionality, appear to reduce the electron heat transport in this TEM dominated regime. Although the physical reason for this triangularity effect still needs to be determined, the strong

effect on electron heat transport might already be used to control the access to electron internal transport barriers (eITBs).

Particle and impurity transport

The main effort in this area was to establish parametric dependencies for the behaviour of density profiles in L-mode and e-ITB plasmas. The study of the phenomenon of 'density peaking' is important since a peaked density profile in a reactor would boost the fusion power and bootstrap fraction, but at the same time would have the undesirable effects of favouring impurity accumulation and of reducing the edge density for a given average density.

Calculations of the particle flux caused by neutrals originating from the edge were performed using the one-dimensional kinetic transport code Kn1D and the 2D Monte-Carlo code DOUBLE. Analysis shows that even for a device the size of TCV, edge fuelling cannot be responsible for the density gradient in the plasma bulk, despite the possibility of penetration by a sequence of typically four charge exchange reactions before a final ionisation. An independent test for the absence of an effect of edge fuelling on bulk density peaking was obtained in Helium plasmas. Due to the low cross section for double charge exchange, stepwise penetration by charge exchange is absent in Helium plasmas. If this mechanism were important, He plasmas should have flatter profiles than D plasmas. Figure 2.1.13 shows discharges that are identical except for the working gas, demonstrating that neutral penetration by charge exchange has no influence on density peaking. Since peaked density profiles are also observed in fully EC current driven discharges, i.e. in the absence of the Ware pinch, the above analysis and the He plasma experiments confirm the existence of anomalous inward pinches.
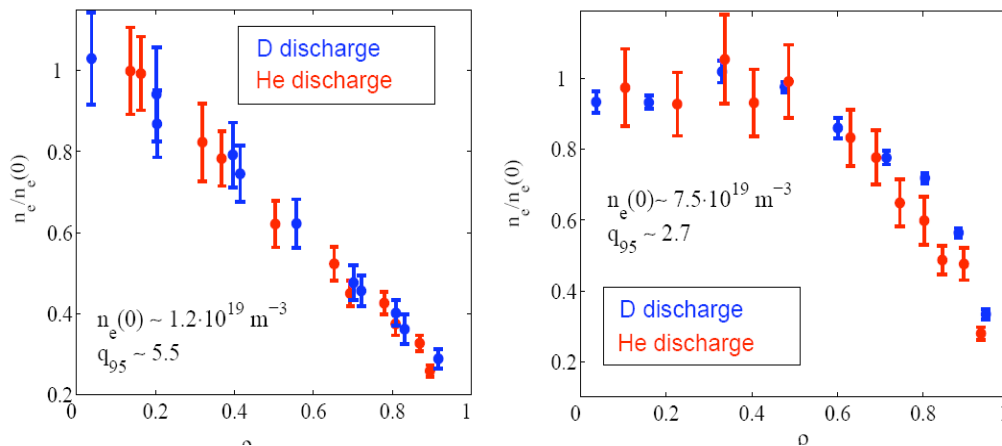
Fig. 2.1.13   *Examples of pairs of discharges in D and He. The working gas has no effect, unlike the edge safety factor, which is strongly correlated with $<j>/(q_0 j_0)$.*

The theoretical framework for interpreting density peaking is that of ITG/TEM drift wave turbulence, which produce convective fluxes proportional to magnetic shear (anomalous curvature pinch) and to the logarithmic temperature gradient (anomalous thermodiffusion). While the former is present in both ITG and TEM unstable plasmas and is directed inward, TEM are predicted to produce outward directed thermodiffusion, thereby reducing the density gradients. One of the issues related to density peaking in reactor conditions is the effect of powerful electron heating by alpha particles from fusion reactions, which may destabilise TEM modes and reduce or suppress density peaking.

This effect has been studied in L-modes plasmas in TCV over a large range of ECH power and depositions location. The peaking factor $n_e(0)/<n_e>$ of the density profile drops from a high value in ohmically heated plasmas to a lower value for some 0.5MW of centrally deposited ECH power and then remains nearly unchanged up to the maximum available power of 2.7MW. A database of 600 samples was established, showing that for ECH heated plasmas at power levels above 0.5MW, the density peaking factor depends only on the parameter $<j>/q_0j_0$, which governs Ohmically heated plasmas, and the normalized radius of deposition of the ECH power.
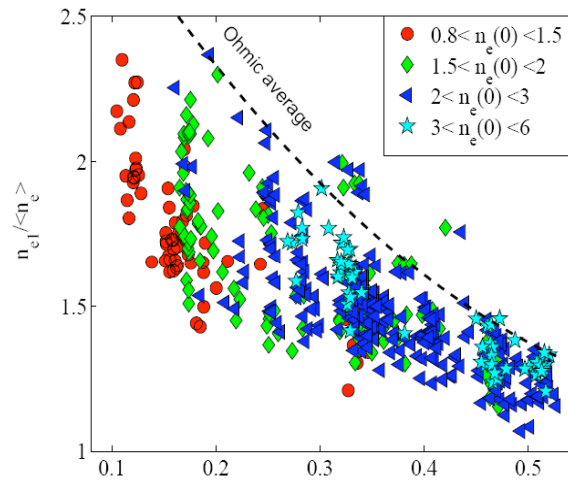
Fig. 2.1.14   *Peaking factor of ECH and ECCD discharges as a function of $<j>/(q_0j_0)$. The broken line is the average of purely ohmically heated discharges.*

A large number of global parameters was tested for their potential influence on density peaking, including $\beta_{e,i}$, $\rho^*_{e,i}$, $\nu^*_{e,i}$, $<n_e>$, $<T_e>/T_e(0)$, $<j>/(q_0j_0)$ and the normalised radius of ECH deposition, ρ_{dep}. Remarkably, a significant dependence was only found on the latter two. It is captured by the scaling relation given by $<n_e>/n_e(0)\approx0.9<j>/(q_0j_0)-0.2\rho_{dep}+0.44$ in ECH plasmas, to be compared with $<n_e>/n_e(0)\approx<j>/(q_0j_0)+0.22$ in ohmic plasmas, Fig. 2.1.14.

Peaking factors similar to or even exceeding the ohmic values are obtained with far off-axis power deposition and in eITB plasmas. Unlike L-modes, strong eITB plasmas show a correlation of density and temperature gradients in the improved confinement zone, $\nabla n_e/n_e\approx0.45\nabla T_e/T_e$, which is suggestive of neoclassical thermodiffusion in the barrier region.

Work on impurity transport has been pursued in collaboration with IPP Prague and KFKI Budapest. Intrinsic carbon impurity profiles, measured using active charge exchange spectroscopy, have been observed to have somewhat larger logarithmic gradients than electron density profiles in the confinement zone. The TCV laser ablation system has been brought into service again recently, with successful injection of Si and Ti. The aim of this work is to characterise and understand impurity transport and its relation to particle and energy transport.

Radially resolved measurements of CV K-α and CVI Lyman-α emission profiles using a four-channel multilayer mirror spectrometer operated jointly with IPP Prague have been modelled using the STRAHL ionisation equilibrium code, demonstrating that transport coefficients for intrinsic carbon in the plasma periphery (r/a>0.7) can be obtained from an analysis of the ionisation equilibrium. Because of the small number of chords, these experiments relied on a radial

compression of the plasma in order to increase the resolution. Recent experiments have shown that, at least for the measurement of CVI profiles, a promising CV charge exchange line is available. If confirmed, this should ameliorate the measurement of impurity transport coefficients in the plasma periphery. The new method is expected to complement data obtained by the injection of medium Z impurities, such as laser ablated Si, in collaboration with KFKI, Budapest.

Isotope substitution experiments

The diffusion of plasma and impurity ions is generally decoupled from the overall behaviour of the plasma electrons. Reactor operation will depend on the cross-diffusion of fuel, ash and impurity ions. The recent installation of the Compact Neutral Particle Analyser, capable of simultaneously measuring neutral fluxes from two ion species (H and D or D and He) has allowed us to start ion transport investigations in isotope substitution experiments. In these experiments, brief puffs of hydrogen were introduced into the discharge and their penetration into the plasma was assessed by measuring the changes in the fluxes of H and D neutrals in the energy range 0.6-3keV. During the H-puff, the flux of hydrogen atoms from plasma increases by a factor of 2-4, while the flux of deuterium neutrals decreases by a factor of 2-3 (Fig. 2.1.15).
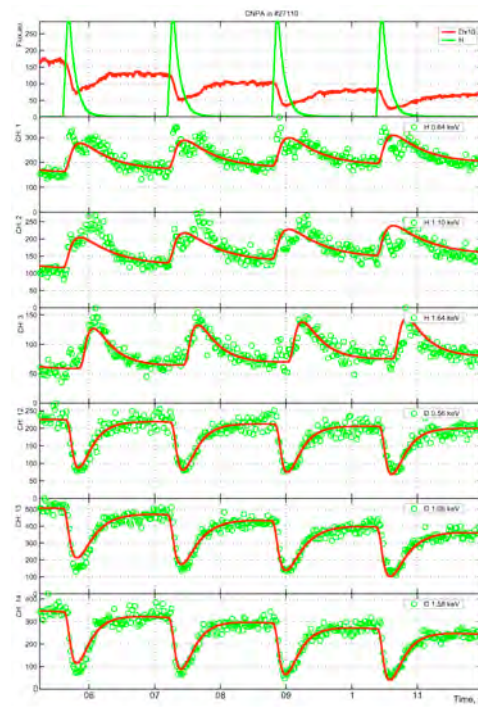
Fig. 2.1.15   *H and D fluxes from gas valves and CNPA count rates at three different energies in a TCV shot with H-gas puff. (D flux is multiplied by 10). Experimental points – green circles, Fit – red lines.*

The time evolution of the fluxes can be modelled (red lines) using an effective confinement time (10-40ms depending on conditions). Similar times are required for the H fluxes to establish Maxwellian spectra of the same temperature as the D background. Initial modelling for the data available suggests diffusion coefficients for H in a D background in the range 0.3-1m^2/s. Systematic investigations of the effects of plasma parameters on ion transport have been initiated. A detailed analysis of these experiments will require the development of analysis algorithms which include a model for neutral and ion transport.

2.1.5   Physics of ECH and ECCD, including Electron Bernstein Waves

During the activity related to the physics of ECH and ECCD was mainly focused on studies of the propagation and absorption of the 3rd harmonic X-mode with a top-launch injection and/or to the 2nd harmonic double mode conversion O-X-B with central Electron Bernstein Wave (EBW) absorption. EBW heating, relying on the O-X-B mode conversion scheme launched from the LFS was demonstrated in TCV for the first time in an overdense plasma of a conventional aspect ratio tokamak. Preparatory work for studying the Ohkawa current-drive efficiency with the X2 has started, but the main experimental activity will be carried out during 2006.

X3-top launch

In experiments dedicated to heating of H-mode plasma it has been possible to reach nearly full single-pass absorption on a target plasma with a central density of $n_{e0}=8.10^{19}m^{-3}$. In these experiments the feedback on the mirror angle could not be used due to perturbations on the presently used observable associated with ELM induced density perturbations as well as fast density variation in ELM free periods occurring during the X3 pulse.

With a total injected power of 1.35MW, an ELMy regime that is significantly different to ohmic/low-power-heating ELMy H-mode has been found. This new regime of ELMy H-mode is highly reproducible and the measured absorbed X3 fraction, is in excess of 85% at central densities of $n_{e0}=8.10^{19}m^{-3}$. The measured level of absorption with the DML is in good agreement with the value calculated with the ray-tracing code TORAY-GA. This result is consistent with the fact that no suprathermal electron population is observed at these high densities.

As shown in Fig. 2.1.16. at the time of the X3 turn-on, the calculated absorbed fraction is approximately 30% and increases up to more than 90% once the stationary X3-heated phase is reached. With a top launch configuration, by the nature of the heating scheme, nearly no control of the deposition profile is possible. However, at the plasma density and temperature reached in these H-mode X3-heated plasmas, the single-pass absorption of an X3 beam injected from the LFS would be greater than 55%. With such absorption, significant control of the deposition profile would be possible.

Beam-tracing calculations with the ECWGB code have been performed in collaboration with CNR Milano, to assess the importance of diffraction effects with the X3 top-launch. The beam-tracing ECWGB code, compared with the TORAY-GA ray-tracing code, includes diffraction effects on the rf-beam propagation through the plasma and also uses a higher number of rays with a better homogeneity in the spatial distribution of the rays. In the top-launch configuration, the condition on ray homogeneity is very important for properly calculating the single-pass absorption. It is also possible to run the ECWGB code in «ray-tracing mode» to directly compare the two different models: beam-tracing and ray-tracing. In the top-launch configuration, since the rf beam is focussed inside the plasma for the ray-tracing calculations, the beam is modelled in free-space with a cylindrical constant cross-section with a gaussian power distribution. In Fig. 2.1.17, the comparison between the two models is made and diffraction effects start to be relevant with strong focussing, $w_0<12mm$.
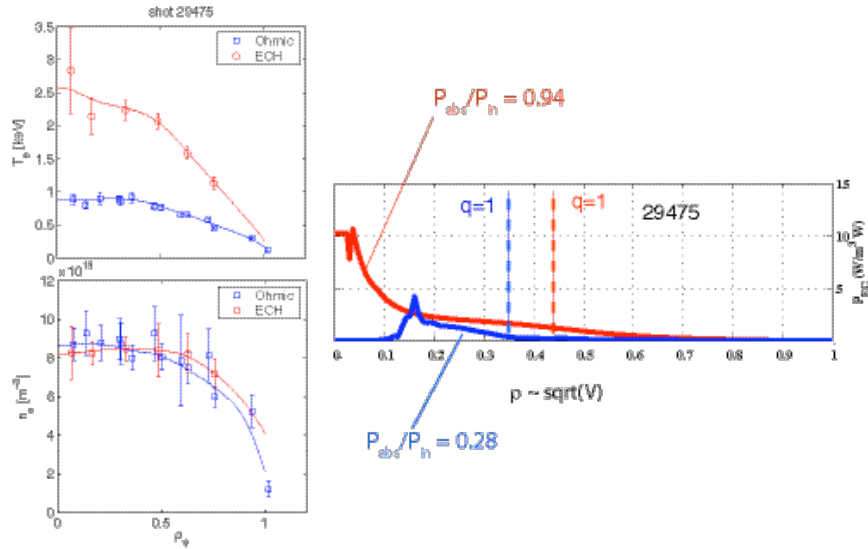
Fig. 2.1.16 *On the left, temperature (top-trace) and density profiles (bottom-trace) measured by Thomson scattering for a typical X3-heated H-mode plasma. In blue are represented profiles during the ohmic heated phase (before X3 turn-on) and in red profiles during the stationary phase of the X3 heating. On the right, with the same color coding, are the calculated absorption profiles for the corresponding phases shown on the left.*
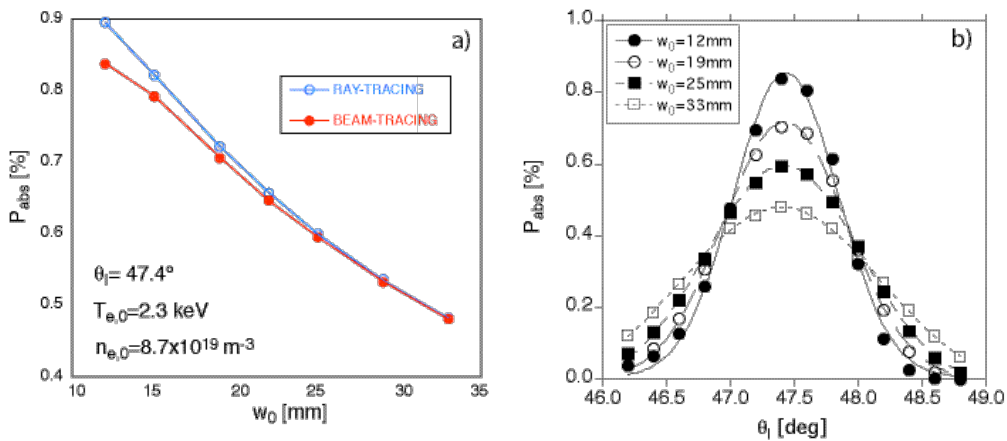
Fig. 2.1.17 *Comparison with ECWGB of the beam-tracing model and the ray tracing model. (a): Comparison of the two models (in blue ray-tracing, in red beam-tracing where the absorbed fraction is plotted against the waist w_0 with the mirror angle at the optimum value $\theta_l = 47.4^o$. The calculation has been performed on a typical L-mode plasma with a central electron density and temperature of $n_e = 10^{19} m^{-3}$ and $T_e = 2.8$ keV. (b) Absorbed fraction versus mirror angle is calculated with the beam tracing model for various waists w_0.*

The rf beam considered in Fig. 2.1.17 is non-astigmatic and the design value has a waist of 30mm. In a recent verification of the upper-launcher mirror design, it was noticed that an error had been made in the machining of the mirror surface and the rf-beam used on TCV was actually strongly astigmatic. Beam-tracing calculations with the ECWGB code have shown that the level of absorption with such an astigmatic beam, $P_{abs} = 70\%$, is equivalent to a 19mm non-astigmatic beam of Fig. 2.1.17a.

Electron Bernstein Wave Heating

Electron Bernstein Waves offer the possibility of heating low-field plasmas like spherical tokamaks or conventional aspect ratio tokamaks with Electron Cyclotron (EC) waves at densities far above the cut-off density of O- and X-modes. In low field machines (B≤3-4T), the EC cut-off density limits are typically lower than the Greenwald density limit, as shown in Fig. 2.1.18.
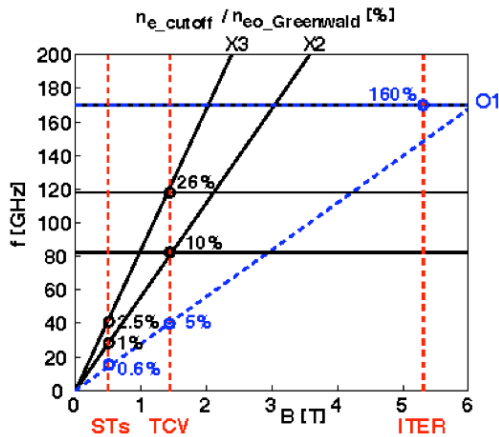
Fig. 2.1.18   *Typical ratio of EC cut-off density to Greenwald density limit (in %) for different gyrotron frequencies and magnetic fields.*

With a low field side (LFS) launch, overdense plasmas are accessible through the double mode O-X-B conversion scheme. The refraction bends the oblique O-mode wave ray path until it is nearly parallel to the magnetic field lines, where O-X conversion occurs, and from where the wave propagates back towards the upper hybrid resonance layer. The X-B conversion occurs naturally in hot plasma close to the upper hybrid resonance layer, from where the converted B-wave propagates further to the centre where it is dissipated at the EC resonance harmonic.

A large O-X transmission-conversion angular window requires a high-density gradient and a central density n_{eo} above O-mode cut-off. For this purpose, a low q_{95} ohmic H-mode target plasma was developed with a slowly rising density, exhibiting ELMy and ELM-free phases, with adequate high edge density gradients. The heating studies use a central density of typically $1.5 \cdot 10^{19} \mathrm{m}^{-3}$.

To prepare heating experiments, the value of the correct O-mode injection angles needs to be determined. Since the power of one gyrotron beam influences the H–mode properties, the determination of the angular conversion-absorption window uses this power at a low power duty cycle (6%). The level of EC stray radiation in an ELM-free phase gives the measure of the converted power, see Fig. 2.1.19

A two-directional scan of the injection angle, searching for the minimum of the stray radiation, yields the optimal launcher angle position through interpolation, Fig. 2.1.20. This angle overlaps to within an error of 2° with ART ray tracing calculations, compatible with the uncertainty in the equilibrium reconstruction.

With a higher duty cycle, the total power absorption is measured from the modulated energy via the diamagnetic probe. An absorbed power of more than 60% of the injected O-mode power has been measured. As a counterproof, using an incorrect injection angle or an X-mode injection, the same measurement yields only very small-absorbed power.
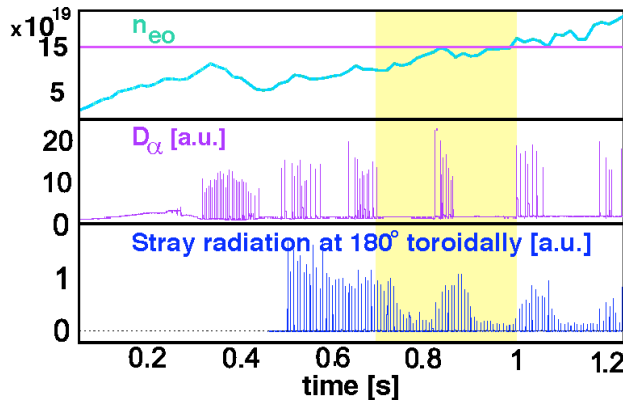
Fig. 2.1.19 *ELMy H-mode with ELM-free phases, with density evolution, D_α-emission, and strong absorption (low EC stray radiation) during ELM-free periods.*
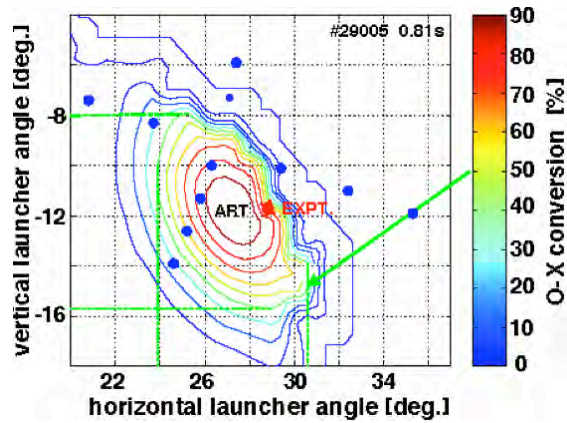
Fig. 2.1.20 *Optimum angular absorption response (EXPT) from two experimental angular scan of the EC stray field (dots) compared with ART calculations.*

Local power deposition is found directly from the evolution of the soft X-ray emission at the heating pulse from the soft X-ray DMPX wire-chamber camera, as well as from Fourier transform, at a location close to the predicted location from the ART code.

These high power EBH experiments demonstrate absorption of EBW wave in a conventional aspect ratio tokamak, both local and global, using the O-X-B scheme for the first time. [IPP Greifswald, D; IPP Garching, D; UKAEA, UK; CompX, USA]

2.2 Theory and numerical simulation

2.2.1 Physics underlying anomalous transport

Nonlinear global gyrokinetic simulations

The mutual interactions between ion temperature gradient (ITG) modes, zonal flows and geodesic acoustic modes (GAM) in tokamak plasmas have been investigated using the global nonlinear electrostatic gyrokinetic code ORB5, in which the time evolution of the temperature profile and its gradient is totally unconstrained. A series of numerical simulations with the same initial temperature, density and magnetic shear profiles has been performed using a sequence of ideal MHD equilibria (Fig.2.2.1) differing only in the value of the total plasma current. On top of a bursty or quasi-steady behaviour, the zonal flows oscillate at the GAM frequency. The amplitude of these oscillations increases with the value of the safety factor q, resulting in a less effective suppression of ITG turbulence by zonal flows for low values of the plasma current. As a consequence, the turbulence driven, volume-averaged radial heat transport is found to scale inversely to the total plasma current. Similar scalings are found in the burst regime, characterised by avalanches, when the temperature gradient is far above marginality, and in the quasi-steady regime when the temperature gradient has relaxed close to marginal stability.
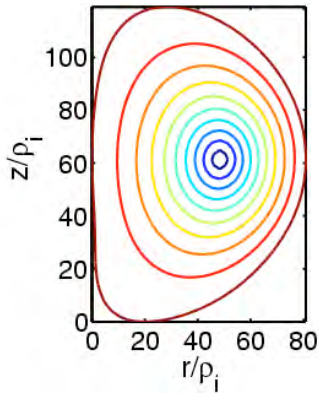
Fig. 2.2.1 *Magnetic surfaces of the equilibrium used in global gyrokinetic simulations of Figs 2.2.2 - 2.2.4.*
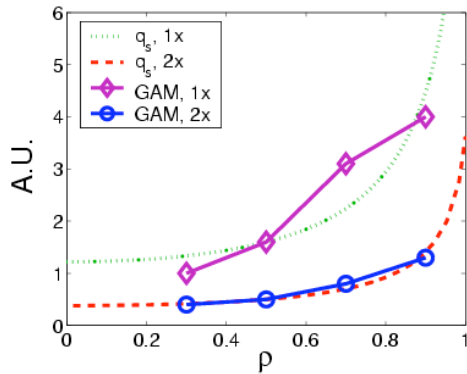
Fig. 2.2.2 *Amplitude of zonal flow oscillations at the GAM frequency, for two equilibria differing only in the value of total plasma current. The dotted lines are the two corresponding q profiles.*

The nonlinear gyrokinetic code ORB5 has been improved in several aspects. A major upgrade has been the introduction of straight-field-line magnetic coordinates, and a magnetic field-aligned Fourier filter that suppresses the unphysical small parallel wavelengths. The upgraded version has been benchmarked against the former version of the code. The first results show a substantial improvement in the noise accumulation for long simulation times (Fig. 2.2.5). In addition, an alternative initialisation of the perturbation has been implemented, replacing the random noise quiet start formerly used. It is expected that once non adiabatic electrons are introduced, these improvements will be crucial in getting low noise simulations.
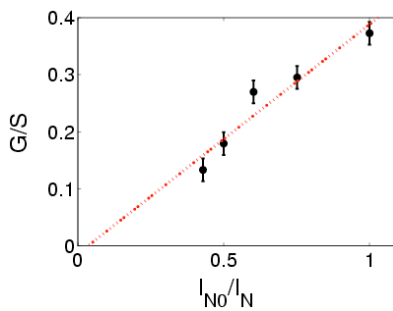
Fig.2.2.3 *Ratio of zonal ExB flows amplitude oscillating at the GAM frequency (G) to the steady zonal amplitude (S) versus inverse total plasma current.*
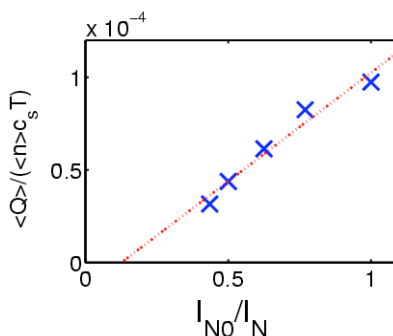
Fig. 2.2.4 *Volume-averaged ITG turbulence-induced radial heat flux versus inverse total plasma current.*

In another study, we have shown how an appropriate choice for the initial distribution function, using constants of motion, is necessary to avoid the spurious generation of axisymmetric *ExB* flows that arise due to magnetic drifts normal to the magnetic surfaces. A method to specify the initial distribution function has been proposed, implemented and successfully tested, simultaneously satisfying the requirements of the quasi-neutrality equation and of being a gyrokinetic equilibrium in the absence of electric fields, valid for general axisymmetric configurations with nested magnetic surfaces.
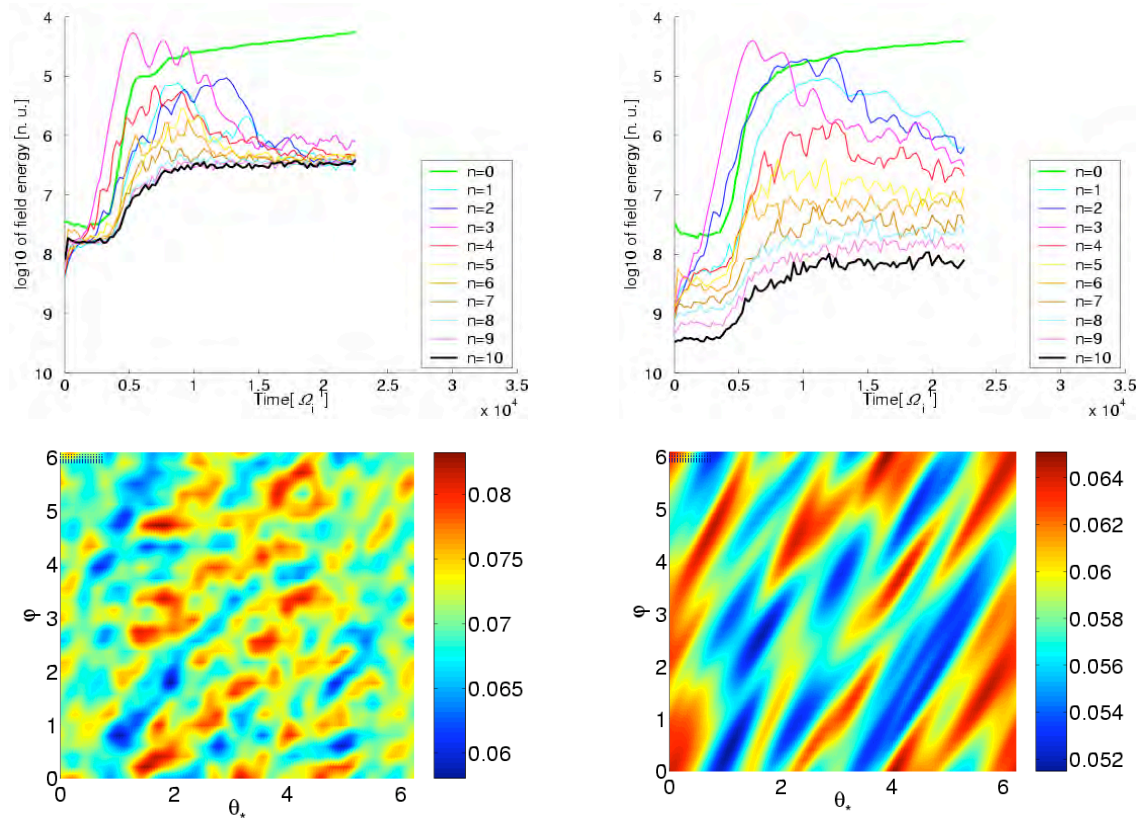
Fig. 2.2.5   *Global gyrokinetic simulations of ITG with ExB zonal flows. Top: field energy versus time for various toroidal mode numbers n. Bottom: contours of perturbed potential on a magnetic surface. Without (left) or with (right) a field-aligned Fourier filter. Without a field-aligned filter, the simulation is drowned in numerical noise.*

With the purpose of identifying the most accurate and efficient algorithm, various Eulerian solvers for Vlasov-type equations have been compared: the standard semi-Lagrangian, the Cubic Interpolation Propagation (CIP), and the Positive and Flux Conserving (PFC) methods. Diffusion and dispersion properties and behaviour with respect to the Gibbs problem of overshoot has been proposed, implemented and successfully tested, which appear as a major issue in gyrokinetic simulations. Applications to nonlinear Landau damping modelled by the 1D Vlasov-Poisson system and to the Kelvin-Helmholtz instability problem in 2D have been performed, the latter providing a good test bed for some of the technical difficulties of the gyrokinetic equation, in particular handling ExB drifts. From these tests, the CIP method turns out to be an interesting alternative to the standard semi-Lagrangian scheme based on cubic B-spline interpolations. In particular, the CIP interpolation scheme, based on cubic Hermite elements, is a local method whereas B-spline interpolation requires global computations. This is an advantage for implementation

on parallel computers. [IPP Garching, D; IPP Greifswald, D; CEA Cadarache, F; JAEA Tokyo, J]

Electron internal transport barriers, transport and current profile modelling

Advanced scenarios characterised by a rapid drop in the central electron heat transport coefficient, and thus improved electron energy confinement, have been obtained in many tokamaks, related to the appearance of an Internal Transport Barrier (ITB). Experiments have been carried out in TCV to elucidate the role of the plasma current density (j_p) profile evolution from peaked to hollow in the electron ITB (eITB) formation, in particular the importance of the occurrence of a zero-shear surface for triggering the barrier. A systematic study of TCV eITB discharges has been carried out with the ASTRA transport code, suggesting a correlation between the barrier formation and the safety factor (q) profile inversion, i.e. that the radial location and time of the eITB triggering are consistent with the spatial and temporal appearance of a minimum in the q profile. In this context ASTRA has been employed in an interpretative mode, constrained by experimentally measured density and temperature profiles, to provide modelling of the q and j_p evolutions, which are not measured. An accurate modelling of the current density profile in both steady-state and transient simulations has been made and comparisons between the numerical results with the experimental profiles have also been discussed. A study of the sensitivity of the j_p profile on the bootstrap current density, the driven electron cyclotron current density and the loop voltage, has been started. Further investigation is needed to understand the interplay between the extension of the negative shear region and the degree of improved confinement.

A study of particle transport in the presence of an eITB and more generally in the presence of electron cyclotron radiofrequency heating (ECR), has been undertaken, with emphasis on the dependence of density profile tailoring on the local characteristics of the current profile and power deposition. In collaboration with the ASDEX Upgrade team, experiments with off-axis ECRF heating in L-mode plasmas have been performed, showing a strong dependence of density gradient on the local shear, independent of the collisionality. For eITBs, an interesting result has been found that density and temperature are strongly coupled for the steady state fully developed eITB.

2.2.2   RF waves

Electron cyclotron current drive compensation of the bootstrap current in stellarators

Self-consistent 3D MHD equilibria with finite bootstrap current and partially compensating electron cyclotron current drive (ECCD) are computed for quasi-axisymmetric and quasi-helically symmetric stellarator reactor configurations. An inner loop convergence between the equilibrium state and the bootstrap current in the collisionless regime is supplemented by an outer loop that determines the necessary current required to avoid the appearance of low order rational surfaces within the plasma domain in the vicinity of which ideal MHD instabilities can be triggered. Schemes based on ordinary mode propagation at the fundamental harmonic (O1;160GHz) and on extraordinary propagation at the second harmonic (X2;385GHz) have been shown to effectively stabilise a 3-period quasi-axisymmetric device modelled on the NCSX stellarator in construction at Princeton for β=6.4%. The O1 mode launched from the low field side requires 5MW to remove the critical rational rotational transform surface iota=2/3 from the plasma while the X2 mode from the high field side achieves the same objective with between 1.5 and 3MW. A mode conversion scenario of OXB (ordinary-extraordinary-Bernstein) has also been attempted with mixed success, motivated by the fact that the electrostatic Bernstein

waves are not subject to cut-offs. The 4-period quasi-helical system examined corresponds to the extrapolation of the HSX experiment to reactor dimensions. This system becomes weakly unstable to an m/n=1/1 global mode for β>0.6%. The critical iota=1 rational surface is removed from the central region of the plasma with 100kW of power with a X-mode at the third harmonic (500GHz) launched from the top of the plasma. [CIEMAT, E; Culham, UK]

Alfvén and ICRF waves in 2D and 3D configurations

The modifications of the dielectric tensor due to warm plasma effects have been introduced in the LEMan full wave 3D code. Thus, Landau damping is included in the formulation and the conversion of modes to the Kinetic Alfvén Wave (KAW) can be modelled. This extended version of the LEMan code has been successfully tested with a cylindrical model, a circular cross section tokamak and a straight bumpy mirror in which the Alfvén wave dispersion relations acquire a simple form. The convergence of the code has been verified through analysis of the Coulomb gauge and the integrated local and global power balances. A helicity induced Alfvén gap eigenmode (HAE) has been computed in a straight helix at 100kHz with oscillations that correspond to KAW on either side of the gap. The propagation of waves in a bumpy mirror in the ion cyclotron frequency range has been investigated using the cold plasma limit and reproduces the magnetic beach absorption expected in such geometry at the fundamental harmonic. Adding toroidal effects (aspect ratio 25) displaces the resonant surface and corresponding absorption. [KTH, Stockholm, S]

2.2.3   Operational limits

Kinetic effects on MHD modes

Studies continue to identify kinetic modifications to modes which are essentially of MHD origin. The drift kinetic treatment employed has recently been generalised to take into account the toroidal and poloidal magnetic drift of passing particles. This has been undertaken through analytical calculation of the orbit averaged magnetic drift frequency of particles in realistic tokamak equilibria, and for realistic plasma parameters. The Fig. 2.2.6 shows the average poloidal and toroidal drifts over the
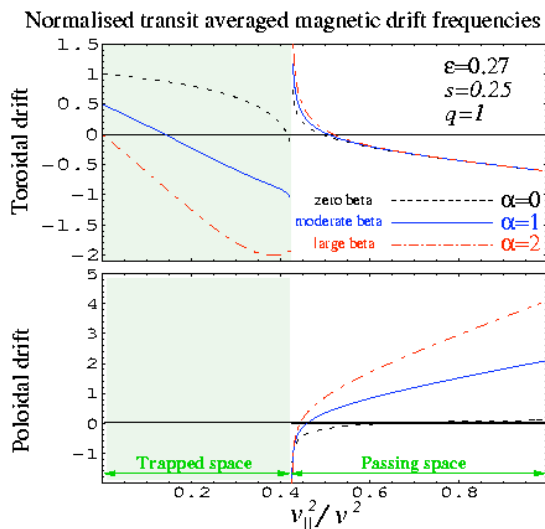
Fig. 2.2.6   *Average poloidal and toroidal drift frequencies over the full range of velocity pitch angle for different plasma beta.*

full range of velocity pitch angle for different plasma β. The poloidal magnetic drift frequency is found to have a strong dependence on plasma β. This is a toroidal

effect, which manifests itself in the Shafranov shift, and generally results in reduced single particle resonance with a parallel wave vector. The inclusion of these effects has recently been published in conjunction with the related issues concerning the effects of pressure anisotropy (Section 2.2.4) on the equilibrium and MHD stability. Studies continue into comparisons of the analytical treatment of the effects of pressure anisotropy on the equilibrium and internal kink mode stability, and the numerical results from VMEC and TERPSICHORE. [Uppsala, S]

Sawtooth behaviour and internal kink mode

A summary of the theoretical interpretation of sawtooth control in present and future tokamaks has recently been compiled. Special consideration is given to the control of sawteeth via the modification of resistive diffusion in the hot core region of the tokamak. The work details the effects of localised current perturbations in various tokamaks. The current perturbations are deliberately deposited near the rational surface of the internal kink mode. JET experiments in which injection of neutral beam ions is orientated in the direction counter to the plasma current are also interpreted. The momentum induced toroidal rotation, which is in the opposite direction to conventional neutral beam discharges, is found to be an important consideration, as is the radial deposition of the hot neutral beam ions. The latter is found to modify the heating to the electrons, and ultimately the timescale of the current penetration and sawtooth repetition time.

Edge Localised Modes (ELMs)

Stability diagrams for ideal MHD edge current density and pressure gradient limits for tokamak configurations with a separatrix at the boundary have been systematically investigated with the global code KINX, showing the robustness of the edge current density limit $J_{edge}/(I_p/S_{pot}) \sim 1$, and of the scaling $w\,n\,q_{95} = const$ for the toroidal mode number n of the most unstable mode, for different pedestal widths w and various q profiles. In relation to ELM triggering experiments by external magnetic perturbations in TCV and AUG tokamaks, we have analysed the effects of boundary deformation (increased squareness) on the stability limits. Increased boundary squareness destabilises edge kink – ballooning modes. This is consistent with the AUG experiment in which ELMs are triggered when the plasma moves down. An ITER plasma has also been analysed, and the current density variation induced by the magnetic perturbation is large enough to destabilise edge kink – ballooning modes. For the case of the TCV experiments, both current density variation and plasma boundary shape modifications are possible candidates for the ELM triggering. [Keldysh Inst. Moscow, RU]

2.2.4   *Optimisation of 3D configurations*

Neoclassical transport in 3D stellarators

A new Monte Carlo delta-f code, VENUS-delta-f, has been developed to determine the neoclassical transport properties, and in particular the bootstrap current, in 3D stellarator configurations with a mono-energetic distribution of particles and a momentum conserving Lorentz collision operator. Several successful tests and benchmarks have been performed for model JT60 tokamak and Wendelstein VII-X stellarator systems. These include the main conservation tests, convergence studies and the dependences of diffusion coefficients and bootstrap currents as a function of the collision frequency and the poloidal angle. [Kurchatov Inst., Moscow, RU; IPP Greifswald, D]

3D anisotropic pressure stellarator equilibria

The fixed boundary version of the 3D VMEC equilibrium code has been extended to investigate anisotropic pressure equilibria. One model uses a modified slowing down distribution that loads particles preferentially with large parallel velocity to model tangential neutral beam injection. The pressure surfaces remain coupled to the flux surfaces and the Shafranov shift increases with parallel anisotropy. A second model is based on a bi-Maxwellian distribution function that can treat parallel and perpendicular anisotropy. Parallel anisotropy yields similar results to the first model. Off-axis deposition with perpendicular anisotropy causes the perpendicular pressure to concentrate in the region of energetic particle deposition. [ORNL, USA; NIFS, J; Nagoya Univ., J]

Global and Mercier stability in stellarators with fluid and non-interacting energetic particles

Formulations of the Kruskal-Oberman energy principle in which the hot particles represent a fully interacting fluid, and of an energy principle proposed by Johnson et al. in which the energetic particles constitute a rigid non-interacting layer have been adopted in the TERPSICHORE stability code. Applications to a current-free 10-period heliotron system with parallel pressure anisotropy at $\beta=3.9\%$ reveal that global n=2 modes and the Mercier stability become marginal when the hot particle contribution to β approaches $1/3$ in the fully fluid model and $1/4$ in the rigid non-interacting model. As the ratio of hot to total β increases, the radial extent of the unstable domain driven by the ballooning/interchange mechanism shrinks. [NIFS, J; Nagoya Univ., J]

J-parallel optimised quasi-isodynamic stellarators with poloidal quasisymmetry

The optimisation of an N=12 period quasi-isodynamic stellarator has been undertaken with targets that included satisfactory properties of fast particle confinement, effective ripple, bootstrap current and MHD stability. Unlike quasi-helically symmetric systems, there is no symmetric analogue of a quasi-isodynamic system. Nevertheless, the MHD stability limit improves with increases in the number of periods and aspect ratio. Nevertheless, the toroidal effect in this configuration is important so that a simple increase of the number of periods with a corresponding enhancement of the aspect ratio does not conserve favourable neoclassical transport and local ideal MHD stability properties. [Kurchatov Inst., Moscow, RU; IPP Greifswald, D]

2.2.5 Tokamak discharge simulation

Work on the DINA-CH full tokamak modelling code continued. The major effort went into simulating the magnetic triggering of ELMs, developed on TCV and confirmed on ASDEX Upgrade. In addition, simulations of the effect of the applied Poloidal Field voltages on ITER during disruptions were made, showing the requirement of appropriate decisions during a disruption. Work continued to identify non-linear behaviour in the vertical position control of MAST, due to the very different vertical field index on spherical tokamaks compared with conventional aspect ratio tokamaks.

Magnetic triggering of ELMs in ASDEX Upgrade showed frequent ELM events when the plasma is rapidly moved vertically. However, the ELMs are triggered when the plasma is moving down, contrary to the previous observation on TCV in which the ELMs occurred when the plasma moved upward.

By simulating the plasma response with a full simulation of the plasma control system, vacuum vessel and PF-coils, the magnetic triggering of ELMs in ASDEX Upgrade has been compared with that in TCV. A new candidate for the explanation of ASDEX Upgrade ELM behaviour, the flux surface deformation pattern, has been suggested. The passive stabilisers located inside the vacuum vessel of ASDEX Upgrade play a role as an external linking flux source and create a local expansion or shrinkage of the flux surface near them. At the same time, they have a shielding effect against other external flux changes caused by the vacuum vessel components and the active PF-coils. Therefore, when the plasmas are moving in opposite direction, upward in TCV and downward in ASDEX Upgrade, they have similar flux surface deformation patterns at the time of the triggered ELMs. This causes the opposite ELM behaviour with respect to the plasma motion. For the validation of this new candidate, experiments with a radial plasma movement have been proposed for ASDEX Upgrade. [Kurchatov Inst., Moscow, RU; TRINITI Inst., RU; IPP Garching, D; CEA Cadarache, F]
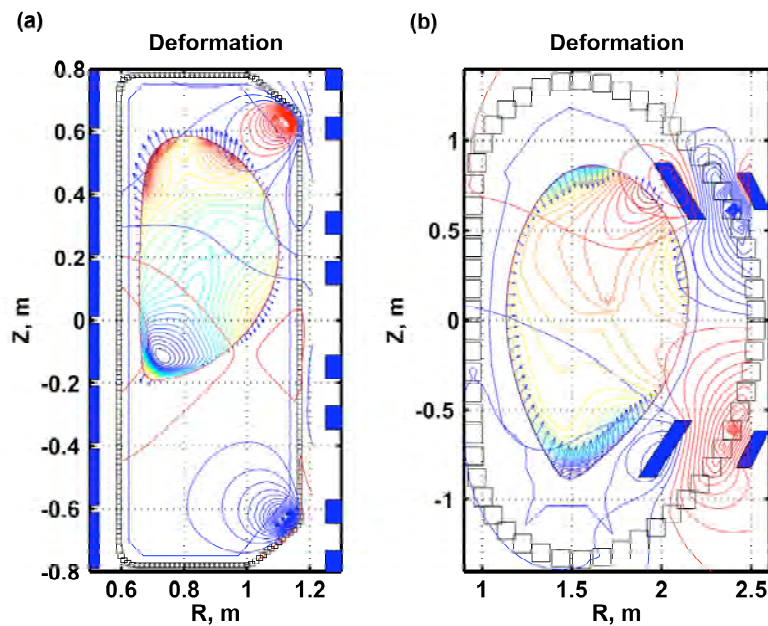
Fig. 2.2.7   *Deformation of the plasma during magnetic triggering of ELMs, comparing TCV (left) with ASDEX Upgrade (right). The role of the Passive Stabilising Loops in ASDEX Upgrade is visible.*

2.2.6   Integrated Tokamak Modelling

Work in 2005 concentrated on the development of suitable structures for sharing data between experiments and codes for the Integrated Tokamak Modelling Task Force. A collaboration with CEA Cadarache, IPP Garching and UKAEA allowed us to propose a structure defined by XML schemas and to explore the advantages of this approach. Overlaying these structures on MDSplus was developed and the data structures were exported to Frascati. This prototyping work should now give way to use of these structures to interface codes. [CEA Cadarache, F]

2.3　Operation of a specialised basic plasma physics device, TORPEX

2.3.1　Fluctuation measurements and identification of instabilities

The relationship between the plasma gradients and the development of instabilities and turbulent phenomena is a key issue for anomalous transport in toroidal plasmas. To characterise this relation, systematic measurements of the 2D spatial distribution of the fluctuation amplitudes, their frequency and wave number spectra, dispersion relation, correlations and phase shifts between fluctuating density and potential have been performed for a wide range of control parameters such as vertical magnetic field, neutral gas pressure, microwave power. Figure 2.3.1 shows the 2D profiles of the density and its fluctuations for a standard Hydrogen plasma (P_{RF}=1.5kW, B_z=0.6mT, p_H=2x10^{-5}mbar), recorded by the HEXTIP probe over 500ms shots. It is evident that the instabilities occur primarily on the LFS, and in the region of a strong pressure gradient, where density and magnetic field gradients are aligned, corresponding to a maximum interchange drive. The power spectra of the density fluctuations for four chosen values of gas pressure, measured in the region of largest rms fluctuation levels, are shown in Fig. 2.3.2. A reduction of the amplitude, and a corresponding broadening of the coherent peaks can be noticed as the neutral pressure is increased. The dispersion properties $S(k,\omega)$ perpendicular to the magnetic field were reconstructed using a the fixed set of AC coupled probes distributed along the poloidal direction and applying a statistical method based on the two point correlation technique, shown in Fig. 2.3.3 for the source region where the instabilities originate. Consistently with the local measurements of the spectrum (Fig. 2.3.2), the coherent character of the peaks apparent in the low pressure case tends to fade as the neutral pressure is increased. The slope in the graph for the low frequency region (f<5kHz) is similar, indicating similar propagation speeds, around 1000m/s in the laboratory frame. In all cases analysed here, the observed direction of propagation is that of the ExB flow, i.e. upwards on the LFS, opposite to the electron diamagnetic drift. Therefore, for drift waves, the magnitude of the phase velocity should be the difference between the two velocities. Nevertheless, the measurements error bars prevent us from using this as a conclusive argument for the identification of the instabilities. The potential fluctuations in many cases are so large that the average, steady-state component of the ExB flow loses significance.
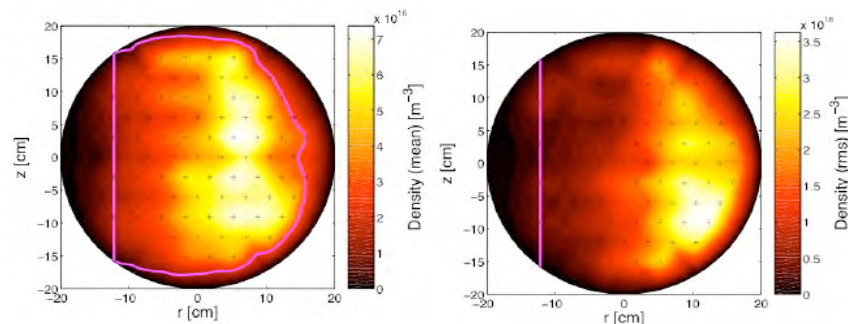
Fig. 2.3.1　　Distribution of density (left) and related rms value of the fluctuations up to 125kHz for a standard Hydrogen plasma.

By applying the same analysis technique to signals from probe sensors aligned toroidally, an estimate of the parallel dispersion relation is obtained. In most of the

cases, spectral components are characterised by a spectrum centred on $k_{||}$ values well distinct from zero. The magnitude of the perpendicular wave number is generally at least an order of magnitude larger than the parallel one, as expected for drift-interchange type instabilities.

A ratio of order unity of the normalised density to potential fluctuations is also compatible with drift instabilities. The measured phase relationship between perturbed density and potential shows complex behaviour, with no indication of extended radial eigenmodes.
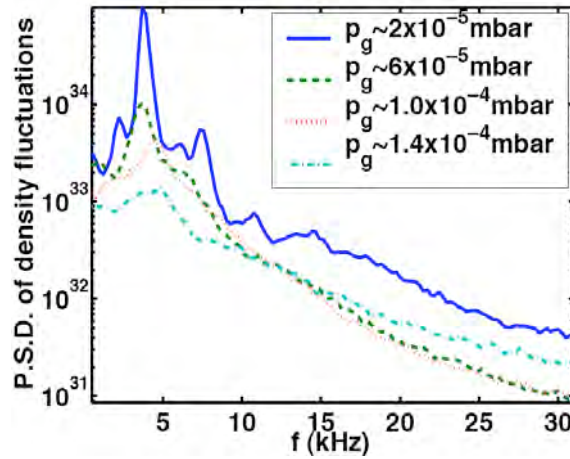
Fig. 2.3.2   *Power spectra of density fluctuations measured in the region of largest rms value for the four values of H neutral gas pressure*
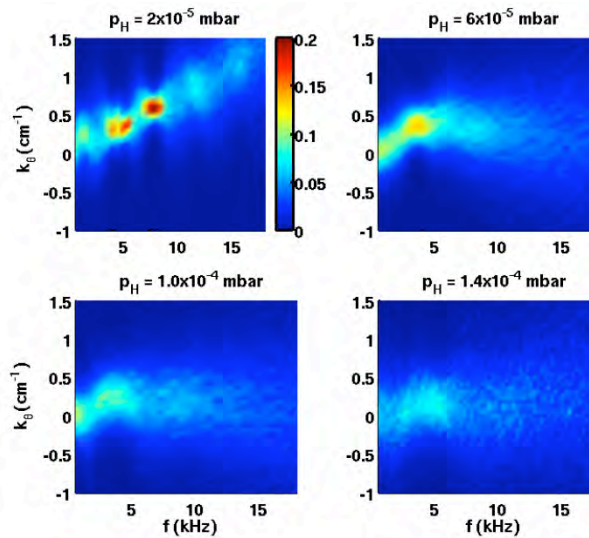
Fig. 2.3.3   *Statistical dispersion relation perpendicular to the magnetic field reconstructed in the source region for four different H neutral gas pressures.*

2.3.2   Fluctuation induced particle flux across the magnetic field

The phase between density and potential influences the value of the turbulence induced particle flux, whose time average value along the radial direction is given by $\langle \Gamma_{radial} \rangle = \langle \tilde{n}\tilde{v} \rangle$. The contributions to the turbulent flux from the space and frequency resolved measurements are selected based on the spectral amplitudes,

the relative coherence, the smoothness of the phase variation with frequency, and the wave number, which has to be in the range compatible with the probe geometry. The results for two neutral pressure values are shown in Fig. 2.3.4, along with the value of the flux integrated over all frequencies and the corresponding density profile. The frequency spectrum of the flux shows contributions for the different spectral modes that differ both in size and sign. For the low pressure case, the flux is larger and is concentrated in the low frequency range, where coherent peaks dominate, but contributions come from a larger spatial region. Conversely, in the higher pressure case, the flux is lower and results from the contribution of a broader spectral region but a narrower portion of the radial profile. In both cases, the sign of the total turbulent flux in the radial direction and on the mid-plane indicates an inward pinch.
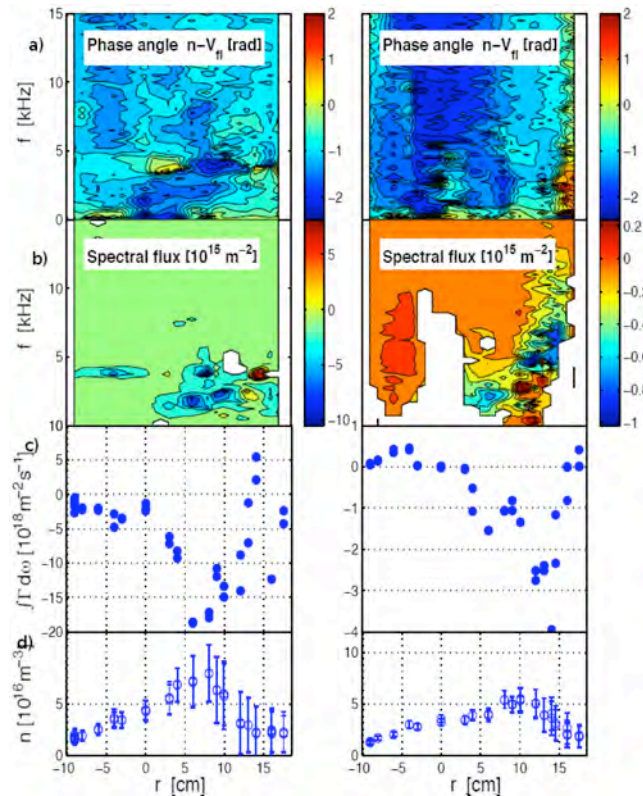
Fig. 2.3.4   *Radial profile on the equatorial plane of the frequency resolved phase between density and potential fluctuations (a), the frequency resolved fluctuation induced flux (b), its integrated value (c), and density (d), for $p_H=2x10^{-5}$ mbar (left) and $p_H=1x10^{-4}$ mbar (right). A negative flux indicates a pinch towards the centre of the device. The error bars on the density indicate the rms value of the fluctuations*

2.3.3   Quantification of structures and imaging

Probability distribution functions can provide information on the instabilities and turbulence and on their possible impact on plasma transport. However, this local description difficult to interpret and cannot constrain unequivocally the theoretical models aimed at simulating the turbulence evolution. A full spatio-temporal imaging of the electrostatic fluctuations and turbulence needs to be undertaken. A new method has been developed and now routinely used on TORPEX. It is based on direct measurements of potential and density fluctuations taken over a single discharge using the HEXTIP probe. A necessary step to characterise the nature of the structures is to identify them as mathematical objects, and construct a set of

observables from measurements of quantities representative of their dynamics, like centre of mass, size, lifetime and velocity. In defining these observables it is important to consider possible applications to the results of numerical codes, which would then be compared on their basis. HEXTIP data is first extrapolated to the whole poloidal cross section, assuming zero fluctuations at the wall, then cut into contours using a contouring algorithm. A structure is delimited by a bounding contour, defined by a minimum level of the excess density, chosen here as the global (i.e. for all signals) standard deviation for the density fluctuations. The trajectories of the centre of mass of the structure (or *blob*) can then be reconstructed by comparing the evolution of consecutive time frames. To represent their statistical distribution, the cross-section is divided into a rectangular grid and we count the number of trajectories that traverse each bin, where the average trajectory velocity is also determined. Figure 2.3.5 shows the statistics of the presence of blob trajectories over the poloidal cross-section, for a standard TORPEX plasma. Only orbits that last for longer than 200μs are considered here. By looking directly at the trajectories, one can infer that, for each mode (Fig. 2.3.2), the blobs originate in the region of large amplitude, but propagate well beyond it. Superimposed on the colour plot, the arrows represent the speed and direction of the motion of the centre of mass of the structures for each bin. Significant differences are found between the motion of trajectories originating from each spectral region. Finally, aspects of the trajectory patterns are compared with the reconstructed averaged ExB flow field. [Risoe, DK; MIT, Cambridge, USA; UCI, USA]
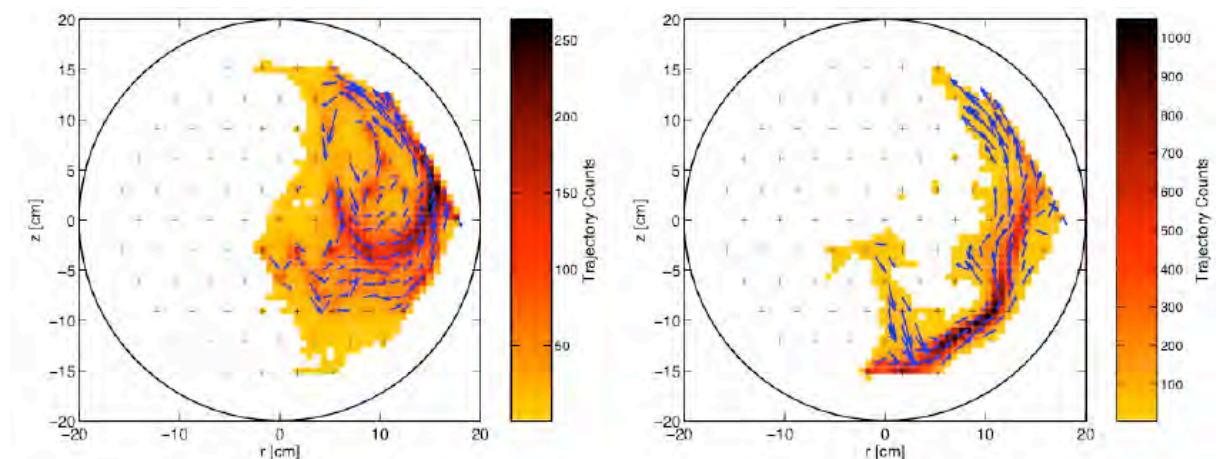
Fig. 2.3.5 *Statistics of the occupation of bins of the poloidal cross-section by trajectories of fluctuation structures and of the velocities of the blob centre of mass, for a standard Hydrogen plasma. The two columns correspond to two separate spectral regions (1.6- 2.8kHz on the left, and 3.3-4.3.3kHz on the right).*

2.4   Materials research

The main objective of the Fusion Technology Materials (FTM) group is to investigate the effects of the damage produced by radiation in a variety of materials, in particular candidate materials for structural components of future fusion reactors but also pure metals and model alloys. The group is located at the Paul Scherrer Institute (PSI) in Villigen.

In fusion reactors, the plasma facing (first wall, divertor) and breeding-blanket components will be exposed to plasma and electromagnetic radiation and will suffer from irradiation by 14MeV neutrons that are the product, together with helium nuclei, of fusion reactions between deuterium and tritium nuclei. The high-energy

fusion neutrons produce atomic displacement cascades and transmutation nuclear reactions within the irradiated materials. From the point of view of materials science, atomic displacement cascades create point structure defects, i.e. vacancies and interstitial atoms, while transmutation nuclear reactions produce impurities, e.g. helium or hydrogen gas atoms.

Key parameters for the first wall in 3 to 4GW fusion power reactors and in quasi-continuous operation include a total neutron flux of 10 to $15 \times 10^{18} n/m^2 \cdot s$, a neutron wall loading of 2 to $3MW/m^2$, an integrated wall load of 10 to $15MWy/m^2$, a surface heat load of 0.1 to $1MW/m^2$ and a volume power density of 20 to $30MW/m^3$. The accumulated dose will amount to 20-30 displacements per atom (dpa) per year in steels, while the gas produced by transmutation nuclear reactions will amount to 10-15 atomic parts per million (appm) of He per dpa and 40-50appm H/dpa.

The final microstructure of the irradiated material results from a balance between radiation damage and thermal annealing. It may contain small defect clusters, dislocation loops, precipitates, stacking-fault tetrahedra, voids and/or helium bubbles (Fig. 2.4.1, left). This microstructure has a strong impact on the physical and mechanical properties of the irradiated material. It may lead to significant hardening (Fig. 2.4.1, right), loss of ductility, fracture toughness and creep strength, as well as macroscopic swelling of the material. These effects are the main factors limiting the choice of candidate materials. The residual radioactivity of a large quantity of exposed material is also of concern and will govern its handling methods, dictate the storage periods and the overall waste management and recycling scenarios. The development strategy that takes these limitations into account has led to the development of so-called low activation materials.

The thermal efficiency of a reactor is proportional to the temperature of the coolant, which is imposed by the upper temperature of the structural materials. From a technological point of view, the temperature window of operation of fusion reactors is mainly limited by the mechanical properties of structural materials. Candidate structural materials for plasma facing and breeding-blanket components have a chemical composition that is based on low activation elements (Fe, Cr, V, Ti, W, Si, C, Ta). They include mainly reduced activation ferritic/martensitic (RAFM) steels, oxide dispersion strengthened RAFM and RAF steels, vanadium-based alloys, tungsten-based materials, and fibre reinforced SiC/SiC ceramic composites. Each alternative alloy class exhibits specific problems of radiation damage. For the time being, the most promising class of alloys are the RAFM steels for which the greatest technological maturity has been achieved, i.e. qualified fabrication routes, welding technology and general industrial experience are already available.

No intense source of 14MeV fusion neutrons is presently available and it is necessary to simulate the effects of 14MeV neutrons experimentally, using for instance fission neutrons. Until December 2003, the FTM group was using the high-energy (590MeV) proton beam of the PSI accelerator, through the Proton Irradiation Experiment (PIREX) facility. Since April 2004, most irradiation experiments have been performed with a mixed spectrum of high-energy protons and spallation neutrons by using a combination of the PSI proton accelerator and the target of the Swiss Spallation Neutron Source (SINQ).

Like 14MeV neutrons, 590MeV protons produce atomic displacement cascades and transmutation nuclear reactions within the irradiated material. One of the main advantages of 590MeV protons is to generate high rates of production of impurities, which cannot be achieved with any other currently available irradiation source. While proton irradiation in PIREX was producing about 130appm He/dpa and 800appm H/dpa in steels, irradiation in SINQ produce about 50appm He/dpa and 450appm H/dpa. However, in order to investigate the material property changes and degradation under different irradiation conditions, the FTM group is also

involved in specific neutron irradiation performed in reactors in the U.S.A., the Netherlands and Hungary.
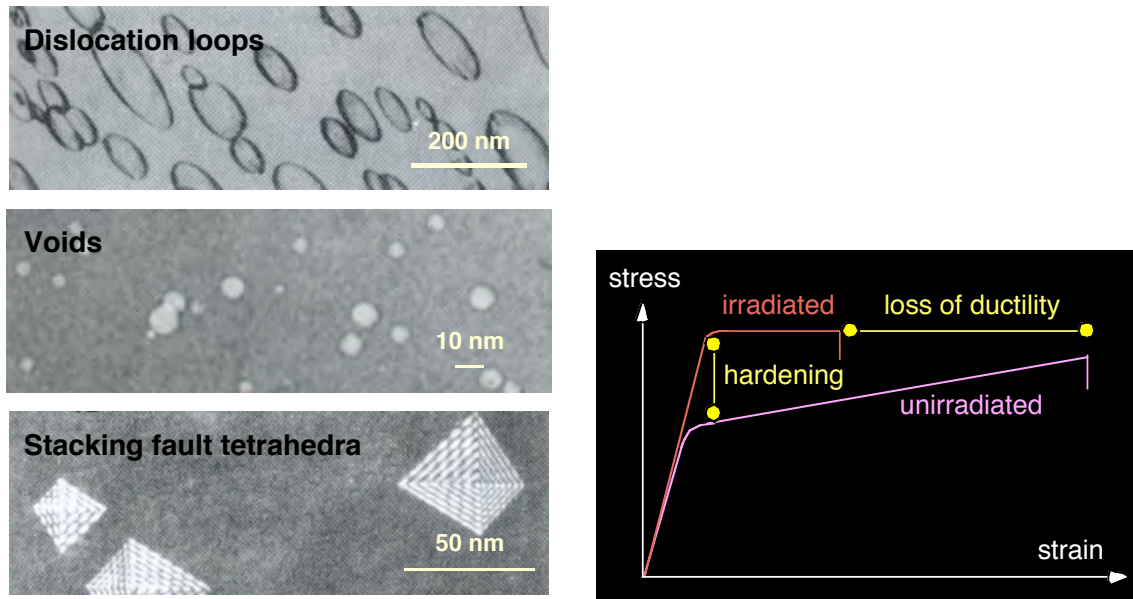
Fig. 2.4.1   *Left: examples of transmission electron microscopy images of irradiation-induced structure defects. Right: schematic of irradiation-induced hardening and loss of ductility, as measured in tensile tests on irradiated specimens.*

The design of materials with adequate properties requires an understanding of the effects of irradiation on their physical and mechanical properties. The FTM group has been active in this field for several years within the framework of the European Fusion Development Agreement (EFDA) and collaborates with many research institutes and industries in Switzerland as well as abroad. The research activities of the FTM group include basic research on radiation damage in pure metals and alloys, characterisation and development of low activation materials for fusion power reactor applications and characterisation of materials for ITER. The scientific approach adopted by the FTM group to understand the fundamentals of radiation damage in metals and alloys is based on investigating the structure/mechanics relationships at different length scales, micro-, meso-, and macroscopical, using a range of experimental and numerical tools. The main experimental tools include mechanical testing on sub-sized and standard specimens, scanning and transmission electron microscopy (SEM, TEM), small angle neutron scattering (SANS) and corrosion resistance experiments. The main numerical tools include ab-initio calculations, molecular dynamics (MD), Monte-Carlo (MC) and dislocation dynamics (DD) simulations and finite element modelling (FEM).

2.4.1   Decommissioning of PIREX

The definitive shutdown of the PIREX facility took place on December 22, 2003. Decommissioning of the PIREX facility was started in March 2004. It will be pursued in a continuous way until the end of 2006. Technically, the PIREX facility was mainly composed of four irradiation heads, referred to as targets, a rectangular port allowing the heads to be inserted into the proton beam line, a helium loop with its compressor (for cooling the heads and specimens during irradiation), and electrical connections. The targets are strongly radioactive and the helium loop is

slightly contaminated with tritium. Most of the dismantling is being performed in hot cells using remote handling.

2.4.2   *Modelling of radiation damage in fcc and bcc metals*

This work is carried out as an Underlying Technology Task.

The irradiation-induced damage in face centred cubic (fcc) and body centred cubic (bcc) metals is being simulated by molecular dynamics (MD). The aim is to produce a data set of atomic displacement cascade-induced defects. It will be used as input for kinetic Monte Carlo (kMC) calculations that allow prediction of the long-term evolution of the defect microstructure at a mesoscale.

One intriguing point is the formation of stacking fault tetrahedra (SFTs), which are observed in large quantities in many irradiated fcc metals, such as Ni and Cu. Their formation depends on the stacking fault energy and the shear modulus. Irradiated stainless steels, however, although they present a low stacking energy and a high shear modulus, do not contain SFTs, or, if present, their number density is low. There is still a lack of knowledge of this phenomenon. In order to unveil the mechanisms behind it, a series of MD simulations were initiated under the hypothesis that in stainless steels there are alloying elements (Fe, Cr and Ni) with differences in atomic radii that could hinder the formation of SFTs. MD simulations were started for the Ni-Al system, for which an Embedded Atom method (EAM) interatomic potential is available, contrary to the Fe-Cr-Ni system, and presents a large difference in atomic radii. In a first step, the formation of a SFT from a triangular vacancy platelet was reproduced. Following the Silcox-Hirsch (1962) mechanism, it should collapse into a SFT. A 15 vacancy-triangular platelet was relaxed at 800K for 3ps, in pure Ni and in Ni-5at.%Al. Figure 2.4.2 shows that both materials allow the platelet to collapse to the same SFT, but with a small difference (one atom in the stacking fault is not hexagonal compact (hcp)-coordinated in the case of Ni-5at.%Al). Work is being continued using different platelet sizes and Al contents (10at.%), and temperatures (10K, 400K).

Fig. 2.4.2   *Resulting atomic configurations, showing a stacking fault tetrahedron, following annealing of a 15 vacancy-triangular platelet at 800K for 3ps. Left: pure Ni, right: Ni containing 5at.% Al. Red atoms: hcp-coordinated atoms, blue: non-fcc, non-hcp, non-bcc atoms.*

On the other hand, series of atomic displacement cascades were produced by MD in bcc Fe with the Ackland interatomic potential and in Fe-He with the interatomic potentials derived by Morishita and Wirth. Cascades were generated for PKA (primary knock-on atom) energies of 1, 5, 10 and 20keV at temperatures of 10, 300 and 523K, in order to compare the obtained results to the experimental ones arising from irradiations and ion implantations. Simulations were made with He either in interstitial or in substitutional position and He contents of 0.1 and 1at.%. The available Fe-He potentials do not reproduce the appropriate energies for the He

interstitial and substitutional locations and for the He migration energy in bcc Fe, as compared to the values obtained by ab-initio techniques. However, there is at present no other set of potentials available.

To improve the statistical relevance of the resulting data on irradiation-induced damage, which results essentially from a stochastic process, every cascade was repeated about 10 times, with randomly varied incidence angle for the PKA. In all cases the resulting interstitial cluster size distribution peaks at about 4 interstitials. When interstitial He is present, the mean cluster size is also 4, but the density of the clusters is higher than in pure Fe. The ratio of He atoms to Fe atoms, i.e. self-interstitial atoms (SIAs), in the interstitial clusters peaks at about 1. This indicates that interstitial He promotes the formation of mixed He/SIA clusters. The case of substitutional He is being analyzed.

2.4.3   *Development and characterisation of nanocrystalline materials for fusion applications*

This work is carried out as an Underlying Technology Task.

Polycrystalline W plates with a purity of 99.95wt.% were provided by Goodfellow Cambridge Limited. This material is composed of well-developed equiaxed grains of about 1μm in size, which contain a low density of dislocations.

Discs with a diameter of 8mm and a thickness of 0.5mm were cut out by spark erosion from the as-received W plates. The discs were sent to the Institute of Physics of Advanced Materials at the Ufa State Aviation Technical University, Russia. There, the W discs were submitted to severe plastic deformation by performing high-pressure torsion (SPD-HPT) to obtain a nanostructured texture. A pressure of 6GPa was applied and the upper anvil was rotated five times by 360° during the compression. The deformed discs exhibit a strongly textured, inhomogeneous microstructure with grain sizes between 40 and 100nm. There is a strong gradient in the grain size from the centre to the edge of the SPD-HPT discs, the smaller grains appearing at the edge of the discs.

Specimens for transmission electron microscopy (TEM) were prepared from the as-received W plates by electrolytical polishing. They were bombarded by 6keV Ar ions at room temperature in a Fischione ion mill to induce radiation damage. The specimens were then heated in-situ in a double tilt Gatan specimen holder in a JEOL2010 transmission electron microscope, from room temperature to 1025°C. Figure 2.4.3 shows the resulting evolution of the microstructure with temperature as observed in TEM. The diffraction condition was set to g={011}, close to a zone axis of the <100> type, at 200kV. The double tilt holder allowed us to preserve the diffraction condition as the specimen started to bend as a result of thermal expansion upon heating. The general microstructure is stable. Particular attention was paid to the nanometric grains and here was no observable grain growth, or shrinking, or grain boundary changes. At high magnification the radiation-induced damage appears to be stable up to 1000°C. At 1025°C the size of a dislocation loop increased. This is a single event, as all other dislocation loops remained stable. Polycrystalline, and possibly nanocrystalline, pure W appears very promising as high-temperature radiation resistant material.
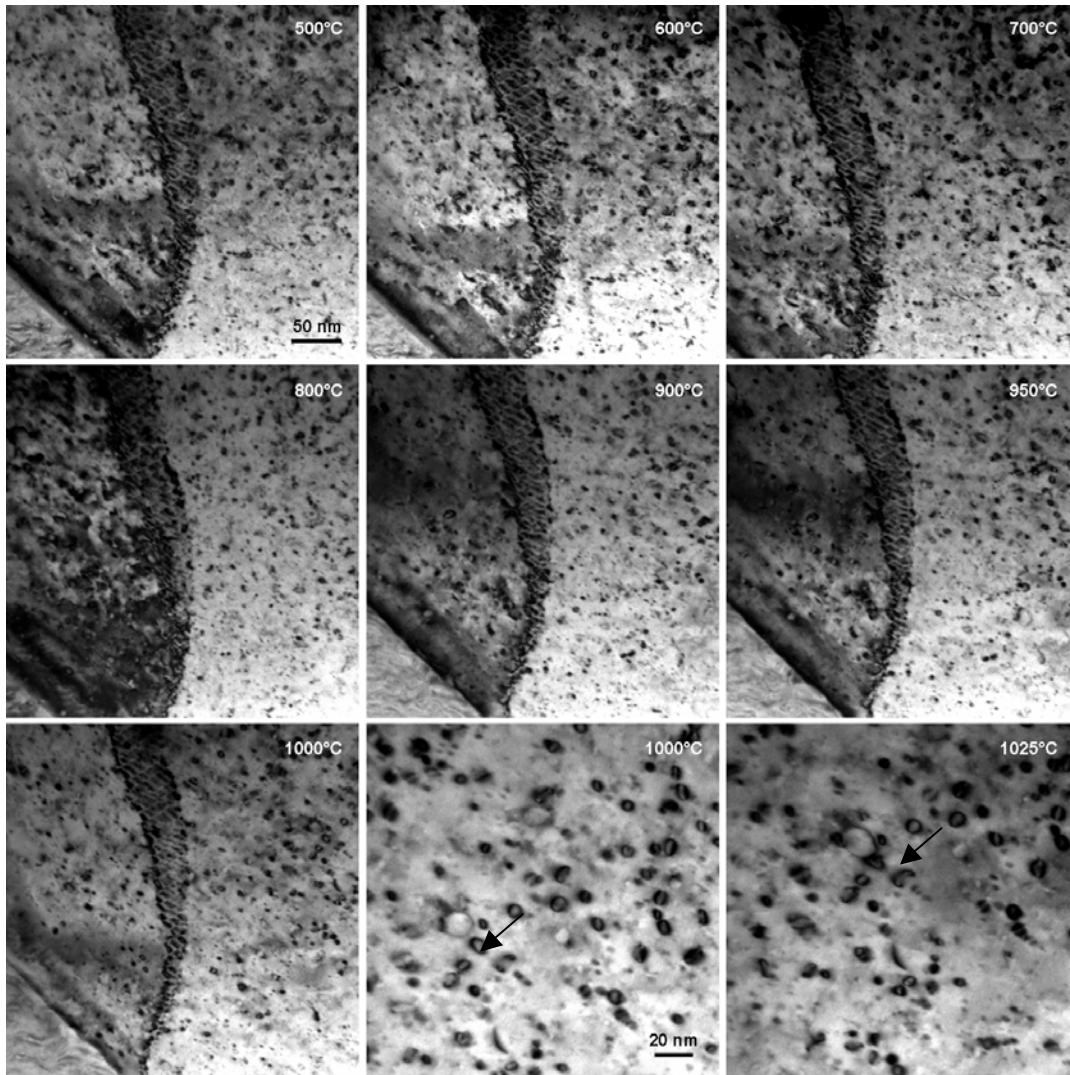
Fig. 2.4.3 *TEM micrograph series of an in situ anneal of pure W implanted with 6keV Ar ions at RT. Same scale for all pictures but the last two at the bottom right, which show a magnified view of the microstructure at the highest temperatures. The arrow indicates the single dislocation loop that changed upon heating.*

2.4.4 Supporting research

Small angle neutron scattering analysis of irradiation-induced defects in pure metals and alloys

Nano-scale irradiation-induced defects are believed to contribute significantly to the hardening and/or embrittlement of metallic materials under irradiation, along with the microscopic defects. Transmission electron microscopy (TEM) allows direct observations of defects whose size is larger than about 1nm in weak beam imaging but other techniques have to be used to reveal ultra-fine scale microstructures. It is well established that small angle neutron scattering (SANS) is an effective technique to characterise nano-scale distributions of features in terms of number density, size distribution and chemical composition. Therefore, SANS experiments have been undertaken on specimens of the EUROFER 97 RAFM steel irradiated with 590MeV protons in the PIREX facility at room temperature, 250°C and 350°C to doses of 0.3, 1 and 2dpa.

SANS measurements were carried out at the PSI. Neutron scattered intensities were obtained using a neutron wavelength of 0.5nm and a specimen-detector distance of 2m, which allows measurements over a range of (q) from 0.35 to 2.6nm^{-1}, q being the scattering vector. The measurements were performed in a strong saturating magnetic field perpendicular to the incident neutron beam with the aim of separating nuclear and magnetic contributions to the scattered intensity. Assuming that the irradiation-induced scattered intensity comes from a dilute distribution of a single type of scattering spherical features, it was found that the mean size of the irradiation-induced defects peaks at about 0.6nm, a value well below the TEM resolution limit. The number density of irradiation-induced defects was found to increase with accumulated dose and to decrease with increasing irradiation temperature. Clearly, the nanometer-sized irradiation-induced defects tend to disappear with increasing irradiation temperature by enhanced recombination of point defects and possible coarsening of the clusters.

A variety of nano-sized irradiation-induced defect clusters may contribute to the additional scattered intensity exhibited by the irradiated specimens: these include small, unidentified defect clusters (of vacancy or interstitial type), voids, helium bubbles, small dislocation loops (of vacancy or interstitial type), carbides and/or precipitates. In an attempt to identify the type of defects responsible for the irradiation-induced scattered intensity, values of the ratio (A) of the nuclear plus the magnetic scattering intensity to the nuclear scattering intensity have been calculated, according to:

$$A = \frac{\left.\frac{d\Sigma}{d\Omega}(q)\right|_{n+m}}{\left.\frac{d\Sigma}{d\Omega}(q)\right|_{n}}$$

where $d\Sigma/d\Omega$ is the differential coherent small angle cross-section, which is proportional to the scattered intensity. The mean A value for $\phi=90°$, where ϕ is the angle between the applied magnetic field direction and the projected observation direction onto the plane perpendicular to the neutron beam, was found to be 2.2±0.2. The ratio A clearly increases with the angle ϕ and the accumulated dose, which suggests that the chemical composition of the diffracting features might be dependent on dose.

For comparison, values of the ratio A have been calculated for a number of complex defects, including carbides and helium bubbles (Table 2.4.1). Various complex defects may give rise to an A value of about 2, such as for instance CrHe or Cr_2FeHe_3 complex defect clusters (in red in Table 2.4.1) or a combination of He bubbles and Cr_3C chromium carbides (in blue in Table 2.4.1). To clarify the situation, we plan to perform SANS measurements on specimens of pure Fe irradiated in similar conditions to EUROFER 97 RAFM steel, as no irradiation-induced carbide formation is expected to occur in pure Fe. SANS measurements will also be performed on irradiated specimens of the EUROFER 97 RAFM steel, subsequently annealed at various temperatures, with the aim of investigating the evolution of nano-sized irradiation-induced defects with temperature. Their temperature behaviour should indeed offer additional information on their intrinsic nature. Simulations of the SANS signal for a wide variety of structural defects will be also performed.

Type of nano-sized irradiation-induced defects and defect clusters	Neutron scattering length density ρ $[\times 10^{10} \text{ cm}^{-2}]$	Contrast $\Delta\rho$ $[\times 10^{10} \text{ cm}^{-2}]$	Ratio A
Void	0	7.3234	1.3558
He bubble	0.8261	6.6063	1.4503
CrHe (Cr_3He_3, Cr_4He_4, etc)	2.6525	4.7798	1.8603
Cr_2FeHe_3	3.4334	3.9990	2.2290
Cr_3C	3.7055	3.7268	2.5301
Cr_2HeC	3.5025	3.9298	2.4069
$CrHe_2C$	3.2195	4.2128	2.2924
$(FeHeCrHe)_7C_3$	4.1169	3.3154	2.7880
$(FeHeCr)_7C_3$	4.7021	2.7302	3.6367
FeHe (Fe_3He_3, Fe_4He_4, etc)	5.0350	2.3973	4.4197
$(Fe_4He_4)C$	5.2792	2.1532	5.2393
$(FeHe)_3C$	5.3537	2.0786	5.5489
$(FeHe)_2C$	5.4979	1.9344	6.2522
$(FeCr)_7C_3$	5.7051	1.7272	7.59
Fe_2C	7.7736	-0.3413	169.7656
Fe_3C	7.813	-0.3807	136.639
Fe_8C	7.9171	-0.4847	84.6522
Fe_2HeC	6.3686	1.0637	18.3693
FeHeC	5.8821	1.5502	9.1786

Table 2.4.1   *Calculated values of the ratio A for different complex defects in the EUROFER 97 RAFM steel.*

Fracture mechanics: 2D Finite element simulation of the stress fields at the crack tip; comparison between compact tension specimens and small scale yield condition

Compact tension specimens

Calculations have been performed using the ABAQUS/Standard (6.5) code that uses Newton's method to solve nonlinear equilibrium equations. Since large deformation levels are expected in the region near the crack tip of compact tension (CT) fracture specimens, geometrical nonlinearity is also expected. A finite strain ('large displacements') approach has been implemented to account for this problem.

The loading level has been determined by means of the "J-integral", calculated for different contours in the model. J refers to the energy release rate. Three different Finite Element (FE) models have been considered the only difference between them being the initial crack tip radius: r_0 (model c1), $2\,r_0$ (model c2) and $3\,r_0$ (model c3), respectively. This difference in the initial crack tip radius allowed us to investigate different load levels without excessively deforming the elements in the region of the crack tip.

Plane strain linear elements with reduced integration have been used to model the CT specimens (Fig. 2.4.4). The loading of the model specimen was carried out through a displacement of a rigid body in frictionless contact with the specimen. The loading level has been determined by means of the J-integral, calculated for different contours in the model. The expected path independence of J is found for contours far enough from the crack tip.
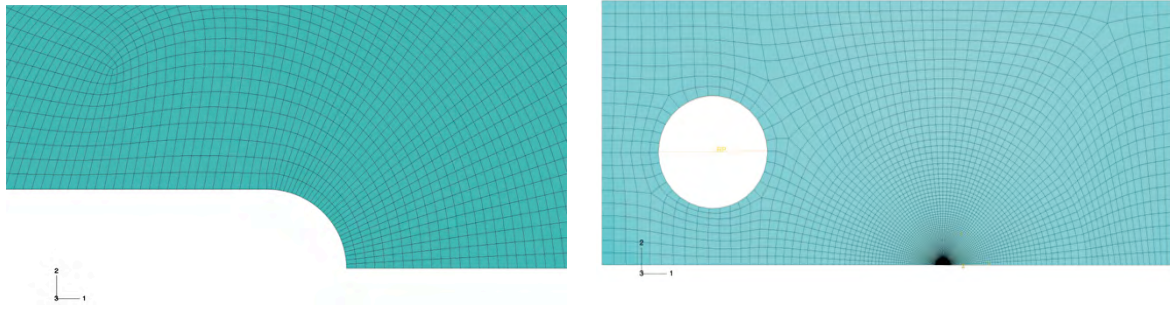
Fig. 2.4.4   *Left: finite element mesh used in the present work. Right: detail of the crack tip in the initial configuration.*

Small scale yielding model

A fully circular model was built, based upon the pure boundary layer model (T–stress=0) containing a small notch radius r_o in the middle (Fig. 2.4.5). The opening of the crack was performed in "mode I" (tensile opening mode) by imposing the standard elastic displacements, Δx and Δy, of the nodes on the outer circular boundary and considering a T-stress equal to zero. Δx and Δy are written as:

$$\Delta x = K \frac{1+\upsilon}{E} \sqrt{R\big/2\pi} \cos\left(\frac{\theta}{2}\right)(3 - 4\upsilon - \cos\theta)$$

$$\Delta y = K \frac{1+\upsilon}{E} \sqrt{R\big/2\pi} \sin\left(\frac{\theta}{2}\right)(3 - 4\upsilon - \cos\theta)$$

where R is the radial distance from the crack tip and θ is the angle between the crack plane and the direction to the node, ν is the Poisson's ratio and E the Young's modulus. Note that the imposed displacements scale with the applied stress intensity factor K. 2D linear reduced integration elements were used. To limit the effect of the initial tip radius on the stress field at the crack tip, we run simulations such that the crack tip opening displacement (d) assures that the ratio d/r_o is larger than 4.
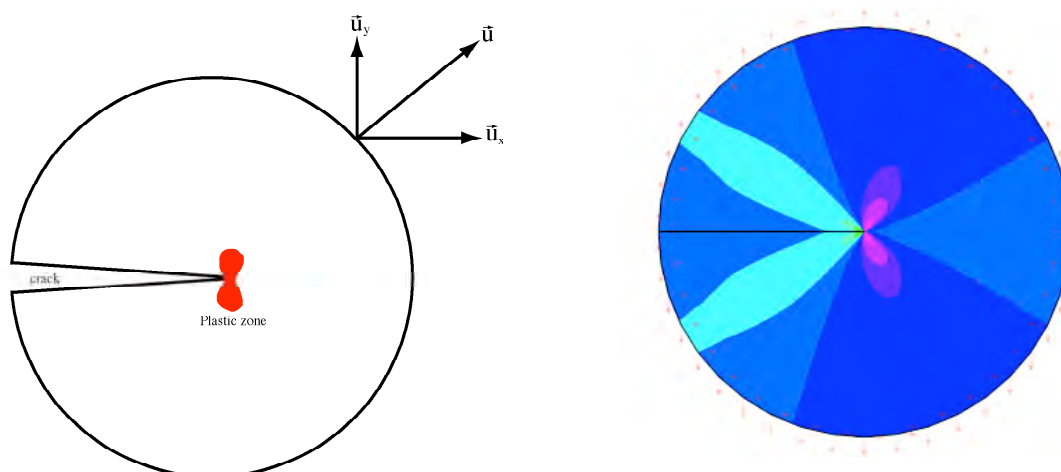
Fig. 2.4.5   *Left: diagram showing the boundary layer problem. Right: FE results for a plane strain calculation. The principal stress levels relate to the different colour contours in the plot.*

Molecular dynamics simulations of structural defects in Fe

Molecular dynamics (MD) simulations of structural defects are being run on single processor workstations, with the MOLDY code, which solves numerically and simultaneously the N Newton equations as a function of time, where N is the number of atoms in the sample. It is based on the embedded atom method that was developed by Daw and Baskes, which, in addition to the interatomic potential, accounts for the electronic configuration around the nucleus of the atoms by a simple functional. The link cell method implanted more recently in the code allows us to compute a larger number of atoms in a given calculation time, as the calculation scales with NLogN as opposed to N^2. MD simulations of various types of structural defects in pure body centred cubic (bcc) Fe have been initiated.

Simulations of transmission electron microscopy (TEM) images of MD-created structural defects are being achieved using an original procedure combining the multislice technique and the Electron Microscopy Software (EMS) code. Simulated TEM images of interstitial dislocation loops in pure Fe, 2nm in diameter, created my MD simulations, are shown in Fig. 2.4.6. These preliminary simulations show that the tools are well established and indicate that the visibility limit of these defects is well below 2nm. Indeed, 2nm-sized defects show TEM image features that can be distinguished the ones from the others. Work is in progress to explore sizes below 2nm. On the other hand, the code based on EMS was modified to simulate the nuclear SANS signal. This technique will be used with confidence to close the gap between MD simulations and experimental SANS measurements.

INTERWELD Integrated Project (IP) of the Fifth European Framework Programme[1]

Irradiation effects on the microstructure, mechanical properties and residual stresses in the heat affected zone of stainless steel welds

The properties of irradiated austenitic stainless steel welds are important for lifetime assessments of reactor internals (e.g. the core shrouds) in light water reactors (LWRs). The effects of neutron irradiation on austenitic stainless steels are the alteration of the microchemistry and the microstructure, and consequently of the mechanical properties. Our study was aimed at extending knowledge of the impact of neutron-irradiation on the heat-affected zone (HAZ) of welded materials, which was influenced by the thermal cycles during welding.

Two types of austenitic stainless steels welds, namely AISI 304 and AISI 347 were produced by FRAMATOME ANP (Germany) using a welding procedure that was a compromise between the conditions applied to real reactor components and the restrictions concerning dimensions and the allowable deformation imposed by our project. The welded test materials were irradiated with neutrons in a High Flux Reactor in Petten (Netherlands) at a temperature of around 573K (approximate operating temperature of LWRs) to 0.3dpa and 1dpa. A welded AISI 304 type austenitic stainless steel was also studied, so-called in-service material, originating from a decommissioned light water reactor in Mol (Belgium), which had operated for 25 years and had accumulated different dose levels to a maximum of 0.3dpa.

For the unirradiated and very low dose irradiated materials, optical microscopy observations showed that the grain size is larger in the HAZ compared with the base material (BM) due to the high temperatures reached during welding. The HAZ extends over around 600μm on both sides of the weld. Transmission electron microscopy (TEM) observations showed that the HAZ contains a higher dislocation

---

[1] Work not belonging to the Association's work programme

density than the BM due to the thermal cycles during welding. The HAZ also contains small body centred cubic (bcc) ferrite islands dispersed in the face centred cubic (fcc) austenite matrix.
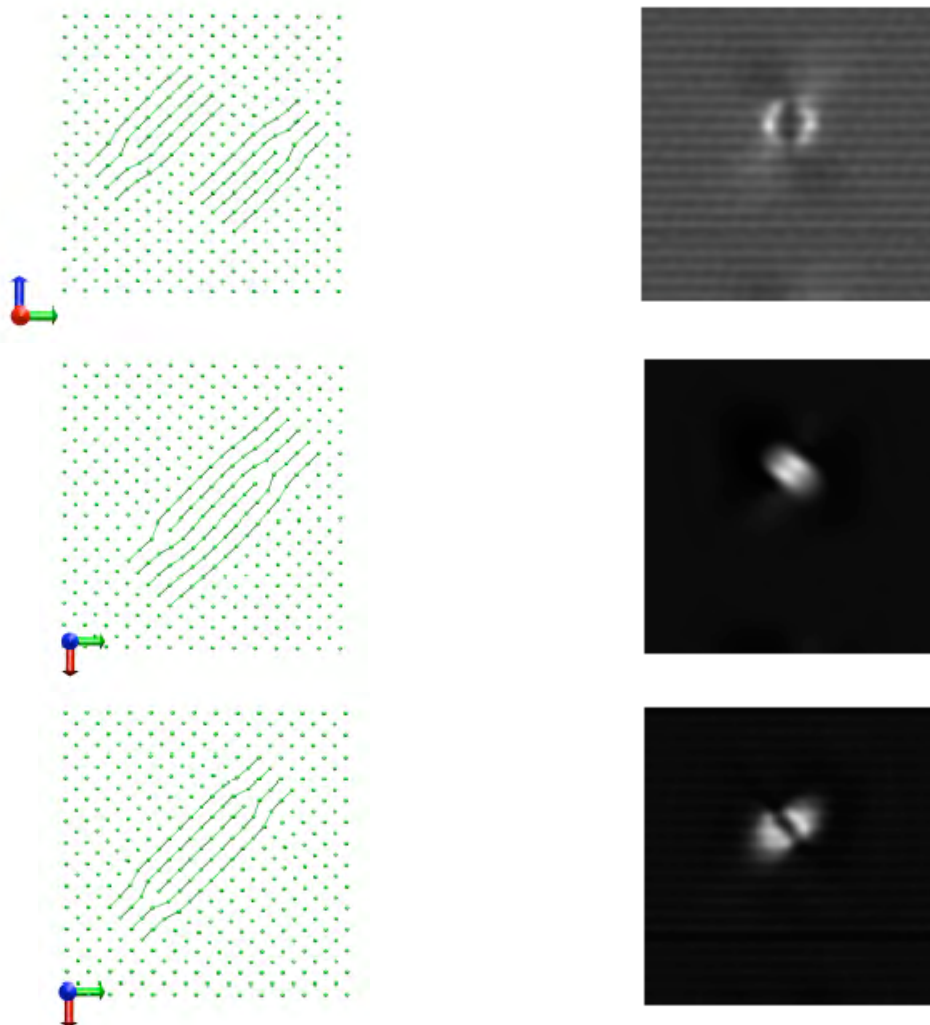
Fig. 2.4.6   *Simulated TEM images of 2nm interstitial dislocation loops in pure bcc Fe, created by MD. Dark field imaging g(1.2g), g=(200), 200keV. Upper part: [001](001) loop; middle part: [111](110) loop; bottom part: [110](110) loop.*

TEM observations of the irradiated materials showed that the austenite matrix contains a large number of irradiation-induced defects. These defects are black dots, too small to be identified in TEM, and Frank loops, which can be either of vacancy or of interstitial type. In the in-service material the irradiation-induced defect density was found to be higher in the HAZ compared with the BM. The higher defect density in the HAZ may be due to the higher grain size in the HAZ compared with the BM, leaving fewer sinks (e.g. grain boundaries) for irradiation-induced defects annihilation. No irradiation-induced defects were observed by TEM in the bcc ferrite interphase, which confirms that the irradiation-induced defects accumulate at a smaller rate in bcc materials than in fcc ones.

Following tensile testing at room temperature the microstructure of unirradiated materials mainly contains twins. Following tensile testing at 573K, the microstructure appears to be composed of dislocation cells. These results are independent of the specimen position from the fusion line. In the case of irradiated materials, the deformation microstructure mainly contains stacking faults and

twins. It seems to present no significant dependence on the material type, the irradiation dose and the test temperature.

Tensile tests performed on all irradiated materials revealed an increase in the yield strength (radiation hardening) and a decrease of the uniform elongation (loss of ductility), at both deformation temperatures. Radiation hardening presents lower values in the HAZ compared with the BM (Fig. 2.4.7 left). The loss of ductility is higher in the HAZ compared with the BM (Fig. 2.4.7 right). Radiation hardening was analysed using the dispersed-obstacle hardening model. The measured radiation hardening cannot be explained solely by the presence of the irradiation-induced defects observed in TEM. Smaller irradiation-induced features (not resolvable in TEM) apparently also contribute to radiation hardening.
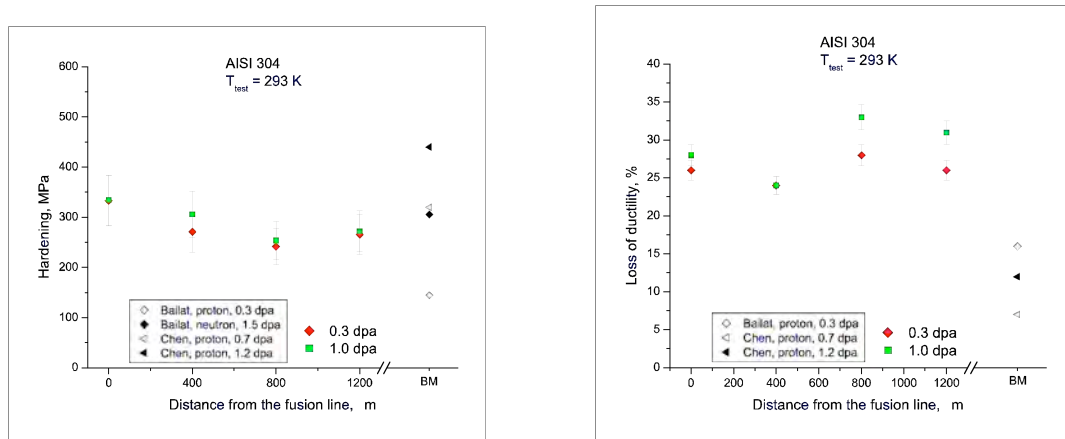
Fig. 2.4.7   *Radiation hardening (left) and loss of ductility (right) versus distance from the fusion line, as measured in tensile tests at RT for the 304 stainless steel irradiated at 0.3 and 1dpa.*

In conclusion, the HAZ presents a resistance to neutron-irradiation that is similar to the BM, in terms of accumulation of irradiation-induced defects (black dots and Frank loops) and changes in mechanical properties (hardening and loss of ductility). The degradation of the mechanical properties of the HAZ clearly results from irradiation and not from welding. It seems that the threshold dose for deterioration of the HAZ, in terms of apparition of cracks or microcracks, was not reached in the present study.

EXTREMAT Integrated Project (IP) of the Sixth European Framework Programme[2]

Activities within the EXTREMAT Project are aimed at:

- Modelling the radiation and radiation effects on pure W;
- Developing reduced activation, radiation resistant, oxide dispersion strengthened (ODS) ferritic steels for structural applications in the future fusion reactors;
- Developing ductile, radiation resistant W-based materials for structural applications in the future fusion reactors.

Modelling of radiation damage and radiation effects on pure W

---

[2] Work not belonging to the Association's work programme

Atomic displacement cascades have been generated with success by molecular dynamics (MD) in pure W using the MOLDY code. For *short-range interaction*, the improved 'universal interatomic potential' has been used. For *long-range interaction*, either of the two available 'Embedded Atom Method (EAM) interatomic potentials' has been used:

- The EAM-type W potential or Finnis-Sinclair potential ;
- The improved EAM-type W potential, with one additional term for distances smaller than 0.27nm.

The short-range and long-range interatomic potentials have been smoothly connected by a function of the type $\exp(c_0+c_1.r+c_2.r^2+c_3.r^3)$. In the case of the Finnis-Sinclair potential, $r_1=0.15$nm and $r_2=0.22$nm. However, the connection is not very smooth in first derivative and can be easily seen as discontinuous in second derivative (Fig. 2.4.8). In the case of the Ackland potential, the fitting distances are chosen as $r_1=0.157$nm and $r_2=0.219$nm to improve smoothness of the first derivative (Fig. 2.4.8).

Both long-range interatomic potentials fail to reproduce the correct energy of defects in body centred cubic (bcc) transitions metals. In the near future, a new potential, developed by UKAEA, should become available.

Development of advanced, radiation-resistant ODS ferritic steels

The aim of this work is to develop reduced activation, radiation-resistant ODS ferritic steels by powder metallurgy techniques. Such materials are expected to be used as structural materials in fusion reactors up to about 800°C. In addition, the numerous interfaces engendered by the presence of oxide particles are expected to act as sinks for the irradiation-induced defects.

Candidate compositions, manufacturing routes, pre- and post-irradiation characterization methods for ODS ferritic steels have been defined. In a first step, the following alloys will be prepared by mechanically alloying basic powders in a ball mill and compacting the milled powders either by hot extrusion with square-shaped die or by high-speed hot extrusion:

- $Fe-14Cr-1.2W-0.3Ti-0.3\%Y_2O_3$
- $Fe-14Cr-2W-0.3Ti-0.3\%Y_2O_3$
- $Fe-12Cr-2W-0.3Ti-0.3\%Y_2O_3$

This activity is complementary to the EFDA Long Term Technology Task TW5-TTMS-006/D4, in terms of compositions and manufacturing routes.
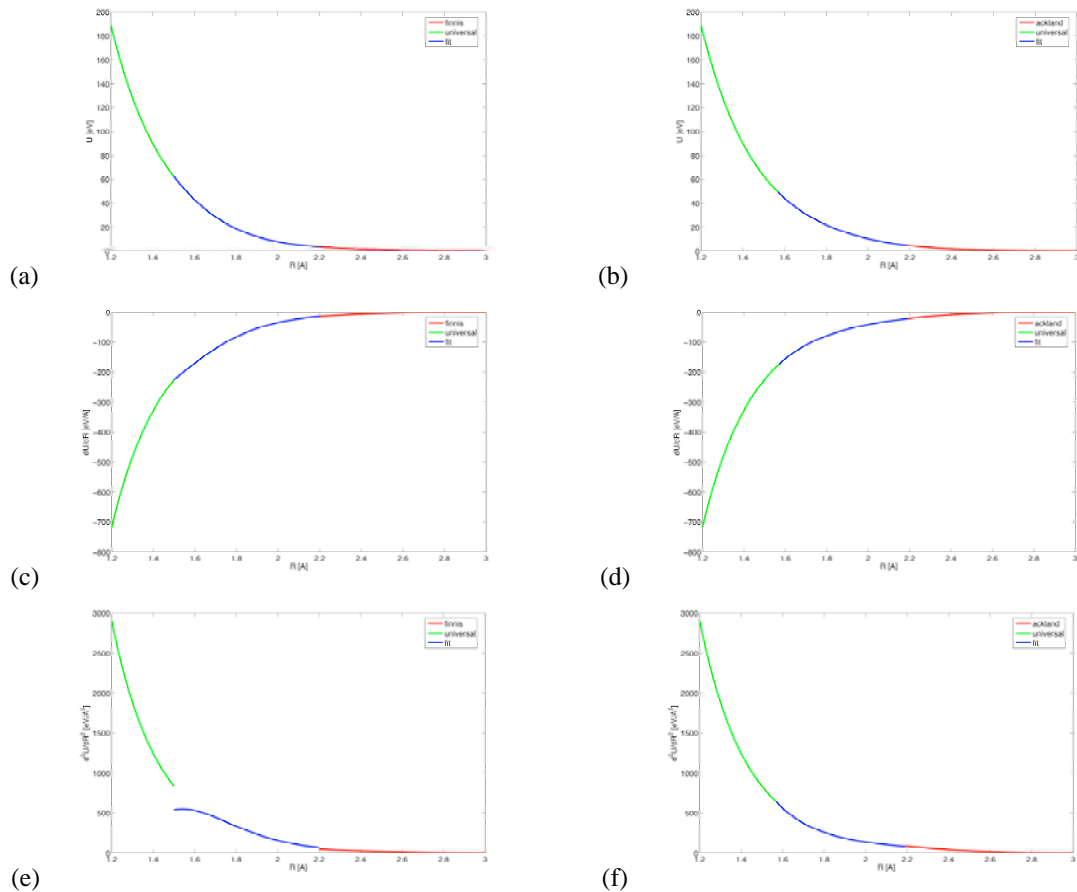
Fig. 2.4.8   *Interatomic potentials for pure W versus distance to an atom centre. (a) Red: Finnis potential; green: universal potential; blue: fit. (b) Red: Ackland potential; green: universal potential; blue: fit. (c), (d) Corresponding first derivatives. (e), (f) Corresponding second derivatives.*

Development of ductile, radiation resistant W-basetd materials

The aim of this work is to develop nanocrystalline W-based materials by severe plastic deformation. Such materials are expected to show improved ductility and resistance to radiation damage. In the latter case, the grain boundaries should act as sinks for the irradiation-induced defects.

Candidate compositions, manufacturing routes, pre- and post-irradiation characterisation methods for W-based materials as have been defined. Three commercial materials have been selected: pure W, W-0.3%Y_2O_3, W-1%La_2O_3. These materials will be mechanically alloyed (in the case of powders) and their microstructure will be made nanocrystalline by high-speed hot extrusion.

PERFECT Integrated Project (IP) of the Sixth European Framework Programme

The aim is to simulate the identification of nanometric irradiation-induced defects in low C alloy steels using transmission electron microscopy (TEM). The focus is given to secondary phase precipitates, that may consist of Cr-rich precipitates or precipitates containing Cr and other alloying elements of the steel. In addition, these precipitates may contain vacancies. The first stage of the study consisted of firstly, establishing the methodology of the simulation and secondly, of establishing the methodology for the creation of virtual samples for the TEM simulations.

Convergent TEM (CTEM) images of the defect clusters have been simulated using the multislice method to obtain their weak beam image at 200kV. The imaging conditions have an influence on the quantification of the actual defect from its image. On the imaging side the parameters of importance are the objective aperture size, the spherical aberration, the beam convergence, and the defocus spread. For the sample itself, its thickness and the depth of the defect cluster are the main parameters which can be changed and the resolution limit that could ideally be achieved can be explored. Limitations are imposed experimentally by sample preparation quality and unwanted structural defects. The technique used is derived from the multislice technique originally developed to simulate high-resolution TEM images. A number of approximations described in the next paragraph were applied to simulate CTEM images.

The CTEM image simulation was performed with the Electron Microscopy Software (EMS) that includes the multislice technique. The sample derived from molecular dynamics (MD) simulations is cut perpendicular to the electron beam direction in slices 0.2nm thick. The sampling in all cases is chosen to be 1024x1024 for slices that have a 10nm side and contain roughly 2000 atoms. The diffraction condition is selected by the beam direction, which is also the cutting direction, so that it allows us to isolate the systematic row defined by the selected diffraction vector. Slices have to be periodic because the multislice method is based on Fourier transforms. In order to comply with this rule the cut direction is chosen to be a crystallographic direction that is close to the originally desired direction. The use of a crystallographic direction for the cut introduces secondary families of diffracting planes that may disturb the image. To reduce the contribution of these secondary systematic rows, relatively high-order crystallographic directions are chosen. One of the advantages of the multislice approach over the classical beam calculation, used for defects defined by their displacement field described by the elasticity of the continuum, is that it allows us to avoid the deformable ion approximation, which may be detrimental to defects as small as those considered here. In addition, this technique allows us to avoid the column approximation generally used in the classical beam calculation. The parameters used to derive the images are close to those of modern microscopes, usually operated at an acceleration voltage of 200kV. For the present CTEM image simulations the beam semi-convergence, the defocus spread and the spherical aberration are set to zero to avoid extraneous effects from parameters that are generally not controlled in this imaging mode. In addition, absorption (both normal and anomalous) is not considered here.

In this first stage, pure Fe samples containing a 2nm cluster of Fe and varying amounts of vacancies have been considered. The aim was to investigate the possibility of quantifying the vacancy content of a cluster based on the magnitude of the intensity of the CTEM contrast. Samples were cubic boxes, $15.1x15.1x15.1nm^3$, or 53^3 lattice cell units, unrelaxed. The selected diffraction condition was a dark field weak beam g(3.02g), with a diffraction vector g=(200), at 200kV. Figure 2.4.9 shows the resulting images, together with a view of the sample in cross-section.

The images are printed with the same greyscale, so the relative intensities can be compared from one image to another. From a content of 40% vacancy, the cluster can be clearly identified; below that, at 20%, there is no visible contrast arising from the cluster. At 20% the residual contrast is from noise in the image. Work is in progress to investigate CTEM images of the same clusters, but relaxed by MD, to highlight any displacement fields.

| Fe & 2nm void | Fe & 20% vacancy | Fe & 40% vacancy | Fe & 60% vacancy | Fe & 80% vacancy |
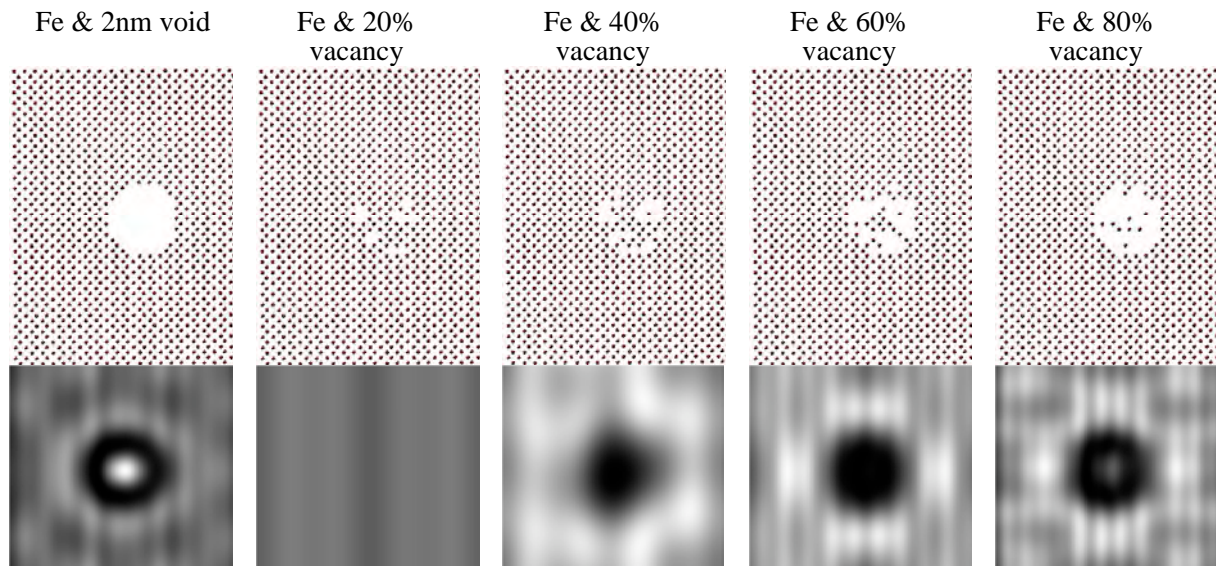
Fig. 2.4.9 *Top: cross-sectional view of the sample containing a precipitate. Bottom: corresponding simulated CTEM image.*

CTI Joint Project[3]

This project is performed in collaboration with the Swiss company ALLPER. ALLPER proposes integrated solutions for the piston, the steel shot sleeve and the lubricants used in the injection of liquid Al and Mg alloys. Erosion, illustrated in Fig. 2.4.10 (left), and deformation of steels used to inject light alloys are problems in the industry of die casting, because of the casting quality and machine down time. Increasing competition in that field, mainly related to the automobile industry, renders subsequent costs prohibitive. To increase lifetime of the shot sleeve steel, an investigation of the causes of this wear was initiated in June 2004.

Material	Surface speed [m/s]	Temperature [°C]	Immersion time [hrs]
GG600	1.0	700	170
GG600	0.1	700	170
QRO90	1.0	700	170

Table 2.4.2 *Matrix of running corrosion tests.*

Three specimens of two different Al-based alloys (GG600, QRO90) were prepared for performing corrosion experiments in a bath of liquid Al alloy using three of the small corrosion devices similar to the ones described under the Task TW2-TTMS-004b deliverable 3 described later. The corrosion parameters are listed in Table 2.4.2 for the three tested specimens. Figure 2.4.10 (right) shows the first specimen of GG600 following immersion for 40 hours in liquid Al at 700°C, using a rotational surface speed of the specimen of 0.5m/s. The wear of small steel specimens will be characterised via loss-of-weight measurements, chemical analyses, scanning and transmission electron microscopy observations of planar and cross-sectioned specimens.

---

[3] Work not belonging to the Association's work programme
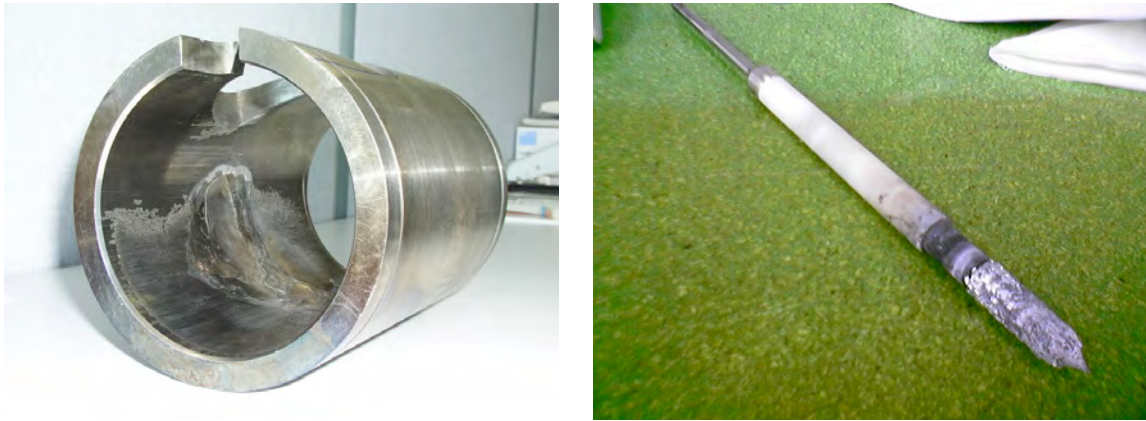
Fig. 2.4.10   *Left: steel shot sleeve used for the injection of liquid Al. Liquid metal is poured from above through the hole. This inner view clearly shows the erosion of the left inner wall at the impact point of the liquid metal. Inner diameter: about 100mm. Right: sample of GG600 after immersion for 40 hours in liquid Al at 700°C, using a 0.5m/s rotational surface speed. Note the macroscopic Al deposit on the surface.*

2.4.5   EFDA Technology Tasks - "long term"

TW1-TTMS-001 deliverable 3 : Proton irradiation of EUROFER 97 up to 1 dpa of plate, for He effect testing

Tensile testing of specimens of the EUROFER 97 RAFM steel, irradiated with high-energy protons in the PIREX facility to various doses ranging between 0.3 and 2dpa and at various temperatures ranging between 50 and 350°C, has been completed. As expected, hardening and loss of ductility have been shown, as a result of proton-irradiations. The magnitude of both phenomena increases with dose and decreases with increasing temperature. Characterisation of the fracture toughness-temperature curve of the EUROFER 97 RAFM steel, using mini-bend bars that have been proton-irradiated in the PIREX facility at 300°C to 1dpa, is in progress at the end of 2005, via 3-point bend testing, following design and construction of adapted specimen holder and load train.

TW1-TTMS-002 deliverable 20 : Tensile and fracture toughness of EUROFER 97, punch testing

These activities were completed at the beginning of 2005. In the last part of this Task, proton-irradiated specimens have been deformed using the small ball punch test (SBPT) technique, developed to extract tensile and fracture properties, to assess the so-called ductile-to-brittle transition temperature and the fracture toughness properties. In Fig. 2.4.11 (left), we show the experimental and calculated SBPT curves obtained for the EUROFER 97 RAFM steel at room temperature. The open circles and squares correspond to the unirradiated and irradiated materials, respectively. In the latter case, the specimens were irradiated with 590MeV protons in the PIREX facility at 423K up to 0.5dpa. The thickness (t) of the specimens is indicated in the Figure. After irradiation a strong increase in the load is observed. The calculated curves in Fig. 2.4.11 (left) were obtained by using the axisymmetric finite element model we developed. Each calculated curve corresponds to a specific constitutive behaviour assigned to the specimen. The constitutive behaviours are plotted in Fig. 2.4.11 (right); the colours of the calculated SBPT curves presented in Fig. 2.4.11 (left) correspond to those in Fig. 2.4.11 (right). Based on these figures,

the effect of the constitutive behaviour on the SBPT curve could be then investigated. The unirradiated SBPT curve is well reproduced by using, for the constitutive behaviour, the experimental tensile true stress–true strain data up to the necking, which occurs at a strain of about 0.05, and by linearly extrapolating the curve at larger strains.
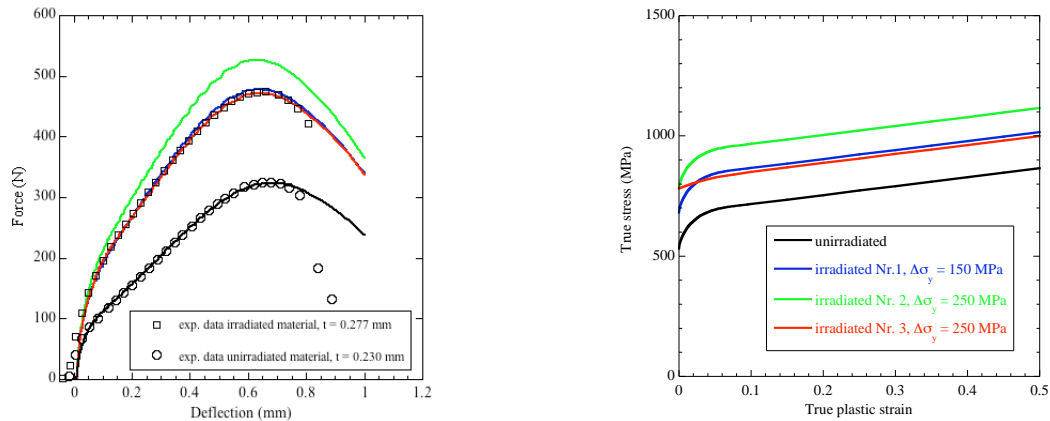
Fig. 2.4.11   *Left: irradiated and unirradiated experimental SBPT force-deflection curves for the EUROFER 97 RAFM steel at 293K. The curves calculated according to the constitutive behaviours shown on the right are overlaid on the data on the left.*

For the SBPT curves obtained for the irradiated specimens, we run three different simulations. Expecting an irradiation-hardening $\Delta\sigma_y$ of the order of 150MPa, we defined three different true stress – true strain curves, plotted in Fig. 2.4.11 (right). Two of these curves (Nr. 1 and Nr. 2) are an upward shift of the unirradiated true strain–true stress curve by respectively 150 and 250MPa. The corresponding calculated SBPT curves show that the constitutive behaviour Nr. 1 closely reproduces the experimental curve. However, a third constitutive behaviour was defined (Nr. 3), with a $\Delta\sigma_y$ of 250MPa, but with a sharp transition at the yield stress followed by a strain-hardening behaviour above a strain of 0.05 identical to the two others constitutive behaviours. In that case, the experimental SBPT curve was also satisfactorily reproduced. This indicates that more than one constitutive behaviour may actually be used to reconstruct a SBPT curve. However, the difference between Nr. 1 and Nr. 3 is only limited to small plastic strains (<0.05) while at larger strains the flow stresses and strain hardening are quite similar. Therefore, the SBPT technique appears to be a more reliable tool to assess the constitutive behaviour at large strains. In order to draw safer conclusions on the irradiation hardening and the strain hardening behaviour at low strains, it would be highly desirable to supplement SBPTs in the future with other mechanical tests for a more accurate assessment of those properties. For example, tensile tests to measure $\Delta\sigma_y$, and compression tests to measure $\sigma(\varepsilon_p)$ over a few percent strain.

TW2-TTMS-004b deliverable 3 : Development and testing of coatings to improve the corrosion resistance vs Pb17Li at T>450°C

Eighteen specimens of the EUROFER 97 RAFM steel were sent to three different European companies for deposition of pure W coatings using three different techniques. Six specimens were coated with a 10μm-thick hard W coating using a galvanic technique (Fig. 2.4.12 left). Six specimens were coated with a 18–22μm–thick W coating using physical vapour deposition (PVD) (Fig. 2.4.12 centre). Six specimens were coated with a 120μm–thick W coating using plasma spraying (Fig. 2.4.12 right). All the coated specimens were received in 2004.

Construction of twelve small corrosion devices were made at the beginning of 2005 to test the resistance of the three types of W coatings as protection barriers for the EUROFER 97 RAFM steel against corrosion in molten Pb-17Li (Fig. 2.4.13). A cylindrical specimen is screwed to the bottom part of a rod that is connected to a small motor. The motor allows the specimen to rotate in a bath of molten Pb-17Li at a speed between 1mm/s and 5m/s and a bath temperature between 300°C and 800°C. Corrosion testing of reference specimens (uncoated EUROFER 97) and W coated specimens was started in summer 2005 at a specimen rotation speed of 1cm/s and a bath temperature of 550°C, for various corrosion times ranging between 500 and 10'000 hours. Corrosion experiments will be completed in 2006.

Fig. 2.4.12   *Optical micrographs of cylindrical specimens of the EUROFER 97 RAFM steel coated with (left) a 10-μm layer of Hardalloy W, (centre) a 20μm-thick layer of W-PVD, (right) a 120μm-thick layer of plasma sprayed W.*
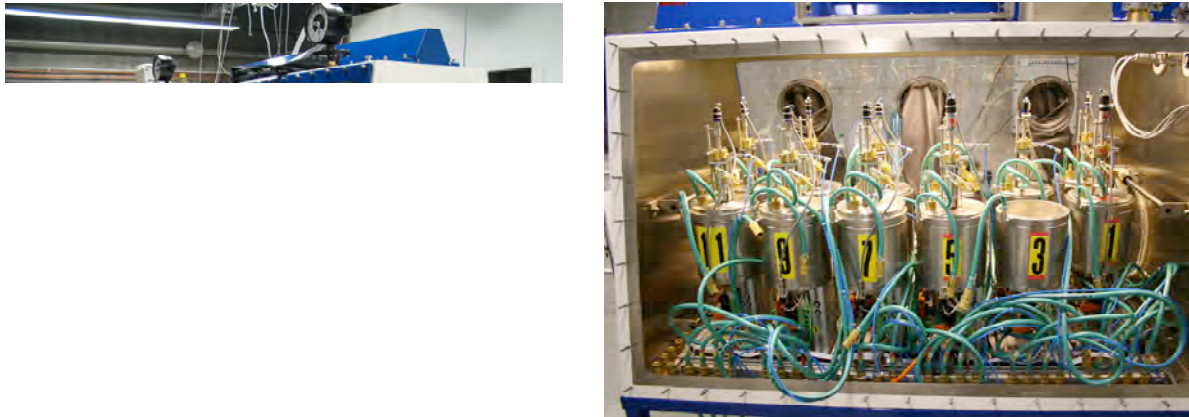
Fig. 2.4.13   *Left: picture of two interconnected glove boxes for the preparation of experiments (melting and cleaning of the Pb-17Li and filling of the Mo containers) and for the corrosion experiments. Right: the corrosion devices.*

TW2-TTMS-005b deliverable 6 : Small-scale fracture mechanics - Modelling of brittle and brittle to ductile transition behaviours using appropriated theories. Formation of rules for transferability to standards and fusion components

Activities were completed at the beginning of 2005. Two capsules of neutron-irradiated specimens of the F82H RAFM steel were tested. The specimen matrix included pre-cracked 0.2T CT and KLST fracture specimens irradiated up to 2.5dpa at 60°C and 300°C, respectively. All the specimens were tested in the lower transition, below 100MPa.m$^{1/2}$, to minimise the loss of constraint effects. Assuming a constant shape of the fracture toughness-temperature curve before and after

irradiation, the irradiation-induced shifts of that curve were determined following the ASTM procedure for the determination of T_o (T_o is the index at $100MPa.m^{1/2}$). The measured shifts are about $0.6\Delta\sigma$, where $\Delta\sigma$ is the radiation hardening measured by tensile tests. This is quite comparable with data obtained for other irradiation conditions on similar ferritic/martensitic steels.

A fracture toughness-temperature reference curve for a 25mm plate of unirradiated EUROFER 97 RAFM steel, was also established using bigger specimens, of the 0.4T CT type, in the lower transition. Such big specimens assure that no constraint loss occurs in the lower transition. The median fracture toughness-temperature curve is significantly steeper than the Master Curve used for RPV (reactor pressure vessel) steels.

TW3-TTMS-005 deliverable 1 : Low cycle fatigue testing of EUROFER 97

This work is aimed at testing the EUROFER 97 RAFM steel in the condition of low cycle fatigue (LCF). The fatigue is strain controlled at room temperature, 150°C, 300°C and 550°C. The tests are run in vacuum using strains of 0.5%, 0.8% and 1.4%. Tests with 500sec hold times are also run, at the same temperatures and using the same imposed strains. The first step of this project consisted of the development of a new LCF mini-specimen, suitable for irradiation in reactors (small size, small mass) and compatible with our testing machine.

The EUROFER 97 RAFM steel exhibits a softening behaviour in LCF tests, as usually observed for ferritic/martensitic steels. The cyclic stress amplitude decreases very rapidly during the first cycles and then saturates to a certain value that then decreases very slowly as the number of cycles is increased. As the crack develops inside the material, a pronounced decrease of the saturation stress indicates failure of the specimen. The number of cycles to failure (N_f) is found by applying a simple graphical method. The intersect of a parallel to the softening stress line placed at a stress 10% lower, defines N_f.

The fatigue endurance measured at room temperature is shown in Fig. 2.4.14 (left). The experimental points may be well fitted by a straight line, probably because the plastic component of the strain is significant, even at low imposed strains. One test was carried out in creep-fatigue, applying a tensile dwell of 500sec. The fatigue life was then reduced by about 25%. This effect is small and not visible in Fig. 2.4.14 (left), drawn in logarithmic scales. The fatigue endurance measured at higher temperatures is presented in Fig. 2.4.14 (right). Again the data points do not deviate strongly from a common line. The influence of the temperature, if any, is not significant.
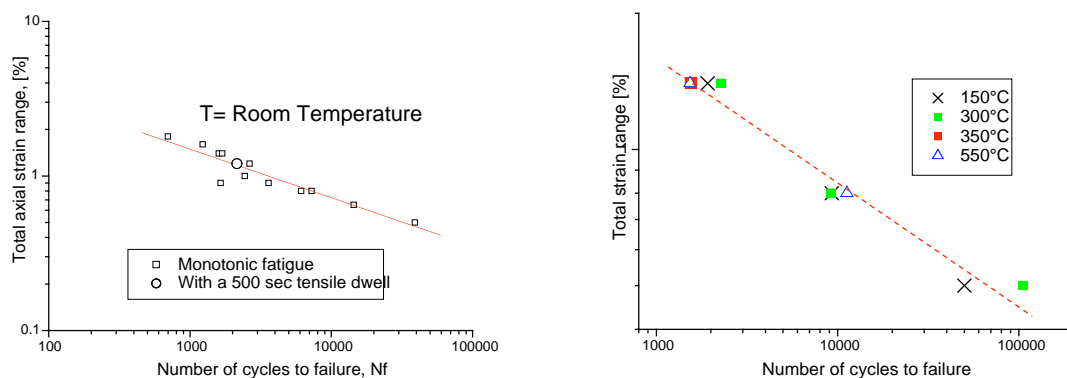
Fig. 2.4.14   *Left: fatigue endurance at RT. Right: fatigue endurance of the EUROFER 97 RAFM steel at various temperatures.*

Figure 2.4.15 shows the influence of relatively long tensile dwells (500sec) on the fatigue life of EUROFER 97 RAFM steel. During the hold times, a strong stress relaxation occurs. In Fig. 2.4.15, the effect of the hold times becomes very strong at 300°C. This indicates that at this elevated temperature, part of the damage also comes from creep. If the number of cycles to failure is then significantly reduced, the total time to rupture is considerably increased, especially for low imposed strains. The high temperature creep-fatigue testing is being pursued and should be completed at the beginning of 2006.
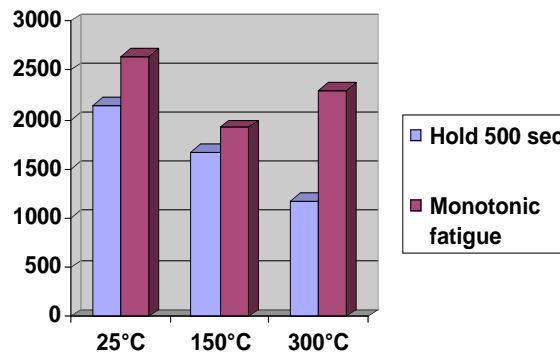
Fig. 2.4.15   *Effect of a tensile dwell of 500sec on the fatigue life of the EUROFER 97 RAFM steel. The imposed strain was 1.4% for the tests at 150°C and 300°C and 1.2% for the test at room temperature.*

TW3-TTMS-005 deliverable 2 : Investigation (tensile and Charpy testing) of PHT and PWHT to improve the design limits and to define the acceptable temperature range

No activity has been undertaken yet since the post-weld heat-treated plates are not available from the EFDA for the time being. This Task will be re-defined in agreement with the EFDA-CSU.

TW3-TTMS-007 deliverable 8 : Irradiation in SINQ

Specimens of the EUROFER 97 RAFM steel, the ODS EUROFER (EUROFER 97 reinforced with 0.3wt.% Y_2O_3 particles) and three Ti-base alloys (Ti-5Zr-2.4Sn, Ti-5Zr and Ti-22Zr), destined to be irradiated in 2004/2005 in the Swiss Spallation Neutron Source (SINQ), have been prepared at the end of 2003. They include mini-Charpy impact specimens ($3x4x27mm^3$), tensile flat specimens (5mm in gauge length x 1mm in width x 0.4mm in thickness), specimens for transmission electron microscopy observations and small ball punch testing (3mm in diameter x 0.25mm in thickness) and specimens for small angle neutron scattering measurements ($8x8x1mm^3$). Specimens were mounted into the irradiation tubes at the beginning of 2004. The irradiation campaign was started at the end of April 2004 for a period of about two years. The irradiation spectrum is a mixture of high-energy protons (original energy: 570MeV) and 30 to 50% of spallation neutrons, depending on the position of the tube inside the target. Mounting was performed so that enough specimens are being irradiated in given irradiation conditions, which will allow us to perform systematic, valuable mechanical tests on irradiated specimens. The doses and irradiation temperatures are expected to range between 5 and 10dpa, and 300 and 600°C, respectively. Irradiation is in progress and will be completed in December 2005.

TW3-TTMS-007 deliverable 10 rev.1 : MD simulations of effects of cavities

Activities were completed at the beginning of 2005. This task was aimed at identifying the irradiation-induced defects that actually contribute to the hardening of Fe and Fe-Cr alloys in presence of irradiation-induced He. For this purpose, particular defect configurations have been created by means of molecular dynamics (MD) simulations. Dislocation loops with a Burgers vector of the <111> or <001> type and lying in {110} or {100} planes, respectively, were created in Fe. In addition, cavities with a radius of 2nm were created, also in Fe. They remained empty or were filled with He. In order to simulate the Fe-He interaction in MD, the interatomic potentials implemented by Morishita have been used. They are based on the interatomic potentials of Ackland, Wilson-Johnson and Beck, which describe the interactions of Fe-Fe, Fe-He and He-He, respectively. The MD code was adapted to the potentials.

A code has been written to generate dislocations for MD simulations with any Burgers vector in a face centred cubic (fcc) or body centred cubic (bcc) lattice. The displacement field is described within the framework of the anisotropic elasticity of the continuum. It can generate any type of dislocation, from edge, mixed to screw dislocations. The procedure was successful as it could reproduce the fact that the edge dislocation core presents a planar dissociation, or core spread, in the {011} glide plane, while the screw dislocation presents a three fold core dissociation in three {011} planes, 120° apart.

The MD code has been adapted to apply a stress and/or strain to the simulation box containing the irradiation-induced defect configurations and one screw or edge dislocation. MD simulation of the interaction between an edge dislocation and a 2nm void in pure Fe showed that the dislocation moves under applied strain rate at a speed of 60m/s. The resulting hardening is about 200MPa. Mobility of the screw dislocations was achieved by applying very high stresses. The hardening was found weakly dependent on temperature, at least for temperatures ranging between 10 and 700K. The size of the simulation box has no influence on the stress value needed to induce mobility, at least for simulation boxes containing between 600'000 and 1'200'000 atoms.

We found that He placed in solid solution does not have any significant impact on the flow stress. The 2nm voids, 2nm He bubbles (with He/vacancy ratios of 1:1 and 2:1), and 2nm $a_o/2$<100>{100} dislocation loops are strong obstacles (500MPa), while $a_o/2$<111>{110} dislocation loops are weak obstacles.

TW4-TTMA-002 deliverable 2 : Development of W-based materials for future divertor application using electrodeposition

Activities were completed at the beginning of 2005. To produce nanostructured W with improved ductility and fracture toughness, due to the reduction in grain size, it was proposed to use electro-deposition. A literature research was made to find the optimum electro-deposition conditions. We found that it is not possible to deposit W alone, but W can be co-deposited with other metals, such as Fe, Ni or Co. We chose to deposit W with Fe, a relatively low activation element from the point of view of irradiation-induced radioactivity. The selected solution consisted of sodium tungstate, ammonia citrate, phosphoric acid, boric acid, 2-butene-4-diol and $FeSO_4$, diluted in water. The W-Fe alloy was deposited electrolytically over a Cu plate, 10mm wide and 0.5mm thick. The deposited alloy was 20μm thick and appeared to be fully dense in optical microscopy. A carefully controlled experiment showed that the deposit is paramagnetic, indicating that it is rich in Fe. X-ray energy dispersive spectrometry showed that the deposit contains 85at.% Fe and 15at.% W. Transmission electron microscopy observations revealed a nanostructured microstructure. Grains are nicely equiaxed and their mean size ranges from 50 to

100nm. The structure is mainly crystalline, of bcc type. A fraction of the volume is amorphous. Its morphology is similar to that of the crystalline phase. The increase in W in the electro-deposition bath favours the amorphous phase formation. The material is extremely stable in the tested temperature range, from room temperature to 650°C. Note that the electrodeposited W-Fe compound presents a much finer microstructure than the one obtained by severe plastic deformation (high pressure torsion).

TW4-TTMS-005 deliverable 4 : Support in development of design rules for structural materials with low ductility

Activities were completed at the beginning of 2005. Tensile tests on the EUROFER 97 RAFM steel were carried out at room temperature to investigate the real deformation range in which the deformation can be considered as homogenous along the specimen gauge length. The uniformity of deformation and the stability of the plastic flow are usually considered up to the maximum load reached during the tensile tests. By loading the specimens up to a load somewhat lower than the maximum load and by keeping the specimens under this load we showed that an instability develops with time as well, which also leads to necking and failure. We therefore concluded that the uniform elongation at maximum load may not be the most appropriate parameter to consider for design rules. The fundamental reasons why the instability load is lower than the maximum load remain to be clarified. Nonetheless, it is believed that they are related to the very low strain hardening of RAFM steels or/and due to relaxation processes of the martensitic structure occurring with time under load.

TW5-TTMS-001/D7 : Assessment of irradiations performed on EUROFER97

We have analyzed the available fracture toughness data on the EUROFER 97 RAFM steel. Rensman et al. have developed a database for compact tension (CT) specimens in the L-T orientation from a 25mm-thick plate and from a 14mm-thick plate of EUROFER 97. Their dataset is shown in Fig. 2.4.16 (left) along with our own dataset obtained from a 25mm-thick plate. In the case of the 25mm-thick plate results, Rensman's data are completely consistent with our results. However, the data obtained from the 14mm-thick plate show a clear difference from the trend drawn for the 25mm-thick plate. Even though the number of results from the 14mm plate is quite limited, the data suggest that this plate may be slightly tougher than the 25mm plate.

In order to compare the fracture properties of the EUROFER 97 RAFM steel with those of the F82H RAFM steel, we carried out our own analysis of the existing fracture toughness database on RAFM steels. To avoid geometry effects, we have considered only data obtained with CT specimens and for different sources. All the data assembled are plotted in Fig. 2.4.16 (right).

Two major observations can be made: i) the amplitude of the scatter is larger for F82H but ii) the lower bound of both RAFM steels seems to be the same. It must be emphasized that even though clear differences in the cleavage toughness in the transition of these two similar RAFM steels are established, their origin, which unambiguously lies in differences in their respective microstructure, is not understood and has not been investigated yet through fundamental comparative studies and modelling.
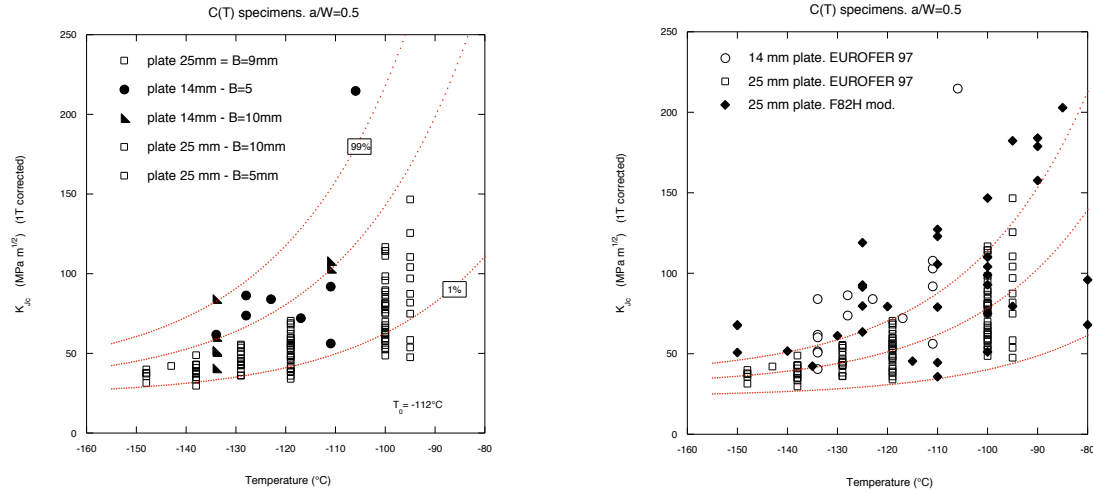
Fig. 2.4.16 *Left: analysis of the available data on the EUROFER 97 RAFM steel. Right: comparison between the F82H and EUROFER 97 data.*

TW5-TTMS-005/D2 : SSTT: Model the brittle transition region - continuation of TW2-TTMS-005b/D6

Analysis of the data obtained under Task TW5-TTMS-005/D11 has been initiated. The scatter in the fracture toughness data, obtained with 0.4T CT specimens of the EUROFER 97 RAFM steel, has been analyzed in the lower transition at three different temperatures, namely -138°C (12 specimens), -119°C (27 specimens) and -100°C (27 specimens). We used the three-parameter Weibull distribution (equation below) to describe the scatter in the fracture toughness values at a given temperature.

$$P_f(K_{Jc}) = 1 - \exp\left[-\left(\frac{K_{Jc} - K_{min}}{K_0 - K_{min}}\right)^m\right]$$

The parameter m is known as the Weibull slope, K_o is the scale parameter and K_{min} is the location parameter. Note that the value of 4 for the Weibull slope arises from the observation that the stress volume $V(\sigma^*)$, the volume encompassing a critical stress σ^*, scales with K_{Jc}^4. In addition, the existence of a threshold in toughness, K_{min}, is the consequence of a mathematical derivation that involves the sequence of two successful mechanisms, namely crack initiation and crack propagation. As we used well-constrained specimens we assumed that the Weibull slope value is adequate and fitted only K_o and K_{min} to our data. In Fig. 2.4.17, we show two examples of failure probability diagram at -119°C where, on the left, two parameters (K_o and K_{min}) have been fitted and, on the right, only K_o has been fitted by taking the usual value for K_{min} equal to $20MPa.m^{1/2}$.

Even if, in the example of Fig. 2.4.17 (left), K_{min} fitted is slightly smaller than $20MPa.m^{1/2}$, no systematic variation of the fitted K_{min} parameter with temperature was found. This indicates that the standard Weibull expression with m=4 and $K_{min}=20MPa.m^{1/2}$ provides an adequate description of the scatter in the lower transition of the fracture toughness-temperature of the EUROFER 97 RAFM steel. Note that a real experimental validation of this point would require much more experimental data to assess the values of the three parameters of the distribution function with high confidence.
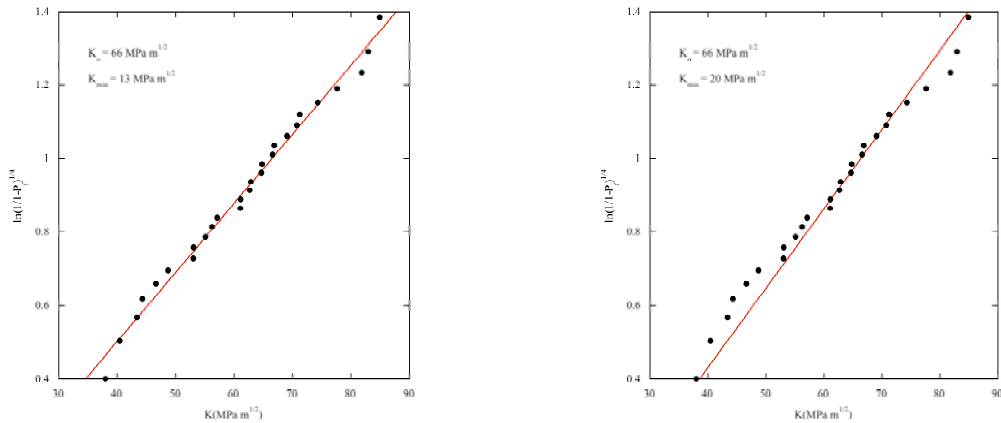
Fig. 2.4.17   *Failure probability diagram at T=-119°C, EUROFER 97 RAFM steel. Left: two parameters fit, K_o and K_{min}, with m=4. Right: one parameter fit, K_o, K_{min}=20, m=4.*

TW5-TTMS-005/D10 : Support in development of design rules for structural materials with low ductility

We started with the experimental constitutive behaviour of the EUROFER 97 RAFM steel at room temperature, represented by the black curve in Fig. 2.4.18. At this temperature the yield stress is 532MPa. The black curve was taken as the reference curve since it corresponds to the experimental data up to a plastic strain of 0.06, which are linearly extrapolated at larger strains. In this figure, we show how the post-yield behaviours have actually been constructed. Three post-yield behaviours were generated using the same strain-hardening law presented by the experimental curve. To vary the shape of the initial plastic regime, three points have been selected along the reference curve at plastic strains of about 0.01, 0.02 and 0.05. Then, the plastic stress-strain curves $\sigma_{pl}(\varepsilon_{pl})$ were generated by considering the segments of the reference curve at the right hand side of the three points and by finally shifting these segments to the original point (0.0-532MPa). Ultimately, SBPT curve simulations were run, using the $\sigma_{pl}(\varepsilon_{pl})$ curves starting at a yield stress of 532MPa, and also with the yield stresses at 632 and 732MPa (in these cases, the curve was simply shifted in stress by 100 and 200MPa). Therefore, in total twelve SBPT curve calculations were carried out.
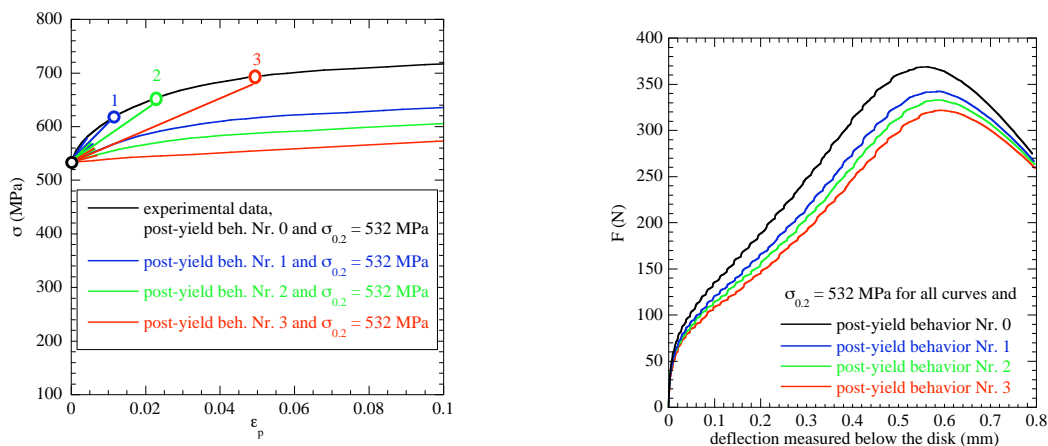
Fig. 2.4.18   *Different constitutive behaviours (left) with the corresponding calculated SBPT curves (right).*

TW5-TTMS-005/D11 : Experiments in support of TW5-TTMS-005/D2

Fracture tests with 0.4T CT fracture specimens of the EUROFER 97 RAFM steel were carried out. Four different temperatures were selected, where a series of specimens were tested to assess the scatter distribution. The testing was done in the lower transition, namely below 100MPa.m$^{1/2}$, in order to ensure a large enough constraint around the crack tip. Bigger fracture specimens, of the 0.8T CT type, are now being prepared to explore the fracture toughness-temperature curve at a higher level while keeping enough constraint at the crack tip. The failure probability is being investigated using the standard Weibull distribution function in order to follow the evolution with temperature of the parameters of the distribution. The data will also serve to calibrate a cleavage model, based upon a local approach. For more details, see also the Task TW5-TTMS-005/D2.

TW5-TTMS-006/D2 : Characterisation of reference EU ODS-EUROFER batch

The objective of this task is to assess the mechanical properties of the reference EU ODS-EUROFER batch produced by the Plansee Company together with Forschungszentrum Karlsruhe (FZK). The mechanical tests will include uniaxial tensile tests at RT, 200, 300, 400, 500, 600, 700, and 800°C and Charpy impact tests at various temperatures between -100 and 300°C to evaluate the ductile-to-brittle transition temperature. In order to save material, it was agreed with other European partners to perform the uniaxial tensile tests on miniaturized cylindrical specimens with a diameter of 2.4mm, while the Charpy impact tests will be performed on KLST specimens (3x4x27mm^3).

Pieces of ODS-EUROFER, cut out from two different products (17mm thick plates and rods, 20mm in diameter), were supplied to us in September 2005. The quantities received will allow the manufacturing of 48 tensile specimens (8x3 specimens per product) and 90 Charpy impact specimens (15x2 specimens from the rod, 15x2 specimens from the plate in the longitudinal direction and 15x2 specimens from the plate in the transverse direction). Subsequently, a call for tender for cutting the specimens by spark erosion has been sent to specialized workshops and fabrication is now in progress.

Prototype tensile test specimens made of EUROFER 97 have been manufactured and tensile tests are being performed at room temperature in a Zwick Z010 testing machine. This work is aimed at verifying the adequacy of a new sample holder, adapted to the miniaturized tensile specimens, and assessing the contribution of the machine elastic deformation displacement to the elongation measured using extensometers.

TW5-TTMS-006/D4 : Nanocomposited ferritic steels for HT application

The aim of this Task is to develop reduced activation, radiation-resistant nanocomposited ferritic steels by powder metallurgy techniques. Such materials are expected to be used as structural materials in fusion reactors up to about 800°C. The numerous interfaces engendered by the presence of oxide particles are expected to act as sinks for the irradiation-induced defects.

Fe-12Cr-2W-(0.1-0.3-0.5)Ti-0.3Y$_2$O$_3$ and Fe-14Cr-2W-(0.1-0.3-0.5)Ti-0.3Y$_2$O$_3$ nanocompo-sited ferritic steels (six compositions) will be prepared by mechanical alloying and hot isostatic pressing (HIPping). Procurement of pure Fe, Cr, W, Ti and Y$_2$O$_3$ powders was completed, and two ball mills for mechanical alloying have been purchased: a high-energy dual mixer/mill of the type SPEX 8000 and a planetary ball mill of the type Retsch PM100. Mechanical alloying of the various powders has been started in summer 2005 in an argon atmosphere. The morphology, structure,

microstructure, chemical composition and mechanical properties of mechanically alloyed powders are being characterized as a function of milling time, milling speed and ball to powder ratio by means of optical and scanning electron microscopy, X-ray diffractometry and Vickers microhardness measurements. Once the optimal mechanical alloying parameters will be clearly defined, the mechanically alloyed powders of different compositions shall be compacted by HIPping in 2006. The microstructure and mechanical behaviour of the various ingots will be subsequently evaluated by performing density measurements, chemical analyses, scanning and transmission electron microscopy observations, Vickers microhardness measurements, tensile and Charpy impact testing.

TW5-TTMS-007/D11 : Ion irradiations for verification analyses on thin foils of Fe-Cr-C model alloys

In order to close the gap between modelling of radiation damage in Fe(Cr,C) model alloys and actual experiments, and to understand the response to irradiation of ferritic and ferritic/martensitic steels, it is proposed to irradiate two Fe-9Cr-C and one Fe-12Cr-C (ferritic and ferritic/martensitic) model alloys with ions and to investigate the resulting microstructure by transmission electron microscopy (TEM).

In a first stage, materials were prepared from high purity casts delivered by Carpenter Inc., USA. Further heat treatments were applied to obtain the desired microstructure, either ferritic or martensitic. The ferritic material is purely ferritic, with equiaxed grains of about 20μm and a low dislocation density. The martensitic material presents a pure martensitic structure, with prior austenite grain boundaries, martensite lathes about 100nm wide and a high dislocation density. Table 2.4.3 summarizes the preparation conditions for the six prepared types of materials.

Samples of Fe-9.02Cr-0.002C (ferritic steel #786), Fe-12.02Cr-0.090C (ferritic/martensitic steel #787) and Fe-9.05Cr-0.098C (ferritic/martensitic steel #788) were prepared in the shape of TEM disks. About 10 disks, 3mm in diameter, were punched from each material. They were mechanically polished down to 0.25mm in thickness. Ion irradiations will be performed at the Hahn Meitner Institute in Berlin in the next few months.

Cast ID	Material	Ferritic - heat treatment	Martensitic - heat treatment
#785	Fe-12Cr	1h@950°C+24h@800°C	
#786	Fe-9Cr	1h@950°C+24h@800°C	
#787	Fe-12Cr-0.1C	1h@940°C+1h@760°C	1h@940°C+WQ
#788	Fe-9Cr-0.1C	1h@940°C+1h@760°C	1h@940°C+WQ

Table 2.4.3   *Matrix of the ferritic and martensitic model alloys. WQ: water quench.*

TW5-TTMS-007/D15 : Dislocation-defect interaction and the evolution of the deformed microstructure in Fe (development of dislocation dynamics methods)

In irradiated ferritic/martensitic steels, irradiation-induced defects like dislocation loops and/or cavities, such as voids or helium bubbles, are believed to lead to substantial hardening and loss of ductility below 400°C. The amplitude of these effects and the underlying mechanisms at the mesoscale (μm) are not clear. This work is aimed at simulating these effects by numerical simulations. Discrete dislocation dynamics (DDD) simulations of the plasticity of Fe and Fe-Cr samples containing given densities of irradiation-induced defects (dislocation loops, voids, helium bubbles) at temperatures between room temperature and 400°C are being

set up and, in a second stage in 2006, they will be performed to quantify the hardening and embrittlement effects and to identify the underlying mechanisms.

In this work the microMegas code from LEM-ONERA is being used to apply the Discrete Dislocation Dynamics model for simulating and visualising dislocation-based plastic deformation in crystals, based on the so-called lattice model. The microMegas code is written in Fortran90 and was delivered under the GNU license. It was implemented in our cluster of G5 Macintosh computers.

In a first step, the irradiation-induced defects have been simulated by means of a population of locked, immobile, short dislocation segments. Figure 2.4.19 (left) shows four such defects in pure Fe, at which one dislocation is pinned. In Fig. 2.4.19 (right), the Fe specimen contains high densities of dislocations and irradiation-induced defects.
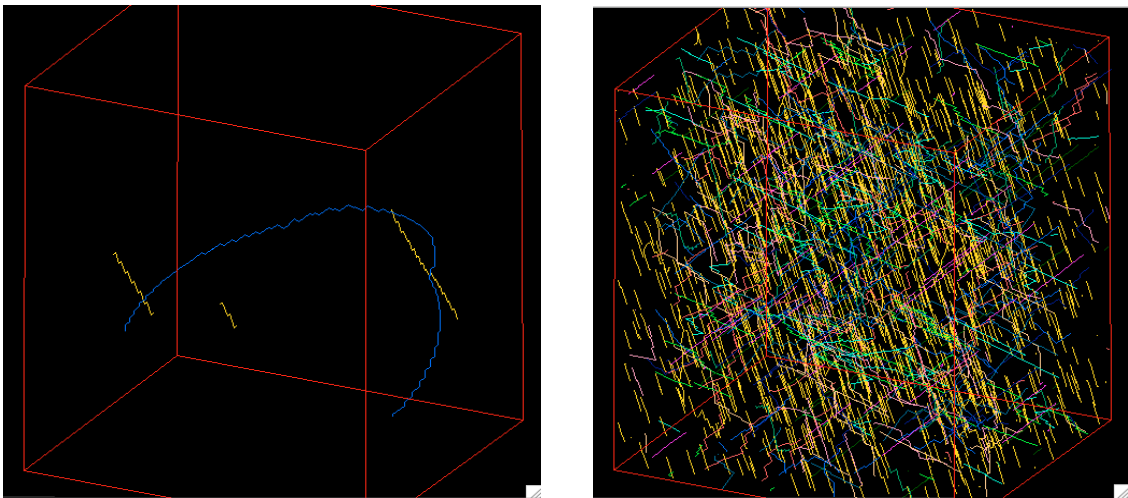
Fig. 2.4.19   *Left: Fe sample containing four defects (yellow) and one pinned dislocation (blue). Right: Fe sample containing a dislocation density of $10^{12}m^{-2}$, defects in yellow.*

Preliminary results of this approach, applied to low strains, showed that the stress-strain curves exhibit a yield drop followed by serrations. It has also been observed that in the presence of obstacles in the matrix, deformation occurs by junction formation and cross-slip events at the onset of deformation and then by increase in the dislocation density as a result from dislocation forest hardening. The next step will consist of implementing defects that are closer to a proper description of real irradiation-induced defects.

TW5-TTMS-007/D18 : Molecular dynamics calculation of the temperature dependence of the dislocation-defect interaction in Fe

Irradiation of ferritic/martensitic steels is known to lead to significant hardening. This work is aimed at pursuing the assessment of the strength of the irradiation-induced defects as obstacles to mobile dislocations in pure Fe by molecular dynamics simulations, as a continuation of the Task TW3-TTMS-007 deliverable 10 rev.1.

The effects of temperature on the interaction of an edge dislocation with defects are being assessed and the mobility of screw dislocations is being explored.

The stress needed for an edge dislocation to overcome obstacles is reduced when temperature is increased, illustrated in Fig. 2.4.20 for the case of a 2nm void. Moreover, the strain needed to overcome the obstacle is reduced when the temperature is increased. It decreases more rapidly than the decrease in stress. Work is continued for the case of a screw dislocation.
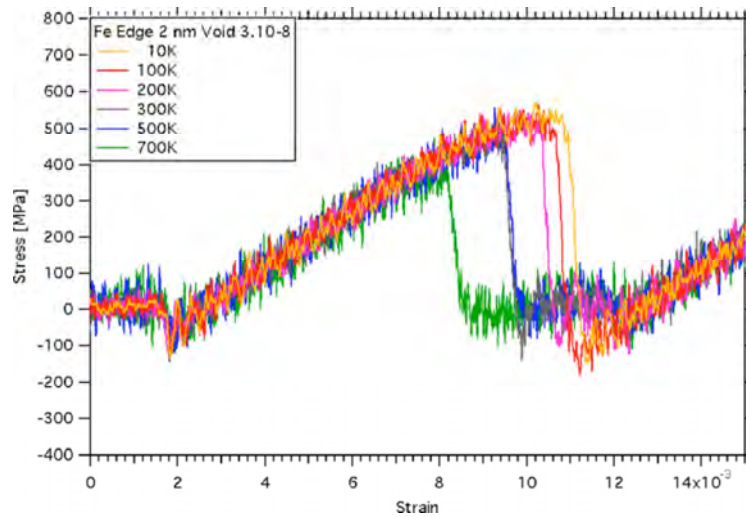
Fig. 2.4.20   *Stress-strain response of an Fe sample containing a 2nm void and one edge dislocation. The sample was deformed by applying a constant strain rate.*

TW5-TTMS-007/D24 : Definition of a programme for verification and validation of the tools developed using multi-ion beam sources

Activities were completed at the beginning of 2005. This work was aimed at preparing a detailed scientific programme of ion implantation of ferritic/martensitic materials, in collaboration with a number of European partners, in view of validating the European effort of modelling radiation damage and radiation damage effects on fusion materials. A draft document, including the contributions from the various implied European partners, was sent to EFDA containing a literature survey of past and on-going experiments of ion implantation of ferritic/martensitic steels. The characteristics of ion implantations and the main obtained results are described. It also contains some advice on the potential use of the French facility JANNUS for investigating the resistance to radiation of fusion materials as a function of irradiation temperature, accumulated damage and damage rate.
Fifteen tasks have been defined, in relation to the EFDA Long Term Technology Programme. These tasks are distributed over four main topics:

- Point defects: configuration, migration, clustering
- Kinetic pathway of the microstructure to high dose and He & H contents
- Phase stability under irradiation
- Mechanical properties

The tasks are time scaled over three years, from 2006 to 2008. In terms of manpower they correspond to 13.5, 17.5 and 15ppy for 2006, 2007 and 2008, respectively, which amounts to a total of 46ppy for the whole programme.

2.4.6   EFDA Technology Tasks - Next Step

TW4-TVM-CUSSPIT : Testing of irradiated CuCrZr/SS joints produced under different blanket manufacturing conditions

CuCrZr/SS joints, where CuCrZr refers to a precipitation strengthened Cu-based alloy and SS to the 316LN austenitic stainless steel, are part of the current ITER design. Their final applicability in ITER will depend on their mechanical properties before and after neutron irradiation, with respect to those of the base materials.

This project is aimed at investigating the effects of different heat treatments on the mechanical properties (joint strength, fracture toughness) of CuCrZr/SS joints. It will be carried out by three European partners: SCK-CEN (Belgium) is responsible for the neutron irradiations, the joints will be tested by VTT Manufacturing Technology (Finland) and the fracture toughness of the base materials will be measured at the CRPP. The neutron irradiations are in progress. Following an extended cooling phase, three sets of six three-point bend specimens each, irradiated to 0.001, 0.01 and 0.1dpa, respectively, will be transported from SCK-CEN to the CRPP. They will be tested in fracture according to the J1C procedure in 2006/2007.

TW5-TVM-COMADA: Investigation of the effect of creep fatigue interaction on the mechanical performance and lifetime of CuCrZr

The CuCrZr alloy is a candidate heat sink material for the first wall of ITER. Therefore, extensive research was conducted in the past on the fatigue properties of the CuCrZr alloy, under relevant ITER operating conditions. Unfortunately little data exist on its creep-fatigue behaviour, mainly due to the very costly testing involved.

The first part of this project has been completed according to the program schedule. It consisted of reviewing the mechanical properties of CuCrZr alloys in fatigue, creep and creep-fatigue testing conditions. A collection of ITER data files, reports, reviews articles and papers on the fatigue and creep-fatigue of the CuCrZr alloy has been delivered to us by EFDA. The existing fatigue data from six different sources are reported in Fig. 2.4.21 (left), and the creep data collected from fourteen different sources are reported in Fig. 2.4.21 (right). In the latter case, the dispersion of the data points is rather large and it is difficult to define a Master Curve that would represent all the data.

The data collected were then analyzed using the time-based approach, as proposed by the French RCC-MR design code, to verify the suitability of the linear damage accumulation rule for lifetime predictions in creep-fatigue tests. This method assumes that fatigue and creep damages are linearly additive and that a lifetime prediction can be made on the basis of the partition of pure creep and pure fatigue lifetimes. It requires knowledge of the relevant fatigue life equations, the cyclic hardening curve and the creep equation. The method can be applied with more accuracy if the particular relaxation curve at the holding point is known, which of course requires the completion of at least one partial creep-fatigue test.

Creep-fatigue data are very scarce. On the basis of the little data available it was found that fatigue and creep damage are actually not linearly additive and that the method needs to be improved before it can be applied to CuCrZr alloys.
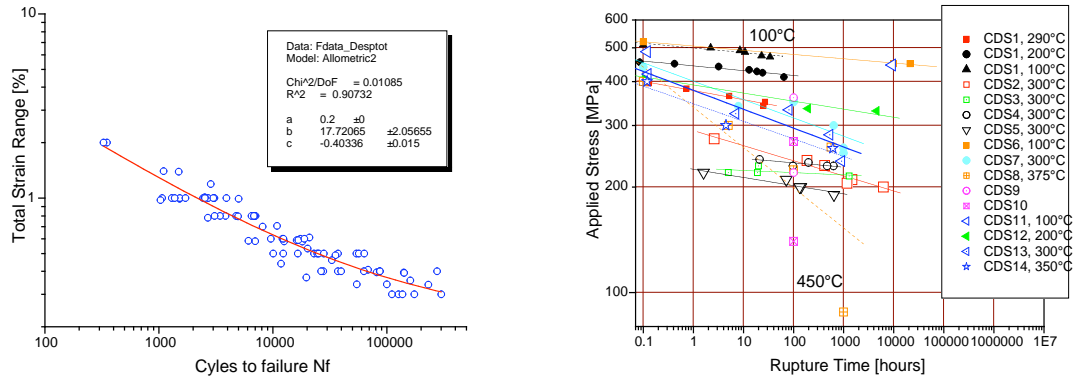
Fig. 2.4.21   *Left: fatigue life curve for the CuCrZr alloy, in the range RT-300°C, as derived from data from six different sources. Right: creep rupture data of the Cu-Cr-Zr alloy, in the range 100-450°C, from fourteen different sources.*

As a result of the first part of this project, an experimental testing program was prepared with the aim of producing the additional data points needed to make reliable predictions for the first wall of ITER. The material to be tested in the second part of this project has been prepared by the CEA-Grenoble and was sent to us by the end of September. The specimens needed have been manufactured, and the creep testing started to be completed in 2006.

2.5   Superconductivity

In 2005, the activities centred around the improvement of the ITER conductors. Individual "advanced Nb_3Sn strands" and a sub-size CICC made of them have been tested with positive results. Full size Nb_3Sn conductors have been heat treated. Investigations of cable layout variations are carried out with sub-size CICC made with different cable patterns. The impact of cycling load on ac loss of NbTi CICC has been experimentally assessed. Thermal-hydraulic campaigns, at room temperature as well as in SULTAN, are carried out on full size NbTi conductors.

The activity on high temperature superconductors (HTS) was expanded, with three tasks about the use of HTS in future fusion reactors. The commissioning of the JORDI test facility was successfully completed and the first results on the resistance distribution on two ITER joints were obtained. An intense design activity for a high field dipole has been carried out in the first half of 2005 in collaboration with EFDA.

2.5.1   EFDA Underlying Technology

Thermal-hydraulic properties of the ITER PFI conductor

The conductor of the ITER Poloidal Field Insert Sample (PFIS) is a NbTi dual channel cable-in-conduit conductor (CICC), in which the coolant flows in parallel in the central channel (i.e. hole, subscript H) and in the annular bundle region (subscript B). Two conductor samples have been investigated at CRPP, one with ($PFIS_W$) and one without subcable/outer cable wraps ($PFIS_{NW}$). After the hydraulic and electric characterization was carried out in 2004, additional investigations were

completed in 2005 for thermal-hydraulic properties at room temperature, as well as in SULTAN.

Pressure drop and friction coefficient

Pressure drop is measured using pressurised water at room temperature. In the first campaign (2004), the central channel was blocked and the friction factor of the bundle region (f_B) was assessed; in the second campaign (2005) the central channel is open. The longitudinal friction factors f_B and f_H are deduced from measurements of pressure drop (Δp) and mass flow rate (dm/dt). The split of mass flow rate between bundle area and central channel is derived by difference of the total mass flow rate $(dm/dt)_B + (dm/dt)_H$, measured in the second campaign, and the mass flow rate in the bundle $(dm/dt)_B$, measured in the first campaign, at the same pressure drop per unit length, $\Delta p/L$.

In the second campaign there are two locations for sensing Δp: (a) at the ends of each sample, as in the first campaign, where the distance between the taps is $L_{\Delta p}=1.944$ m, referred to as the 'outer' Δp location, and (b) along each sample ($L_{\Delta p}=1.0$ m), referred to as the 'inner' Δp location. The $(\Delta p/L)_{in}$ is lower than $(\Delta p/L)_{out}$ by 6-8%. This means that the turbulence due to the flow adjustment at inlet/outlet have a small, but measurable impact on the $\Delta p/L$ results.

The friction factor is deduced from the $\Delta p/L$ results and is plotted vs. Reynolds number in Fig. 2.5.1

$$f = 2\frac{\Delta p}{L}\frac{d_h}{\rho v^2} \qquad\qquad \mathrm{Re} = \frac{v d_h \rho}{\eta}$$

where d_h is the hydraulic diameter, η is the fluid viscosity, ρ the fluid density and v the flow speed. The $f_H(\mathrm{Re})$ is of the order of 0.1. The minimum observable in the $f_H(\mathrm{Re})$ curve is actually buried in the error bar. The friction factor of the spiral of the PFIS conductor is 40-50% lower than predicted by the correlation $f_{Showa}=0.3024\mathrm{Re}^{-0.0707}$, deduced for a similar spiral. The friction factor in the bundle $f_B(\mathrm{Re})$ is lower than the value predicted by the Katheder and ITER correlations as already stated from the first campaign in 2004. In the second campaign, with the hole free, the difference of pressure drop per unit length between $PFIS_W$ and $PFIS_{NW}$ is 5.6% using the 'inner' Δp location and 3.5% using the 'outer' Δp location.
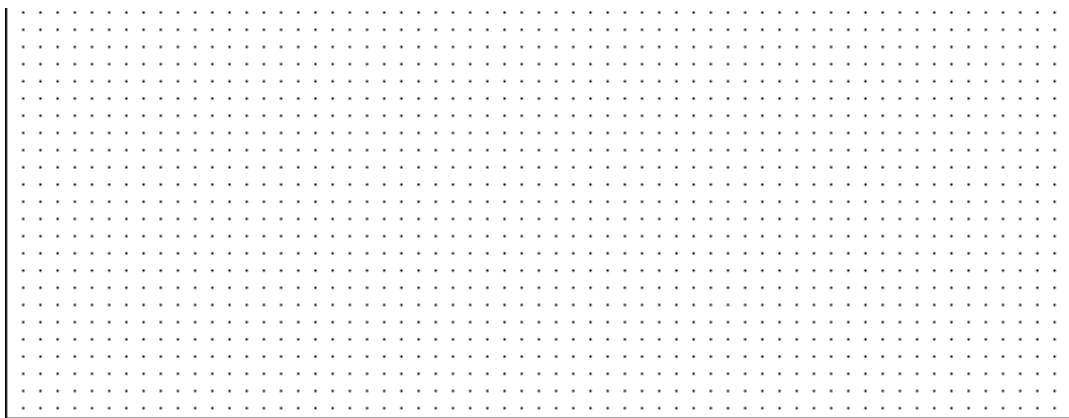
Fig. 2.5.1   *Friction factor in the central channel of the sample $PFIS_{NW}$ vs. Reynolds number, using the 'outer' Δp location (distance 1.944m). The Showa correlation for the hole is also shown for comparison.*

Transverse heat transfer coefficient between bundle and central channel

This activity has focused on a new method for the determination of the equivalent transverse heat transfer coefficient between the helium flow in the cable bundle and the flow in the central channel, h_{BH}, based on the experiments carried out in SULTAN in October 2004. The simplest representation of the helium hydrodynamics of CICC's with central cooling channel is a parallel of two 1-D flows exchanging heat and mass through a perforated wall. The main unknown in the model is the mechanism and amount of heat transfer at the boundary between the two flows. We use the response of the cable temperature sensors (placed on the conductor jacket) to a heat slug to deduce the global heat exchange coefficient.
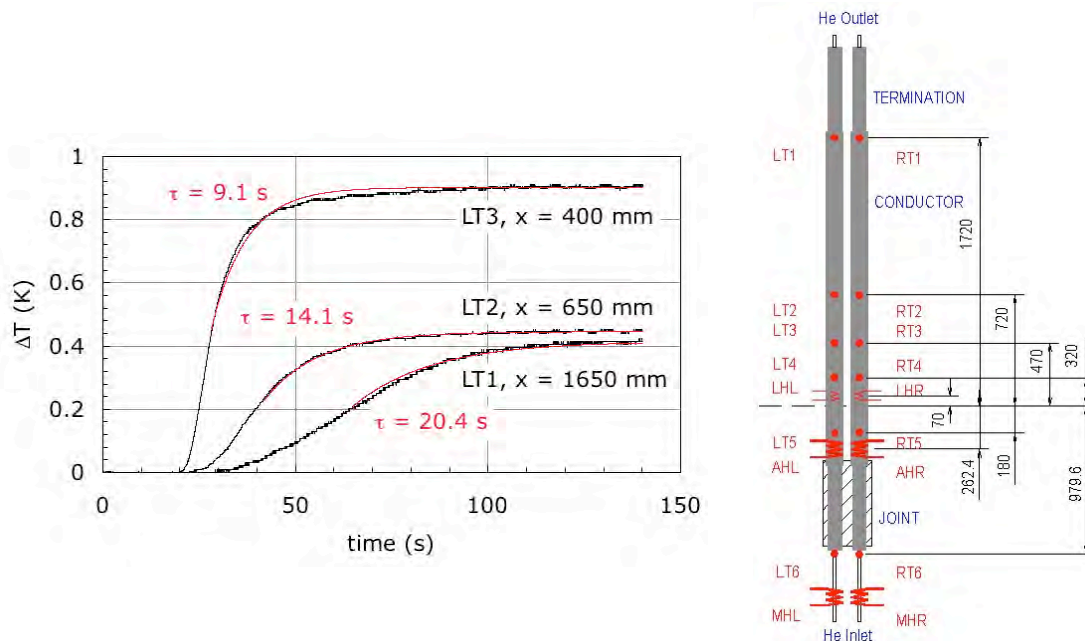
Fig. 2.5.2 *Response of selected temperature sensors in a heat-slug propagation experiment performed on the left leg of the PFIS sample, with the exponential fits of the temperature rise. The location of sensors and heaters along the sample is shown on the right hand side*

The result of a typical heating experiment is reported in Fig. 2.5.2. In the selected run, the heater fired is LHL, inducing a temperature step visible in the response of the downstream thermometers, and in particular LT3 at 400mm, LT2 at 650mm and LT1 at 1650mm from the heater. The front of the heat slug has a delay that increases as a function of the distance of the thermometer from the heater. In addition, the temperature front is smeared. The amplitude of the temperature step is lower at the downstream thermometers. This is most likely a measurement artifact, which, however, does not affect the dynamics of the temperature evolution. The time evolution of the asymptotic part of the front is well fitted with exponential curves. The time constant of the exponential fit increases as the heat pulse moves downstream, as expected by the theory.

The same data fitting procedure is applied to a series of experimental runs performed in different operating conditions, and with different heaters. The time constant follows broadly a square-root dependency on the longitudinal position. The average velocity is known from the measured mass flow, as well as the conductor geometry and the helium density at the measured operating conditions. It is then possible to find the diffusivity k that best fits the set of characteristic times obtained from the analysis of the experimental data. The final step of the analysis is to use the diffusivity k and derive the value of h_{BH}. To perform this calculation we

remark that the velocities in the cable bundle and hole v_B and v_H need to be computed iteratively from the total mass flow and the friction factors of
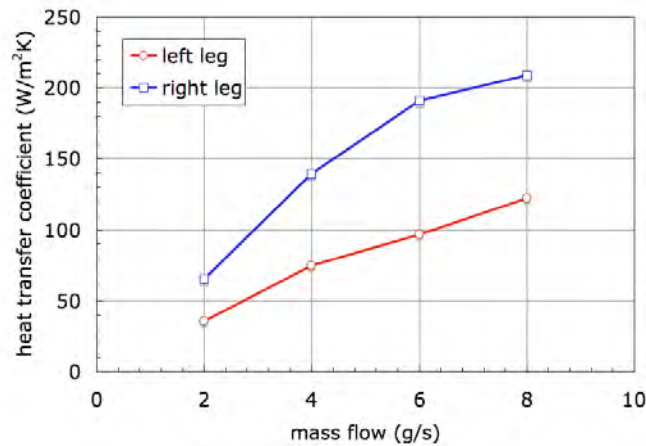
Fig. 2.5.3   *Transverse heat transfer coefficient deduced from the analysis of the heat slug experiments on the PIFS short sample, plotted as a function of the mass flow or the two legs of the sample*

each flow channel. A sufficient approximation is obtained assuming steady state, incompressible flow, and balancing the two flows so that the pressure drop along the two channels is the same. The result is shown in Fig. 2.5.3, and gives the value of the transverse heat transfer in the two legs of the PFIS sample, inferred from a series of about 15 heat pulses in different operating conditions. The results are shown as a function of the mass flow in the sample. The direct comparison of the two legs shows that the conductor in the left leg of the sample has a much smaller transverse heat transfer than the conductor used for the right leg. A plausible explanation for this result is that the subcable wrap decreases the transverse heat and mass flow and gives a lower effective heat transfer.

Test of sub-size Nb$_3$Sn CICC with cable pattern variations

Irreversible degradation, likely due to microscopic filament damage, has been observed in the past years for large size Nb$_3$Sn cable-in-conduit conductors (CICC). The effect of the cabling pattern on the transverse load degradation including cyclic loading has been investigated in two Nb$_3$Sn cable-in-conduit conductor samples with identical parameters (number of strands, void fraction, and jacket material) except the cabling pattern, either braid- or triplet-based. The pattern of strand crossovers affects the transverse load transmission. The dc performance difference has been found to be about 10% in favour of the braided CICC.

The main characteristics of the two Nb$_3$Sn cable-in-conduit conductors are listed in the following table. One of the conductors, "T", is a fully stranded, multi-stage cable, with a triplet being the first cable stage (see Fig. 2.5.4 top). The rope of the other conductor, "B", consists of five twisted braids (transposition pitch of 370mm), each containing 29 strands (see Fig. 2.5.4 bottom). The strand for the two CICC's is a single length (about 3.5km) left over from the Vacuumschmelze production for CSMC. The twist pitch of the strand is 9mm. At 4.2K and 12T, the strand critical current density and the *n* factor reach values of 624A/mm^2 and 33, respectively.

	CICC "T"	CICC "B"
Strand diameter [mm]	0.81	
Cu : non-Cu	1.5	
Cable space diameter [mm]	12.50	12.52
Steel conduit diameter	14.50	14.52
Stainless steel outer wrap	0.055mm × 22.4mm, 45% overlapped	
Number of strands	144	145
Total Cu cross-section (non-twisted) [mm^2]	44.52	44.83
Total non-Cu cross-section (non-twisted) [mm^2]	29.68	29.88
Cable pattern	3 × 3 × 4 × 4	29 (braid) × 5
Twist pitches [mm]	51 / 76 / 136 / 167	167
Estimated cos θ	0.96	0.97
Estimated void fraction [%]	34.47	34.89

A first important feature is a comparison of the dc performance of the two sub-size Nb_3Sn CIC conductors with the values expected from the strand data. Measurements of the critical current of other Nb_3Sn sub-size CIC conductors with a stainless steel conduit as a function of the axial tensile strain suggest that the thermal strain in the filaments may reach values between -0.6 and -0.7%. In the present report a thermal strain of -0.7% is retained for the Nb_3Sn strands in the cable.
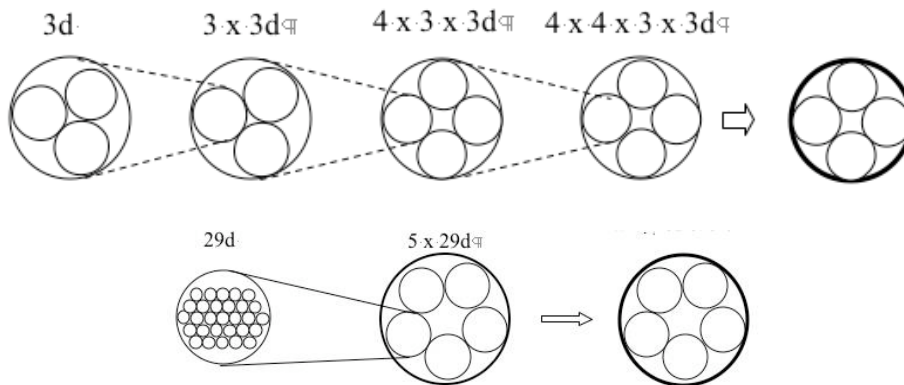
Fig. 2.5.4   *Cable-in-conduit conductors of type "T" (upper) and "B" (lower).*

In Fig. 2.5.5 the critical currents (0.1μV/cm criterion) of the braid- and triplet-based Nb_3Sn cables are compared with the I_c values obtained with the Durham scaling laws for the background, the effective ($B_{eff} = B_b + k_{eff} I$) and the peak magnetic field ($B_{eff} = B_b + k_p I$). The peak field factor (k_p), which is simply determined by the conductor geometry including the field generated by the return conductor, reaches a value of 0.0365T/kA. The effective self-field factor (k_{eff}) can be estimated by means of the uniform current and insulated strand model. The resulting values of k_{eff} are between 1/5 and 1/2 of k_p depending on the supposed n factor of the strands in the cable. In the comparison of strand and cable performances, a k_{eff} value of 0.0122T/kA has been retained, corresponding to n factors of ≈20. The comparison with the Durham scaling law suggests that a reduction in the cable performance occurs even before the cyclic loading. This reduction is slightly more pronounced for the triplet-based conductor.
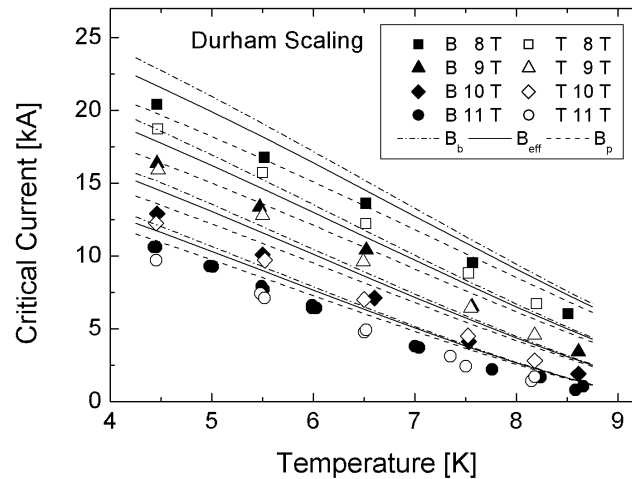
Fig. 2.5.5   *Comparison of the critical currents measured before cyclic loading in the braid- and triplet-based Nb₃Sn cable-in-conduit conductors with the cable critical currents expected from the Durham scaling law (ε = -0.7%) for the background, the effective and the peak magnetic field.*

The cable critical current has been measured before and after 1000 load cycles. The evolution of the critical current and the n values with increasing number of load cycles is illustrated in Fig. 2.5.6. The data have been collected at 11T and 4.5K. In the case of the braid-based conductor, both the critical current and the n index show a pronounced decrease during the first 25 cycles. Nevertheless, I_c and n remain considerably higher than for the triplet-based conductor. The total reduction in I_c caused by more than 1000 load cycles is ≈5%. For the triplet-based conductor, the critical current and the n index after the first cool-down are considerably lower than for the braid-based CICC. Both, I_c and n decrease continuously and do not show a pronounced reduction during the first load cycles.

The reduction of the critical current accompanied by a reduction of the n value suggests that the degradation caused by the load cycles is related to a microscopic damage of the filaments in the strands. The highest n values found before cyclic loading do not exceed a value of 16 even for fields as low as 8T. These values are much smaller than the strand n value of 33 measured at 4.2K and 12T. In addition, the I_c values measured before cyclic loading are well below the expectations from the strand data for ε = -0.7% and an effective self-field factor of 0.0122T/kA. Both results suggest that the first cool-down and the first load cycles cause an irreversible damage of the filaments in the strands of both conductors which continuously increases during the following load cycles. The braid-based conductor seems to be slightly less sensitive to degradation than the triplet-based conductor.

Supposing a thermal strain of -0.7% and an effective self-field factor of 0.0122T/kA, the reduction in the effective superconductor cross-section (degradation) has been estimated by means of the Durham scaling laws. The effective cross-sections obtained for braid- and the triplet-based conductors before cyclic loading are 89.2 and 84.3% of the nominal strand values, respectively. The over 1000 load cycles reduce the superconductor cross-section to 87.8 (braid) and 77% (triplet) of the nominal strand values. In the case of the braid-based conductor, the value of 89.2% of the nominal cross-section obtained before cyclic loading has to be considered as an average over the first 30 load cycles.
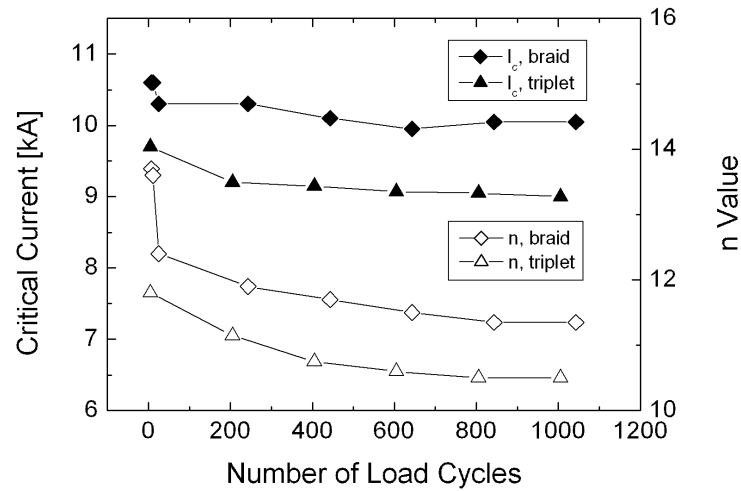
Fig. 2.5.6 *Development of I_c and the n factor with increasing number of cycles for the braid- and the triplet-based conductors.*

The ac loss is measured by gas flow calorimetry. An ac field of amplitude ±0.3 T with frequency in the range of 0.5-6Hz is applied perpendicular to the conductor axis and to the background field of 2T, over a length of 390mm. The loss results, including the hysteresis and coupling currents contribution, is plotted in Fig. 2.5.7 for both conductors before and after the cyclic loading.
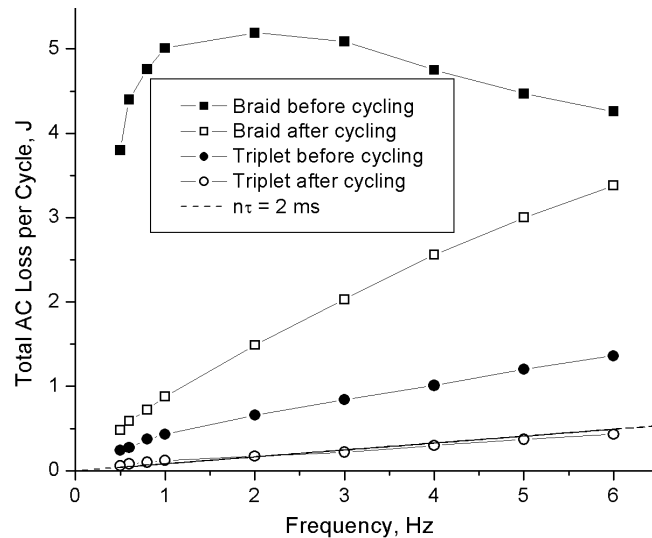
Fig. 2.5.7 *AC loss curves, before and after cyclic loading, for braided and stranded conductor*

As observed in all the Nb_3Sn, Cr plated CICC's, the ac loss is substantially reduced after cyclic loading. The surprising feature in Fig. 2.5.7 is that the braid based conductor has about ten times higher loss compared to the triplet-based conductor although the Nb_3Sn strand, void fraction and twist pitch of the last cable stage are identical. The large difference may be due to the different transposition path, i.e. higher linked area for the inter-strand current loops in the braid, and to the likely lower contact resistance at the crossovers of the mechanically stiffer braid. The loss curves in Fig. 2.5.7 are not linear and a reliable assessment of the coupling loss constant ($n\tau$) is not possible from the initial slope. In the triplet-based conductor the coupling loss is after cyclic loading at the level of the inter-filamentary loss, with

nτ of the order of a few ms. The calculated coupling loss for $n\tau$ = 2ms is also plotted in Fig. *2.5.7* for comparison. From the position of the loss maximum, $n\tau$ is larger than 150ms before cycling in the braid-based conductor.

Design and development of a react-and-wind conductor

The use of Nb_3Sn in large size, high current cable-in-conduit conductors (CICC) is limited by the transverse load damage, see above, proportional to the product B·J·R, where B is the operating field, J is the current density in the cable space and R is the radius of the cable space. In 2003, an experiment carried out at CRPP demonstrated that the transverse load damage is cured by solder filling the cable space, i.e. improving the mechanical support of the cable and restricting the bending of the strands.

Stimulated by this result, a cable design, an option to the CICC, has been developed based on the react-and-wind technique. Contrary to the CICC, the cable is flat, with high aspect ratio and very low void fraction. It is heat-treated at 950K without any structural material, which substantially reduces the thermal strain in the Nb_3Sn filaments. After heat treatment, the cable is filled with a low melting alloy and encased in a steel conduit, also providing an adequate cooling channel for forced flow operation. The superconductor is close to the midline to limit the bending strain down to ±0.1% during the winding of the TF coils, with variable radius, from 2.2m to infinity. The heat treatment should be carried out on a circular drum of 4.5 m diameter to minimise the bending in the D-shaped TF coils.

Nb3Sn Strand
Cu:non-Cu = 0.8
ø = 1.3 mm

First cable stage
Pitch ≈ 50 mm
ø ≈ 3.64 mm

Stainless Steel strip, ≈ 29 x 0.1 mm
Flat cable of 22 first cable stages = 154 strands
Cable pitch ≈ 250 mm
≈ 6.6 x 36 mm, rounded edges, R ≈ 3 mm

One layer of 46 soft, Cr plated, copper wires, ø = 2.1 mm
Twisted in opposite direction to the cable, pitch ≈ 350 mm
≈ 10.6 x 40 mm, rounded edges, R ≈ 4 mm

Total non-Cu = 113.5 mm^2 (non-twisted)
Total Cu = 90.8 + 159.3 = 250.1 mm^2
Void fraction ≈ 8%

Stainless steel sheath, 2 mm thick, folded and welded
Cable space, 11 x 50 mm, R = 4 mm
filled by low melting (160-200 C) alloy ≈ 33 mm^2
5% loaded with PrB6 powder
Cooling channel ≈ 103 mm^2
Outer size 15 x 54 mm, R = 6 mm

Fig. 2.5.8   *Layout of the react-and-wind conductor*

The sketch in Fig. 2.5.8 shows the layout of a conductor to be used in the ITER TF coils with an operating current of about 45kA. The non-Cu cross section is much smaller than in CICC because of the smaller thermal strain degradation and the missing transverse load damage. To limit the ac loss, the strands are Cr plated and the low melting alloy filling the residual voids has high resistivity at low temperature. A short length prototype is being built to demonstrate the potential of this design at full size. The superconducting strand, ordered at Outokumpu, was delivered in October. The cabling parameters have been tuned with trials on copper

"dummy" cables at Brugg AG. Heat treatment, filling and encasing in steel jacket will be completed at CRPP. The test of the prototype is planned for earlyof 2006.

2.5.2   EFDA Technology Tasks

SULTAN Operation (TW5-TMSC-SULT)

The operation of the SULTAN facility was covered during six months in 2005 by a EFDA technology task. The objects of the task were the preparation and test of a sub-size, rectangular Nb_3Sn CICC (pre-prototype for the high field dipole), the cyclic load test up to 10 000 cycles of a NbTi sample and the thermal-hydraulic test, with sophisticated instrumentation, of a full size NbTi sample ("Low Cost Joint Sample").

Test Results of a Small Size CICC with Advanced Nb_3Sn Strands

In the scope of the design activities for a 12.5T dipole magnet, a short length of cable-in-conduit conductor (CICC) with steel jacket was prepared in spring 2005 as a pre-prototype of the high field dipole conductor. The small, rectangular conductor uses "advanced" Nb_3Sn strands for the first time, with J_c=1100A/mm^2 at 12T, 4.2K, also planned in the qualification samples for the ITER conductors. At CRPP, a hairpin sample for SULTAN has been prepared from the short conductor length, heat treated and instrumented. The test program included pressure drop, ac losses and full dc characterisation before and after cyclic loading. The test results indicate that the high performance of the advanced strands is preserved in the small size, steel jacketed CICC.

The observed performance drop in the large Nb_3Sn CICC's of the ITER Model Coil and short samples, likely due to transverse load degradation, motivated the use of "advanced", higher current density Nb_3Sn strands, made available on the market since the production of the KSTAR conductors and the R&D for high field accelerators. The main properties of the Nb_3Sn CICC are listed in the table. A picture is shown in Fig. 2.5.9. The SULTAN sample is hairpin shaped, with the helium inlet in the U-bend. The advanced strand, supplied by Oxford Superconducting Technology (OST) has a non-Cu critical current density of 1100A/mm^2 at 4.2K, 12T and an electric field criterion of 0.1μV/cm.

In the Nb_3Sn conductors tested so far in SULTAN, the cable *n* values were generally found to be much smaller than the strand *n* values. In the conductor, fabricated of the advanced strands, the cable *n* reaches a value as high as 25 at the highest critical currents. The highest cable critical current of 28.15kA corresponds to an average strand I_c of 335A, which is comparable to the strand I_c of 297.5A at 4.2K and 12T. The corresponding strand *n* value is 26. Hence, the cable and strand *n* values are not significantly different, which suggests that the strands in the CICC are not degraded.

Strand diameter	0.81mm
Strand Supplier	OST
Strand Cu : non-Cu	1.0
Cabling pattern	3 × 3 × 3 × 4 (84 Nb$_3$Sn + 24 Cu)
Twist pitch	58 / 95 / 139 / 213mm
Total strand area	56.76mm^2 (cos ϑ = 0.97)
Conductor dimensions	7.7mm × 18.4mm
Jacket thickness	1mm
Void fraction	35% (calculated)

Fig. 2.5.9   *Photo of a short piece of the rectangular cable-in-conduit conductor.*

The comparison of strand and cable performance is based on the use of the Durham scaling relations. Effective self-field factors (k_{eff}) are defined in such a way that $I_c^{cable} \cong N\ I_c^{strand}(B_{eff})$, where N is the number of the Nb$_3$Sn strands, I_c^{cable} the measured cable critical current, $B_{eff}=B_b+k_{eff}\ I_c^{cable}$, and B_b the background field. The effective self-field factors (k_{eff}) are determined by a least squares fit to the measured cable I_c data. Because of the fact that the exact value of the strain experienced by the Nb$_3$Sn filaments in the cable is unknown, the optimum value of k_{eff} has been determined for a range of strain values. In Fig. 2.5.10, the optimum values of k_{eff} and the sums of the squares of the differences of the measured cable critical currents and the I_c values expected from the strand data for B_{eff} are shown. The results are based on the use of the Durham scaling relations and the assumption that the Nb$_3$Sn strands are not degraded. The best agreement of the measured data and the strand data is reached for a strain of –0.625%. The corresponding optimum value of k_{eff} is 0.0109T/kA. Analogously to k_{eff}, a peak field factor (k_p), can be defined, determined only by the conductor geometry. Field calculations, taking into account the field generated by the return conductor, provide a k_p value of 0.0352T/kA.

Another way to compare the strand and cable performance is the assumption of insulated strands and a uniform current distribution among the strands. Due to the twist pitch, the strands cycle in and out of the high field region. Thus, the cable critical current is expected to be between the sums of the strand I_c values for the background and the peak magnetic field. The averaging of the electric field along the strand is based on the assumption that each of the strands is found with the same probability at any position in the rectangular conductor cross-section. Field calculations indicate that the variation of the magnetic field in the direction perpendicular to the background field within the conductor can be well approximated by a linear field gradient. In Fig. 2.5.10, $\Sigma(I_c^{cable} - I_c^{UCD,IS})^2$, obtained for insulated strands and a uniform current distribution at different strains, is also shown. The minimum of this sum is reached for ε=-0.615%, which is in good agreement with the results of the k_{eff} fit.
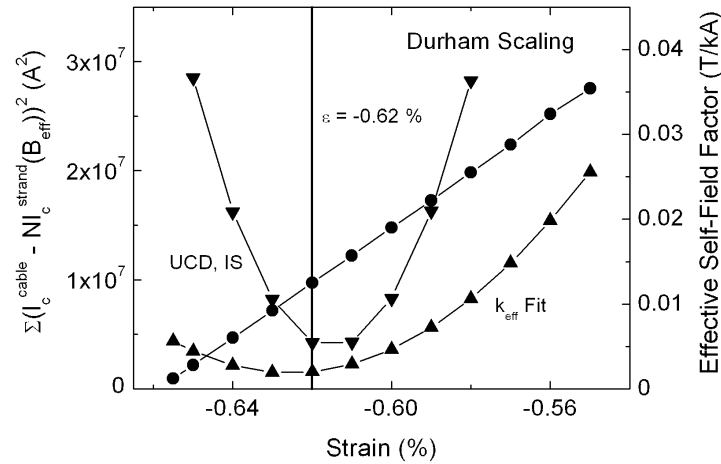
Fig. 2.5.10 *Minimum values of $\Sigma(I_c^{cable}-N\,I_c^{strand}(B_{eff}))^2$ and the corresponding values of the effective self-field factor obtained for different strains. For comparison, $\Sigma(I_c^{cable}-I_c^{UCD,IS})^2$ versus strain is also shown.*

In Fig. 2.5.11, the measured cable critical currents are compared with the critical currents expected for insulated strands with a uniform current distribution ($I_c^{UCD,IS}$) and a strain of -0.62%. Moreover, the values expected for the background ($I_c(B_b)$), the effective ($I_c(B_{eff})$) and the peak field ($I_c(B_p)$) at $\varepsilon=-0.62\%$ are included in Fig. 2.5.11. The measured cable critical currents are between the expectations for the background and the peak field. The cable I_c values are very close to (10 & 11T) or slightly above (8 & 9T) the values expected for a uniform current distribution and insulated strands. A fit based on $k_{eff}=0.0125T/kA$ and $\varepsilon=-0.62\%$ is in excellent agreement with the measured data.
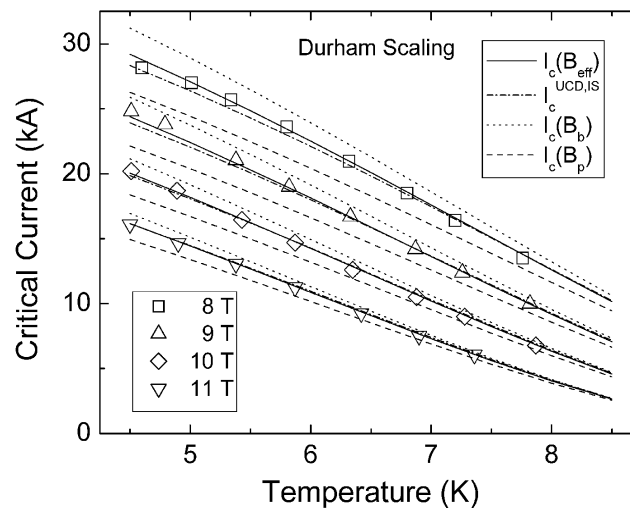
Fig. 2.5.11 *Comparison of the measured cable critical currents with the I_c expected for insulated strands and a uniform current distribution. The sum of the strand critical currents for the background, the peak and the effective magnetic field is indicated ($k_{eff}=0.0125T/kA$, $\varepsilon=-0.62\%$).*

To study the effect of large transverse loads, the conductor has been charged over 1000 times with a current of 22kA in a field of 9T. The resulting peak load reaches 12MPa. The cable critical current and the n values, measured at 11T and 4.5K as a function of the number of load cycles, are shown in Fig. 2.5.12. The data indicate a

significant drop of the n value from ≈ 18 to ≈ 13 within the first 280 cycles. The reduction in the n value suggests that the strands in the cable are slightly degraded. In the region of damaged filaments the current has to flow across the bronze matrix, which is reflected by a lowered n value. On the other hand, the observed reduction of 2.1% in the critical current is rather small.
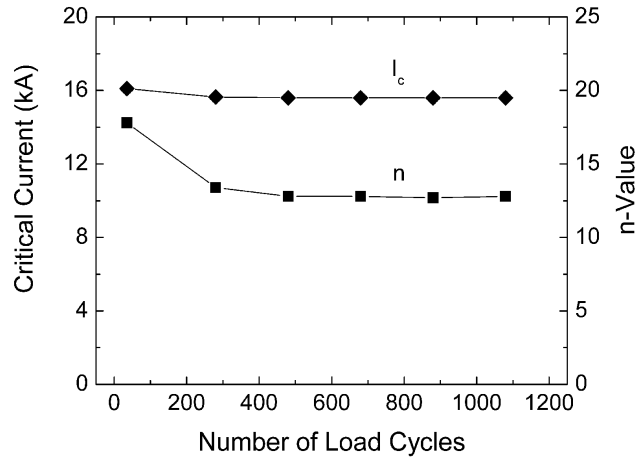
Fig. 2.5.12   *Cable critical current and n value as a function of the number of load cycles.*

The ac loss has been measured before any loading and after more than 1000 load cycles at B_{dc}=2T and B_{ac}=±0.3T. The total loss per cycle normalised to the cable volume, including the Cu strands, is shown in Fig. 2.5.13. The hysteresis loss in the Nb_3Sn filaments reaches $\approx 59mJ/cm^3$ compared to a value of $3.5mJ/cm^3$ found for a sub-size CICC made of bronze route Nb_3Sn strands. The $n\tau$ value from the initial slope of the loss curve is as high as 99ms. After more than 1000 load cycles the $n\tau$ value is reduced to 18ms. The reduction of the $n\tau$ due to the cyclic loading is consistent with former results on Nb_3Sn CICC's.
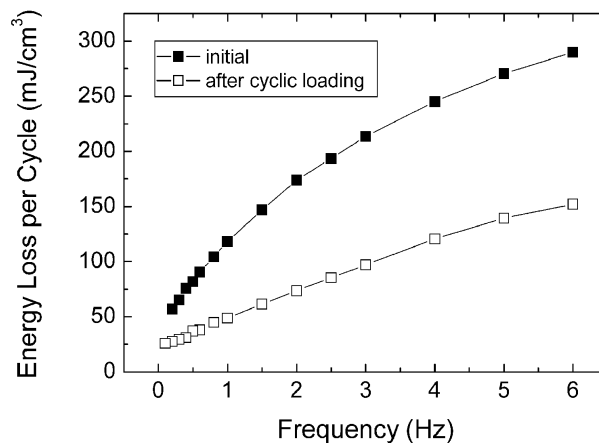
Fig. 2.5.13   *Energy loss per cycle normalised to the cable volume as a function of the frequency.*

Cycling load test of a NbTi CICC up to 10 000 cycles

The Condopt#3 is a sample of medium size NbTi CICC, without central channel and subcable wraps, with 336 Ni strand coating. It was extensively tested in SULTAN in 2002 and 2003. A section of the same conductor was used at University of Twente

(UT) for ac loss tests as a function of the cyclic load, up to 40'000 cycles in a mechanical press at 200 kN/m. The results of UT indicated that after a moderate loss reduction in the first 100 cycles, the loss increases starting from 1000 cycles, doubling eventually the value of the time constant compared to the initial values.

In SULTAN, the sample current is raised 10'000 times from 0 to 25kA in the background field of 8 T to generate a transverse body force of 200kN/m. The ac loss is measured periodically at tero load, B=2T and ΔB=0.4T. The raw data are shown in Fig. 2.5.14 as energy per cycle vs. frequency. After the initial, ≈30% loss decrease (which is a common feature of the Ni coated NbTi CICC's), the loss remains basically at the same level within a few percent. The drop observed at 2800 can be correlated with the history of the cycling. The sample was cycled up to 1400 cycles in 2002 and three years later cycling was resumed. The test at 2800 cycles is the first after long storage and the loss reduction (recovered in the following cycles) may be due to surface oxidization. The test in SULTAN suggests that the loss stays substantially constant even after a large number of load cycles. The different application of load, either mechanical in the UT press or electromagnetic in SULTAN, may be invoked as a reason for the different behaviour. [Univ. of Twente]

European Dipole Design (TW5-TMS- EDDES)

The conceptual design activities of CRPP for the layout of a dipole winding for a conductor test facility have been carried out through frequent iterations and meetings with EFDA and the other Associations involved in these design activities between December 2004 and May 2005. In agreement with EFDA, the activity of CRPP concentrated on three subjects:

- Conceptual design of a planar race-track, bath cooled winding based on a flat cable;
- Conceptual design of a planar race-track force-flow winding based on a cable-in-conduit;
- Thermo-hydraulic analyses in support of the conceptual design given by EFDA.
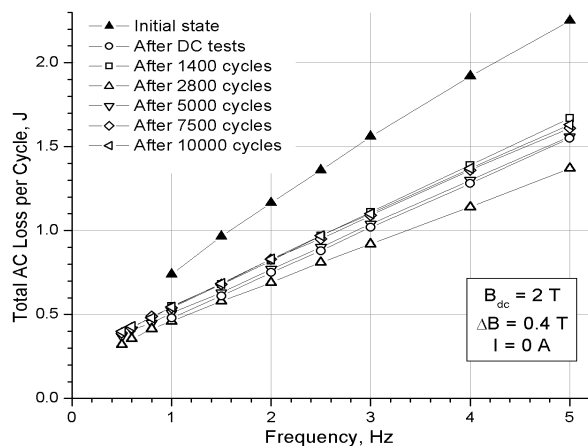
Fig. 2.5.14   *Energy loss per cycle measured after different steps of the cycling*

The advantages of a non-planar winding layout (superconductor and space economy) overcome the drawbacks (complex winding tools and barely predictable local load at the 3D bent Nb_3Sn) when a series production of dipoles is envisaged. The additional effort in design and R&D is perhaps paid back. In the case of a single device, the economy of superconductor does not justify the additional cost of 3D winding at the bends. A non-planar design implies a minimum number of R&D

steps to assess the integrity-degradation of the Nb$_3$Sn at the 3D bends. If no time/resources are allocated for R&D trials, the risk factor of a non-planar design becomes a driver for the preference of a planar winding layout.
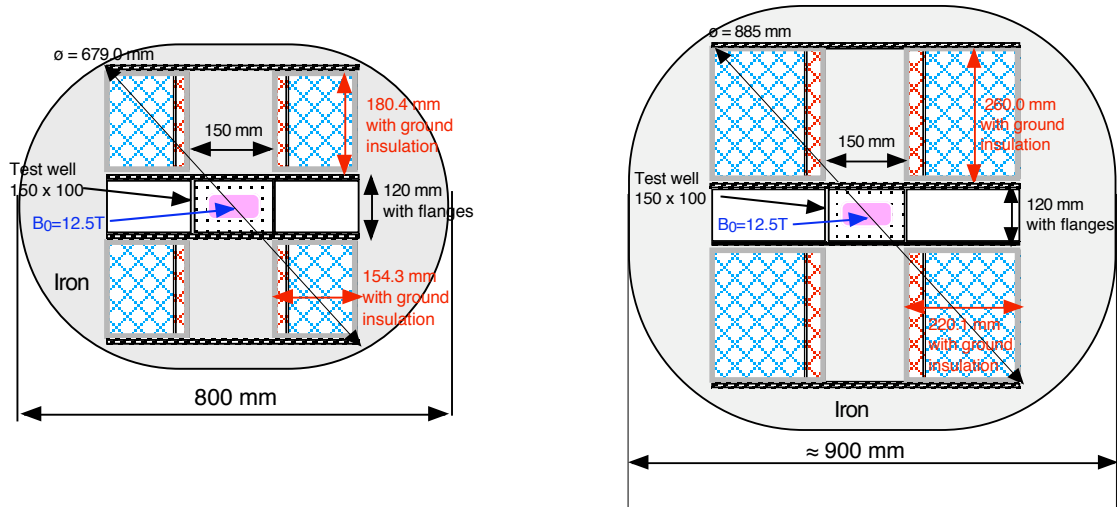
Fig. 2.5.15 *Cross section of the assembled winding packs (same scale) around the rectangular test well, including the iron clamp: left, the flat cable/bath cooled option, right, the CICC forced flow option*

After three design iterations, the results of the final conductor and winding layout for the planar race-track options are listed in the tables below, including a sketch of the conductors, and shown in Fig. 2.5.15 and 2.5.16. A full set of thermal-hydraulic computations have been produced for the planar CICC option, as well as for the non-planar design provided by EFDA, including pressure drop, heat removal, quench pressure and hot spot temperature. Magnetic field maps have been produced at CRPP for both planar options. Stress analyses have been carried out in collaboration with CIEMAT.
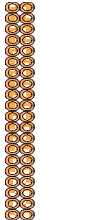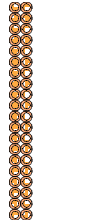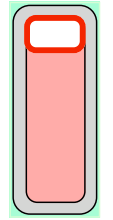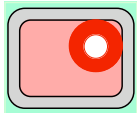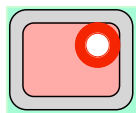
	Flat cable/bath cooled		CICC / forced flow		
	high grade	*low grade*	*high grade*	*medium grade*	*low grade*
Strand diameter, mm	1.31	1.13	0.85	0.90	
Cu:non-Cu	2.2		1		
Coating	none		Cr		
RRR	200		100		
# of sc/cu strands	40/ø	25/21	144/ø	54/27	27/54
Copper pipe	-		7.2 x 4, s = 0.8mm	ø 6.5 x 3 mm	ø 5.5 x 3 mm
Non-cu cross section	16.8 mm^2	7.8 mm^2	40.85 mm^2	17.17 mm^2	8.59 mm^2
Cu cross section	37.1 mm^2	38.3 mm^2	54.8 mm^2	60.4 mm^2	59.5 mm^2
Helium channel			5.6x2.4=12.9mm^2 D_h = 3.3 mm	ø=3 =7.1 mm^2 D_h = 3 mm	ø=3 =7.1 mm^2 D_h = 3 mm
Helium cross section			bundle 46.7 mm^2 channel 12.9 mm^2	bundle 29.5 mm^2 channel 7.1 mm^2	bundle 28.0 mm^2 channel 7.1 mm^2
Jacket thickness	-		1.5 mm	1.4 mm	1.6 mm
Bare Size, Δx Δy	2.5x24.4 mm	2.15x24.4 mm	10.2x25.2 mm	15.3x12.2 mm	15.1x12.2 mm
Insulation thickness	0.4 mm				
Insulated size, Δx' / Δy'	3.3x25.2 mm	2.95x25.2 mm	11.0x26.0 mm	16.1x13.0 mm	15.9x13.0 mm
Bending (Δx/R)	3.1%	2.0%	12.3%	11.7%	7.8%

Table 2.5.1   *Conductor layout*

	Flat cable/bath cooled		CICC / forced flow		
	high grade	*low grade*	*high grade*	*medium grade*	*low grade*
Winding thickness, Δx	26.4 mm	123.9 mm	44.0 mm	64.4 mm	105.7 mm
Winding height, Δy	176.4 mm		260.0 mm		
# of layers	8	42	4	4	7
# of turns/layer	7		10	20	20
Total # of turns	56	294	40	80	140
WP with g.i. , Δx / Δy	154.3 / 180.4 mm		220.1 * / 264.0 mm		
Nb$_3$Sn strand weight	≈ 691 kg		≈ 576 kg		
Non-cu strand weight	≈ 216 kg		≈ 288 kg		

Table 2.5.2   *Winding pack layout*

	Flat cable/bath cooled		CICC / forced flow		
	high grade	*low grade*	*high grade*	*medium grade*	*low grade*
Peak field in WP	13.7 T	10.8 T	13.17 T	10.67 T	8.22 T
T_{cs}	6.45 K	6.67 K	6.20 K	6.31 K	6.34 K
Operating current	11.6 kA		19.35 kA		
Operating temperature	4.2 K		4.5 - 4.7 K		
Equiv. Iron Radius	400 mm		500 mm		
Temperature margin	*2.25 K*	*2.47 K*	*≈ 1.6 K*	*≈ 1.7 K*	*≈ 1.7 K*
Ret. thermal strain	-0.3%		-0.6%		
Stored Energy/m	12.6 MJ/m		17.8 MJ/m		
Inductance /m	188 mHy/m		95.1 mH/m		
Hot spot temperature	150 K	117 K	138 K	149 K	124 K

Table 2.5.3   *Basic performance assessment*

To summarise, the conceptual design has detected no major obstacle for the feasibility of planar, race-track windings, with both bath cooled, impregnated flat cable and force flow CICC.

The dc and ac field generation required for the dipole facility must be in any case done by different windings. The ac coil is at best a quasi-steady state copper winding.

The reference input initially retained in the conceptual design, e.g. about non-cu J_c, operating strain, insulation thickness, is much too aggressive. Either a relaxation toward proved criteria and available material or a validation by experimental demonstration is mandatory to proceed to an engineering design phase. The conductor performance has the highest priority in the list of criteria to be validated.

Under the pressure of the "design option comparison", the conceptual design activity has been devoted mostly to detail refinement and optimisation of the conductor/winding. Other important design aspects, including mechanical and cryogenic engineering, power electronic, facility integration, have been either neglected or limited to a shear "feasibility" check. A qualified cost analysis, ranging from the coil manufacturing to the high current components, cryogenic layout and operation, should be carried out by independent experts to complete the overview of the design options.

For the flat cable, bath cooled winding option, the conclusion is that:

- The optimum engineering current density is at ≈150A/mm². Higher values would not save substantial amount of superconductor and may lead to dangerous transverse compressive load.
- The originally selected operating current, ≤12kA, is not the best choice; increasing the operating current up to 18-20kA with j_{eng}=150A/mm² would allow to reduce by 40% the number of turns and increase the cu and non-cu cross section at cost of the insulation; the result would be a dump voltage <1kV, a temperature margin up to 3K and improved heat removal.

For the force flow CICC winding option, the conclusion is that:

- The low engineering current density is the main issue for CICC, due to the steel and helium cross section, as well as the high thermal strain; increasing the

operating current, i.e. reducing the number of turns, brings obvious advantages reducing the insulation cross section and the self-inductance; opposite to the flat cable design, the feasibility of a larger CICC conductor is not straightforward due to the sharp bends at the heads. A prove of principle test is mandatory;

- In the hydraulic behaviour, the high quench pressure (thermal-hydraulic-quench-back) and the poor heat removal rate are the surprising results of the analyses; a pressure release channel becomes the recommended option for CICC up to 20kA.

Based on the perception of risk (superconductor performance), simplicity of manufacture (winding tools), modest size and weight, the preference of the CRPP is for a race-track, planar coil made by a flat, Rutherford type cable, fully impregnated and pool cooled at 4.2K, with operating current 18-20kA. [CEA Cadarache, CIEMAT, E; ENEA, I; FzK, D]
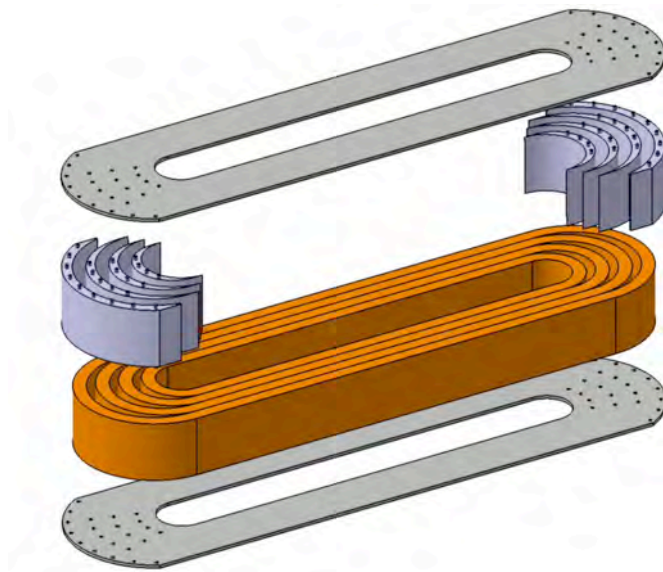
Fig. 2.5.16   *3D view of the assembled winding pack, with the spacers used to smooth the peak field at the bends*

Advanced Strand Test (TW3-TMSC-ASTEST)

The performance drop in large Nb_3Sn CICC's, probably due to transverse load degradation, motivated the use of advanced (i.e. higher current density) strands to maintain the operational margins in the ITER CS and TF coils. The objective of this task is to characterise the recently developed advanced strands procured in the frame of an EFDA technology task. These investigations are considered as a cross-check of the formal acceptance tests performed by the strand supplier. Advanced strands, supplied by European Advanced Superconductors (EAS) and Oxford Superconducting Technology (OST), were tested in October-November 2005 at CRPP. From these advanced strands the next European full-size conductor TFAS 1 has been fabricated and is tested in the SULTAN facility. The heat treatment of the full-size conductor sample and of witness strand samples has been performed at CRPP. Additional specimens from both strands wound onto ITER Ti_6Al_4V barrels have been heat treated in a small furnace (two different heat treatments). First measurements of the critical current of the advanced strand samples have been done in liquid helium. Measurements of the critical current in a temperature variable cryostat at temperatures up to 9K are underway. The measured strand data will be used as a basis for the comparison of the performances of the full-size conductor and the advanced strands. [CEA, F; ENEA, I]

Heat Treatment of two Full Size Samples (TW4-TMSC-SAMFSS)

Two Nb$_3$Sn full size European conductor samples are being manufactured by industry based on advanced strands. CRPP is responsible for the heat treatment of the conductor sections prior to assembly.

The first sample (TFAS1) was heat-treated in August 2005, see Fig. 2.5.17, and sent back to the industry. The heat treatment is in the CRPP vacuum furnace, with a small flow of helium gas maintained in the cable space. The duration of the heat treatment is about three weeks. The temperature is monitored by 5 thermocouples attached to the sample. The temperature homogeneity over the 3.5m long conductor section is within 5 degrees. A number of I$_c$ "barrels" (strand specimens for I$_c$ test) have been prepared and heat treated together with the sample.

The second sample will be supplied for the heat treatment within the end of 2005.
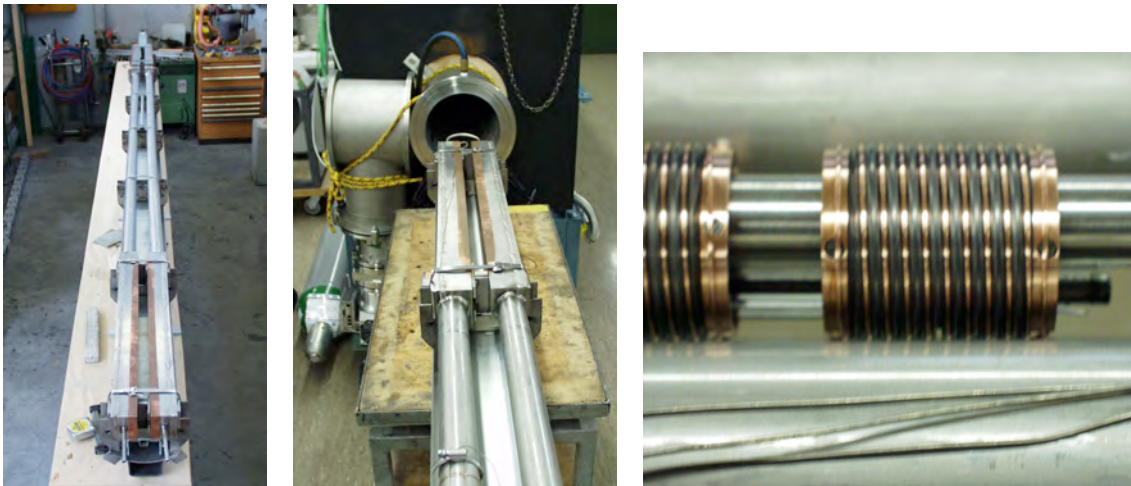
Fig. 2.5.17   *From right to left: the conductor section fixed on their support, the assembly being introduced in the furnace and a detail of the strand witness samples*

Joint resistance distribution (TW1-TMC- JSPREP)

JORDI (JOint Resistance DIstribution) has been successfully commissioned at CRPP and is a dedicated test facility for the measurement of contact resistance distribution in full-size, ITER type conductor terminations. The facility and the sample layout were already reported in 2002 and 2004. This year the first test results are reported.

For the termination prepared and tested in 2005, conductor sections of the "new full size Nb$_3$Sn CICC" (2003) and "low cost joint" NbTi conductor (2004) were used. The cable of the NbTi termination, tested in summer 2005, was split into **96** current carrying elements, corresponding to the first cable stage, made by one copper core surrounded by nine NbTi strands, see Fig. 2.5.18.
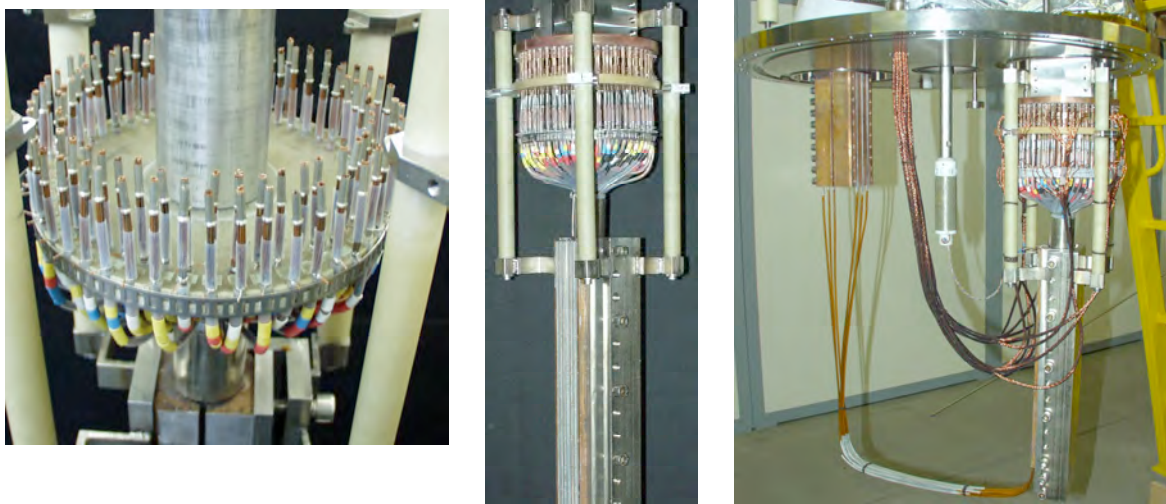
Fig. 2.5.18   *The JORDI NbTi samples. Left: a detail of the termination, opened in 96 current carrying elements placed in two concentric rings. Middle: the full sample, soldered to the shunts and copper disk. Right: the sample assembled and wired in JORDI.*

The cable of the Nb_3Sn termination, tested in October 2005, is opened into the **42** basic braids (first cable stage): each braid contains 14 Nb_3Sn and 15 copper wires. The copper wires are cut away and only the 14 superconducting strands are soldered to the shunt resistors. The preparation of the Nb_3Sn sample was very demanding as the exact geometry had to be fixed during the heat treatment, with the open cable and the 42 elements kept exactly in the final position, see Fig. 2.5.19. After heat treatment, the metallic fixture has been carefully replaced by insulating spacers before soldering to the copper disk (acting as a current terminal) with the 42 shunt resistors to impose a balanced current among the current carrying elements.
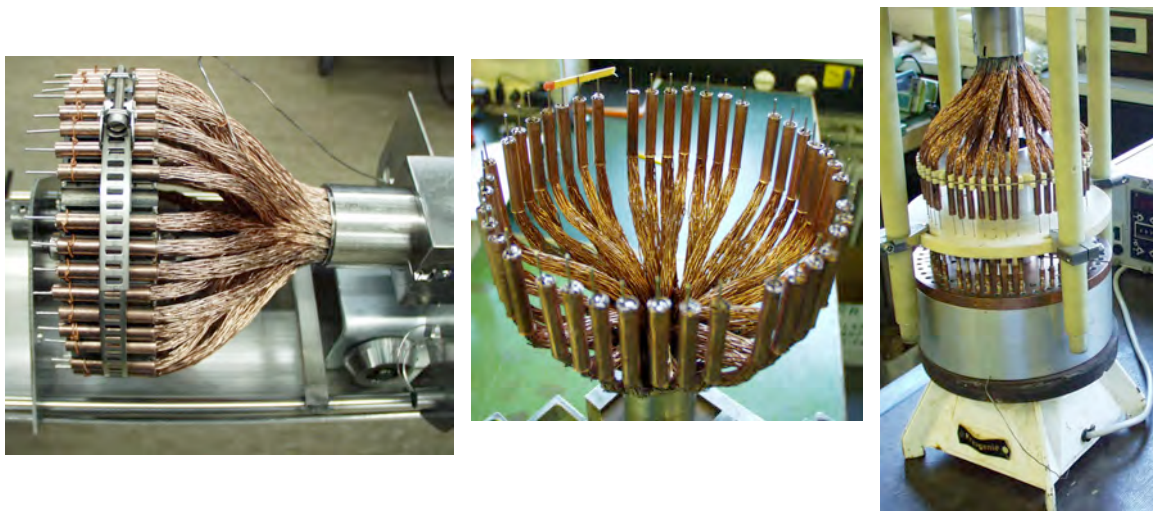
Fig. 2.5.19   *The JORDI Nb_3Sn samples. Left: the termination prepared for the heat treatment. Middle: after removing the heat treatment supports, with 42 current carrying elements. Right: soldering (upside down) of shunts and copper disk.*

The imposed current distribution, obtained by the calibrated cryogenic shunts (40$\mu\Omega$), was indeed very flat, with overall scatter smaller than 2%. The resistance distribution among the 96 elements is shown in Fig. 2.5.20. In the plot at the left side, the channels are grouped according the 6 last but one cable stage. No clear trend is observed, i.e. there is not a specific subcable with higher resistance. Within each sub-cable there are low and high resistance elements. In the plot on the right hand side of Fig. 2.5.20, the results are plotted as histogram of electrical conductivity. If the measured resistance of the 96 channels is considered as a parallel network, the result matches the overall joint resistance, $\approx 1n\Omega$ at zero applied field, as reported in 2004 from a SULTAN experiment.

In a real coil, the operation is at imposed voltage (from the power supply) and, in dc mode, the current distribution among the cable elements is driven by the resistance (or conductance) distribution at the joint. From the right hand side of the plot in Fig. 2.5.20, we deduce that the two "first cable stages" (those with highest conductivity) will have an overload of about a factor of two compared to the average of the elements. At the level of individual strands, the distribution may be less flat and the overload factor for individual strands may be higher by a factor of two. When a large size NbTi conductor operates at high current density, the superconducting transition occurs without observable current sharing (2003 and 2004) and a current overload on an individual strand cannot re-distribute, leading to a much poorer cable performance than the average strand.
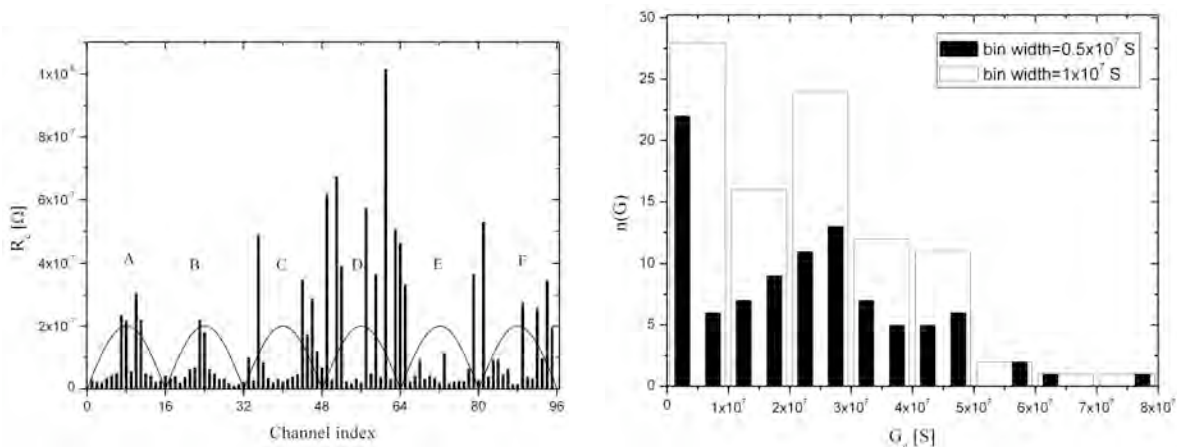
Fig. 2.5.20   *Results of resistance distribution. Left, the channel are grouped according to the sub-cables. Right, a population histogram of the electrical conductivity*

Use of High Temperature Superconductors for Fusion Applications

CRPP and the Forschungszentrum Karlsruhe were responsible for the development and test of a 70kA high temperature superconductor (HTS) current lead demonstrator for the magnet system of ITER. The use of HTS current leads for ITER offers considerable savings in the refrigeration investment and operation costs. These encouraging results, reported in 2004, triggered the start of a new study about the replacement of the water-cooled aluminium bus bars of ITER by HTS bus bars (Task TW4-TMSF-HTSCOM finished in June 2005). In a second task (TW5-TMS-HTSMAG), the potential advantages of the use of HTS for the magnet system of future fusion reactors beyond ITER are considered. In parallel to this task, measurements on industrially fabricated HTS are performed to provide a data base for the investigation of the impact of the use of HTS in future fusion magnets (Task TW5-TMSC-HTSPER). [FzK, D]

Conceptual Design of External HTS Bus Bars (TW4-TMSF-HTSCOM)

In a collaboration between CRPP and the Forschungszentrum Karlsruhe the possibility to replace the water-cooled aluminium bus bars by HTS for the TF, CS and PF coils of ITER has been investigated at the conceptual design level. The design is based on the availability of 50K helium gas and a bus bar warm-end temperature of 65K. These operating conditions have been found to provide a minimum refrigerator input power necessary to cool the HTS current leads.

The TF bus bars are designed for a rated current of 68kA and 17.5kV to ground. The 12m long ITER TF bus bars consist of two aluminium conductors, each 200mm in width and 107mm in thickness (see Fig. 2.5.21). Two pipes, each 25mm in diameter, are embedded for the required water cooling. The aluminium cross-section of the TF bus bars is approximately 41000mm^2. The minimum tolerable bending radii (on-site bending) vary between 428 and 1200mm, depending on whether the thicker or the thinner side of the rectangular bus bar is bent. The duty factor for the steady state DC operation of the TF bus bars is 32%. The rated current of the PF and CS aluminium bus bars is 45kA in pulsed mode. In the case of the PF coils, a back-up mode with currents up to 52kA is foreseen. The rated voltage between poles and to ground is 17.5kV. The PF and the CS bus bars consist of two aluminium sub-conductors, each 200mm wide and 53mm thick (see Fig. 2.5.21). The diameter of the cooling channels is 20mm. The total aluminium cross-section is approximately 20000mm^2. The minimum tolerable bending radii (on-site bending) vary between 212 and 1200mm.

I, kA	a, m	b, m	c, m	d, m	e, m	g, m	h, m	i, m	m, m	l, m	k, m
68kA	107	200	229	25	210	236	217	221	280	260	520
45kA	53	200	121	20	210	128	217	221	280	152	412
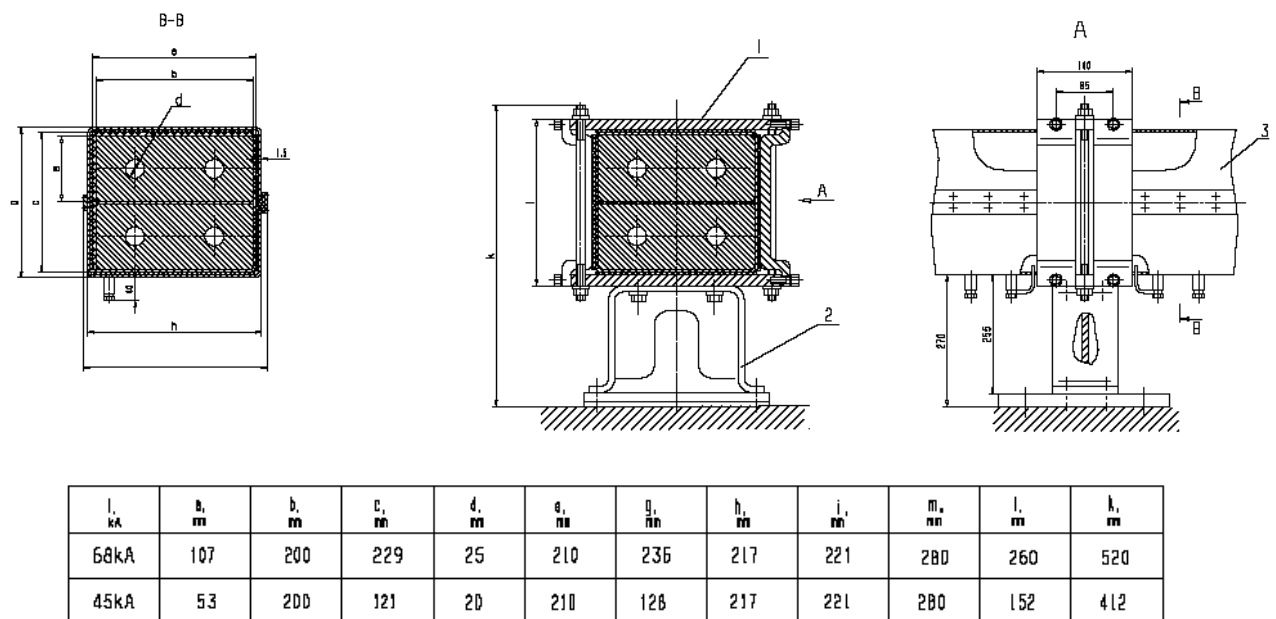
Fig. 2.5.21   *Layout of the single water-cooled aluminium bus bars.*

The design of the HTS bus bars is similar to that of superconducting power transmission cables. A sketch of a superconducting power transmission cable with a room temperature dielectric is shown in Fig. 2.5.22. The superconducting Bi-2223 tapes are wound onto a flexible stainless steel former. The coolant flows in the space between the superconducting layers and the inner corrugated stainless steel pipe of the vacuum thermal insulation system. The estimation of the bus bar critical current is based on the data for AgMg/Ag/Bi-2223 tapes fabricated by European Advanced Superconductors (EAS) (I_c@77 K=115A). The effect of the cable self-field on the current carrying capacity of the Bi-2223 tapes has been taken into account. To limit the ratio of the operating to the critical current to a value of 0.8

the minimum required critical current is 85kA for the TF bus bars and 65kA for the PF (retained here identical to the CS).
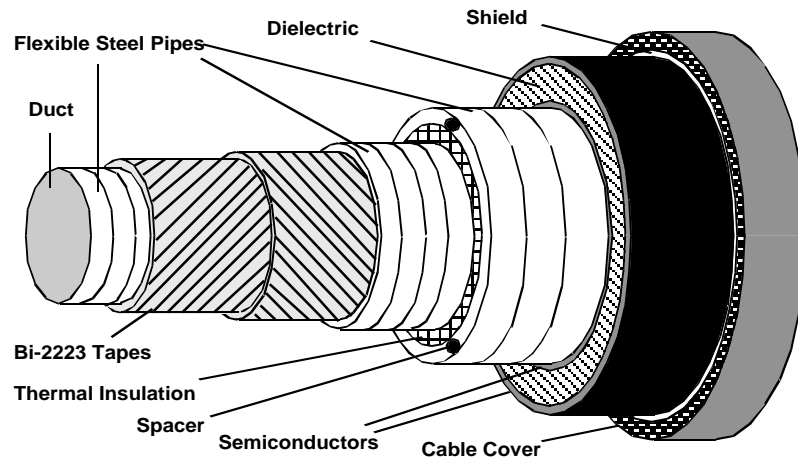
Fig. 2.5.22 *Schematic illustration of a single phase power transmission cable with warm dielectric.*

The examples of TF and PF HTS bus bar designs given in the table are based on the use of flexible stainless steel pipes with optimised dimensions and a maximum electric field of 5kV/mm in the dielectric. The space needed for the evacuated superinsulation is at least 20mm. The outer radii of TF and PF HTS bus bars are 85mm (TF C, 12 layers) and 75mm (PF B, 12 layers), respectively. The cross-section of the HTS bus bars is by a factor of 2 smaller than that of the water-cooled aluminium bus bars. The availability of Bi-2223 tapes with I_c(77K, sf) >150A would reduce the number of layers in the designs TF B and PF A to 12 and the outer bus bar radii to 76 and 67mm, respectively. The cross-sections reduction would be >2. The minimum bending radius of 2000mm is determined by the limited flexibility of the outer corrugated steel pipe of the thermal insulation system. To reach a reasonably small number of layers in HTS bus bars the operation temperature has to be 65K or lower.

The heat leak of the order of 1W/m has been found to be the main loss contribution. The AC loss in the PF and CS bus bars averaged over a full plasma cycle has been found to be negligible as compared to the thermal losses. The cooling power required for a combination of HTS bus bar and current lead is expected to be not significantly larger than that necessary to cool only the HTS current lead.

For the use of HTS bus bars it would be desirable to have a limited number of bends with a sufficiently large bending radius. The design of the terminations and the aspects related to the large short circuit currents have to be investigated in further studies.

Design	TF A	TF B	TF C	PF A	PF B	PF C
Former inner radius [mm]	25.0	32.5	40.0	25.0	32.5	40.0
Former outer radius [mm]	26.5	34.0	42.25	26.5	34.0	42.25
Superconductor	AgMg/Ag/Bi-2223 tapes (4mm×0.22mm), I_c(77K, sf) = 115A					
Tapes/layer	35	46	57	35	46	57
Number of layers	24	16	12	16	12	8
Outer radius of sc layer [mm]	31.78	37.52	44.89	30.02	36.64	44.01
Thermal insulation inner radius	34.78	40.52	47.89	33.02	39.64	47.01
Thermal insulation outer radius	65.29	72.28	81.27	63.14	71.21	80.20
El. insulation inner radius [mm]	65.29	72.28	81.27	63.14	71.21	80.20
El. insulation outer radius [mm]	68.89	75.87	84.85	66.74	74.80	83.78
Operating conditions						
Temperature [K]	65	65	65	65	65	65
Current [kA]	68	68	68	45(52)	45(52)	45(52)
Critical current [kA]	86	84	84.5	65	68.5	62.5
Voltage [kV]	17.5	17.5	17.5	17.5	17.5	17.5
Maximum electric field [kV/mm]	5	5	5	5	5	5
Losses						
Averaged AC loss [W/m]	-	-	-	0.012	0.008	0.004
Heat leak [W/m]	0.71	0.80	0.93	0.68	0.79	0.91

Table 2.5.4   *Summary of the bus bar designs*

Scoping Study of HTS Fusion Magnets (TW5-TMS-HTSMAG)

High temperature superconductors (HTS) are not only characterised by critical temperatures above the boiling point of liquid nitrogen but also by extremely high upper critical fields. The use of HTS in fusion magnets could provide higher operating temperatures and/or higher operating fields. In the scoping study on the use of HTS for fusion magnets the following options will be considered:

- High field and low temperature option (T_{op}=4.5K) based on the use of Bi-2212 ($Bi_2Sr_2CaCu_2O_{8+x}$) or Bi-2223 (($Bi,Pb)_2Sr_2Ca_2Cu_3O_{10+x}$);
- Intermediate temperature option (T_{op}: 20-40K) at fields comparable to the present ITER design (i.e. 11.8T in the TF coils); potential conductor candidates are Bi-2212 and Bi-2223;
- High temperature option (T_{op}=65K) using Y-123 ($YBa_2Cu_3O_{7-x}$) coated conductors.

In general, the use of HTS at intermediate or high operation temperatures would provide savings in the refrigeration operation and investment costs. Higher operating fields would provide the possibility to enhance the fusion power, which is roughly proportional to the plasma volume and the fourth power of the toroidal field.

As a first step, a literature study of the physical properties of different HTS materials has been performed. A comparison of the current carrying capacity of HTS, MgB_2 and Nb_3Sn indicates that MgB_2 needs further improvements to reach the critical current densities achievable in Nb_3Sn at 4.5K. The critical current densities

of Bi-2212 and Bi-2223 are in high fields ($B \geq 16T$) and at 4.5K larger than those reached in Nb_3Sn. In addition, the critical current densities achievable in the Bi-based superconductors are even at operating temperatures of 20K or above sufficient for magnet applications. Operation of fusion magnets at temperatures as high as 65K (sub-cooled liquid nitrogen) may be feasible using Y-123 coated conductors.

The stress tolerance of stainless steel reinforced Ag/Bi-2223 tapes reaches 300MPa at 77K. The corresponding critical strain is 0.45%. These values seem to be sufficient for the Ag/Bi-2223 tapes to be used in magnet applications. In Bi-2223 tapes with an AgMg matrix (dispersion-strengthened silver) a similar good stress tolerance has been achieved (critical stress of 210MPa at 77K).

At operating temperatures of 20K or above the metal specific heat is at least two orders of magnitude larger than at 4.5K. As a consequence superconductor stability is no longer a critical issue. Moreover, the temperature margins estimated for Bi-2223 at 20K are larger than those of Nb_3Sn at 4.5K. The temperature margin and the conductor performance are mainly determined by the field component perpendicular to the broad face of the tapes.

Analytic expressions for the estimation of the hysteresis and the coupling losses in tape conductors can be found in the literature. In general, the tape geometry is unfavourable with respect to the ac loss reduction for magnetic fields perpendicular to the broad face of tape conductors.

Aspects needed to be considered in more detail are:

- Optimum operating temperatures and fields for Bi-2212, Bi-2223 and Y-123 taking into account the anisotropy of the superconductor properties with respect to the direction of the applied field;
- Mechanical loads and limitation of the magnetic field in case of a high field option;
- Manufacture of high current conductors using tape conductors; conventional cable manufacturing techniques can be applied (e.g. Rutherford cable) only for Bi-2212 round wires; however, the operating temperature of magnets fabricated of Bi-2212 round wires seems to be limited to 20K;
- Consequences of the use of HTS for the whole system including thermal insulation requirements, AC losses, refrigeration operation and investment costs, generated fusion power, interaction of HTS with high energy neutrons.

HTS Materials for Fusion Magnets (TW5-TMSC-HTSPER)

In the framework of this task, industrially fabricated HTS wires and tapes will be characterised for critical current as a function of field, temperature and axial tensile strain. First measurements on AgMg/Ag/Bi-2223 tapes made available by European Advanced Superconductors (EAS) were carried out in summer 2005. The tape dimensions are 4mm in width and 0.22mm in thickness. The critical current of the AgMg/Ag/Bi-2223 tape measured at 77K and zero applied field is 95A.

The critical current is shown in Fig. 2.5.23 as a function of the magnetic field applied parallel (parallel to the crystallographic ab planes) and perpendicular (parallel to the crystallographic c direction) to the broad face of the tapes. The results indicate that the critical current is considerably larger for fields applied along the broad face of the tapes. This anisotropy of the critical current with respect to the direction of the applied field is more pronounced at higher temperatures. For the favourable field direction the critical current at 27K is well above 100A even in fields of 11T. On the other hand, the critical current at 27K falls below 100A in a field of 4T applied perpendicular to the broad face of the tape. The results indicate

that the operation temperature and field of AgMg/Ag/Bi-2223 tapes is limited by the field component parallel to the crystallographic c direction.
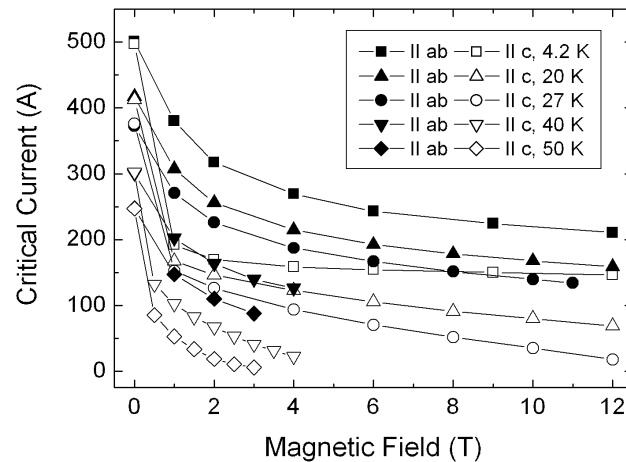
Fig. 2.5.23   *Critical current of an industrially fabricated AgMg/Ag/Bi-2223 tape as a function of the magnetic field applied parallel (parallel to the crystallographic ab planes) and perpendicular (parallel to the crystallographic c direction) to the broad face of the tapes.*

An interesting feature of the AgMg/Ag/Bi-2223 tapes is a considerable hysteresis in the critical current depending on whether the critical current has been measured in successively increasing or decreasing fields. The hysteresis of the critical current for fields parallel to the broad face of the tapes is shown in Fig. 2.5.24. The effect is negligible for temperatures of 40K and above. At low temperatures, the critical current measured in decreasing fields is considerably larger than the value found for increasing fields. This observation may be related to the granularity of high temperature superconductors. It is well known that the critical current densities within a single grain are considerably larger than the transport critical current density, which is limited by the current carrying capacity of the grain boundaries. For measurements in successively increasing fields, the magnetic field generated by the screening currents induced within in the single grains adds to the applied magnetic field in the grain boundaries. On the other hand, the field generated by the screening currents flowing in the individual grains for decreasing fields is opposite to the applied field at the grain boundaries. At the highest temperatures the flux lines are only weakly pinned in Bi-2223. As a consequence the critical current density across the grain boundaries becomes comparable to the intragrain critical current density, and hence the hysteresis is vanishing at the highest temperatures.

It is intended to measure additional HTS samples. Moreover, the dependence of the critical current on the axial tensile strain will be investigated. The results of the measurements of the critical current as a function of field and temperature should provide the basis for scaling laws describing the critical surface of HTS.
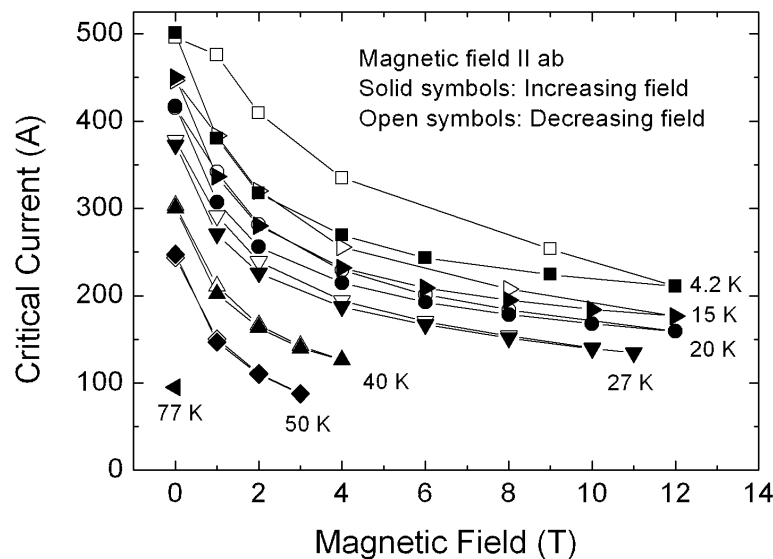
Fig. 2.5.24   *Critical current of an industrially fabricated AgMg/Ag/Bi-2223 tape measured in increasing and decreasing magnetic fields. The field is applied parallel to the broad face of the tapes (i.e the crystallographic ab planes). At low temperatures, a considerable hysteresis in the critical current has been observed.*

2.6   *Industrial process plasmas*[4]

As in the past years, projects on large area capacitively coupled RF plasmas for the deposition of thin film solar cells and for flat displays have been one of the main activities of the industrial plasma group. The diversification of the research topics of the group has continued. The up-scaling of small plasma reactors to industrial reactors in most cases implies a considerable increase in electrical power. This increase leads to additional problems such as arcing and other parasitic discharges which can hinder introduction into industrial production lines. Therefore arcing and parasitic discharges in industrial plasmas constitute a new line of research and development topics for the industrial plasma group. First approaches to investigate arcing phenomena in large area RF reactors such as our KAI reactor have been tried. Arcing is also important in the space environment and in space equipment, underlined by a new mandate from Mecanex SA in Nyon on behalf of the European Space Agency (ESA). Micro discharges used in Electrical Discharge Machining (EDM) and in other applications are another topic which shall be investigated in the future. Discharge plasmas physics is the underlying feature in these interesting projects linked to successful industrial applications.

Modelling of process plasmas, not just in large area RF plasmas, is not only important for designing and developing new reactors but also for the interpretation of ongoing experiments. Modelling is also favoured by modern software such as convenientpartial differential equation solvers and multi-physics software facilitating the modelling of the complex plasma environment and plasma sources.

---

[4] Work not belonging to the Association's work programme.

2.6.1 *Electromagnetic nonuniformities due to standing wave and electrode asymmetry effects in large area, high-frequency capacitive plasma reactors*

Capacitively-coupled, parallel plate radio-frequency (rf) reactors are commonly used for plasma enhanced chemical vapor deposition (PECVD) and dry etching of thin films such as amorphous silicon or silicon oxide. Large area ($>1\,m^2$) reactors are used, for example, for the production of photovoltaic solar cells and thin film transistors for flat screens. These industrial applications typically require a uniformity in film thickness to better than +/-10%. Many phenomena can give rise to nonuniform deposition or etching in large area rf parallel plate reactors, including inappropriate gas flow distribution, clouds of dust particles, imperfect contact of the substrate with the electrode, or electromagnetic wave propagation effects. The plasma nonuniformity considered here is due to electromagnetic wave propagation effects. These effects cause nonuniformities in plasma rf potential which are responsible for a nonuniform power dissipation and consequently nonuniform deposition or etch rates.

When higher frequencies are combined with large areas, electromagnetic standing wave effects can become a major source of nonuniformity in conventional parallel plate reactors. Taking this effect into account, the standing wave nonuniformity already becomes important when the reactor size is about one tenth of the free space wavelength (2.2m at 13.56MHz, but only 0.3m at 100MHz).The telegraph effect is associated with asymmetric electrodes, which necessitate the redistribution of rf current along the plasma to maintain rf current continuity. The case of high frequency excitation in asymmetric reactors requires simultaneous treatment of both the standing wave effect and the telegraph effect. The aim of this work was to place the electromagnetic description of the standing wave and telegraph effects in the same context by deriving general field solutions, dispersion relations and equivalent circuits for both of them.

The electromagnetic field solution has been derived for a capacitive, high-frequency, cylindrical reactor with asymmetric electrode areas containing a plasma slab. It was shown that two modes are necessary and sufficient to determine the electromagnetic fields everywhere within the reactor except close to the sidewalls. These two modes give rise to the interelectrode rf voltage standing wave effect and the telegraph effect. The interelectrode rf voltage standing wave effect is associated with high frequencies in large reactors, the telegraph effect is associated with asymmetric electrode areas. This is analogous to propagation along a lossy conductor in a transmission line, hence the term telegraph effect.

It has been shown that the combination of the standing wave effect, the telegraph effect and edge-localised modes all appear in the analytical solution of the field equation for a high-frequency plasma reactor with asymmetric electrode areas. In particular, it has been shown that the electromagnetic field solution can be written as the sum of even and odd modes and that only the first even mode and the first odd mode propagate inside the reactor and directly affect the plasma uniformity above the process area (a few centimeters away from the reactor sidewall). The first even mode is responsible for the interelectrode rf voltage standing wave effect and the first odd mode, which is excited only in asymmetric reactors, is responsible for a perturbation of the plasma rf potential due to the telegraph effect. The first even mode and the first odd mode are necessary and sufficient to describe the electromagnetic fields everywhere within the reactor except in the immediate vicinity of the walls, where the higher-order evanescent modes contribute. Finally, the equivalent circuit was derived for each first mode from the corresponding dispersion relations. The electromagnetic solution presented here explains the physical origins of the electromagnetic nonuniformities in large area capacitive plasma reactors. This is of practical importance for reactor design because methods

have been proposed to suppress both sources of nonuniformity. The interelectrode rf voltage standing wave can be suppressed by using a shaped electrode and the telegraph effect can be suppressed by using a symmetric sidewall.

2.6.2   Design of a new large-area high density RF plasma source (HDS)

Due to their apparent design simplicity, capacitively-coupled parallel plate radio frequency (rf) plasma reactors remain one of the main choices for large area plasma-enhanced chemical vapour deposition (PECVD) or dry etching of thin films such as amorphous silicon, silicon oxide or silicon nitride. Large area rectangular reactors exceeding $1m^2$ are used for production of thin film photovoltaic solar cells and thin film transistors for flat screens. These industrial applications typically require a uniformity in film thickness to better than +/-10%. Generally, these reactors are driven at a standard excitation frequency of 13.56MHz, but there is a strong interest in using higher frequencies because of advantages such as high deposition rate and reduced sheath voltage and ion energy bombardment.

In order to suppress the standing wave nonuniformity, discussed in the previous section, in a large area cylindrical reactor, a proposal was based on an analytical solution of Maxwell's equations in vacuum. This was to use a Gaussian shaped electrode together with a thin dielectric plate in order to confine the plasma in a constant interelectrode gap in place of the conventional flat electrode. By analogy with an optical dielectric lens, the variable gap between the shaped electrode and the dielectric plate has been called a lens due to its property of correcting the electromagnetic standing wave.

Previous measurements in a 1m diameter cylindrical reactor at 67.8MHz had proven that this new lens solution was effective for suppressing the radial standing wave nonuniformity for a wide range of plasma parameters. Recently, it has been shown that the gaussian lens solution is not valid for rectangular geometry. A numerical method based on a two-dimensional quasi-planar circuit model has been developed, to calculate the electrode shape that can suppress the electromagnetic standing wave nonuniformity. In particular, it has been shown that the electrode shape depends not only on the reactor dimensions and excitation frequency, but also on the number and position of the rf connections to the electrodes.

A commercial KAI 1000 reactor obtained from Unaxis Display can coat substrates of $1m^2$ and was installed at the CRPP. The plasma diagnostics on the KAI 1000 reactor were optical diagnostics and electrical probe measurements. 24 fibre optics were installed in the ground electrode to monitor the optical uniformity of the plasma. During the past year this reactor has been equipped with the new rectangular lens design to suppress the standing wave effect at 67.8MHz. The experiments showed that the lens concept is a powerful technique to compensate the standing wave effect in an industrial large-area RF plasma reactor.
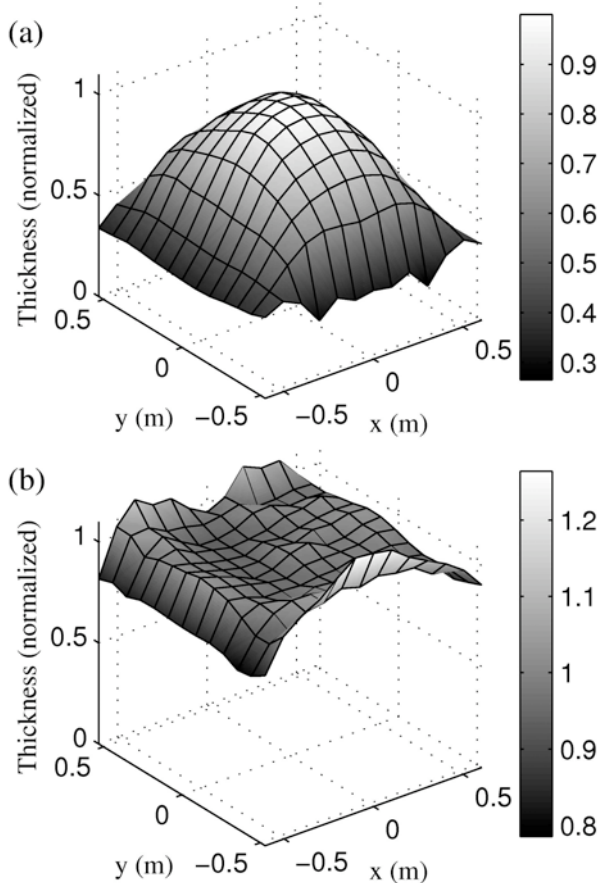
Fig. 2.6.1 *Normalised a-Si:H film thickness uniformity deposited on a 1.1m by 1.2m substrate placed on the base of a KAI-1200 asymmetric reactor at a 40.7MHz excitation frequency, (a) for the parallel plate configuration and (b) for the shaped rf electrode configuration.*

A second reactor used in these investigations was an industrial KAI-1200 type Plasmabox reactor commercialised by UNAXIS. for thin film deposition. This reactor at UNAXIS Solar differs essentially from the first one by its larger lateral dimensions which are 1.35m long and 1.25m wide. Depositions of amorphous silicon (a-Si:H) were performed from a silane hydrogen gas mixture, and the process uniformity was characterised from the *ex situ* thickness measurements of the thin films deposited on glass substrates.

Figure 2.6.1 shows the normalised a-Si:H film thickness profiles deposited in this commercial KAI reactor. Figure 2.6.1(a) corresponds to the parallel plate electrode configuration at a 40.7MHz excitation frequency and Fig. 2.6.1(b) to the shaped rf electrode configuration. The nonuniformity of the thin film deposited in the parallel plate configuration (Fig. 2.6.1(a)) is about +/-58%, with a maximum deposition rate at the centre of about 4.5Å/s. For the thin film deposited with the shaped rf electrode configuration (Fig. 2.6.1(b)), the thickness nonuniformity is about +/-23%, with a deposition rate at the centre of about 3.6Å/s. These results confirm the ability of the shaped electrode technique to reduce the nonuniformity due to the interelectrode voltage standing wave in large area rectangular capacitive plasma reactor for PECVD processes. The film thickness nonuniformity for the shaped electrode case is essentially confined to the substrate periphery. If we exclude 10cm from the edges of the substrate in the calculation of the nonuniformity, then the film thickness nonuniformity decreases from 23% to 7.5% over the remaining 0.9m by 1m substrate central area.

2.6.3   *A new large area very high frequency (VHF) reactor for the high rate deposition of microcrystalline silicon for thin film solar cell applications*

The scientific and technological aim of the present project is to apply the newly-developed technology of the high density reactor with its characteristic shaped electrode(s) to the production of large-area solar cells. This new reactor should represent the second generation of reactors in the PV equipment production line of UNAXIS Solar.

The production of thin film solar cells is the first straightforward application for this new reactor type. The reasons are that higher plasma excitation frequencies are required for this type of application. Higher deposition rates together with moderate to high material quality can most probably only be obtained with such a process. In addition, the higher excitation frequency also allows the industrial deposition of microcrystalline or micromorph layers, required by the photovoltaic (PV) industry for future solar cells. On the other hand, the commercial KAI plasma box concept has proven to be adapted to PV applications and, coupled together with higher plasma excitation frequencies, could be of benefit for the production of amorphous and microcrystalline silicon for application in solar cells. The new high density reactor generation could therefore be most appropriate for thin film solar cell production.

Besides these more technical problems, the development of the process for amorphous and microcrystalline silicon deposition in this new device is necessary and will therefore be a large part of the project. Particular care will be taken regarding the electronic quality of the layer, including roughness and film density as well as the deposition rate and the uniformity of the layer over the whole $1x1m^2$ glass substrate. One scientific aim of the present project is to develop an industrial process for the deposition of these highly demanded PV materials.

In order to reach a high deposition rate of μc-Si:H films, we have investigated a low interelectrode gap (11mm) version of the standard (25mm) KAI-S PECVD reactor. This low gap reactor has shown very interesting behaviour concerning film crystallinity. Indeed, all samples were μc-Si:H at a RF power input of 1.5kW, which is lower than the 2kW needed to obtain μc-Si:H material at a standard 25mm gap over a wide process window. However, the process window at 11mm is limited to high pressure >6mbar in order to have an acceptable thickness uniformity (±15%) and this means that no increase in deposition rate is observed, because of the strong powder formation at high silane concentration (>3%) used in this process.

The only advantage of such a low gap reactor compared with the standard version is that the necessary power to obtain μc-Si:H deposition is reduced, and thus the power consumption and the risk of parasitic plasmas are reduced.

We have performed a reactor modification to reach an interelectrode gap of 18mm. Compared to both the 11 and 25mm gap reactor, the mid-gap reactor presents very high deposition rates (up to 12Å/s). This large improvement is not due to changes in plasma parameters or in the fraction of depleted silane, but to the fact that very little powder formation occurs in this mid-gap configuration. Mid-gap reactor (18 and 15mm) investigations are still going on and if this tendency to produce a small amount of powder is confirmed, they will be of great interest for high rate μc-Si:H deposition with low silane losses in powder. This increases silane consumption efficiency and decreases risks related to small particles.

An analytical model for RF PECVD deposition of amorphous and microcrystalline silicon for solar cells has been studied and validated against experimental measurements. This model is based on a simple set of chemical reactions that take

place in the plasma and at the surface of the substrate (plasma – solid interaction). It can reduce the number of dimensions of the plasma parameter space from 7 (excitation frequency, power density, pressure, temperature, silane concentration, total flow rate and interelectrode gap) to 2, which are silane concentration and the ratio of dissociation rate to the pumping rate. The output of this model is the transition region from amorphous to microcrystalline silicon in this new 2–D parameter space (Fig. 2.6.2). A study of various chemical reactions has shown that the plasma chemistry does not affect the final behaviour of the model.

To validate this model, we had to install a Fourier Transform Infrared (FTIR) absorption measurement directly in the exhaust line of the KAI-S reactor to have a direct measurement of the ratio of the dissociation rate to the pumping rate. Raman spectroscopy performed at the Institut de Microtechnique (IMT) of the University of Neuchâtel gives information on the crystalline fraction of the samples. A combination of these two measurements and comparison with the model is used to adjust the model and find the transition region between amorphous and microcrystalline silicon deposition regimes, (Fig. 2.6.2).
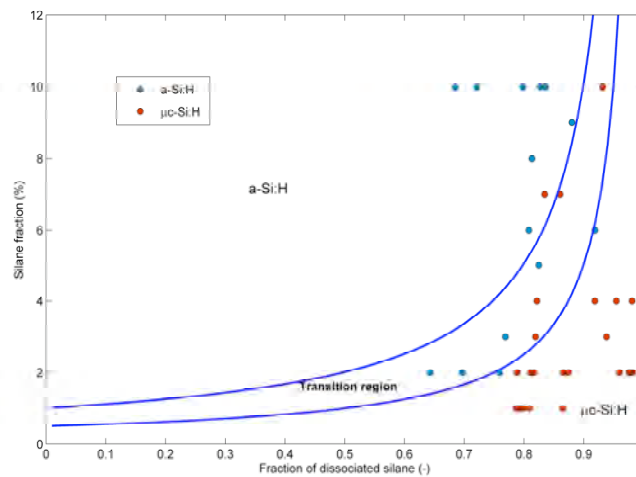
Fig. 2.6.2   *Transition region calculated by the analytical model and experimental data points with microstructure.*

2.6.4   *From conventional Plasma Spraying to Reactive Thermal Plasma CVD*

The plasma torch is one of the most elementary plasma sources used in industrial applications. It has brought atmospheric thermal plasma spraying to commercial and economic success. Many daily applications would not be possible without this widespread industrial process. However the applications are limited to relatively porous and thick coatings compared with vapour deposition techniques, and the spray materials are restricted to substances with a convenient melting point.

Recently, the plasma torch has been operated and investigated at very low pressures. Low pressure plasma spraying (LPPS) operates down to pressures in the mbar range and more closely approaches the thin film technology which is mainly dominated by conventional RF plasma sources. This broad operation range has a large potential for a wide variety of industrial applications and will widen the traditional market of plasma spraying and plasma spray equipment.

Fig. 2.6.3   _Injection of Kr into the plasma jet generated by a F4 Sulzer Metco torch._

The plasma torch is the only plasma source up till now which successfully allows the use of solid, liquid and gaseous precursors. This great advantage is due to the high enthalpy content of the plasma jet. The existing plasma torch will be the basis for a new technology of reactive thermal plasma CVD. In reactive thermal plasma CVD, the evaporated solid or liquid precursors and the gaseous components contribute to a complex plasma chemistry which leads to film deposition. With reactive thermal plasma CVD, the residual porosity of the plasma spray coatings can be suppressed and dense layers should be obtained at high deposition rate. However, this needs a completely new development of processes and a deeper understanding of the underlying plasma physics and chemistry, the main aims of this project.

During the past year, detailed investigations have been performed on the behaviour of the injection of neutral gas into the plasma jet. A movable gas injector and a cooled substrate holder were designed and constructed, Fig. 2.6.3. Xenon and krypton have been used and the torch was operated at different parameters, in particular at different gas pressures. This study clearly showed that neutral gas feeding of the fast plasma jet is only possible if the gas injection point is located inside the barrel shocks which surround the hot supersonic plasma jet. In addition, high diffusion transport is responsible for fast and homogeneous distribution of the injected gas within the plasma jet. The excitation of the noble gas atoms within the jet, shown up by optical emission spectroscopy, indicates that intense plasma chemistry can be expected if reactive species are introduced. All these results are promising for the following phases when reactive precursors will be injected.

For injection of liquids, a small commercial nebulator has been used to inject water without any very convincing results. It seems that liquid injection is more efficient

using direct injection into the plasma torch through the existing powder injection hole of the F4 torch. New unmachined nozzles obtained from Sulzer Metco have been adapted for liquid precursor injection experiments.

2.6.5 Design, characterisation and modelling of a reactive Low Energy Plasma (LEP) Source for SiGe processing

Industry needs plasma sources capable of driving high deposition rate processes for high quality coatings. In particular, the semiconductor industry needs high deposition rates in epitaxial processes in order to decrease the production costs of the sources.

The underlying physical principle of the LEP is that an intense low energy plasma can be generated by sustaining a low energy arc discharge by a large electron current emitted from a hot filament. The plasma source (Fig. 2.6.4) contains a tungsten filament heated by a current. The plasma is sustained by applying a voltage of about 20-30V between the grounded chamber walls and the hot filament. Discharge currents in the range 10-100A can easily be obtained. The low energy electrons ionise and excite the argon as well as the admixed gases and therefore create a dense reactive plasma in the chamber. The main advantage of the low energy plasma is the low energy (<12eV) ion bombardment of the substrate leading to interesting industrial applications such as the epitaxial growth of layers such as SiGe.
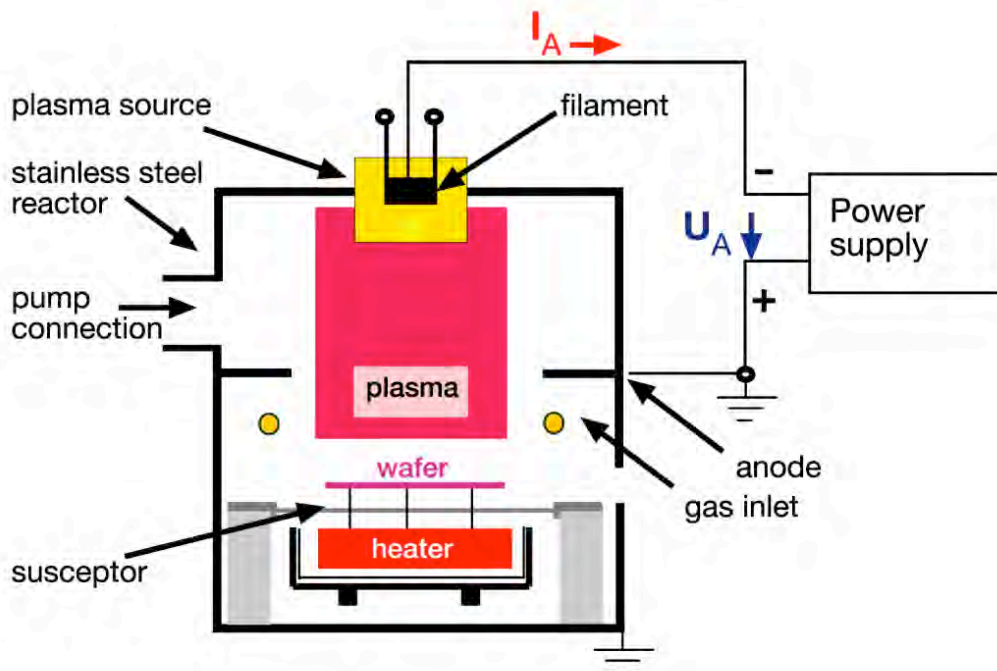
Fig. 2.6.4   *Schematic of the LEP plasma reactor*

The first successful applications of the low energy plasma source showed several difficulties which are directly related to plasma physics and chemistry, and to the technology of the plasma source design. One major problem inherent in the principle of the plasma source is the influence of the design of the ionisation source on the resulting plasma. Process stability and film inhomogeneity are two other topics which need to be clarified before successful industrialisation of the reactor and of the process. Therefore, diagnostics of the plasma obtained are needed to

optimise the process plasma from the point of view of deposition rate and uniformity. For semiconductor applications, the process development for plasma cleaning and for solving the problem of the reactor self-cleaning have to be investigated.

The LEP reactor has been installed at the CRPP and is now running with a new control system designed at the CRPP. This simplified control system replaces the industrial control system which was too complex for experimental work. The design of the ring anode and its construction at the CRPP have been finished.

Using double Langmuir probes, uniformity profiles of the plasma density, electron temperature and floating potential have been measured for various conditions; such as different pressures, source configurations, different anode geometries and different magnetic field coil configurations and magnetic field strength. The plasma stability (plasma flickering) was also investigated under these conditions. Furthermore, investigations of the hot electron beam with and without orifice plate have been performed using a shielded probe.

Filtering of the arc power supply allowed substantial plasma noise reduction plasma. In addition, an electrical resistive path between the filament and the source was discovered, depending on metal film deposits, which could cause irreproducible process conditions.

A dummy substrate has been prepared with 59 surface electrical probes for homogeneity measurements and the vacuum electrical feedthrough has been installed. A multiplexer and a digital multimeter controlled by Labview software will read out the probes and enable instantaneous monitoring of plasma uniformity and stability at the substrate surface.

Using the Femlab and Matlab software a fluid model was written for the argon plasma in a magnetic field and will be used for comparison with the experiment and later for process development.

2.6.6   Low Energy Plasma Processing for Wear Resistant Coatings

Existing technologies for wear resistant coatings have their limitations. Thermal CVD technology is not flexible enough in the selection of the precursors for a determined temperature range to compete with PVD and the thermal load limits the free choice of substrate material. Existing technology for plasma-enhanced CVD for wear resistant coatings has mainly been developed for diamond and diamond-like deposition.

The objective of this project is the deposition of wear resistant coatings on metallic and insulating substrates by a new plasma-enhanced CVD process. The new process approach will take advantage of existing DC plasma technology. The basis of the process used is the same as for the deposition of diamond and in the project for epitaxial SiGe growth running at the same time at the CRPP. The LEP plasma process is based on a DC arc discharge. The discharge operates at high currents and at low voltages. All gases fed to the discharge are more or less completely dissociated. However, the operating pressure is orders of magnitudes lower than in conventional CVD and also lower than in PECVD for diamond in the same reactor.

The commercial BAI plasma reactor at the CRPP was modified to be run in the Low Energy Plasma (LEP) mode. This implied the addition to the device of a turbo pump with high pumping speed in order to reach working gas pressures down to 10^{-4}mbar. The BAI reactor was successfully modified with the help of our industrial partner Balzers, which supplied the CRPP with a turbo pump. First experiments

showed that the anode became coated by an insulating layer, leading to plasma extinction after several minutes of processing. Modification of the anode design was needed to circumvent this problem.

Layers were deposited on glass and silicon wafers with a thermal native oxide layer, on uncoated cemented carbide inserts and on TiN coated inserts. After the deposition process, the samples were analysed by different ex situ surface characterization methods such as Scanning Electron Micrsocopy SEM (E. Hollenstein, EPFL), X-Ray Photon Spectroscopy XPS (Prof. Mathieu, EPFL), Rutherford Back Scanning RBS (Dr. Döbelin, ETHZ) and X-Ray Diffraction XRD. In particular a FTIR was used since this method allows rapid measurements at the CRPP and a fast validation of the validity of the process.

First coatings of SiN have been made on various substrates and various process conditions such a different discharge currents, pressures, substrate positions and gas mixtures. Two different gas mixtures have been used, namely silane and nitrogen diluted with hydrogen and silane and ammonia mixtures. SiC layers have also been deposited with a mixture of silane and methane. Initial results suggested that nearly stoichiometric, probably nanocrystalline Si_3N_4 coatings were deposited at typical deposition rates around 100nm/min. However, the films still contain hydrogen which should still be removed.

2.6.7   *Plasma diagnostics for electrical discharge machining (EDM)*

EDM is a widely-used machining technique. With this technology, numerous industries produce moulds, dies and finished parts with complex shapes. Compared with other conventional machining techniques, EDM has several advantages: machining of all conductive materials regardless of their hardness, no contact and stress for the workpiece during machining, complex cutting shapes, good finishing surface and machining precision. The principle of EDM is to use the eroding effect of electric spark discharges on the electrodes. This effect was first discovered by Priestley in 1770, and has been used in a controlled way for machining since the 1940's. The process consists of successively removing small volumes of workpiece material, molten or vaporised during a discharge. The sparks are created in a flowing dielectric, generally water or oil. The liquid dielectric plays a crucial role for cooling the electrodes and for removing the material: it increases the force on the molten metal when the plasma collapses, then it solidifies the molten metal into small particles, and finally it flushes them away.

In collaboration with Charmilles SA the EDM plasma has been investigated, which lies at the heart of the process. Optical emission spectroscopy is one of the plasma diagnostics applicable to EDM plasma. With this method, the electron temperature, the electron density and the influence of the discharge parameters on the plasma emitted light have been measured. Time-resolved spectroscopy that the EDM plasma is weakly non-ideal, especially in the very beginning of the discharge. Imaging is another diagnostic applicable to EDM discharges. It has already been used to understand the breakdown mechanism. A spatio-temporal characterisation of the EDM plasma with imaging and optical emission spectroscopy has been made during the last year.
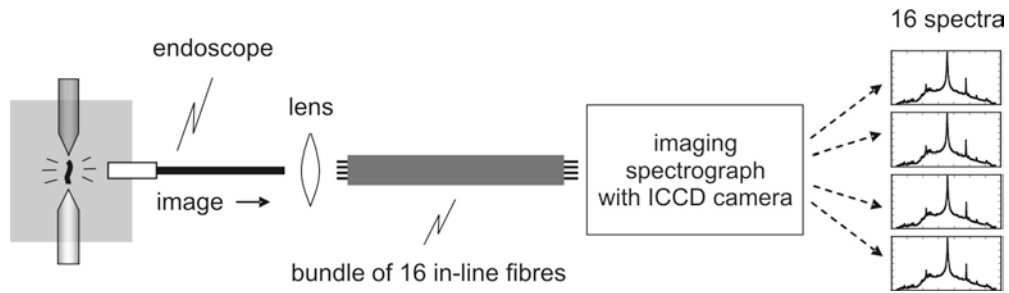
Fig. 2.6.5   *Experimental setup for spatially-resolved spectroscopy.*

In order to have spatial resolution of the emitted light, the magnified plasma image captured with the endoscope is projected onto an in-line array of 16 fibres. Each fibre collects the light coming from a different zone of the emitting region. The fibre bundle brings the sampled light into a imaging spectrograph. The 16 different spectra are recorded simultaneously with the same ICCD camera used for imaging, Fig. 2.6.5.
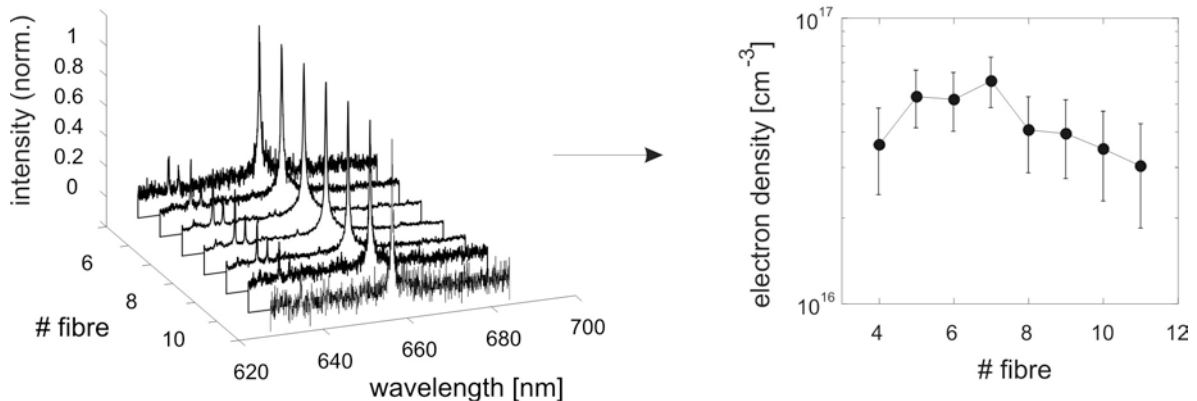
Fig. 2.6.6   *Vertical profile of the electron density calculated from spatially-resolved $H\alpha$ broadening measurements. The spectra are normalised to the intensity of the H_α line at 656.2nm. The light measurement is time integrated over thousands of discharges.*

In dense plasmas such as EDM plasma, line broadening is by far dominated by Stark broadening. From the H_α line width at half maximum, the electron density has been determined using calculations of the hydrogen Stark broadening. Figure 2.6.6 shows spatially-resolved H_α spectra, along with the electron density vertical profile calculated from them. The central spectra have a better signal to noise ratio than the outer ones because the light intensity is higher in the center.

The values found are in good agreement with our previous results, around $5 \cdot 10^{16} cm^{-3}$. Despite large error bars, the electron density seems to be slightly higher in the plasma center.

The plasma is contaminated by impurities and several lines of atomic copper and chromium are present in the emission spectrum coming from the electrode. The spatially-resolved emission spectroscopy measurement showed that the plasma contamination coming from the electrodes is mostly located close to them.

(a) image

(b) optical emission spectrum
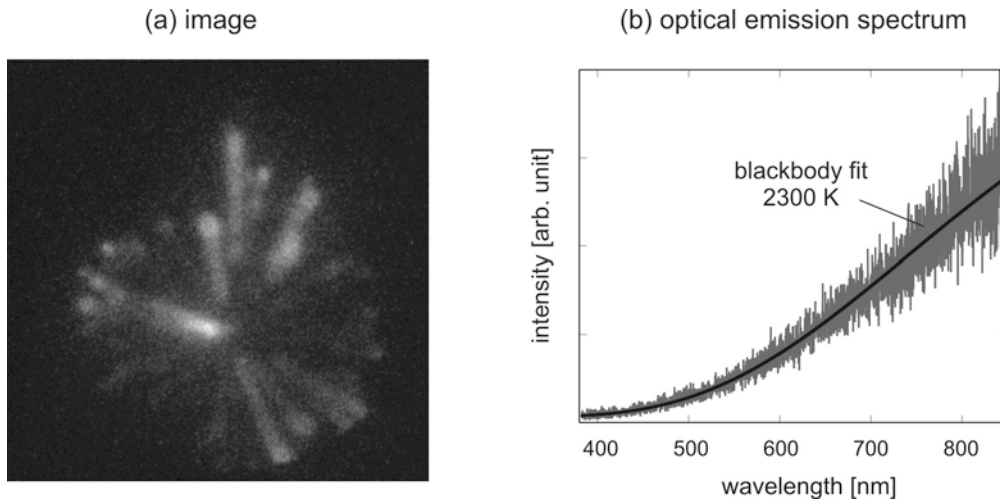
Fig. 2.6.7 *Incandescence of the particles removed after a discharge: (a) Image of a single post-discharge; (b) Optical emission spectrum, with a 2300 K blackbody fit. The light measurement is time integrated over thousands of post-discharges.*

Figure 2.6.7(a) shows that the weak light emitted after the discharge originates from particles of heated metal. These particles originate from the molten metal pool created in the workpiece during the discharge, and are then removed from the workpiece and ejected in the dielectric when the discharge is shut down. We see their path, rather than just luminous dots, because they are moving during the camera exposure. Spectroscopy shows that this post-discharge light emission is close to blackbody radiation, which confirms that the emitters are heated metal particles. The spectrum in Fig. 2.6.7(b) is quite noisy, due to the low intensity of the afterglow emission. Fitting the afterglow spectra with Planck's law, the temperature of the emitters is found to be around 2200K. Since the melting point of steel is about 1700K, the particles are still in a liquid state in the very beginning of the post-discharge. The particle size can be measured from the images. We found that the largest particles have a diameter of about 30μm, which is consistent with previous work on spark-eroded particles. The particle speed can also be estimated from images, the maximum speed being around 3m/s.

2.6.8 Atmospheric plasmas for thin film coating

Plasmas at atmospheric pressure are thought to be an alternative way for the production of coatings for various applications. Avoiding vacuum technology for depositing coatings on polymer films is certainly one possible route for cost reduction. However, there are various problems related to the process of RF plasmas operated at atmospheric pressure, such as controlling the discharge type.

The discharge is generated between two alumina (Al_2O_3) plates (10cmx10cm), metallised on their back face, 2mm apart. One is at the high voltage potential; the other is grounded through a 50Ω shunt. The power supply consists of a low frequency function generator, a power amplifier (130V-8A) and a high voltage transformer (130V/10kV, 3kVA, 1-20kHz). A matching network composed of an adjustable inductance and capacitances is connected in parallel. Primary and secondary currents and voltages can be measured. Gases are injected parallel to the electrodes and the pressure (1-1000mbar) is adjusted with a valve between the chamber and the pump.

A preliminary study of the glow discharge as a function of the pressure (10^3 to 10^5Pa) in different neutral gas mixtures (He, N_2, Ar) has been done to determine the basic plasma characteristics. The discharge regime for depositing SiO_x is filamentary because of the large gap used and the adjunction of reactive electronegative species (HMDSO+O_2). However, at lower pressure, a glow regime is obtained. The SiO_x layer is deposited on polyethylene (PE) films from a mixture of hexamethyldisiloxane (HMDSO) and oxygen diluted with nitrogen.

The FTIR analyses of the deposited polmer films are used to determine coating composition as a function of the position in the discharge along the gas injection axis and of the process duration. FTIR analyses are carried out with an Absorption in Total Reflectance unit installed on a FTIR spectrometer. A higher coating roughness is observed for positions on the PE substrate at the exit of the discharge zone. The coating morphology deposited on PE and measured by Atomic Force Microscopy can be related to powder accumulation in the gas phase near the discharge exit, as demonstrated by laser light scattering.

Particle formation is well known in low pressure plasmas but less studied in atmospheric processes. Laser light scattering is used to investigate dust formation in the plasma. A 300mW argon ion laser beam at 488nm with a vertical or horizontal polarization is focused in the electrode gap in the opposite direction to the gas flow. Images of the discharge gap are captured with a 12 bit CCD camera viewing perpendicularly to the laser beam through a 488nm band pass filter.

The absence of a scattered signal in the core of the discharge (0 to 5cm) could be interpreted either (i) that the particles grow as they travel with the gas flow and are still too small to be detected before the end of the substrate, or (ii) that they are blown out and accumulate at the edge of the electrodes as they reach a size sufficient to be detected. The difference between the scattered light with vertical or horizontal polarization is evidence for a Rayleigh region where light is scattered by particles much smaller than the incident wavelength. The remaining scattered light follows the Mie theory. This can explain powder dynamics in our discharge: small particles (<50nm) are trapped in the plasma, grow until they are pushed beyond the edge of the discharge by the gas, and then probably agglomerate at the edge of the dielectric.

2.6.9   *Nano powder synthesis by thermal plasmas*

The goal of this joint project between the EMPA Thun and the CRPP is to monitor the process of nanometer particle formation in a thermal RF plasma. The aim is to understand nano-particle synthesis and the growth mechanism and to develop *in situ* process monitoring for nano-particle processing in inductively coupled RF thermal plasmas. Several *in situ* powder and plasma diagnostics have been designed, constructed and are available now available at the EMPA Thun to study plasma processing of nano-powders. Extinction measurements simultaneously available at two distances from the torch exit enable the monitoring of the amount of non-evaporated, primary powder. An additional diagnostic, optical emission spectroscopy, is simultaneously applied at the same location. The emission spectroscopy can be used to obtain basic information on the plasma chemistry, in particular the plasma composition. The use of a digital camera gives qualitative information on plasma flow and powder flow pattern. The melting and/or evaporation zone of the injected powder below the torch nozzle exit was diagnosed by an enthalpy probe. These diagnostics can be used to optimise the thermal plasma with respect to enthalpy which is related to the distribution of available RF power in the plasma-powder reaction zone. Various plasma parameters such as gas mixtures and gas flow rates have been varied to find the most appropriate process parameters for nano-powder formation.

In order to obtain high quality mono-dispersive nano-powder, no primary particle should pass the reaction zone untreated. The chemical composition of the primary particles, the plasma source and the powder feeding rate must all be optimised to obtain complete evaporation of the primary particles. In the melting and evaporation regionm chemical reactions take place, as well as the nucleation phase finally leading to nano-particle formation.
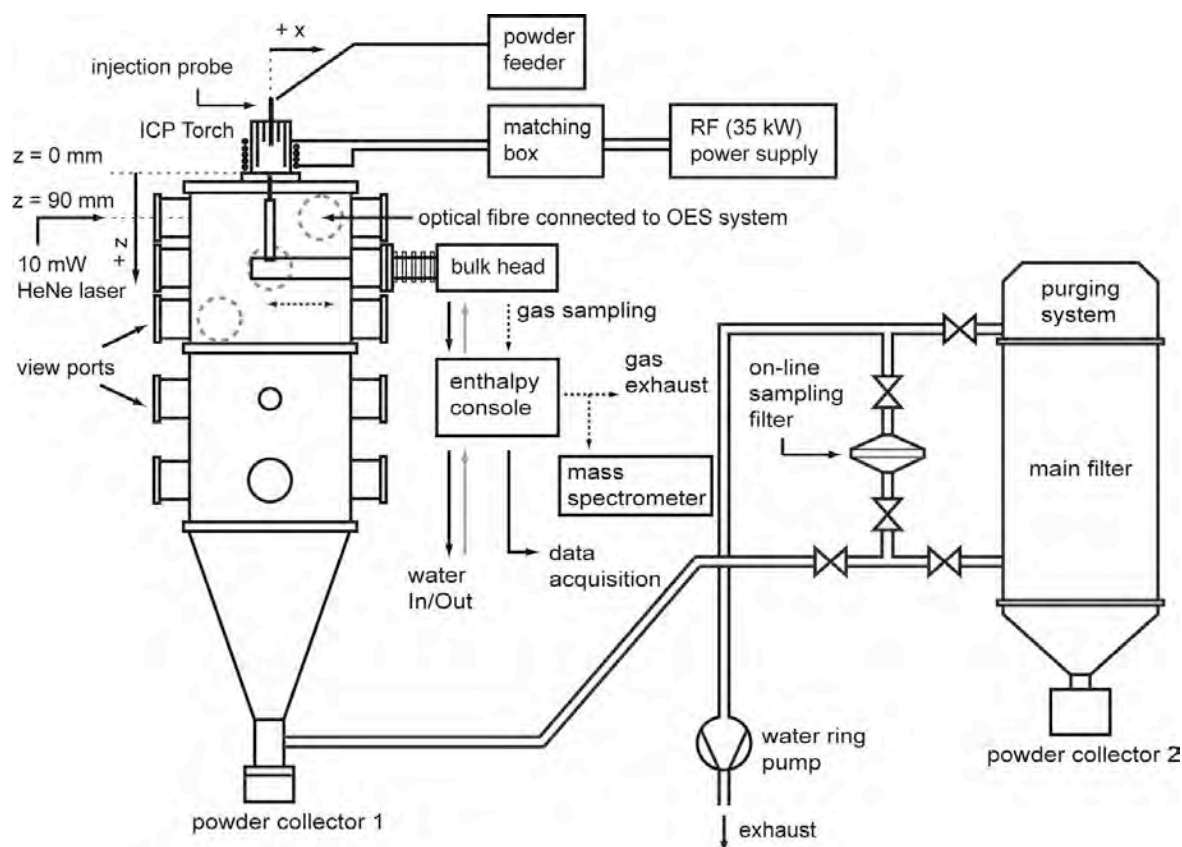
Fig. 2.6.8   *Schematic of the experimental set-up at the EMPA Thun for nano-powder synthesis.*

The nano-powder synthesis system consists of an induction plasma torch, a synthesis reactor, a filtration unit, and a powder feeder illustrated schematically in Fig. 2.6.8. The induction plasma torch used at 13.56MHz is mounted on the top of the synthesis reactor and operated with argon and hydrogen gases with a maximum RF power of 35kW. Argon is used as the core gas and a mixture of argon and hydrogen as sheath gas. This powder injection probe is connected to a commercial powder feeder operated by continuous volumetric dosing.

Two sampling stations allow extraction of samples for *ex situ* characterisation. *Ex situ* characterisation of the produced powders by various methods such as SEM, TEM, X-Ray Diffraction (XRD) and BET showed consistent results with the above mentioned process behaviour.

We found that the central gas flow of the RF torch has an important influence on the melting and evaporation of the primary particles. For low central gas flow rates, the flow pattern is laminar and the powder flow remains in the hot central part of the plasma jet. High central gas flows leads to turbulent gas and powder flow patterns. Furthermore, a higher enthalpy was measured for low central gas flow rates. The influence on nano-particle formation is shown by the fact that at low particle/carrier gas flow rates, a higher volume fraction of finer particles and a

lower fraction of untreated particles were measured by the *ex situ* powder characterisation methods.

Optical emission spectroscopy and laser light extinction measurements are carried out to monitor the on-going process *in situ*, which gives real-time information on precursor evaporation. Alumina powder was used as precursor material. After injection of the alumina precursor, specific emission lines of aluminium metallic vapour indicated the dependence on the process parameters. Besides this, extinction of laser light is used to estimate the number density of non plasma-treated powder on the laser path, from which the number fraction of evaporated particles can be estimated. Finally, particles are collected after the synthesis process and their size and morphology are characterised *ex situ*.

Optical emission spectroscopy showed that the intensity of the Al emission lines is a reasonable monitor for the vaporisation of the Al_2O_3 precursor particles. The maximum in the Al emission intensity as a function of the powder feeding rate indicates that for low feed rates, a precursor deficient regime is reached. The Al emission intensity also decreases for higher feed rates indicating that the energy deficient regime is obtained. The maximum volume fraction of large particles can reach a few tens of percent at these locations and for the highest feed rates.
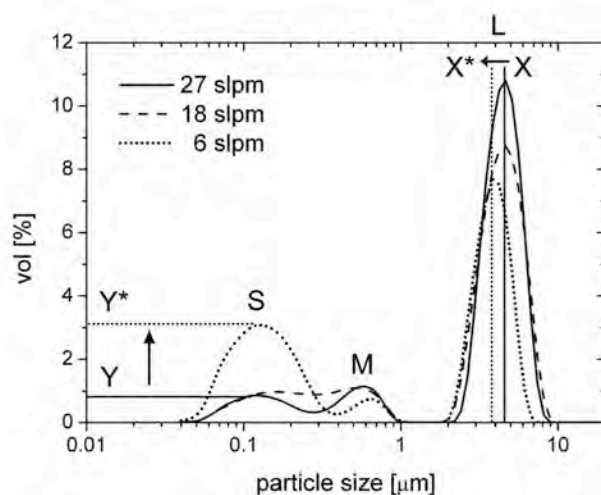
Fig. 2.6.9   *Particle size distribution of the collected alumina powder.*

The synthesized particles are collected by an on line sampling system and characterised *ex situ*. Figure 2.6.9 shows the size distributions of the collected particles. As for all three central gas flows, multimodal distributions have been obtained. The measured particle size of the large particles is at 4-5μm which corresponds well to the mean size of the alumina precursor powder. The presence of large particles implies that a part of the injected precursor has not been plasma-treated. However, a decrease in the volume fraction as well as in the size of the large particles is observed with decreasing central gas flow as illustrated by the centre line shift from X to X* (3.7-3.1μm) in Fig. 2.6.9. This decrease can be explained by more precursor powder being plasma-treated and evaporated with the lower flow rates of the central gas as the OES results show. One peak is around 100nm, marked as S, and the other is around 600-800nm marked as M. The M particles are assumed to be large hard agglomerates made up the fine particles which cannot be separated from each other by an external shear force such as ultrasonic treatment. The S particles are expected to include the synthesised primary nano-particles and the small agglomerates. The flow rate of 6slpm central gas creates a drastic increase of S particles in the volume fraction 0.8-3.1% (Y to Y*) compared with the higher flow rates of central gas. This can be due to the increased

precursor evaporation and the higher plasma cooling rate, as shown by the optical emission spectroscopy and the enthalpy probe measurements.

2.6.10   Arc Phenomena in Space Environment and Equipment

The arc is one of the oldest topics in plasma physics. Arcing is once again a key issue in the application of plasma in industry and also, as in this project, in space environment and space equipment. Modern satellites, in particular transmission satellites, require larger and larger electrical power systems. This tendency leads to complication due to possible arcing in the satellite power system. Arcing starts to be the limiting factor in several other plasmas applications, thus triggering intense research and development on this topic.

In the present work for ESA in collaboration with Mecanex SA in Nyon and ONERA in Toulouse, the fundamentals of arcing will be established and applied to the space equipment, to reduce or suppress arcing in space environment and equipment.

In order to investigate arcing, a micro-plasma device has been mounted in a small UHV vacuum chamber in which a controlled atmosphere can be created. The distance between two electrodes is accurately controlled with a piezo-actuator allowing for distance control within the nano-meter range (Fig. 2.6.10). Various gases at pressures from ultra high vacuum up to several mbar pressure can be used for the different arcing experiments.

The sustaining voltage of such a discharge should be similar to the one encountered in the slip-ring on the spacecraft. Furthermore, the plasma is accessible for further characterisation, an important point for advancing the understanding of arcing in the space environment.
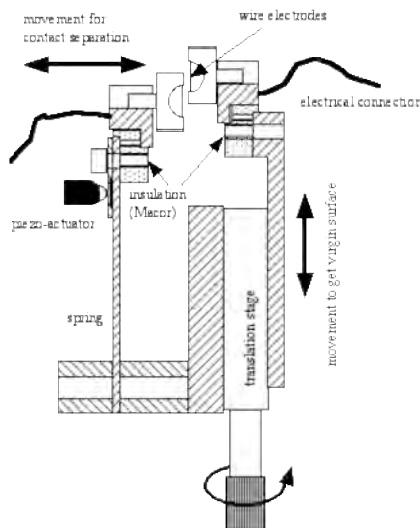
Fig. 2.6.10   *Experimental set-up for precise contact opening under high vacuum conditions.*

Contact openings under various conditions (<60V and 1.5A) have been investigated at atmospheric pressure. It was found that several distinct arc events occur before the final contact opening cuts the current to zero. Depending on the experimental set up, more than 7 different successive arc events could be observed. During such an experiment the final contact opening was at a separation of about 5-6μm, occurring 0.5s after starting the wire movement. Each of these events consists of a series of individual arcs since the voltage traces and the light simultaneously detected by a photomultiplier are correlated. During such an event, the current delivered by the power supply decreases very fast in a first phase, followed by a

slower exponential current decrease. The arcing clearly consists of several spikes indicating that many short time (sub-microsecond) arcs occur. This period suddenly finishes and the current recovers exponentially to its starting value. During this second part no light is emitted indicating the absence of any plasma. If the separation is large enough, the current decrease in the first phase approaches zero. This arc interruption is followed by exponentially-damped oscillations driven by the energy stored in the different elements of the electrical circuit. A first interpretation of the observations is that the arc melts sufficient material from the wires that a liquid bridge can be formed between them, establishing full contact again. However, if the separation of the wires is too large the arc interruption is followed by the contact opening.

Presently, the dependence of the number of events, the event duration and the decrease of the current is investigated as a function of the key elements in the electrical circuit such as inductance, capacitance and the current. In addition, the emitted light from the arc will be analysed spectrally by means of a fast camera coupled to an optical monochromator.

2.6.11   Modelling for industrial plasmas: Uniformity study in large-area showerhead reactors

Large area plasma-enhanced chemical vapour deposition (PECVD) of thin films such as silicon nitride is widely used for thin film transistor fabrication in the flat panel display industry. The uniformity requirement of the film properties over the substrate becomes more and more stringent due to the high-quality market demand. Despite this attention on PECVD reactors, only a few comprehensive models have been developed, mainly due to the complexity of the plasma behaviour and of theengineering requirements. In fact, large area reactors are affected by a considerable number of process parameters such as reactor geometry, gas injection distribution, powder contamination, voltage nonuniformity, and perturbations due to reactor edges. In this context, this project plays a crucial role in proposing a valid computational tool to understand the fundamental physics of the SiN thin film deposition process better.

A detailed model of PECVD in rectangular geometry requires the simultaneous three dimensional solutions of Maxwell's equations, the mass continuity equation, the momentum equations, and the neutral and charged species mass transport equations. CFDRC ACE® software by the ESI group offers the capability of dealing with such a complex problem in the fully three dimensional space. To decrease the computational complexity of the problem, Maxwell's equations for the electromagnetic effects (voltage nonuniformity due to standing waves, and perturbations due to reactor edges) and the flow injection distribution thorough showerhead electrode are solved separately and then coupled to the main solver by CRPP software. The present model can not only predict the overall deposition rate profiles, but also characterise the film composition. Figure 2.6.11(a) represents the overall deposition rate profile on the substrate, and Fig. 2.6.11(b) gives the film composition (Si to N ratio) for the same process conditions. By varying the process parameters such as the flow injection distribution, the relative gas injection flow rate and the input power distribution, the model will be able to predict deposition rate profiles and degree of nonuniformity leading to a possible new reactor configuration.

(a)   (b)
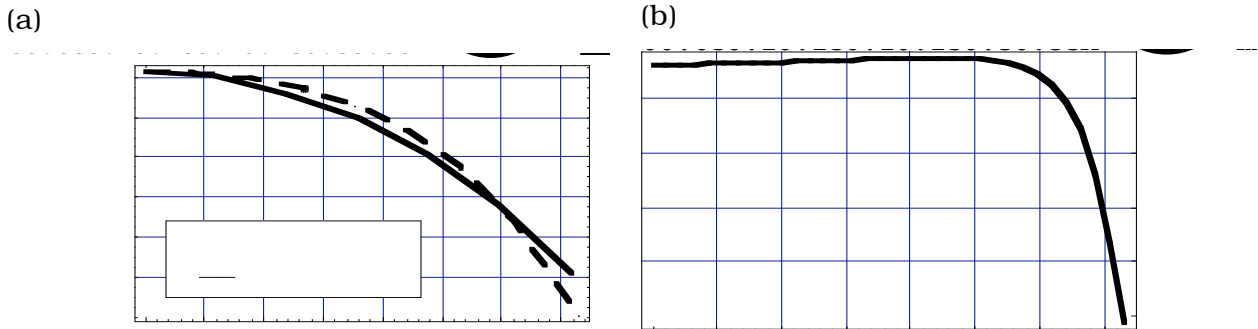
Fig. 2.6.11 *a) overall deposition rate profile on the substrate, b) film composition (Si to N ratio).*

The non-uniform deposition of silicon nitride in the UNAXIS KAI-1 800 Plasmabox reactor cannot be reproduced by taking into account only the standing wave effect, whereas good agreement is found when the local power dissipation into the plasma accounts for both the electrode dimension effect (standing wave) and electrode edge asymmetry (telegraph effect). The experimental observations show two distinct deposition profiles in the rf and ground sheath which cannot be explained by the standing wave effect alone. The telegraph effect provides different distributions in each sheath, which give the sources for the different deposition rates on each electrode. The results of the present work are also compared with the outcomes of the two-dimensional model previously elaborated to demonstrate the importance of electromagnetic non-uniformities in film deposition. The deposition profiles of each electrode have been measured in two different experiments.

2.6.12 *Influence of a weakly ionised boundary layer on transonic and supersonic air flow*

The project proposes an experimental investigation of the modification and dispersion of shocks that arise in transonic and supersonic flow by use of a weak ionisation of the gas generated by a surface discharge. The modification of the flow structure and shock wave structure with the ionised air are investigated and compared with the model and the former experiments without the plasma layer. The investigations also include studies on the effect of the surrounding flow on the stability of the glow discharge. This project is performed in a collaboration between the Laboratoire de Thermique Applique et de Turbomachines (LTT) and the Laboratoire d'Ingénierie Numérique (LIN) of the Energy Institute (ISE) from the Faculty of Engineering (STI) and the CRPP.

The experimental research at the beginning of this project focused on two problems. First, to choose or develop materials that can withstand the atmospheric plasma for a long duration and in the presence of a fast airflow. Second, to identify measurement techniques suited to the characterisation of the plasma and the aerodynamic measurements in the presence of plasma, in particular, the evaluation of the power dissipated in the plasma.

The development gave two very important results: the lifetime of the dielectric barrier discharge plates increased to more than 10 hours and an interaction between the plasma and the airflow was demonstrated using spectroscopic techniques. Various diagnostics have been evaluated and adapted to study the small-sized faint plasma: high voltage and current probes are used to measure the input power and estimate the power dissipated in the plasma. Photomultiplier

signals are correlated to the current signals to investigate the nature of the plasma (which has a glow and a filamentary component). CCD imaging gives information about the plasma geometry and emission integrated over the whole visible spectrum. Finally, optical emission spectra are analysed to study the excited species in the plasma. All these diagnostics confirmed that more power is dissipated in the plasma with higher excitation frequencies. This power dissipation takes place in the glow component of the discharge. The efficiency of the system has been estimated (20-30%). It turns out that optical emission spectroscopy is the most promising diagnostic for gaining information about the plasma characteristics and it shows an effect of airflows as slow as 15m/s on the emission from the plasma.
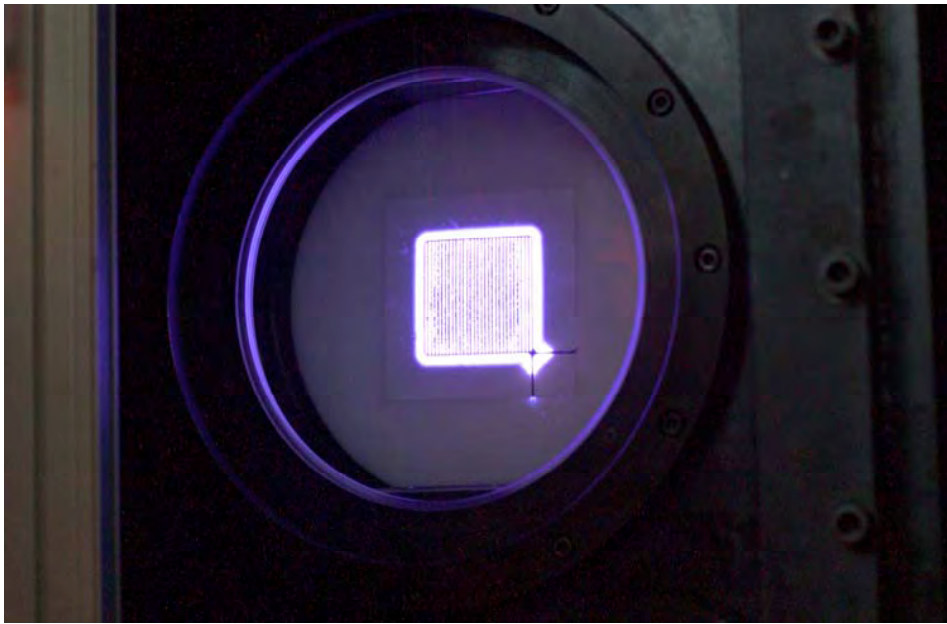
Fig. 2.6.12   *View of the plasma in the Laval nozzle*

A second measurement campaign has been carried out on the effect of airflows up to 65m/s on the dielectric barrier discharge. The power dissipated in the plasma is reduced when the airflow speed is raised. A change in the geometry of the discharge is visible on the CCD images as a function of the airflow speed. When the velocity of the flow is higher, the filamentary nature becomes more important compared with the homogeneous, glow nature of the plasma. To prepare the third measurement campaign to study the effects of transonic flows over the flat discharge, the high voltage electrical circuit has been rebuilt to make it transportable from CRPP to LTT and the plate has been placed in the Laval test nozzle of LTT, on a newly designed polyoxymethylene window. The flow was regulated to Mach=0.6, and the plasma could be started, Fig. 2.6.12. The first important result is that it is possible to sustain the plasma at this speed.

2.6.13   Helyssen SARL, a start-up company at the CRPP

Helyssen SARL; a new start up company, has installed a test bed in the laboratories of the industrial plasma group to evaluate the performance of an innovative plasma source based on the Birdcage Antenna. The performance of this plasma source will be compared with standard Helicon plasma sources. The magnets and the equipment for benchmarking and necessary infrastructure have been lent to Helyssen SARL by the CRPP, including equipment for plasma diagnostics and know-how quantify the performance of the two RF plasma sources.

The results of the development and research of Helyssen SARL during the last year resulted in an extremely efficient Helicon source which is of considerable interest to some industries.

This collaboration was established with the help of the Service des Relations Industrielles (SRI) of the EPFL.

2.6.14   Teaching and education

In Switzerland many companies use various types of plasmas in research and production. However, basic knowledge of the plasma physics and of the plasma processes are usually lacking. In addition, our experience over the past years clearly showed that in general a wrong picture of the plasma exists. In collaboration with Prof Keppner of the Haute Ecole Arc Ingénierie at Le Locle, an introductory course into plasma physics and its application in industry has been prepared and will be given for the first time on 25/26 November 2005 in LeLocle. This course will be given in the frame work of the Swiss Vacuum Society (Swiss Vacuum). The course is addressed primarily to people in the field of plasma applications such as deposition, etching or applications of plasma surface modification, decoration, optics and microelectronics.

The competence of the plasma industrial group in vacuum and vacuum physics was also used in an introduction course to vacuum and its applications. This course as well in the frame of the Swiss Vacuum Society, has been given twice this year on request of the CERN.

3 Technical achievements of the CRPP in 2005

3.1 TCV Operation

TCV operation resumed early in January 2005 after a 3 month shutdown at the end of year 2004. It was entirely devoted to the scientific exploitation of the device on a basis of 5 days of operation per week, except for small interruptions and maintenance periods, and will continue so until the end of 2005. Operation was however suspended during July and August because of summer holidays and for the acceptance tests and the commissioning of a repaired X2 gyrotron.

3.2 Diagnostics

Over the last year the general trend has been the stabilisation of the main diagnostics installed on TCV, the commissioning of some newer diagnostics and the design phase of diagnostics which are being prepared to answer physics issues which the present diagnostic array can not address. As we approach this more mature phase of the TCV diagnostic set, some of the simpler diagnostics, which had often migrated from TCA, are being removed from TCV because their yield is less to the TCV physics programme, than other diagnostics which require the same port access. In general it is the combination of diagnostic measurement, addressed physics issue and the availability of suitable TCV access and operating personnel that must be reconciled.

This is becoming especially true for the diagnostics still at the planning stage when their installation necessitates the displacement or temporary removal of existing diagnostics and where their operation will require the full time attention of one or more of the available physics personnel. The new range of diagnostics are often more intricate and experimental than the range of fundamental diagnostics already installed on TCV.

In the rest of this section some of the most important changes in the diagnostic array of TCV are reported.

3.2.1 Thomson scattering

Alignment stability is a major concern of the Thomson scattering system. Even small angular deviations of the laser beams lead to loss of calibration and result in unreliable measurements of the electron density profile. From the laser output to the TCV vacuum chamber the laser beam paths are ~20m long, including several folding mirrors and a focusing lens combination. Although the requirements for good passive stability were considered in the design, occasional perturbations and slow drifts of this path cannot be excluded. In order to verify the alignment on a regular basis, a set of 4 CCD cameras has been installed at several reference points (see Fig. 3.2.1). They view the actual laser beam pattern by recording the scattered light from an intercepting optical surface (mirror, window or lens) together with a fixed marker or reference point which is also in the camera's field of view. In this way a deviation of the beam from its nominal location may be immediately detected. Small "Webcams" are used for this purpose; they have adequate intensity response at the laser wavelength of 1.06 microns (Nd:YAG laser wavelength), are compact and may be connected to a server-PC using relatively inexpensive commercial

software. The real-time images from all the cameras are accessible from a Web browser with a high-speed connection to the CRPP communications network. This installation has proven to be extremely useful in the early detection of alignment problems and as a tool during the alignment procedure.
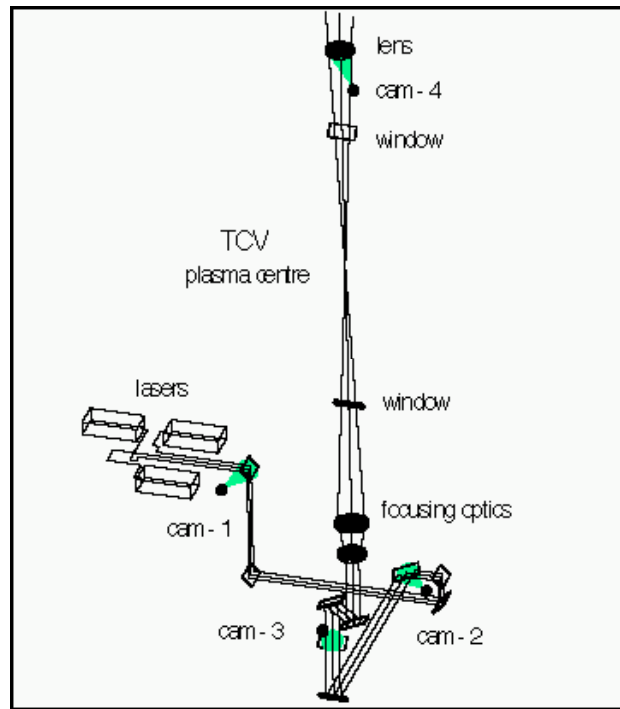
Fig. 3.2.1   *Alignment scheme for Thomson control using CCD cameras*

The interest in measurements of T_e and n_e near the edge with improved spatial resolution (1cm instead of 3cm in vertical direction) continues. Following the return of a system on loan from Consorzio RFX had and before a new dedicated system of our own design is available, we have installed some existing equipment that was modified for the purpose. Using a set of 10 spectrometers with 3 spectral channels, it will be possible to cover the range of Z=+51cm to Z=+62cm (top of the TCV vessel). The given filter set (Fig. 3.2.2) is suitable for temperatures ranging from 20eV to 1keV. However, the sensitivity was found to be marginal at low densities ($<1.10^{19}\text{m}^{-3}$) which should improve with the new design currently in progress.
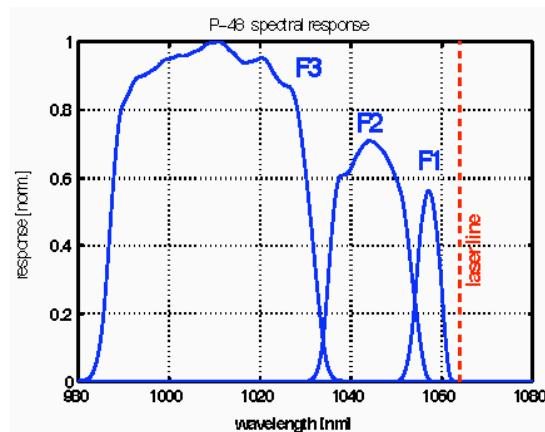
Fig. 3.2.2   *Thomson filter set for measurements near the plasma edge*

3.2.2   *Diagnostic Neutral Beam Injector (DNBI) Operation*

The DNBI was operated throughout 2005 with a mean energy 46keV and mean ion current of 2.2A. The reduction in the beam energy (nominally 50keV) and the beam current (nominally ~3A) were due to degradation in the capacitors of the DNB power supply. A new set of capacitors with a higher voltage specification have been ordered and should solve this issue. The beam and control software performed reliably with relatively few discharges lost due to problems or maintenance requirements such as cryopump regeneration. The beam availability was about 95%, and DNBI was used for 831 plasma tokamak discharges (of 1913 TCV plasma shots). The H^+ (primary energy) fraction was ~50 % of the total beam ion current. In order to increase the beam purity and reduce a beam divergence the RF-plasma generator will be replaced with an Arc plasma source early in 2006 in a contract with Budker Institute (Novosibirsk, Russia). This upgrade is hoped to increase the ratio of active to passive signals in CXRS measurements by a factor of 2-2.5 increasing the signal quality and the density range of CXRS ion measurements.
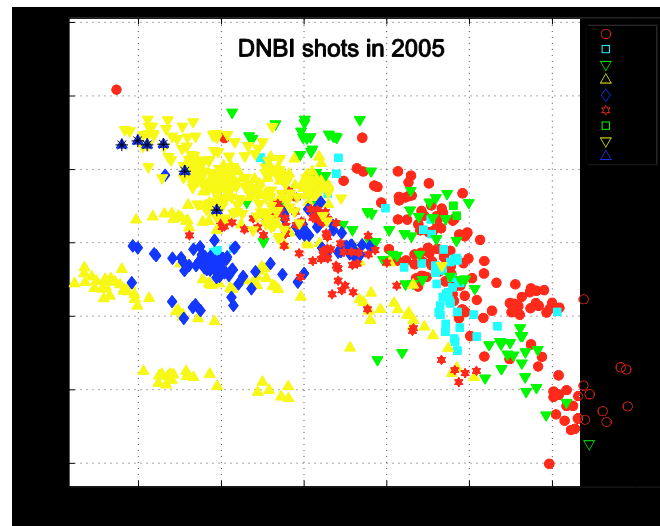
Fig. 3.2.3   *Beam Energy vs. Ion current during the 2005 campaign*

3.2.3   *Neutral Particle Analyzers*

The control of both Compact NPA (CNPA) and a scanning 5-ch. NPA has been migrated to the new plant control system of TCV. This has significantly increased the availability of NPA measurements since they may now be selected by any of the diagnosticians.

To calibrate the energy scale of the CNPA and to monitor changes in the channel sensitivities, a heated alkali ion source with a high voltage accelerating potential was installed in the beam line of the CNPA. Like the similar source in the other NPA, the source may be inserted in the CNPA flight line without breaking the NPA vacuum. The system injects ions in the 100-2000eV energy range and will also be used to calibrate the mechanical shields that will be installed for the low energy CNPA channels in 2006.

Low density discharges on TCV, especially used for ECH experiments, can produce a high intensity of high energy X-rays. The proximity of the CNPA to TCV and the relatively large size of the CNPA detectors can result in a strong Hard X-ray driven pollution to the CNPA detectors. A 7cm thick lead screen has been installed

between CNPA and plasma volume of TCV, (Fig. 3.2.4), which has significantly reduced this problem. The remaining problem with the scattering of light inside the CNPA (recorded by the detectors) will be addressed by inserting extra baffles in the CNPA flight line and possibly inside the CNPA chamber.
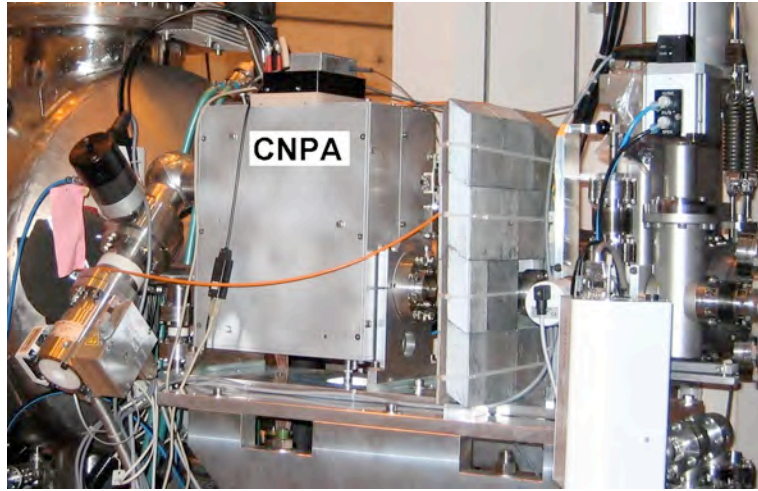
Fig. 3.2.4 *The CNPA device with the lead wall across the flight line to TCV (on the right).*

3.2.4 Tangential X-ray detector array

A new tangential X-ray diagnostic has been designed in collaboration with RRC-Kurchatov Institute (Moscow, Russian Federation) and is currently under construction in Moscow, with installation on TCV scheduled for early 2006 (Figs 3.2.5 and 3.2.6). The diagnostic features six movable, tangentially viewing CdTe detectors to provide fast ($10\mu s$) and radially localised (2cm) measurements of 2-200keV Bremsstrahlung emission in the direction parallel to the magnetic field, from a chosen location in the plasma, by orientating a collimator arrangement. These measurements are intended to provide insight into the physics of magnetic island formation, of runaway electron production and of electron acceleration associated with electron cyclotron current drive. [RRC Kurchatov Inst., Moscow, RU]
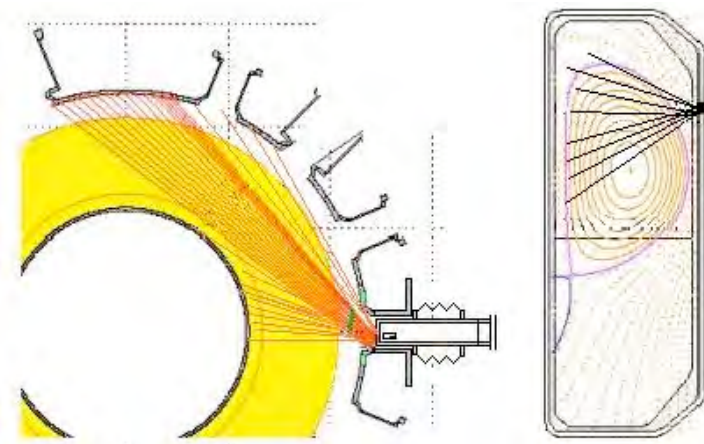
Fig 3.2.5 *Toroidal (left) and poloidal (right) projections of the available lines of sight of the tangential X-ray detector system*
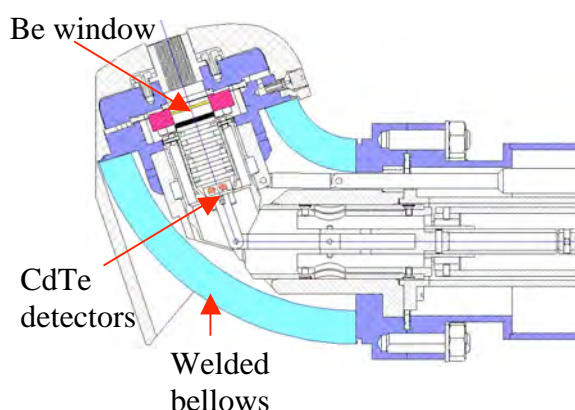
Fig. 3.2.6   *Schematics of the Tangential X-ray camera showing the flexible bellows that allows the sight line to be orientated externally.*

3.2.5   CXRS diagnostic

The installation of the vertical Charge eXchange Recombination Spectroscopy diagnostic has been completed, with the upgrade of the observation head together with corresponding changes to the spectrometer and detector setup.

The system observation head is located on a port under the Neutral Beam Injector under the machine vessel. This configuration permits the measurement of the poloidal component of plasma rotation from the Doppler shift of the measured CXRS spectral lines compared to the unshifted thermal wavelength. The collected light is focused onto a set of 40 optic fibres, and transmitted to the monochromator. The observation head, like the head of the existing horizontal observation optics, has been equipped with a calibration neon pen lamp, which may be placed in front of the fibres by means of a remotely controlled pneumatic translator, providing a reference calibration light source. The lamp is remotely installed in the optical path after a TCV plasma discharge calibration so that thermal and other mechanical changes to the absolute spectral calibration may be followed, Fig. 3.2.7.

For the spectral analysis of the collected light, a SPEX750Mi spectrometer in a Czerny-Turner arrangement has been installed, equipped with a 2400 l/mm holographic grating. The fibre ends are vertically aligned at the entrance slit and then imaged on to a back-illuminated CCD detector (XCAM, 512x512 pixels, 0.67x0.67 mm^2). A 3 coaxial lens optical adapter was designed and installed at the exit slit of the spectrometer, to reduce the size of the image by a linear factor of 2 to match the vertical size of the CCD. In order to maximise the registered signal/noise, the detector is operated while cooled to -30°C by a Peltier stack, itself cooled by a refrigerated water circuit, and kept in a N_2 atmosphere to avoid ice deposition on the chip. This arrangement covers a spectral range of 50Å at the central work wavelength of 5291Å used at these wavelengths, Fig. 3.2.8.
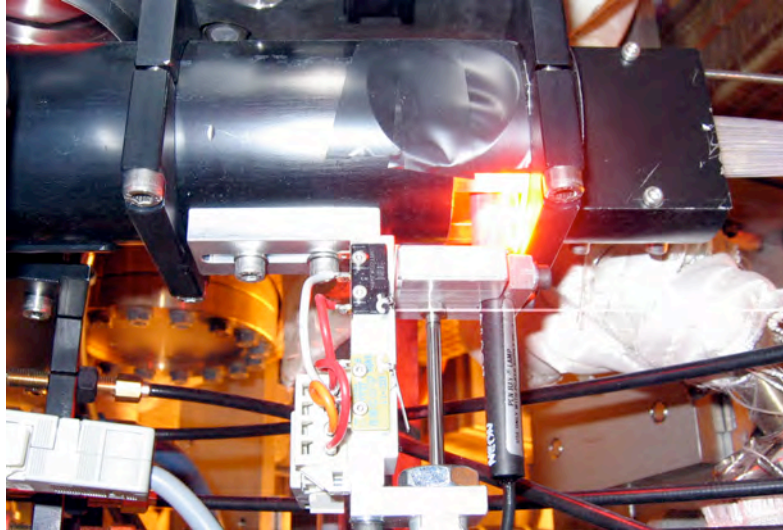
Fig. 3.2.7 *Photograph of the vertical observation head during a wavelength calibration: the Ne pen lamp moves in front of the fibre ends (on the left) illuminating the spectrometer with light of a known wavelength.*

Up to 40 vertical measurement chords from the vertical camera span the external region of the plasma, to measure the poloidal rotation, providing edge profiles with a high spatial resolution (5mm). This diagnostic will be particularly important in the measurement of edge ion temperature, density and rotation, particularly in the H-mode and eITB studies, where the radial electric field (which can be inferred once the toroidal and poloidal rotation are known) is expected to play a major role. Furthermore, the reduced distance of the vertical camera to the plasma compared to the horizontal camera results in a stronger spectroscopic Charge-Exchange signal (less polluted by the passive plasma component) which extends the diagnostic potential to higher plasma densities without a beam upgrade, Fig. 3.2.9.
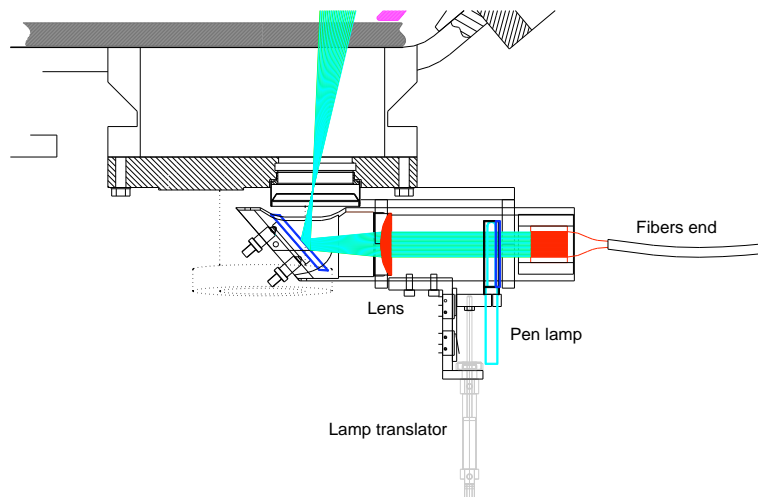
Fig. 3.2.8 *Scheme of the observation head. The optical system is composed of a mirror and a lens focusing the light coming from the plasma onto the fibre ends. The Ne wavelength calibration lamp is also shown.*
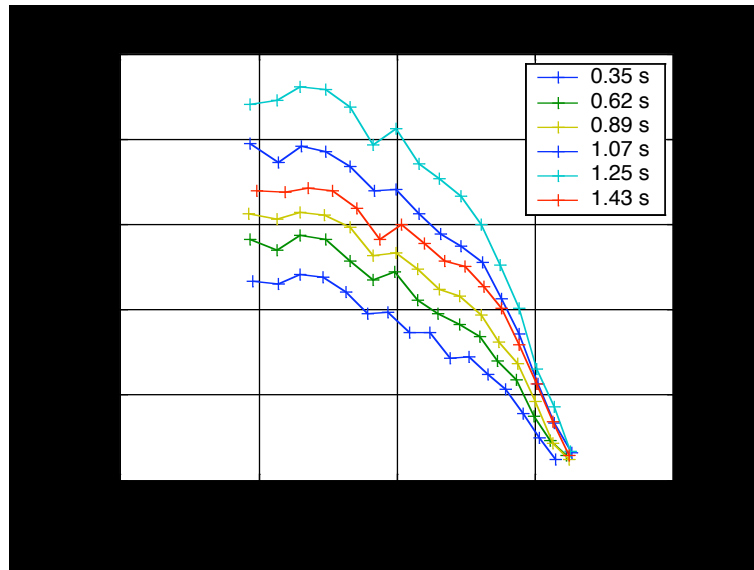
Fig. 3.2.9   *Emissivity profiles of the Carbon VI 529.1nm spectral line, measured by the vertical CXRS diagnostic, indicating the increase of the carbon content during a plasma density ramp.*

3.2.6   PHA-Vertical

The vertical Pulse Height Analysis diagnostic installed on TCV measures the soft X–ray emissions from 700eV up to 10keV along a vertical line of sight, with an energy resolution of 150-175eV. A compact Silicon Drifted Detector (SDD) Peltier cooled diode, consisting of a thin (~300μm) fully depleted silicon wafer sensitive in the soft X-ray range and virtually transparent to X-ray energies above 15keV. The radiation entrance side is a non-structured p+ junction, giving a homogeneous sensitivity over the whole detector's sensitive area (~5mm^2), Figs 3.2.10, 3.2.11.

Preliminary experiments employing a commercial CAMAC based DSP card with fluorescence radiation excited by X-ray radiation from an X-ray tube, showed that the energy resolution starts to degrade with over 100kHz input count rate. Between 1-3MHz, the detector is still able to deliver spectroscopic information with a resolution that is satisfactory for fast counting PHA applications.

Signal conditioning and processing for TCV experiments is achieved with a commercial multichannel analyser (MCA3) installed in the PCI bus of a personal computer. The throughput capacity is in excess of 1Mevents/s depending on the shape and duration of the input pulses. It has been possible to obtain spectra with spectroscopic quality and observe the temperature evolution every 100ms during a 2 second pulse.
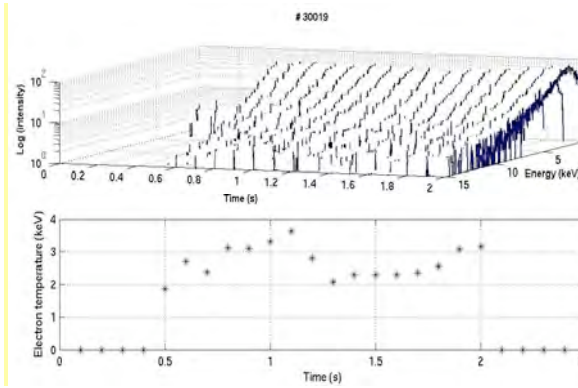
Fig. 3.2.10 *The logarithm of the soft X-ray intensity against photon energy at different instants in time for two operational TCV regimes (Ohmic Heating Only)*
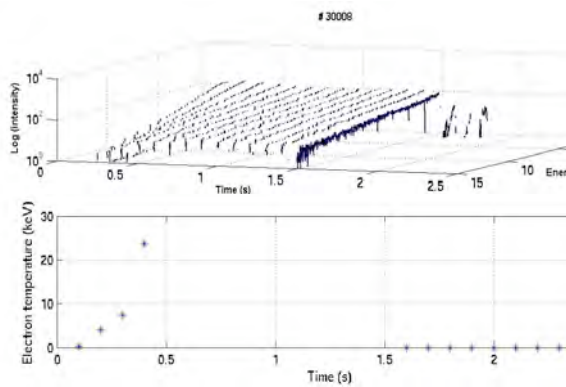
Fig. 3.2.11 *With ECH and ECCD*

3.2.7   Fast Infra-Red camera

There are currently two IR camera and associated relay optic systems operating on TCV, viewing in-vessel surfaces corresponding to the target areas of typical diverted plasmas. Each system is equipped with un-cooled micro-bolometer IR cameras which are limited in time resolution and cannot observe surface heating due to transient events such as Edge Localised Modes (ELMs) and disruptions. Recent observation of large ELMs during X3 heated X-modes on TCV have motivated the replacement of one of the present systems with a fast camera capable of resolving power deposition on the ELM timescale and possibly the fine, filamentary structure now known to characterise the instability as it propagates in the scrape-off layer. To this end, the CRPP has recently ordered the highest performance commercially available IR camera. A unique feature of the Thermosensorik CMT 256 M HS high speed IR camera is the 880Hz framerate (at T_{int}=1.2ms). In subframe mode, rows or columns of pixels on the FPA (minimum 8 pixels wide) can be freely chosen and the snapshot acquisition frequency increased up to 20kHz for the lowest T_{int}. In a joint agreement with IPP Garching (who are buying the same camera) and CRPP, Thermosensorik will provide direct optic fibre coupling to the camera head for noise-free, real time digital data transfer to the host PC.

A Cadmium-Mercury-Telluride (CMT) 256x256 pixel focal plane array (FPA) maintained at liquid nitrogen temperature using a closed cycle Stirling cooler. The camera operates in the 3.4-5.1μm waveband (MWIR) using snapshot (integrate while read) operation with integration times, T_{int}, in the range 10μs – 1.2ms and 14 bit digital data output. A unique feature is the 880 Hz framerate (at T_{int}, 1.2ms). On TCV, as elsewhere, the typical risetime for surface power deposition at the arrival of the ELM front is expected to be in the range ~100μs, within the range of the highest available subframe rate, but the ELM power deposited will be considerably lower than on larger devices (like JET) and the surface temperature rise provoked by the ELM is unlikely to be measurable at the lowest T_{int}. It is known, however, that in

tokamaks containing carbon (like TCV), thin, poorly adhered surface layers can be present on target tiles which result in anomalously high surface temperatures in response to transient events. It is hoped that such phenomena might allow the ELM temporal fine structure to be resolved. All the traditional physics of steady state divertor power deposition will nevertheless continue to be possible, with the added benefit of significantly higher baseline full frame rates (880Hz compared to 50Hz with the existing system).

The current lower divertor relay optics system will be reused, albeit with a likely switch in material from the present ZnSe vacuum window and with some of the Germanium lens elements replaced to account for the reduced wavelength range and the slightly smaller FPA size in comparison with the existing camera. As before, soft-iron magnetic shielding will be provided for the camera, largely to prevent damage to the Stirling cooler during tokamak operation.

3.2.8 Absolute extreme VUV (AXUV) bolometer and Lyman-alpha camera system

The installation on TCV of a new system of 7 AXUV diode cameras has been completed in 2005. Each camera contains two identical diodes (International Radiation Detectors), one for bolometry allowing the measurement of total photonic plasma radiation (at energies in the range ~10eV - 6keV) and a second filtered for L_α radiation at 120nm from excitation of Hydrogenic atoms located in the cool plasma periphery. Spectroscopic selection is achieved using VUV transmision filters (Acton Research Corporation) mounted directly in front of the diodes. These are pinhole cameras using slit apertures and their design is a modification of the concentric cylinder, re-entrant mechanical structure already employed on TCV for the soft X–ray tomography diagnostic. This new system will, in fact, eventually replace a set of 2 vertically viewing prototype AXUV bolometers and a third lateral camera used for testing the L_α filter concept.

With 7 cameras, the system provides a total of 280 viewing chords, 140 for each of the two diode sets (bolometry and L_α), giving unprecedented coverage of the TCV poloidal cross-section at a single toroidal location for tomographic inversion of total radiation and recycling emission. These diodes are extremely fast, with a time resolution limited to ~100kHz, essentially only by the modular transimpedance amplifier electronics mounted onto printed circuit boards which plug directly onto the vacuum feed-throughs. Acquisition is performed using 3, 96 channel, 16 bit differential input digitisers, running as a networked Linux appliance.

The system is presently operating routinely on TCV – it is a passive diagnostic not requiring regular calibration once installed. Whilst the bolometer diodes are functioning correctly, there are persistent problems with the L_α systems which have not yet been identified and further tests are underway at the time of writing. Primary aims of the AXUV diagnostic are the investigation of fast transient events (ELMs and disruptions) through their radiation characteristics and, in conjunction with modelling using the SOLPS5 fluid-Monte-Carlo code package, the study of neutral recycling distributions. This will hopefully be facilitated by comparison of the AXUV data with that from an existing set of foil bolometer cameras, also measuring plasma radiation, but sensitive to both photons and the energy deposited by neutral particles. Estimates of total core plasma radiation on a fast timescale will also be possible - the absorption of some radiation by the diode passivation layer in the 10-50eV region is of little importance in the inference of emission from the hot bulk of the plasma.
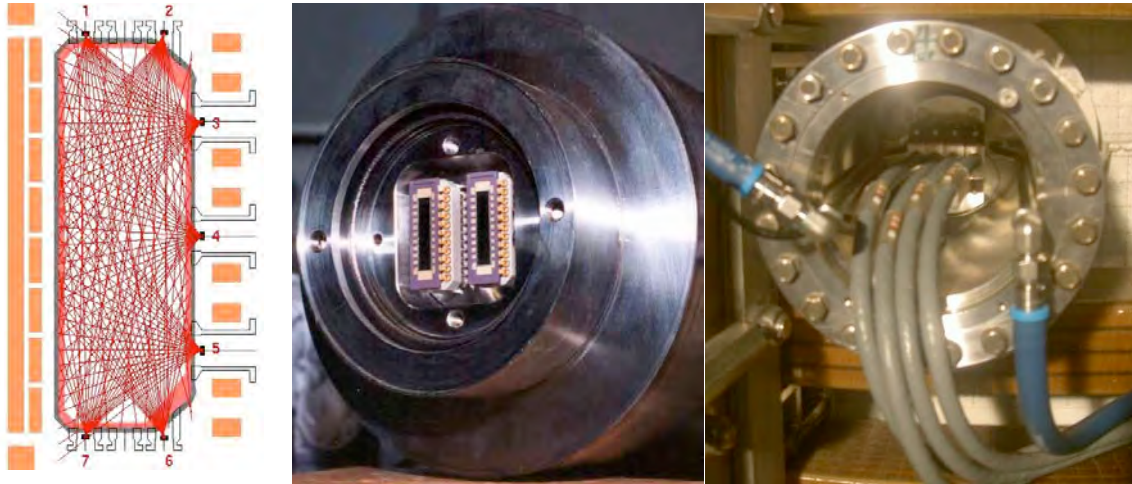
Fig. 3.2.12   *Left: Coverage of poloidal cross-section by AXUV viewing chords Centre: Stainless steel vacuum flange housing the camera with the two 20 channel AXUV 20EL linear photodiodes arrays mounted on a 22 pin DIP feedthrough. Right: One of the lateral cameras installed TCV illustrating the re-entrant port and detector water cooling.*

3.2.9   Electron Bernstein Antenna

The installation of the spare ECRH launcher in "reception" mode has been proposed. An existing damaged ECRH launcher will be repaired and installed in 2006 in a rectangular equatorial port on TCV. An oversized waveguide line, similar to the one on the existing ECE system, will lead the collected signal to a free input of the ECE radiometer.

This launcher will allow a more efficient determination of the optimal injection angle during electron Bernstein wave heating (EBWH) directly from the plasma EB emission (EBE) relying on the O x B mode conversion scheme. This arrangement offers EBE observation and the possibility of an intelligent feedback system for the injection mirror angle in EBWH and current drive (EBCD) operation. Other future applications, such as the observation of tangential electron cyclotron emission ECE, are also planned.

3.2.10   Heavy Ion Beam

The HIBP constitutes a major new diagnostic for TCV and will add a new range of measurable plasma parameters. The system can be used to determine the electric and magnetic potential and the evolution of the plasma current distribution. Correlation data of electron density fluctuations and their propagation may also be obtained and the measurements used to contribute to an improved reconstruction of the mean density profile.

A detailed design study of this diagnostic has been performed whose main results are as follows:

-   A suitable design for TCV is possible (!)
-   Single shot radial profiles up to half the plasma effective radius can be obtained
-   The total radial profile can be obtained from a shot-to-shot procedure

- There are attractive prospects for measuring poloidal flux in the plasma core region.

Due to its cost and the significant impact on TCV operation during the commissioning phase (a long shutdown will be required), it was necessary to perform an international call for tender. The deadline was 3rd of October 2005. As was expected from the small expert community in this field, a single application was received: from the UDIF company in Moscow, operating in collaboration with the HIBP group at the Kurchatov Institute. This tender is currently being analysed in detail, in view of a final decision on implementation.

A conceptual layout of the proposed equipment is shown in Fig. 3.2.13.
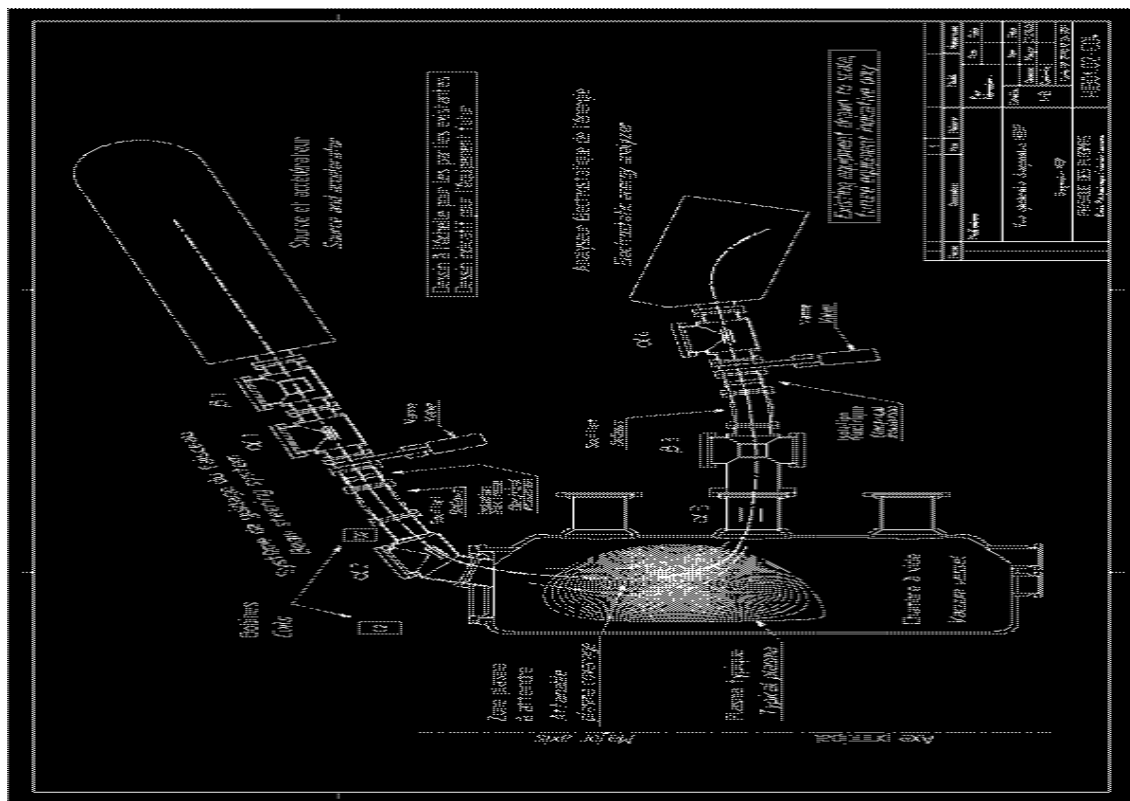
Fig. 3.2.13 Conceptual layout of the HIBP.

3.2.11 Polarimeter

A new far-infrared (FIR) polarimeter diagnostic is under construction on TCV. Following the method proposed by Dodel and Kunz (Infrared Phys, 18, 1978, 773) and successfully employed on MST (D.L. Brower et al, Rev. Sci. Instrum. 74. 2003,1535), it uses two FIR lasers at 432.5 μm, which are optically pumped by a 150W continuous wave CO_2 laser. The two FIR cavities are detuned by about 750kHz (IF) and combined using a quarter wave plate producing a laser beam with a linear polarisation rotating at the IF frequency. The beam will be split into ~10 plasma channels and one reference channel, each equipped with a Schottky diode and wire grid analyser. Faraday rotation angles relative to the reference detector will be measured by standard coherent detection. Since TCV already has two diagnostics for measuring plasma density, no simultaneous interferometry will be attempted. This leads to a substantial design simplification with respect to a previously installed polarimeter-interferometer systemon TCV, which was abandoned as a combined diagnostic ~4 years ago. As in MST, a resolution of better

than 1mrad should be achievable, permitting measurements of TCV plasmas in ECCD regimes. The lasers and Schottky diodes were previously used on the RTP device and were obtained from FOM as part of a hardware exchange agreement.

3.3 Control and Acquisition

3.3.1 Plant control and Data acquisition

A new plant automation software has been implemented on TCV. The new system allows different tasks to be performed simultaneously. Individual systems can be selected for different tasks. When a task starts, it loads the selected systems which execute their actions. The task then releases each system as soon as it has finished with it. All tasks and systems have their own processes to ensure a parallel treatment, but follow the same state machines. Moreover, each task or system is controlled by two processes, one for navigation in the state machine and the other for executing the corresponding actions. This was implemented to prevent errors in user defined action codes from perturbing the navigation in the state machine. Another independent process checks the presence of all processes and warns in case of failure.
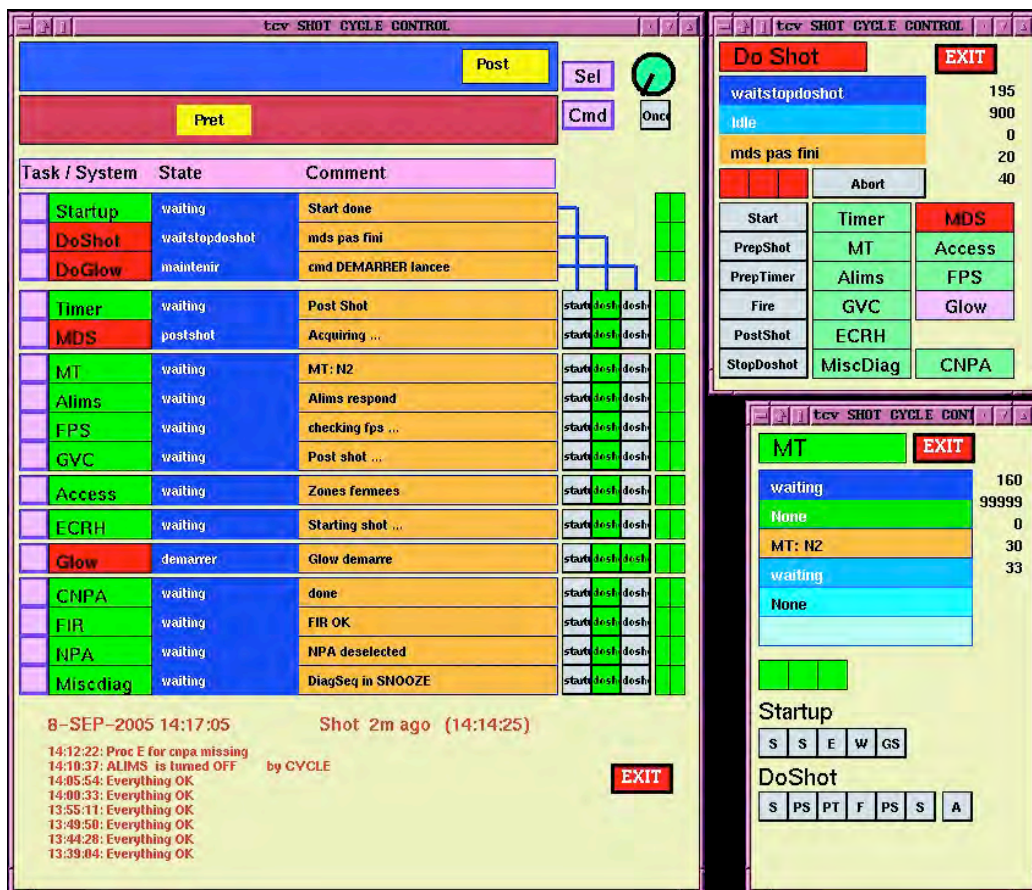
Fig. 3.3.1   *View of the plant automation*

The software is written in TDI (MDS plus) and uses a Vsystem real time database. One of the main advantages of this new system is the clear separation between task, system, state machine description, the navigation in the state machines and the actions to be executed at the different states for each system. The task and

system list is contained in one text file, the state machines, one for each task, are also described in text files. The navigation and the execution code are clearly separated from the used defined action codes.

The Vsystem GUI is used to provide the TCV pilot with a global view of all these processes. Figure 3.3.1 shows the overall survey image, together with details of one task (DOSHOT) and one system (MT).

On the data acquisition side, for the period of this report, there have been 2500 TCV shots, each generating around 250MB of data, which are compressed and stored to disk. All the TCV data, acquired and calculated, are kept on-line on hard disks, for immediate access. At the end of the year they occupy 800GB, backed up entirely on another set of hard disks and, separately, on tape.

3.3.2   Plasma control system

The upgrade of the present analogue plasma control system is based on a kernel made of 36 intercommunicating DSPs. The system developed by the IST in Lisbon has been fully assembled and is approaching its nominal specifications. Coding the control algorithms in the DSPs must avoid the use of C and assembler because the inherent risk of programming errors. In place an ad-hoc language comprising a fixed set of high-level commands was written in-house. This will permit the users to easily and safely program or modify control algorithms. This will also simplify the migration toward future digital technologies.

3.4   Heating Systems

3.4.1   X2 heating system

Gyrotrons

In December 2004, one of two repaired X2 gyrotrons passed its on-site acceptance tests. The output power and polarisation were calibrated in January 2005 and the tube was available for TCV operations from the start of the 2005 campaign. A second repaired tube passed its on-site acceptance tests in the month of July, was calibrated and made available for TCV operations from August 2005 bringing the total available X2 power back to 2.7MW. This second repaired tube suffered a short in the filament heater circuit, internal to the gyrotron, on 3 October 2005 and must be returned to GYCOM-NN for repair under warranty. A spare tube is on-hand and will be installed, calibrated and made available for TCV operations when required by the physics programme.

Auxiliaries

The gyrotron system has been upgraded to improve overall system reliability and avoid excess maintenance. The 14 collector coil power supplies of the X2 system were supplied by GYCOM, falling within the scope of delivery. Many of these power supplies have failed and were repaired. After discussions with GYCOM, and with their consent, it was decided to replace all X2 collector coil power supplies with modern, readily available, off-the-shelf supplies selected by CRPP. A modification to the control slave units was required to permit control of these new supplies. Initial tests were successfully carried out during the acceptance tests of the 1st repaired gyrotron, to the full satisfaction of GYCOM. The new supplies and modified slave units were installed on the first cluster of 3 gyrotrons before the start of operations in 2006 and on the second cluster during the June break.

Launchers

The two new launchers, installed in autumn 2004, were used for the first time, successfully, at the start of 2005. All launchers were realigned in February using the sensitivity of the sawtooth instability to the local EC driven current density at the q=1 surface to provide an *in situ* target, as usual. While the newer simplified launcher design allows a more rapid assembly, it has not improved the reliability of reaching the largest angles. Sticking still occurs on one of the two new launchers and several of the older launchers, previously free from this defect. The largest angles are required for central ECH of plasmas vertically centered in the TCV vessel and for some ECCD cases. The sticking is due to the tight tolerances required for precise aiming combined with thermal deformation of the torus during baking. If required in future, these tolerances could be relaxed to permit the largest angles, albeit with reduced precision.

Operations

Two new gyrotron operators have been trained this year.

3.4.2   X3 heating system

Gyrotrons

During the first 6 months of 2005, the three X3 gyrotrons have been routinely operated with a total injected power in the plasma of 1.35MW. From June 2006, a failure of the brazing on one of the gyrotron cryogenic-windows (sapphire cooled at LN_2 temperature) has prevented the operation the X3 system for EC-heating studies of H-mode plasmas. For this type of experiment, the maximum installed power of 1.35MW is required. The damaged gyrotron is ready to be sent back to the factory and is expected to be operational again on TCV for the second half of 2006.

Launcher

Further improvement of the real-time feedback system on the top-launch mirror angle has been achieved by adding to the proportional term an integral term into the analogue controller. The relevant signals are shown in Fig. 3.4.1.
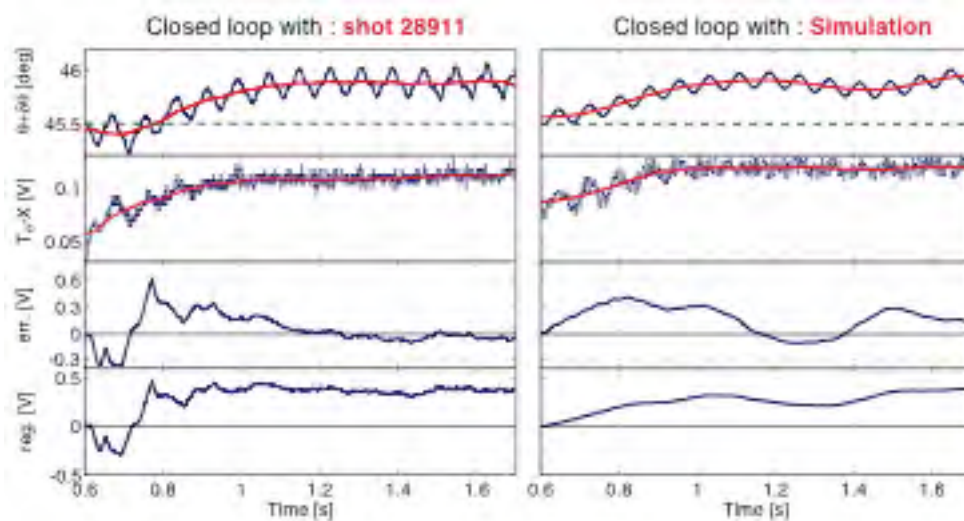
Fig. 3.4.1 *On the left, dynamics of the closed-loop feedback system on a plasma shot where the external reference has been set to a constant angle of 45.5^0. In this shot a PI controller was used and one can see that after a transient period of approximately 250ms the error signal (third-signal from top) reaches a constant zero value consistent with the presence of the integral term in the controller. On the right, simulated dynamics of the closed-loop feedback system using the Simulink software package.*

As discussed earlier, in order to further increase the single pass-absorption from the level reached with the present launcher optics, a new mirror giving a non-astigmatic beam with w_0 =15mm has been designed and constructed. This new mirror will be mounted on TCV in the first half of 2006.

3.5   Upgrades to the TORPEX device

During 2005, minor upgrades in the TORPEX diagnostics system have been completed. A new radially movable Langmuir probe system has been fabricated. The probe consists of four tips arranged vertically in close proximity to each other and measures plasma density and potential fluctuations, and relative phases, with a sampling rate up to 10MHz. Using this probe on long pulses (t_{pulse}>500ms) has allowed us to measure the turbulent particle flux, as described in Section 2.3.

3.5.1   Towards an ohmic transformer operation

Among the open questions on turbulence and related transport in magnetized plasmas is the dependence of the character of fluctuations and turbulence upon the topology of the magnetic field. A power supply to drive the ohmic circuit and the poloidal field coils has recently been installed on TORPEX. The ohmic drive will allow us to induce longitudinal electrical field and then to investigate the change in the character of the electrostatic fluctuations and turbulence in the presence of closed flux lines. Calculations of the expected plasma current for equilibrium cases have been performed. Supplementary diagnostics (Fig. 3.5.1) have been developed, calibrated and installed on the TORPEX device. There are a 3D movable magnetic probe to measure any temporal variation for the magnetic field and two Rogowskii coils among which one can be moved in the radial direction. The possibility to use

AXUV detectors for soft X-ray measurements in those conditions has been explored. The entire ohmic system has been tested using a copper wire loop instead of plasma column. An optimization of ohmic transformer coil system to maintain the plasma equilibrium via poloidal "parasitic" magnetic field has been started. Non-equilibrium plasma current has been experimentally obtained. Further improvements of the system are still required in order to decrease the parasitic vertical magnetic field and achieve the plasma equilibrium.
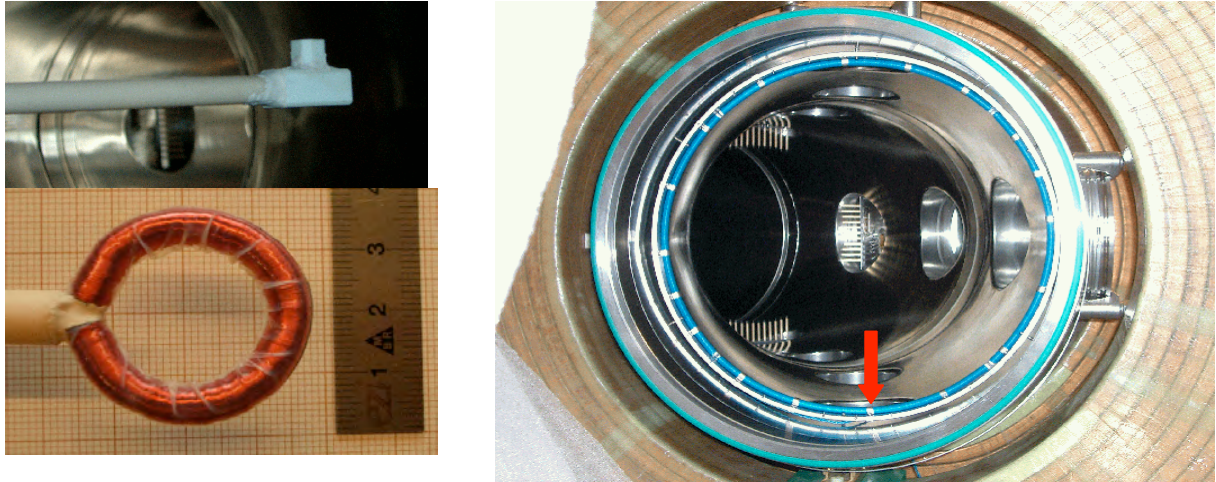
Fig. 3.5.1   *Specific diagnostics for the ohmic operation: a 3D d-B probe (top-left) and two Rogowskii coils.*

3.6   Superconductivity

3.6.1   The SULTAN facility

Damage on the main high voltage transformer of PSI by a blizzard forced the cryo-plant to a shut down at the end of October 2004. The three week break was also used for the yearly maintenance program of the cryo-plant. Operation was resumed in mid November 2004.

A new version of the SATTLINE controller for SULTAN, compatible with WINDOWS XP, was installed in January, upon re-start of operation. The SULTAN facility was not warmed-up and the re-cooling due to the Christmas shut down lasted only one week.

From beginning of February 2005 to mid October 2005 the facility operated continuously, without major break down. The yearly maintenance program started mid October 2005.

At the end of 2005, the EFDA announced its decision to implement the European Dipole facility at the CRPP near to SULTAN. The Dipole will increase the testing capabilities for ITER conductors.

3.6.2 *The JORDI Facility for Resistance Distribution Test on Joints*

The final commissioning of the JORDI facility was carried out in spring 2005, with the first sample test (Section 2.5.2).

In cryogenic operation, precaution needs to be taken at cool down, to prevent a very fast cool down, with large, sudden load to the cryo-plant, affecting the stability of the cryogenic supply for SULTAN. In the case of overload of the cryo-plant, the cryogenic port of JORDI is shut (principle of SULTAN priority) and the cool-down has to be re-started manually.

The automatic liquid level regulation in the JORDI cryostat worked satisfactorily since the first cool-down, independently on the power dissipation during the experiment, up to 100W.

The data acquisition of JORDI was a new challenge because of the large number of channels and the low level of voltage to be sensed. The 96 voltage signals measured between the 96 elements in the termination and the common equi-potential surface of the joint (obtained using a superconducting solder) together with the 96 current signals (voltage drops over calibrated shunts) were read using a National Instruments® data acquisition system with 200 channels. The voltage measurement is done independently by two Hewlet-Packard digital voltmeters, one for the voltage signals and the other for the current signals. Each volt-meter is connected to the data acquisition system through a low noise 1x100 multiplexer array.

After the current in the termination is ramped-up to 10kA (this corresponds to each strand being charged to around 100A) and after the thermal equilibrium in the cryostat has been reached, the data acquisition is started. After a few hours at full current, the power supply is ramped down and the data acquisition is continued for another couple of hours to register the offset values of all measuring channels.

A full cycle of data acquisition for the 200 channels lasts 27s. The volt-meter is switched every 0.27s. Most of this interval is used for low noise switching and communication. The actual sensing time of the volt-meter is 3ms (integration time). A typical test run last several hours, collecting 500 to 1000 points for each channel. After averaging for each channel the results at high and zero current, the zero-current signals (offset) are subtracted from the voltage values at full current before being used in the calculation of the contact resistance.

The "offset" was in many channels of the same order as the actual signal. The resolution of the voltage was eventually better than 50nV, i.e. the resolution of the resistance is better than $0.5n\Omega$

3.7 *ITER 170GHz gyrotron and its test facility*

For the electron cyclotron wave system of ITER the European Party plans to deliver 2MW CW sources at a frequency of 170GHz. Compared with the reference design of ITER based on 1MW sources, a high power unit source (2MW) allows a lower system cost. In 2004 the contracts for the main elements such as gyrotron, superconducting magnet, power supplies were placed to industry. During 2005 CRPP members participated regularly in meetings with EFDA and other participating Associations as well as the contract follow-up concerning all elements

of the project. A significant progress in the construction of the test facility at CRPP has also been accomplished during 2005.

3.7.1 Gyrotron development

Gyrotron

The fabrication of the first 170 GHz gyrotron (out of a possible total of three) is underway, with an expected delivery date in 2006. CRPP is the leading Association, responsible for the contract follow-up, as well as the organisation of the regular bimonthly progress meetings.
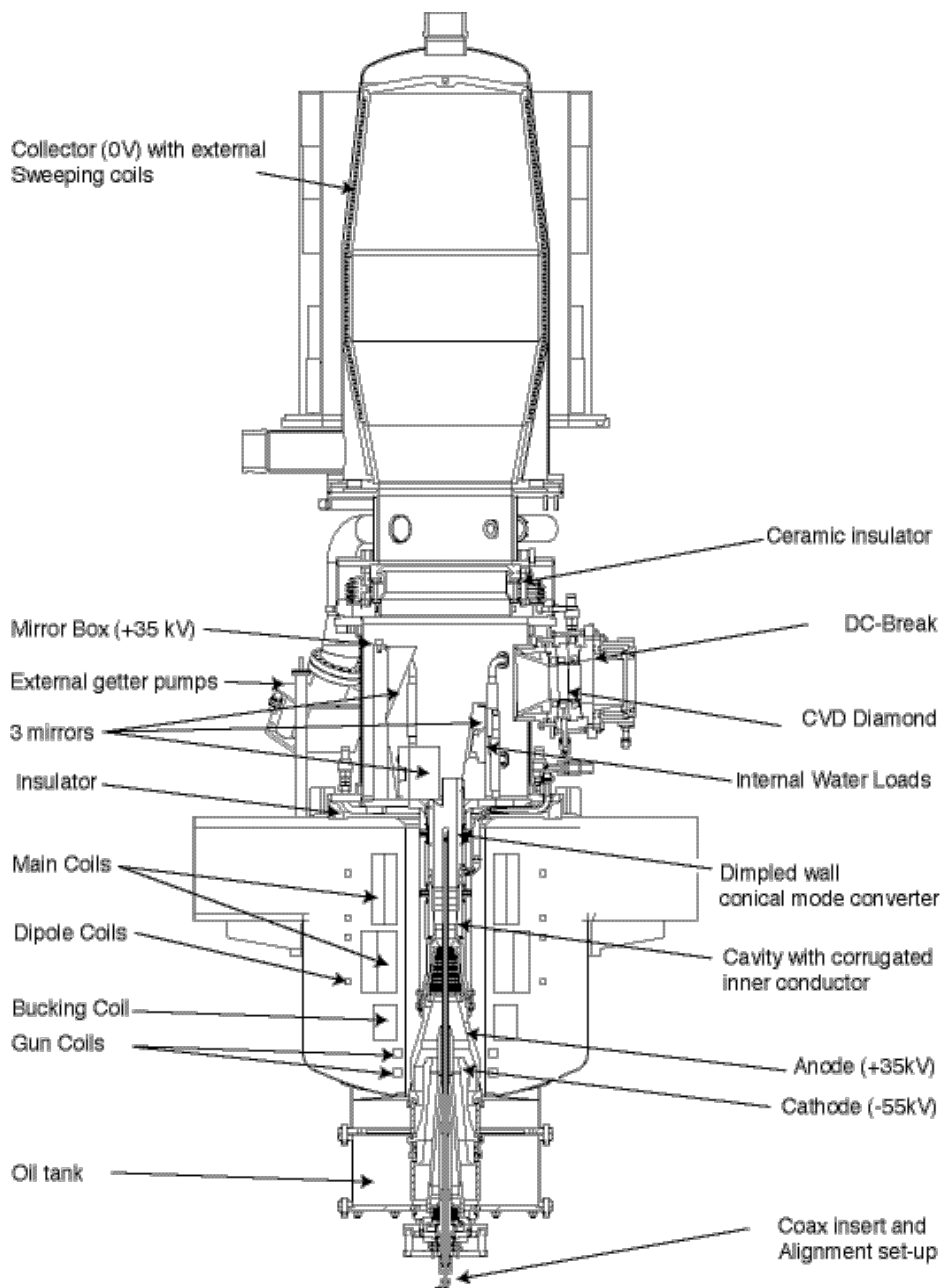
Fig. 3.7.1 *Schematic of the 170GHz/2MW/CW gyrotron first prototype.*

The tube is shown in Fig. 3.7.1. The first prototype performance goals have been fixed to 2MW/1s, with the possibility to test the collector heat evacuation capacity at full performance in CW. In 2005, the design of critical parts of the tube has been continued and was finalised on Aug. 31st, which was the deadline fixed by the supplier (Thalès Electron Devices, TED, France) to ensure on-time delivery, with the exception of the RFCU which will be delivered 3 months later. The identified critical issues, for which the tests planned in Lausanne are of crucial importance, are:

- The coaxial insert assembly, for which vibration eigenmodes have been identified through numerical simulations. The experiments on this prototype will constitute the first 'long' pulse (>100ms) tests of such an assembly.
- The collector power loading. The present collector and sweeping coils design has been shown to have the capacity of evacuating the heat deposited on the collector wall in nominal operation. However, such performance is marginal and further work is required to improve the design
- The stray radiation handling. Internal loads, consisting of a water-cooled ceramic tube, will damp the radiation trapped inside the tube for the first time.
- The quasi-optical mode converter. The present design is not perfect. Nevertheless significant progress has been accomplished in 2005, and the version to be implemented in the second prototype should have a much better profile, as well as a lower level of stray radiation.

Magnet

The design of the 7T magnet has been completed by Ansaldo Superconduttori Genova (ASG), Italy. The magnet manufacturing started in the last quarter of 2005 and the acceptance tests at CRPP are foreseen to be terminated by the end of May 2006. The main difficulties for this type of magnet are related to first, the tight mechanical tolerances on the alignment of the magnetic field axis with respect to the warm-bore mechanical axis, and, secondly, to the mechanical and electrical interfaces with the gyrotron. The gyrotron, which will be mounted in the magnet warm-bore, has metallic surfaces which are brought to high-voltage (50kV max) in the very-near vicinity of the magnet top-plate. Therefore, the design of all the different penetrations on the magnet top-plate (current leads, cryogenic services, alignement rods), has required particular attention.

Radio Frequency Conditioning Unit (RFCU)

The complete gyrotron launcher redesign by FZK using an advanced quasi-optical mode converter for a coaxial gyrotron has allowed us to significantly improve the rf-beam characteristics at the gyrotron window in terms of amplitude and phase patterns. The E-field patterns calculated for a free-space propagation at various distances from the gyrotron window (L=0.2-1.2-2.2-3.2m) are shown in Fig. 3.7.2. The TEM_{00} content of the beam is in excess of 95%. With such a high rf-beam quality, the diffraction losses inside the RFCU will be significantly decreased compared to the previous design and at the same time, the coupling to the HE_{11} waveguide mode will be significantly improved. Quantitative calculations of the RFCU diffraction losses and the HE_{11} mode content are presently underway.
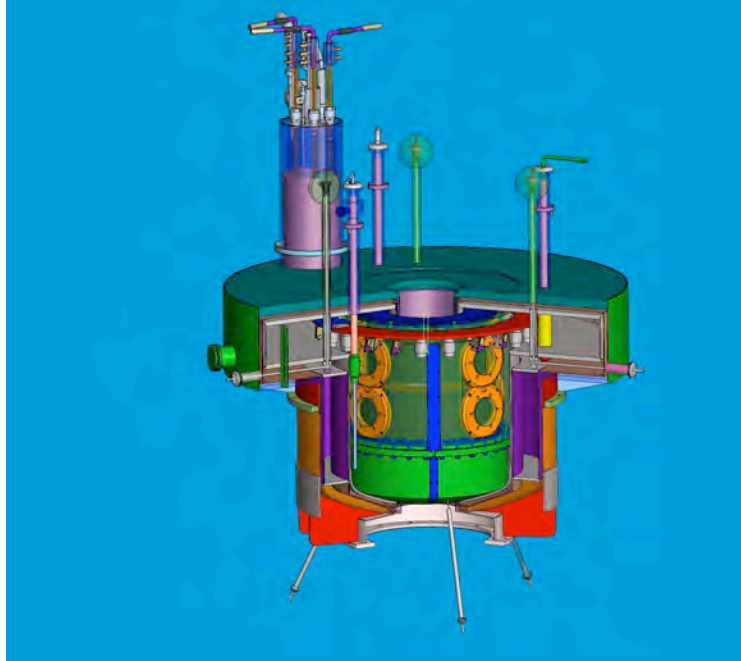
Fig. 3.7.2   *Present design by ASG of the 7T superconducting magnet. This magnet is essentially composed by a set of 5 solenoids aligned on the warm-bore mechanical axis. To verify in situ the gyrotron electron-beam alignment, a set of transverse dipole coils has been implemented. The alignement of the magnetic axis to the warm-bore mechanical axis is insured by a system of 9 alignment rods, placed by groups of 3 on the top, side and bottom of the magnet.*

Different moments (1st and 2nd moments) of the E-field pattern shown in Fig. 3.7.3 allow to calculate the axis of propagation of the rf-beam as well as the equivalent spot-size evolution along the axis of propagation. These quantities are shown along the propagation axis in Fig. 3.7.4.
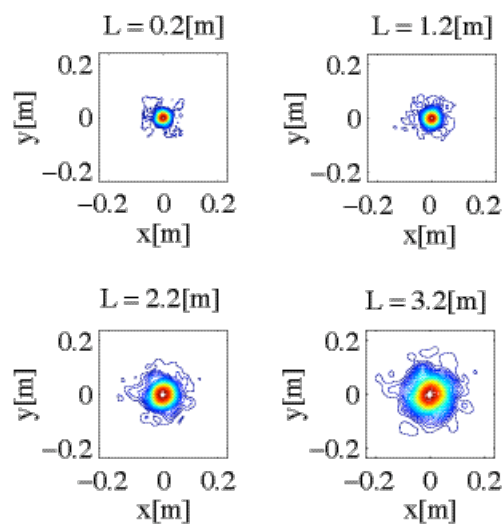
Fig. 3.7.3   *Calculated E-field pattern at various distances from the gyrotron window. A very slight astigmatism is observed. The TEM$_{00}$ mode content of such a beam is in excess of 95%.*
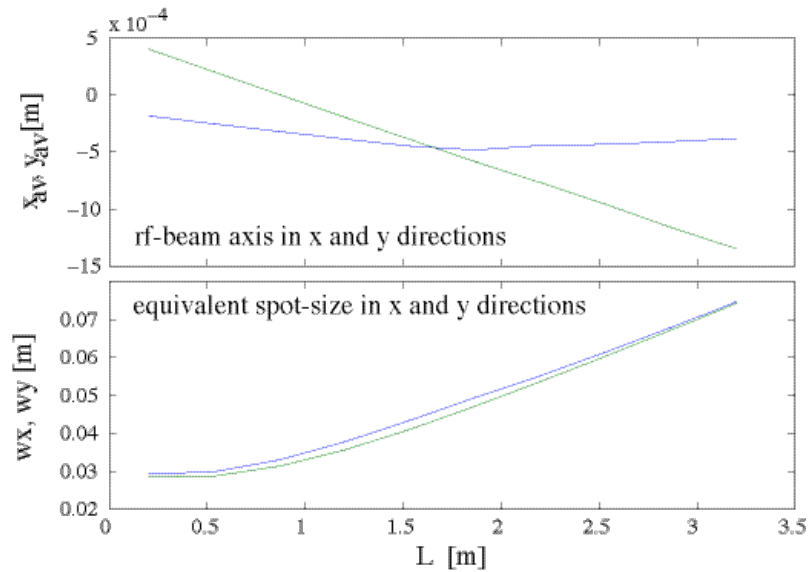
Fig. 3.7.4 *Calculated E-field pattern at various distances from the gyrotron window. A very slight astigmatism is observed. The TEM$_{00}$ mode content of such a beam is in excess of 95%.*

The GT170 RFCU design proposed at the end of the design contract in 2003 can now be retained with minor modification, as the data shown in Fig. 3.7.2 can also be approximated by a paraxial beam of nearly identical characteristics to those used in the original design (the focal plane of the gyrotron output is projected a further 257mm from the gyrotron window than in the original).

3.7.2   C-GT170 Test Facility

Power supplies

During 2005 the work on the power supply structure for the gyrotron C-GT170 has continued. The contracts for the two main supplies, the MHVPS and the BPS, applying together the beam voltage required for RF wave generation, were signed by the EU Commission in May 2005. These power supplies will be delivered by OCEM, based in Bologna, Italy. A CRPP representative attended several progress meetings at OCEM to finalise the technical choices and to design the interface of these supplies with the Test Facility in preparation at Lausanne.

For the BPS, the work is more advanced since a similar power supply will be delivered to ENEA by the end of this year.

Since the contract for the HVSSS (HV Semiconductor Series Switch) has been canceled by EFDA, due to the lack of confidence of the manufacturer to achieve the technical requirements asked by specifications, the MHVPS contract will be amended in order to include the HVSSS requirements in addition to the ones to be fulfilled by the MHVPS. A CRPP representative defined and followed the contract amendment in collaboration with EFDA. Consequently, the delivery of the MHVPS has been delayed, and a revised project time table will be agreed by the end of 2005.

In order to be able to supply the gyrotron and start the tests by July 2006, the existing CRPP HV supply used on the additional heating for TCV will be shared with the C-GT170 test Facility, during 2006 and at least during the first quarter of 2007.

A study of the modifications of the present installation has been launched. The hardware adaptation has started and the additional equipment has been ordered.

Infrastructure

The infrastructure of the test facility has advanced significantly in 2005. All equipment not related to the test stand has been removed from the installation zones on the -1 and 0 levels. As seen (partially) in Fig. 3.7.5, the false floor has been completed, equipment racks installed including power cabling, cable trays laid, security barrier erected and the control room has been furnished with computers, tables, printers, power and internet connections.

Fig. 3.7.5   *View of the entry ramp to the test facility security enclosure as of 21 September 2005. Inside the clear barrier are stored, temporarily, the liquid Helium dewars (blue striped – 66l, 100l, red striped – 250l) and 2MW transmission line components (in boxes).*

The design of the gyrotron tower is underway and will be completed by early 2006, depending on detailed mechanical interface input from the external suppliers of equipment (gyrotron, magnet, RF loads). It includes the water connection interfaces, both high- and low-voltage electrical connection interfaces, mesurement connection panels, as well as alignment reference planes. Initial testing of the gyrotron will take place without the RFCU in place, using the short pulse, high power, calorimetric, RF load supplied by ENEA/CNR Milano. A support and height adjustment structure, including the vacuum pumping equipment, provides the interface between the tower reference plane and the carriage supplied by the RF load manufacturer. The same reference plane is used for RF measurements and the RFCU, when installed.

Cooling water system

Design activity related to the cooling water system was started late in 2004 and continued up to the summer 2005.

The lake water, which is potentially corrosive, is not directly used for the gyrotron cooling. It will extract the heat of the closed cooling circuits through stainless steel heat exchangers.

The second design phase focused on the secondary closed loop cooling circuits. Based on the data available both from the gyrotron manufacturer and from the auxiliary providers (RF load, HV supply etc.), and considering that the main aim is to measure the efficiency of the gyrotron by calorimetry, the CRPP has decided to install three independent circuits.

1. The gyrotron collector circuit, which is the most important. Designed to evacuate up to 3000kW, its nominal flow is 50 litres/second with a pressure of 3.2bar. Thanks to a 30kW pump with variable speed drive, it will be possible to adapt to the real needs of the gyrotron without wasting pumping power. For similar reasons, the amount of lake water will be regulated as a function of the power to be dissipated, Moreover, the temperature of the cooling water will be kept nearly constant to allow for precise colorimetric measurements thanks to a water storage tank of 6000 litres.

2. The Microwave load circuit will extract the thermal load generated by the microwaves in the RF load. The nominal power to be extracted is 2000kW with 14 litres /second at 6bar. A 15kW pump with variable speed drive also allows us to tune the cooling circuit to the actual losses. As for the previous circuit, the amount of primary water is regulated and a 6000 litres storage tank is available.

3. Finally, the gyrotron auxiliary circuit supplies about 15 different equipment groups required for gyrotron operation. Two series connected pumps, each with a variable speed drive, will provide cooling water flow at two different pressure levels, 3.5bar and 7.5bar. The amount of primary water is also regulated and a tank with 5000 litres helps stabilise the temperature variations. The auxiliaries are very sensitive and most of them are placed at high electrical potentials. As a result, this water will be continuously deionized and filtered. For the calorimetric measurements of the separated elements, each circuit contains one flowmetre and two thermometers.

Orders were placed early this year and circuit construction started in May. Installation is completed at 80%. The distribution manifolds for the 15 auxiliary circuits as well as the last pieces of piping up to the gyrotron collector and the microwave load will be completed this year. The complete piping will then be isolated to prevent excessive heat load within the halls (return water temperature may reach up to 60ºC) and to reduce errors in the colorimetric measurements.

Cryogenics

The Helium recovery and liquefaction system for the entire EPFL has been completed and will be operational by the end of 2005.

Gaseous Helium (GHe) recovery system

The GHe recovery system for the entire EPFL has been completed. Each laboratory on the campus has been equipped with manifolds allowing the recovery at low pressure of the GHe which is conveyed to two $10m^3$ baloons located in the basement of the PH and BSP buildings. From these balloons, by means of a special gas turbine system, the GHe is pushed through a 1.3km pipe to a $20m^3$ balloon located in the TCV building at CRPP. A two compressor system with a total

maximum capacity of $100m^3/h$ compresses the GHe at 200bar in a system of 9 spheres ($4m^3$ each). A control and acquisition system for the GHe recovery is presently being designed and constructed and will be operational in the first quarter of 2006.

Helium liquefaction system

The Helium liquefaction system installed in the PPH building of CRPP is shown in Fig. 3.7.6. The liquefaction capacity is of 45l/h without LN_2 pre-cooling and of 78l/h without LN_2 pre-cooling. The liquefier is connected to a 130kW compressor with a mass flow capacity of 13g/s. The gas purifier, integrated in the liquefier, is connected to an $8m^3$ pure-helium storage tank (18bar max) and directly feeds the high-pressure line of the liquefier.

Fig. 3.7.6   *Liquid Helium refrigeration system in the test facility hall (0 level). On the right: Helium liquefier (LINDE L140) with a liquefaction capacity of 45l/h without LN_2 pre-cooling and 78 l/h with LN_2 pre-cooling. The liquefier includes a Helium purification system and accepts gaseous Helium with impurities up to 15%. The typical impurity level in the recovered gas is below 5%. The liquefier operation is nearly fully automatic and controlled via a computer interface. On the left: 5000l Liquid Helium storage dewar from where the mobile dewars (3x450l, 3x250l, 20x100l, 15x65l) are filled and will be distributed over the entire EPFL campus.*

The LHe is stored in a 5000l fixed dewar from which a set of different size mobile dewars (65l, 100l, 250l, 450l) are filled. These mobile dewars will be transported to the different laboratories on the EPFL campus by vehicle.

Transmision line

The transmission line system was delivered at the beginning of 2005, compatible with the transmission of $\geq$2.0MW over a relatively broad bandwidth (>±20GHz)

centered at 170GHz. The components include a straight HE_{11} waveguide (>10m), two miter bends (90° bends), power monitor miter bends (couples ~80dB into a low power mm-wave detector), and adaptation flanges from the waveguide to standard conflate flanges mounted on the RFCU and calorimetric load.

Data acquisition and control

Data Acquisition

The data acquisition system comprises 3 sub-systems. These are

    (i)   A 288 channel slow system that is to be used to stream data to disk drive in real-time at rates below 1kHz.

    (ii)   A 96 channel medium subsystem that acquires data at rates below 250kHz during multiple pre-programmed bursts.

    (iii)   A 16 channel fast subsystem that acquires data at <10MHz on detection of a fault or trip (e.g. an electrical arc in the gyrotron).

The entire data acquisition system has been purchased from D-TACQ Solutions Limited of Scotland. The system was delivered in February 2005 and hardware testing and software development has been on going since then.

The data acquisition cards came supplied with a control computer (a high end IBM PC running LINUX). Required software for the control of the data acquisition was installed and commissioned.

Hardware tests of signal-to-noise, harmonic distortion and crosstalk have shown that all data acquisition sub-systems are within specification.

In close collaboration with D-TACQ, software has been developed, in house, to stream slow data to disk and render it useable in quasi-real time. Real time data streaming was demonstrated at the IAEA technical meeting on data acquisition & control in Budapest, Hungary June 2005. so far, the real-time data streaming has been demonstrated using an internal clock and needs to be done using an external clock.

The CRPP designed and fabricated a slave unit to provide external clocking, synchronization and trigger pulses for the data acquisition system. This slave unit has been interfaced with the Test Stand Control system and the ensemble has been successfully commissioned and tested.

Control

Test stand control is being defined, constructed and implemented.

The decision was made early on in the development process to adopt V-SYSTEM, by VISTA control systems, control interface software to provide the interface to the control electronics. This package provides the database, graphical user interface and a means of state-machine event logging. This package was chosen because it is in use on TCV. This software has been installed and commissioned on a dedicated IBM PC in the gyrotron test stand hall.

Drivers that are required to allow communication between the PC/V-SYSTEM and the hardware is being developed and has been developed for communication with the slave unit that communicates with the trigger/clock generator for the data acquisition.

The electronics for the control of the water cooling pumps and circuitry has been defined and is being manufactured. The software for this application has been specified and is being developed.

4 International and national collaborations

4.1 Exploitation of the JET facilities

4.1.1 Scaling of density peaking in JET H-modes

Results from an extensive profile database analysis of JET density profiles in H-mode, show that the density peaking factor $n_{e0}/\langle n_e \rangle$ in JET H-modes increases as the effective collisionality $\nu_{eff} \approx 10^{-14} R Z_{eff} n_e / T_e$ [SI, eV] drops from ~1 to below 0.1, as expected for ITER. Density peaking is also correlated with Greenwald number, particle outward flux Γ_{NB} from the neutral beam source and T_i/T_e. The influence of parameters related to magnetic shear, such as l_i and q_{95} is weak. There is no significant correlation with β_N, ρ^*, L_{Te} and L_{Ti}. H-modes heated only by ICRH are on average only slightly less peaked than H-modes dominated by NBI, demonstrating that neutral beam fuelling can only explain a modest part (~20%) of the peaking (Fig. 4.1.1). Scaling expressions were developed using many combinations of parameters, confirming that ν_{eff} is the most important scaling parameter. The best fit obtained, expressed as

$$R_0/L_{ne} = 0.78 - 1.28\log_{10}\nu_{eff} + 1.28 R_{0\_NB}/(n_e\chi_{eff}) + 0.7 T_i/T_e,$$

where local quantities are taken at r/a=0.5 suggest a relatively low value for the ratio of the effective heat diffusivity and the particle diffusion coefficient $\chi_{eff}/D \approx 1.3$, consistently with expectations from anomalous transport theory. An extrapolation to ITER suggests $R_0/L_{ne} \approx 3$, corresponding to $n_{e0}/\langle n_e \rangle \approx 1.5$ in ITER, providing a boost of fusion power of some 30% for fixed β_N and N_G with respect to the usual assumption of a flat density profile.
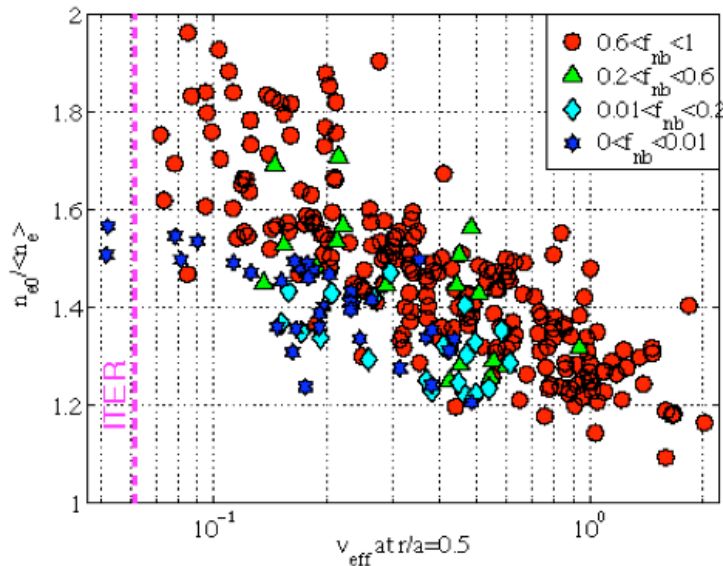
Fig. 4.1.1 *Peaking of density profiles in JET H-modes. Symbols refer to fraction of NB heating $f_{NB}=P_{NB}/P_{TOT}$.*

4.1.2   Collaboration with the JET-EFDA Task Force E (Exhaust)

The traditional CRPP support of JET Task Force Exhaust (TF-E) activities has continued through 2005 in the form of leadership of the Task Force. This has taken the usual form of campaign planning (establishment of edge physics experiment schedules for the 2005-2006 JET Campaigns), detailed clearance of all TFE journal and conference submissions and organisation of regular TF meetings. One such general meeting was hosted over a three day period in Lausanne with over 20 participants.

The extended JET maintenance shutdown from March 2004 until essentially the end of 2005 means that no new experimental data has been gathered since the previous Annual Report. Instead, further data analysis and interpretation has continued, in particular with regard to the high ELM ion energies detected in the JET far scrape-off layer using the CRPP-built retarding field analyser (RFA) probe head. The RFA cannot be used to scan the ion energy distribution (and hence to extract T_i directly) on the ELM timescale. By fixing the internal postive retarding grid bias of the device to the highest possible values, however, if any collector current (i_{coll}) is registered during an ELM, it must have originated from ions able to surmount this potential barrier.

An example is shown in Fig. 4.1.2a), where the RFA entrance slit current, retarding grid bias, V_{grid}, and collector current are shown for a single ELM captured by the probe at a distance of ~80mm from separatrix at the probe location (corresponding to ~30mm mapped to the outside midplane and just inside JET ICRH antenna limiter radius) during a Type I ELMing H-mode in pure hydrogen plasma with hydrogen neutral beam injection. The ELMs in this discharge typically expel ~50kJ of energy from an edge pedestal with $T_i = T_e$~400eV. With V_{grid}~400V (Fig. 4.1.2b), there is signifciant i_{coll} (Fig. 4.1.2c) at this far SOL radius, implying that ions with parallel energies exceeding 400eV have entered the device.

To be more quantitative, the magnitude of this current must then be compared with theoretical expection on the basis of a model of the ELM plasmoid as it propagates radially in the SOL towards the main chamber walls, losing energy along the magnetic field in the parallel direction as it does so. Just such a model of ELM transient loss has recently been developed within Task Force E and has received its first serious and successful test by confrontation with the RFA data. As illustrated in Fig. 4.1.2c), the model prediction (when combined with an analytic description of RFA function) for the RFA i_{coll} compares rather favourably with experiment, confirming both that ELMs do convect hot ions to surfaces in the far SOL and that the new fluid transient model is a good approximation to the ELM propagation.
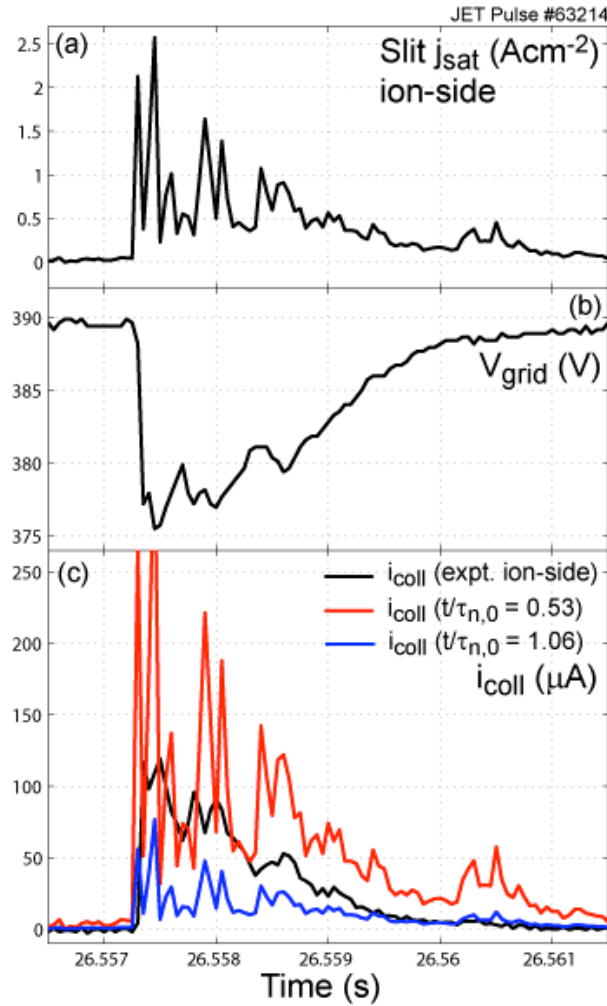
Fig. 4.1.2   *(a) Slit current density, (b) ion retarding grid voltage and (c) collector current for a single Type I ELM captured in the JET far SOL by the CRPP built RFA probe. Fine structure inside the ELM is readily seen in (a), demonstrating the "filamentary" nature of the instability as it is manifest in the SOL. The dip in the grid voltage in (b) is due to ion current entering the RFA during the ELM and being drawn by the retarding grid itself. In (c), the black line is the measured collector current – the fine structure seen on the slit is absent here as a consequence of the restricted bandwidth on the measurement. The red and blue lines are the predicted i_{coll} using a fluid transient parallel loss model of the ELM plasmoid assuming that it originates with "mid-pedestal" plasma paramteters ($T_i = T_e = 300eV$) and that it propagates through the SOL with radial velocity of $0.6kms^{-1}$. Maxwellian distributions are asumed at the RFA entrance slit and sheath and presheath ion acceleration to the probe is accounted for. The two predicted lines correspond to the upper and lower limits of the "normalised transit time, $t/\tau_{n,0}$, due to the uncertainty in the ELM propagation distance, which ranges from top of the pedestal to the probe (blue line) to separatrix to the probe (red line). The theoretical collector currents are computed assuming the measured slit current as input and thus possess exactly the same fine structure.*

4.1.3   Collaboration on Alfvén Waves and Fast Particle Studies

The study of Alfvén waves and their interaction with fast particles is an important topic in the JET programme. During 2005, JET was shut down for the installation of various new diagnostic systems, hence our activities have mainly focused on the analysis of previous experimental results and on the design, manufacturing and installation of a new dedicated antenna system for the excitation of Alfvén Eigenmodes (AEs) with high toroidal mode number, CRPP being directly responsible for this project.

Regarding data analysis, our work has focused on:

- completing the study of the dependence of the TAE stability upon the direction of the ion ∇B-drift;
- studying the decay time of AEs driven by resonant fast particles at the switch-off of the Ion Cyclotron Resonance Frequency (ICRF) heating power to benchmark theoretical modelling.

In 2005, CRPP completed the manufacturing and the testing of the two new AE antenna frames and of the related control and protection electronics, which were delivered to the JET facilities on schedule. However, due to delays in the procurement of the feedthroughs (not CRPP responsibility), only one antenna frame could be installed during the present shutdown, with the in-vessel installation finally successfully completed in Juneby the JET remote handling group. This was then followed by the installation of the ex-vessel hardware. The commissioning of this new diagnostic system (KC1T) is now underway, in preparation for the forthcoming JET experimental campaigns, which are due to start late November 2005. The second antenna frame will be installed during the 2006 summer shutdown.

Furthermore, we have also contributed to:

- the assessment and calibration of the prototype for a new set of high frequency magnetic probes;
- the analysis of the neutrons produced by the proton-triton fusion reaction.

The following sections present the main results of these activities.

TAE stability as function of the ion ∇B-drift direction

The ion ∇B-drift direction is found to be an important parameter for accessing the high-confinement regime known as H-mode. For very similar background plasma parameters and eigenfunctions, the damping rate of $n=1$ TAEs is measured on JET to be a factor three larger when the ion ∇B-drift is directed away from the divertor. A theoretical explanation for these measurements is still lacking, other than the simple observation that ion ∇B-drift terms are present in gyro-kinetic codes, whereas fluid codes only include equilibrium gradients depending on density and temperature.
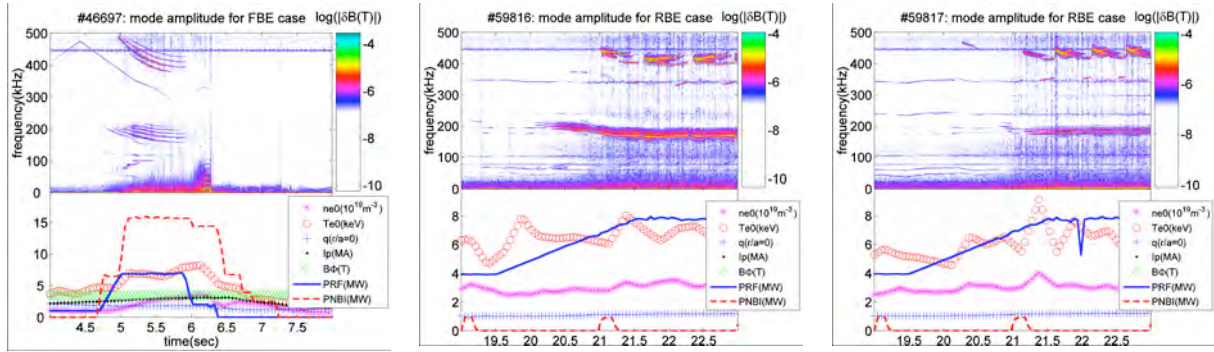
Fig. 4.1.3 *Left: Measurement of the AE activity for the FBE case #46697: even with $P_{NBI} \approx 6.5MW$, the n=4 TAE is unstable at $P_{ICRF} \approx 3.5MW$. Middle: Measurement of the AE activity for the RBE case #59816: here the n=5 TAE becomes first unstable at $P_{ICRF} \approx 5MW$. Right: Measurement of the AE activity for the RBE case #59817: here the n=8 TAE becomes first unstable at $P_{ICRF} \approx 6.5MW$.*

A possible explanation for the difference in the measured γ/ω for n=1 TAEs can be associated with the observation of different flows at the plasma edge and scrape-off layer for the forward (FBE) and reverse (RBE) ion ∇B-drift directions. In addition to a possible direct effect on the TAE damping rate, these flows change the e-folding length for the edge density from the scrape-off layer towards the first wall, hence possibly affecting the interaction of the TAE modes with the Alfvén continuum at the plasma edge. To provide further insight into this idea, we have considered the experimental measurements of the TAE instability threshold as a function of the toroidal mode number, in the range |n|=3-10. TAE modes with higher-n are more localised towards the plasma centre, hence less sensitive to edge effects than more global, lower-n, TAEs. These |n|=3-10 modes are destabilised by the MeV-energy protons (H) produced by the H(D) minority ICRF heating scheme in a deuterium (D) plasma.

Figure 4.1.3 shows the measurement of the AE mode activity for the FBE and RBE case. We note that for the two RBE cases a different spectrum is excited at different levels of P_{ICRF}, due to differences in the background plasma parameters, hence in the damping and drive for the modes. This scatter is then fully reflected in the plot summarising our database, presented in Fig. 4.1.4. As shown in Fig. 4.1.4, larger fast ion drive is found to be required to destabilise TAEs with |n|=3-10 when the ion ∇B-drift is directed away from the divertor, with the difference increasing for decreasing n.

This result is also consistent with previous measurements of γ/ω for stable n=1 TAEs actively driven with in-vessel antennas. We suggest that the different flows measured at the plasma edge and scrape-off layer for the forward and reverse ion ∇B-drift directions may play an important role in modifying the Alfvén continuum, either directly on the TAE damping rate or through a modification of the Alfvén continuum, affecting the TAE edge damping mechanisms, such as continuum damping and mode conversion to kinetic Alfvén waves. High-n, more core-localised TAEs will be less affected by edge damping mechanisms than lower n's, typically more global modes.
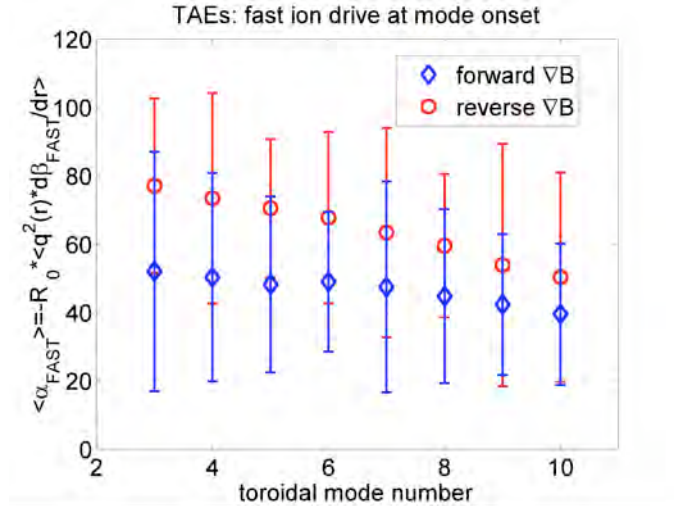
Fig. 4.1.4 *TAE instability threshold as function of the ion ∇B-drift direction for different n.*

We conclude that the measurements of the dependence of the damping rate and the instability threshold on the ion ∇B-drift direction as a function of the toroidal mode number can be used to test the predictions of fluid and gyro-kinetic models of the AE wavefield.

TAE decay time at the ICRF switch-off.

One of the effects determining the AE instability limit in the presence of fast ions is the phase de-correlation between the ICRF and AE wavefield over the ion gyromotion. A piece of information that provides a constraint to the modelling of this effect is provided by the decay of AEs at the ICRF power switch-off, which is observed to occur on time scales much shorter than the fast ion slowing-down time τ_{SD}. Figure 4.1.5 shows an example of the measurement of the AE decay time during ICRF modulations and switch-offs: the modes decay over a typical time scale of $\tau_{DECAY} \approx$ 100-400ms (depending on the n's), compared to a typical volume-averaged $<\tau_{SD,H}> \approx$ 600ms for the fast protons driving the modes.

A qualitative theoretical explanation for this phenomenon has been previously proposed. High energy ions interacting with AEs are displaced along characteristics intersecting the resonance surfaces in phase space. In parts of the phase space the distribution function increases with energy along these characteristics and drives the modes, which in turn flatten the distribution function itself. In other parts of the phase space the distribution function decreases with energy along the characteristics, which leads to a damping of the mode by the fast ions themselves. ICRF heating can partially restore the inverted distribution function on a longer time scale, leading to a non-linear oscillation of the mode energy, which appears as a splitting of the Fourier-decomposed signal. As the ICRF heating is turned off, the restoration of the inverted distribution function ceases and the AE is damped out by wave-particle interactions from the stable part of the distribution function. To provide for a quantitative validation of this theoretical model, various JET discharges with a monotonic q-profile have been analysed to compute the AE decay time from the measured time evolution of the mode amplitude.
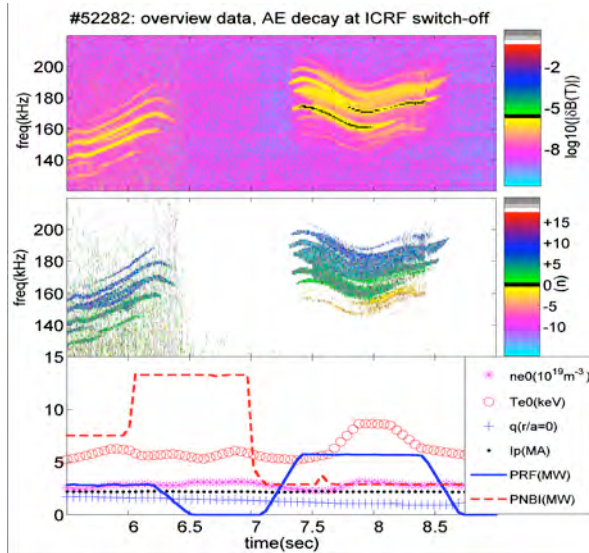
Fig. 4.1.5 *Decay of TAEs and EAEs at constant P_{NBI} during a modulation of the ICRF heating power*
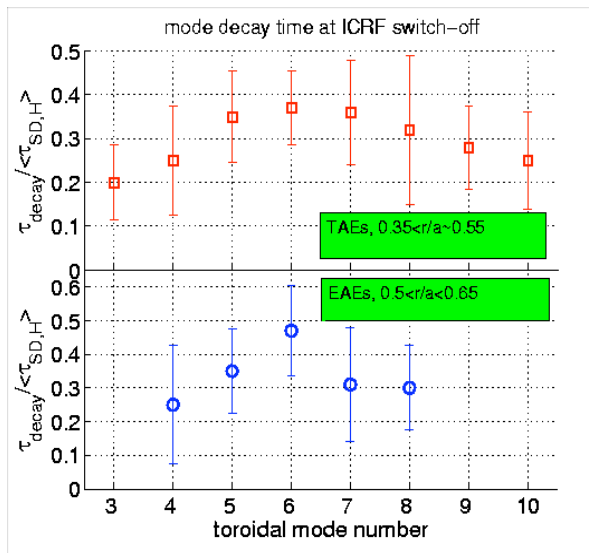
Fig. 4.1.6 *Decay time for TAEs and EAEs at the ICRF power switch-off (or ramp-down) as function of n'.*

Figure 4.1.6 shows the summary result of our database: the scatter indicates the measured range of $\tau_{DECAY}/<\tau_{SD,H}>$ (here the average is over the mode radial structure) for the different plasma conditions analysed in this work. We notice that $\tau_{DECAY} \approx <\tau_{SD,H}>/3$, and it is larger for n=5÷7 modes. The relative roles of MHD modes in flattening the fast ion distribution function on time scales shorter than τ_{SD} compared to the ICRF-induced diffusion can be analysed based on these observations. Reproducing this measured n-dependence becomes in particular the crucial point for validating quantitatively the available theoretical model.

Manufacturing and installation of the new AE antennas

The previous antenna geometry limited the active AE excitation to low toroidal mode numbers, n=0-2, whereas intermediate or high toroidal mode numbers characterise the most unstable AEs, which are already detected in JET and are similarly predicted for ITER. Hence, a direct excitation and tracking of the same modes is of clear interest for preparing the next step experiment. To this end, two antenna structures optimised for the excitation and detection of AEs with n≈10-15 were designed and built by CRPP, and one has been installed in-vessel during the 2005 JET shutdown, Fig. 4.1.7.

CRPP has also been responsible for the modifications and upgrades to a significant fraction of the ex-vessel hardware: amplifier, isolation and distribution unit, control and protection electronics, and the data acquisition modules. CRPP has also significantly participated in the design, testing and assembly of the new link boxes. The installation of ex-vessel hardware and electronic for the octant 8 antennas has been performed mostly by CRPP staff seconded to the JET facilities, and has being completed by mid-September. The commissioning of this new diagnostic system (KC1T) is underway, in preparation for the beginning of the experimental campaigns, which are scheduled to start in late November 2005.
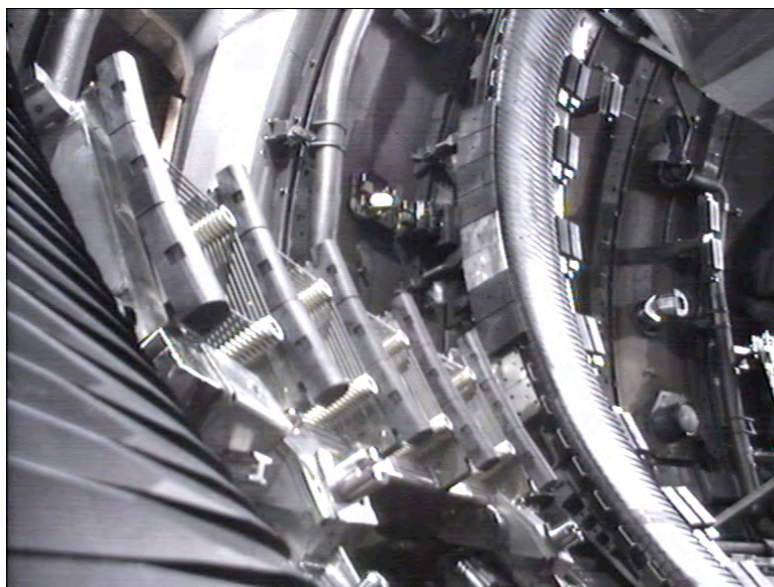
Fig. 4.1.7   *In-vessel view of the TAE antenna structure installed in octant 8.*

Contributions to the testing of the prototype high frequency coil

In collaboration with ENEA and the CREATE consortium, Italy, a new set of high frequency pick-up coils was designed to improve the equilibrium reconstruction and the measurement of MHD activities in JET. In 2005, CPPP has contributed to these activities with the measurement of the frequency response of the prototype high-frequency coil. Following this work, the coil design was changed as the frequency response was found to be inconsistent with the original technical specifications.

Measurement of the neutron produced by the proton-triton fusion reaction

Following the recent Trace-Tritium experiment on JET, CRPP staff have contributed to the measurement of the neutrons produced by proton-triton fusion reaction, and to the analysis of its scaling as a function of the proton temperature and energy.

Further collaborations outside JET

Part of the work reported here on the installation of the ex-vessel hardware for the new AE antennas has been performed in collaboration with staff from MIT-PSFC. MIT-PSFC staff has also contributed to the analysis of the data reported here. [MIT, Cambridge, USA]

The work on the design of the magnetic system has been conducted in collaboration with staff from ENEA and the CREATE consortium, Italy. [ENEA, I; CREATE, I]

4.1.4 Work on MHD physics

The main activities were dedicated to the analysis of the results from the 2003-2004 campaign and the preparation meetings related to the 2005/2006 campaigns. In particular, CRPP has provided active inputs to the TF-S1 and TF-M meetings for the reporting of previous results and the preparation of the forthcoming campaigns, as well as to the main TF-T beginning of 2005.

Dedicated experiments during the recent reversed toroidal field campaign at JET demonstrated that counter-neutral beam injection (NBI) results in shorter sawtooth periods than in the Ohmic regime. The clear dependence of the sawtooth period on the NBI heating power and the direction of injection also manifests itself in terms of the toroidal plasma rotation, which consequently requires consideration in the theoretical interpretation of the experiments [see also Section 2.2.3]. Sawteeth with repetition times less than half that of Ohmic sawteeth were reproducible. A minimum in the sawtooth repetition time was obtained for a moderate neutral beam power of 4 MW. The counter NBI injection discharges investigated here add to a class of regimes which aim at increasing the rate of sawtooth oscillations, thus preventing the triggering of NTMs at low plasma beta.

The marginal beta limit for both the 3/2 and 2/1 modes are being studied in several tokamaks. Preliminary cross-machine scalings show that ITER will be clearly above this limit as soon as it is in H-mode, for both modes. This means that, similarly to present JET experiments, NTMs will be destabilised as soon as a large enough seed island is triggered. A detailed scaling of the marginal island width is also necessary since it directly impacts on the ECCD requirements for full stabilisation. Preliminary scalings indicate that the marginal island is of the order of twice the poloidal Larmor radius, but further experiments are needed to span a larger parameter space.

4.2 ITER

4.2.1 ITER Tasks

EFDA/04-1208 Diagnostic Design for ITER: Magnetics Diagnostic (Task Coordination and Design Analysis)

The ITER magnetic diagnostic system provides the main electromagnetic parameters of the plasma, the position or vertical speed of the plasma centroid, the shape of the plasma boundary, supplemented by some internal parameters and the amplitude and mode number of MHD fluctuations, Fig. 4.2.1. It is therefore of primary importance for machine performance. A subset of these measurements will be used for plasma current, position and shape control.

As ITER host, the EU will supply the magnetic diagnostics for ITER; CRPP has bid for the leadership for this procurement package. During this year, CRPP participated in the EFDA contract 04-1208, reviewing the implementation of the magnetic diagnostic system in ITER, initiating outline design for specific sensors, developing a work plan for their design and development, defining specification for subsequently required R&D, defining the electronics specification, assessing the existing documentation and supporting the ITER International Team in writing the procurement package. In addition the CRPP is responsible for co-ordinating the

activities within the participating EU Fusion Associations, namely ENEA-RFX (Italy), CEA (France) and CIEMAT (Spain).

The contract encompassed the following overall activities in 2005:

- Review the implementation of the magnetics diagnostic systems in ITER.
- Initiate outline design of specific types of sensors.
- Develop a work plan for the design and development of these sensors.
- Define specifications for the subsequently required design, R&D and performance analysis task.
- Define the needs for electronics.
- Assess the existing documentation and support the ITER International Team in writing the procurement specifications.

These activities applied to the following sensor types:

- Diamagnetic loop dedicated sensors
- Inner vessel high-frequency coils
- Inner vessel dedicated MHD saddle loops
- Divertor equilibrium coils
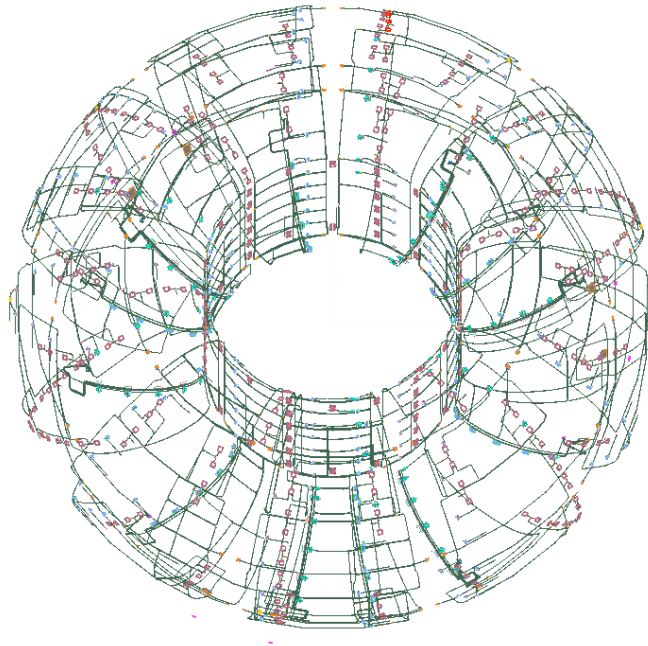
Fig. 4.2.1   *3D view of the magnetic sensors in ITER*

In the framework of this ITER R&D task, we also assessed and developed the technical and scientific specifications for the high frequency (HF) coils. The HF coils are the main diagnostic system responsible for measuring MHD modes with low poloidal/toroidal (m/n) mode numbers, such as sawteeth and disruption precursors, as well as high frequency macro-instabilities, such as fishbones and TAE modes. These coils are also foreseen to be used as backup diagnostic for determining the plasma current, plasma position and shape. The spatial distribution was analysed so as to optimise the measurement capabilities. Routine operation of the coils was studied in different operating scenarios to assess the detection needs (frequency, bandwith, digitisation, mode number resolution). Failure modes were also investigated, to evaluate possible backup/alternative measurements.

Coordination of the ITER Technology Workprogramme 2005

The CRPP is responsible for the coordination of the ITER tasks WP5-THHE-CCGDS2 and TW4-THHE-CCGDS3 for the Coaxial Cavity Gyrotron and Test Facility: Design, Support to the Industrial Development and Preparation of the Technical Specifications (cf 3.7.1 and 3.7.2). This requires the supervision of the gyrotron, superconducting magnet, body/main high voltage power supplies, crowbar and liquid helium recovery/refrigeration plant, data acquisition and transmission line contracts as well as the installation of the auxiliary equipment necessary to operate said equipment. The latter includes the definition and construction of 1) the security and control system, 2) the cooling water plant and 3) the civil works, power and measurement infrastructure; including equipment and/or input from other EURATOM associations (FZK, ENEA, ENEA/CNR). The tasks are coordinated through regular internal meetings at the CRPP, separate external progress meetings with the various manufactures and milestone meetings with all participating associations and EFDA. All tasks are advancing. A delay in the delivery of the main power supply will be handled by implementing a fall-back solution, temporarily using one of the RHVPS power supplies available at TCV.

4.2.2   *International Tokamak Physics Activities (ITPA)*

The management of the International H-mode Threshold Power DataBase is still ensured by a member of the CRPP. Statistical techniques dealing with errors in variables were used for the evaluation of the power law scaling describing the threshold power. Two reference scalings, one based on the full data set and the other on a reduced set of ITER like conditions, were evaluated for the Tokamak Physics Basis document

4.2.3   *ITER upper port ECH front steering launcher*

CRPP is responsible for the mm-wave design of the front steering (FS) ECH launcher for the upper port plug, see Fig. 4.2.3. This development is being advanced in parallel with the design of an alternative launcher design using a remote steering (RS) concept. A preliminary study of the FS launcher was performed by CRPP in 2004, which demonstrated an enhanced performance of the launcher relative to the base design (RS launcher). The encouraging results of the study prompted a contract with EFDA to advance the design to an equivalent technical level to that of the RS system. The development has continued into 2005, with both mm-wave designs at an equivalent level of design. The FS concept has been selected as reference design, while the deveopment of the RS will continue as a fall back option.
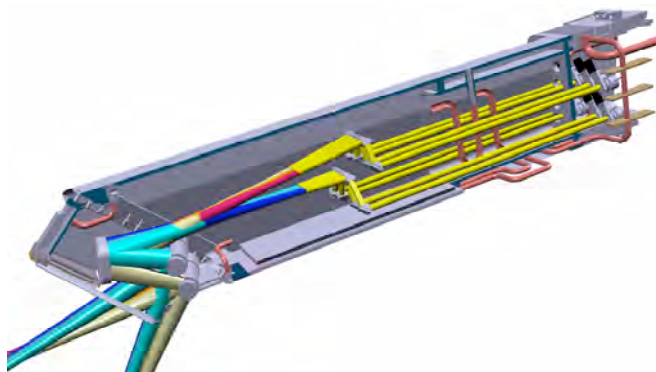
Fig. 4.2.3   *Present design of the FS launcher compatible with injecting eight 2.0MW RF beams*

The preference with the FS launcher is motivated by the enhanced physics performance. The main role of the upper port launcher is to stabilise the Neoclassical Tearing Mode (NTM) when it occurs in the ITER plasma. In order to stabilise the NTM, a very localised current source (j_{CD}) has to be deposited in the magnetic island of the relevant q-surface (q=2 or 3/2). The magnitude of the current must be larger than the local bootstrap current (j_{BS}). The NTM stabilisation efficiency figure of merit (η_{NTM}) is given by max(j_{CD})/j_{BS}, the requirement for complete NTM stabilisation has been formulated as

    sufficient: η_{NTM} > 1.2
    marginal: 1.0 < η_{NTM} < 1.2
    insufficient: η_{NTM} < 1.0

In addition to providing a localised current source, the launcher must be able to direct (or steer) the ECH beam so that the beam is deposited in the island over the entire range that the q=2 and 3/2 surfaces are expected to occur in the relevant ITER scenarios (2, 3a and 5), see Fig. 4.2.4.
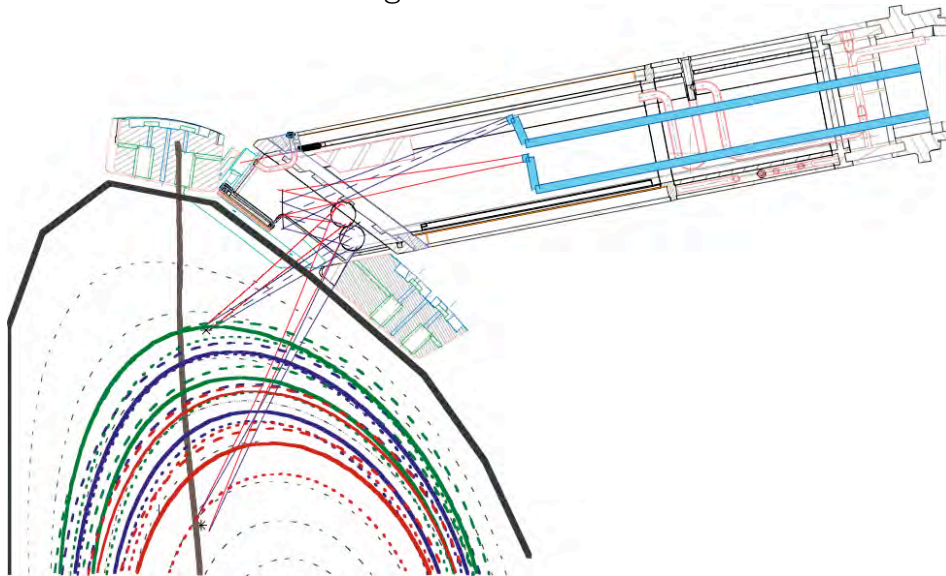
Fig. 4.2.4   *The steering range required of the FS launcher to access all relevant q=2 and 3/2 flux surfaces susceptible to NTMs.*

The FS launcher is designed to provide an optimal focusing of the mm-wave beam into the plasma. This is achieved by allowing the beam to expand from the waveguide aperture to the focusing mirror. A large spot size (~64mm) at the focusing mirror allows the beam to be focused to a relatively small size (~20mm) far into the plasma (~2.1m from the focusing mirror). A steering mirror is placed after the focusing mirror so that the steering and focusing functions are decoupled,. The optimised focusing of the FS launcher has a significant improvement in the NTM stbilisation efficiency as shown in Table 1. On average there is a factor of 3 enhancement for q=2 and 4.3 for the q=3/2 comparing the two launchers. This implies that with the FS concept for all scenarios the NTMs can be stabilised with only two of the three port launchers to be implemented on ITER..

	Scenario 2		Scenario 3a		Scenario 5	
	q=3/2	q=2	q=3/2	q=2	q=3/2	q=2
η_{NTM} FS	2.52	3.54	1.82	2.69	1.93	2.07
η_{NTM} RS	0.56	1.27	0.36	0.69	0.53	0.91

Table 4.2.1 *Comparison of the stabilisation efficiency of the two launcher designs for the three scenarios of interest on ITER. The FS launcher outperforms the RS launcher by a factor of 3 for the q=2 NTM and 4.3 for the q=3/2 NTM.*

In parallel an alternative FS launcher design is being developed with an extended physics applications for ITER. The FS launcher can be designed to access further inward or outward to be used for other physics applications, such as control of the sawteeth, ELMs and FIR. This extended physics FS launcher could also alleviate the requirements of the ECH launcher located in the equatorial port (being designed by JAEA), such that the two launcher can be re-designed for an optimum ECCD system for the ITER physics requirements.
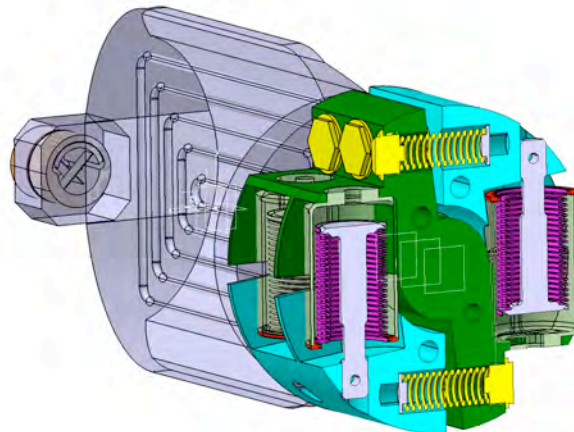
Fig. 4.2.5 *Exploded view of the conceptual steering mechanism design with the principle components identified.*

The present FS launcher (as shown in Fig. 4.2.3) consists of 8 waveguides entering into the port plug. All 8 beams (up to 2.0 MW per beam) are incident on one single focusing mirror and then reflected down to two steering mirrors. The steering mechanism uses a frictionless, backlash-free pneumatic system, as shown in Fig. 4.2.5.

The concept has arms of the mirror positioned between a set of bellows and springs, see Fig. 4.2.6 Increasing the pressure in the bellows pushes the mirror against the springs, which compres due to the applied force. The mirror can be rotated back by decreasing the bellows pressure resulting in the springs pushing the mirror against the bellows.
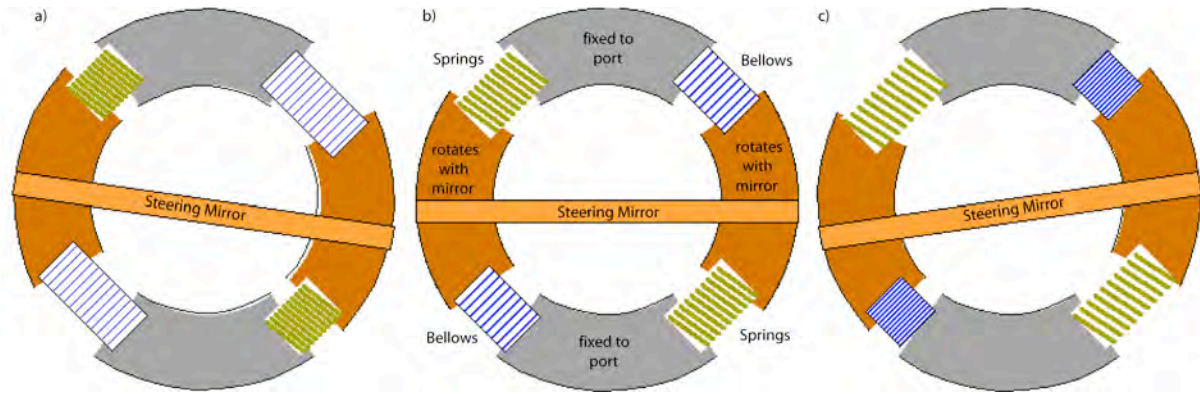
Fig. 4.2.6 *Conceptual design of the pneumatic actuator system of the FS steering mechanism. The mirror rotation is achieved by controlling the bellows pressure. Increasing the pressure compresses the springs and rotates the mirror. The mirror is rotated backwards by decreasing the bellows pressure and the spring forcing the mirror back..*

Traditional ball-bearings are replace with flexure pivots, as shown in Fig. 4.2.7a). The flexure pivot is made from a set of co-axial cylinders held together by thin fins. The fins bend permitting rotation of one cylinder relative to the other as illustrated in Fig. 4.2.7b). One cylinder is connected to the stator (green section of Fig. 4.2.5 and 4.2.7b) that is fixed to the port plug. The rotor (blue sections of Fig. 4.2.5 and 4.2.7b) is attached to the mirror and rotates.
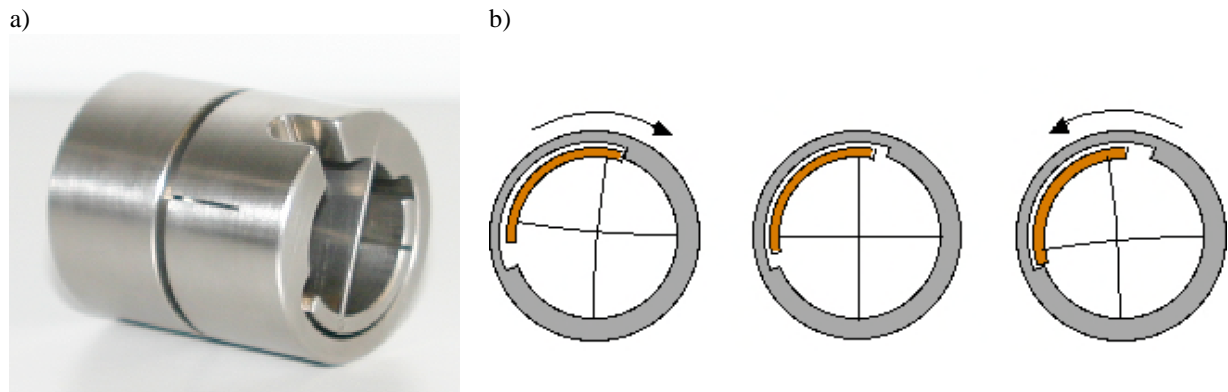
Fig. 4.2.7 *a) A flexure pivot machined at CRPP for the FS steering mechanism. B) the conceptual workings of the flexure pivot, which uses a set of thin fins that bend to allow rotation of the rotor (blue) relative to the stator (green).*

This steering mechanism design is capable of satisfying the steering requirements for the first four years of operation on ITER without incurring cyclic fatigue and withstanding >1'000 Vertical Disruption Events.

The overall launcher design is compatible with the safety and operational requirements as outlined by ITER documents. In the event of a steering mechanism failure, the cooling and pneumatic systems can be isolated and evacuated to reduce the quantity of contaminates introduced into the ITER volume. For example a coolant leak in the cooling tubes to the steering mirror woult leak ~10liters into the torus before the lines could be remotely closed and evacuated. This volume would result in a ~22mbar pressure rise in the torus, which could be evacuated by the ITER pumping system without triggering a venting of the torus volume. The steering

mirror would no longer be functional, but could be repaired at the next scheduled torus opening. ITER operation can continue, the nuclear heat load will be evacuated from the mirror via blackbody radiation.

The preliminary design of the steering mechanism is nearing completion, with construction of the first prototype schedule to begin before the end of 2005 and testing at the beginning of 2006. The whole launcher design is to be advance so that a build-to-print model is available by the beginning of 2008. [EFDA-CSU Garching, D; ITER-IT and the Associations ENEA-CNR-Milano, I; FZK, D; IPP-Garching, D]

International collaboration

Informal discussions between CRPP and JAEA on the design of the two FS launchers (upper and equatorial ports) have progressed during 2005. The goal is to share design and analysis of the two launcher designs in order to provide an optimal set of launchers for ITER. Development of specific mm-wave components compatible for use on both launcher designs is also in progress.

Informal discussion between CRPP and GA, USA have been held to discuss the design of the upper port FS launcher (GA had been responsible for the launcher design prior to 2000). Also, GA is a world leader in providing the HE_{11} corrugated waveguide to be used in the launcher design. The expertise has been solicited to optimize the design of the waveguide components.

4.2.4   *Superconductivity*

A large number of specific R&D technology tasks were dedicated to studies of different superconductivity issues, mostly described in detail in section 2.5, partly funded by EURATOM preferential support. These are summarised as:

TW5-TMSC-SULT : SULTAN Operation
TW5-TMS-EDDES : European Dipole Design
TW3-TMSC-ASTEST : Advanced Strand Test
TW4-TMSC-SAMFSS : Heat Treatment of two Full Size Samples
TW1-TMC-JSPREP : Joint resistance distribution
TW4-TMSF-HTSCOM : Conceptual Design of External HTS Bus Bars
TW5-TMS-HTSMAG : Scoping Study of HTS Fusion Magnets
TW5-TMSC-HTSPER : HTS Materials for Fusion Magnets

4.2.5   *Materials*

Long term and next step tasks are performed by the materials group, described in detail in section 2.6.

Tasks Long Term

TW1-TTMS-001 deliverable 3 : Proton irradiation of EUROFER 97 up to 1 dpa of plate, for He effect testing
TW1-TTMS-002 deliverable 20 : Tensile and fracture toughness of EUROFER 97, punch testing
TW2-TTMS-004b deliverable 3 : Development and testing of coatings to improve the corrosion resistance vs Pb17Li at T>450°C

TW2-TTMS-005b deliverable 6 : Small-scale fracture mechanics - Modelling of brittle and brittle to ductile transition behaviours using appropriated theories. Formation of rules for transferability to standards and fusion components

TW3-TTMS-005 deliverable 1 : Low cycle fatigue testing of EUROFER 97

TW3-TTMS-005 deliverable 2 : Investigation (tensile and Charpy testing) of PHT and PWHT to improve the design limits and to define the acceptable temperature range

TW3-TTMS-007 deliverable 8 : Irradiation in SINQ

TW3-TTMS-007 deliverable 10 rev.1 : MD simulations of effects of cavities

TW4-TTMA-002 deliverable 2 : Development of W-based materials for future divertor application using electrodeposition

TW4-TTMS-005 deliverable 4 : Support in development of design rules for structural materials with low ductility

TW5-TTMS-001/D7 : Assessment of irradiations performed on EUROFER97

TW5-TTMS-005/D2 : SSTT: Model the brittle transition region - continuation of TW2-TTMS-005b/D6

TW5-TTMS-005/D10 : Support in development of design rules for structural materials with low ductility

TW5-TTMS-005/D11 : Experiments in support of TW5-TTMS-005/D2

TW5-TTMS-006/D2 : Characterisation of reference EU ODS-EUROFER batch

TW5-TTMS-006/D4 : Nanocomposited ferritic steels for HT application

TW5-TTMS-007/D11 : Ion irradiations for verification analyses on thin foils of Fe-Cr-C model alloys

TW5-TTMS-007/D15 : Dislocation-defect interaction and the evolution of the deformed microstructure in Fe (development of dislocation dynamics methods)

TW5-TTMS-007/D18 : Molecular dynamics calculation of the temperature dependence of the dislocation-defect interaction in Fe

TW5-TTMS-007/D24 : Definition of a programme for verification and validation of the tools developed using multi-ion beam sources

Tasks Next Step

TW4-TVM-CUSSPIT : Testing of irradiated CuCrZr/SS joints produced under different blanket manufacturing conditions

TW5-TVM-COMADA: Investigation of the effect of creep fatigue interaction on the mechanical performance and lifetime of CuCrZr

4.3 Collaborations on other tokamak experiments

4.3.1 Measurement of the equilibrium using positional modulation

Experiments have been performed on Tore Supra to test the method developed in TCV simulations using DINA-CH. The analysis is pending available effort.

4.3.2 Triggering of ELMS

No new experiments were performed on ASDEX Upgrade, but simulations were made to test the usefulness of radial modulation, which has been proposed for future ASDEX Upgrade experiments.

4.3.3   *Intermediate mode number Alfvén Eigenmodes in Alcator C-mod*

The first experiments on the damping of Alfven Eigenmodes in alcator C-mod have been performed using the recently commissioned active MHD excitation system. Clear resonances corresponding to Toroidal AEs of intermediate toroidal mode numbers have been identified, demonstrating the possibility of driving intermediate n TAEs with localised loop antennas. Damping rates are observed to depend on the plasma-wall distance and on the plasma shape, but in a different way from the low n AEs extensively investigated on JET.

4.4   *Plasma surface interactions in collaboration with the University of Basel*

All optical diagnostic systems on ITER will be based on metallic first mirrors. The possible deterioration of their surface reflectivity as a result of erosion and re-deposition processes represents a serious concern and has recently become the subject of a concerted effort within the tokamak community, both to characterise the effect and seek methods by which it might be mitigated. In partnership with the Univ. of Basel Physics Department, where a high level of expertise in surface analysis and optical characterisation techniques has been developed, CRPP is participating in this first mirror, community-wide effort.

Highly polished mirror samples manufactured in a variety of different materials of interest to ITER (Mo, W, Si) are prepared at the University of Basel and installed on a specially designed manipulator which allows sample insertion into the divertor floor region of TCV (Fig. 4.4.1). A separate pumping system allows the mirrors to be easily inserted and retrieved following exposure without any requirement for a vacuum vessel vent. Samples are recessed behind the front surface of the graphite divertor floor tiles to avoid direct plasma impact, with 5 cm being a typical recess distance (although several distances are being tested). The manipulator location places the samples far from the outer strike point of standard TCV single null lower discharges and hence, it is hoped, simulates the situation of mirrors placed well away from the main plasma-wall interaction area in ITER.
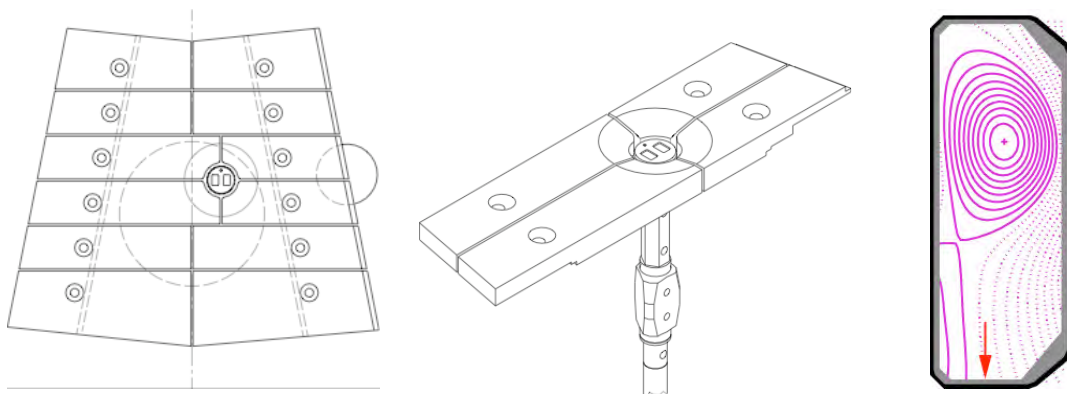
Fig. 4.4.1   *Illustrating the insertion of mirror samples into the TCV divertor floor. Special chamfering is provided around the sample entrance hole to prevent strong plasma-surface interactions in the sample vicinity. The red arrow in the TCV equilibrium at left indicates the sample location.*

The large variety of magnetic equilibria studied on TCV and the absence of any shutter system protecting the samples means that most exposures are integrated across short campaign periods of 2-3 weeks, including regular helium glow discharge conditioning. Before and after each sample exposure, optical measurements and surface analysis are performed at the University of Basel. Spectroscopic ellipsometry is used to determine the optical properties of the samples and the deposited layer thickness, whilst XPS and SEM give information on the layer composition and morphology.

In experiments to date, very thin carbon layers have been found on the sample surfaces, but strong carbon accumulation has in some cases been found at the border between area open to the plasma and area protected by the sample head (Fig. 4.4.2). Under identical exposure conditions the mirror substrate can strongly influence the deposit thickness found on the sample: the carbon layer thickness on a Si sample is found to be five times higher than on a Mo substrate. This is thought to be an interesting demonstration of the preferential reflection, by a given substrate, of incoming neutral atoms, leading to enhanced sputtering of the surface layer. It has potentially important consequences for first mirror material choice and dedicated laboratory experiments are running in Basel to investigate this further. Meanwhile, exposures continue on TCV of varying substrate, exposure duration and recess distance.
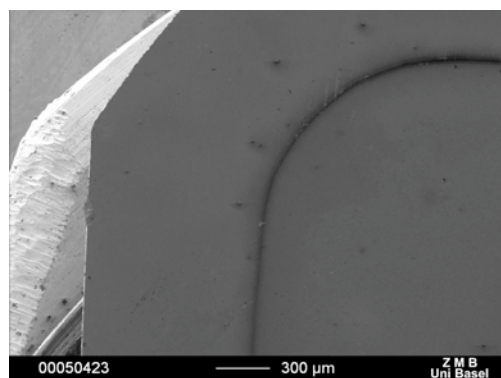
Fig. 4.4.2 *SEM picture of the carbon accumulation found at the border between the exposed and non-exposed areas of a Mo mirror sample recessed 10 mm below the TCV divertor floor surface. The zone inside the thin black ridge (to the right of the image) corresponds to the exposed area. These results were obtained during a dedicated exposure on TCV comprising 19 identical standard ohmic lower single null diverted discharges with 320 kA of plasma current, corresponding to a total of 21 s of plasma exposure.*

SEM picture of the carbon accumulation found at the border between exposed and non exposed areas.

4.5   Socio-Economic Studies

In July 2005, the Organising Committee (initially) comprised of G. Bechmann ITAS, T. Flüeler ETH (principal investigator), A. Grübler IIASA, E. Jochem ETH, D. Spreng ETH (chair), GC. Tosato EFDA met for one day in Zurich. They discussed the main questions to be answered in the project as well as the research plan. In the preparatory discussions it was agreed to enlarge the scope and open the project up to a multi-client study involving diverse relevant energy technologies. It was also decided to invite more members to join the Organising Committee in order to better cover the possible research fields relevant to the project.

Due to the idea of transforming the project to a multi-client study there is a delay in starting preparation of the planned workshop(s). A meeting with the enlarged

organising committee will take place early in 2006 and it is hoped that the project can still be completed in 2006. The work undertaken so far shows that extreme care has to be exercised not to fall into the trap of having one world view or one scientific outlook dominate the project.

4.6   Collaborations with other EURATOM Associations

J-F. Artaud, V. Basiuk, Association EURATOM-CEA, France, *"Coupling of the DINA-CH and CRONOS codes to simulate the ITER hybrid scenario"*

F. Castejon, CIEMAT, Madrid, Spain; **F. Volpe**, Culham Laboratories, UK, *"Electron Bernstein Wave Current Drive in Stellarators (and Tokamaks)"*

S. Cirant, F. Gandini, EURATOM-ENEA-CNR Association, Italy, *"Electron transport studies on TCV via shear modulation experiments with ECCD"*

G. Conway, IPP, Garching, Germany, *"Planning of a reflectometer diagnostic for TCV"*

A. della Corte, Association EURATOM-ENEA, Italy, **D. Ciazynski**, Association EURATOM-CEA, France, *"Test in SULTAN of the ITER TFAS (Advanced Strand)"*

W. Fietz and **R. Heller**, Association EURATOM-FzK, Germany, **A. della Corte**, Association EURATOM-ENEA, Italy, **J. Rifflet**, Association EURATOM-CEA, France, **F. Toral** and **J. Lucas**, Association EURATOM-CIEMAT, Spain, *"Conceptual design of 12.5 T EFDA Dipole"*

R. Heller, Association EURATOM-FzK, Germany, *"EFDA task on design of high temperature superconducting bus bars"*

Y. Ilyin and **A. Nijhuis**, University of Twente, The Netherlands, *"Assessment of AC losses results from tests in SULTAN"*

H.P. Laqua, IPP Greifswald *"Electron Bernstein Waves on TCV"*, Successful experimental determination of optimum ECRH injection angles for mode conversion from O- to X- and finally to Bernstein mode.

D. Mazon, Association EURATOM-CEA, France, *"Temporary loan of imaging hard-x-ray camera"*

Ph. Moreau, Association EURATOM-CEA, France, *"Equilibrium diagnosis by modulation"*

S. Nowak, EURATOM-ENEA-CNR Association, Italy, *"Modeling of X3 top-launch on TCV with beam-tracing code ECWGB"*

Y. Peysson, J. Decker, Association EURATOM-CEA, France, *"Quasilinear Fokker-Planck simulations and modelling of hard X-ray emission in TCV"*

V. Piffl, IPP Prague, September-October. The aim of this collaboration is to study the carbon ionisation equilibrium using Charge Exchange Spectroscopy and to infer transport coefficients for carbon ions.

A. Rodrigues, L.A. Pereira, C. Varandas, CFN Lisbon, *"Advanced plasma control for TCV"*. This project consists in upgrading the central analogue controller of the

TCV plasma control system with a system based on an array of DSP boards connected together to provide about 32 inputs and 32 outputs.

I. Tigelis, S. Mallios, Association Euratom Hellenic Republic, *"Modeling of the EM field distribution at 2.45GHz in the empty TORPEX torus"*

I. Tigelis, G. Latsas, Association Euratom Hellenic Republic, *"Instability calculations in the 170GHz coaxial-cavity-gyrotron beam-duct"*

G. Veres, HAS, Budapest on impurity transport using laser ablation. A first visit took place in March, which allowed the apparatus, supplied by KFKI in 1997, to betaken into service again. A follow-up visit will take place in October-November, with the aim of injecting Ti into eITB plasmas.

F. Volpe, Association UKAEA Fusion, Culham, UK, *"Electron Bernstein wave (EBW) modelling with the ART ray tracing code, planning of EBW experiments on TCV"*

M. Windridge, Association UKAEA Fusion, UK, *"Non-linear modelling of MAST"*

4.7 Other international collaborations

J. Egedal, W.Fox, M.Porkolab, PFSC, MIT, USA, *"Investigation of the physics of magnetic reconnection in the collisionless regime in a dedicated laboratory device, the Versatile Toroidal Facility"*

Dr. Debasis Chandra, IPR, Bhat, Gujarat, India, *"Comparison of theoretical and experimental stability properties of resistive MHD modes with plasma shape"*

R. Gruber, EPF-Lausanne, Switzerland, **S.P. Hirshman**, ORNL, USA, **K.Y. Watanabe, H. Yamada, S. Okumara, Y. Narushima, S. Sakakibara, C. Suzuki, T. Yamaguchi**, NIFS, Japan, **K. Yamazaki**, Nagoya Univ., Japan, *"3D anistropic pressure equilibrium and fluid magnetohydrodynamic stability"*

R.W. Harvey, A.P. Smirnov, E. Nelson-Melby, CompX, San Diego, CA, USA, *"Development of a fully relativistic ray tracing solver for study of mode conversion and electron Bernstein wave propagation in TCV"*

W. Heidbrink, H. Boehmer, UC Irvine, USA, *"Sources for energetic ions for a simple magnetized torus"*

Y. Igithkhanov. T. Andreeva, C. Beidler, J. Kisslinger, H. Wobig, Max Planck Institut fuer Plasma Physik, Greifswald, Germany, *"Bootstrap Current Effect on Stability in a 4-Period Helias Reactor"*

M.Yu. Isaev, Russian Research Centre Kurchatov Institute, Moscow, Russia *"Development of the VENUS-df Code for Bootstrap Current and Neoclassical Transport in Stellarators"*

M.Yu. Isaev, Kurchatov Inst. Moscow, Russia, **H. Maassberg, C. Beidler, J. Nuehrenberg, M. Schmidt, J. Geiger**, IPP-Greifswald, Germany, **A. Bergmann**, IPP Garching, Germany, *"Nontecarlo-delta_f neoclassical transport in 3D systems"*

K. Kim, KBSI, South Korea, **K. Okuno**, JAERI, Japan **J. Minervini**, PFSC, MIT, USA, **V. Pantsyrny**, ASRIIM, Russian Fed., and **P. Weng**, CAS, China, "Preparation of ITER conductor qualification samples"

S.Yu. Medvedev, A.A. Martynov, A.A. Ivanov, Yu.Yu. Poshekhonov, Keldysh Institute of Applied Mathematics, Moscow, Russia, **M.Yu. Isaev, V.D. Shafranov, A.A. Subbotin**, RRC Kurchatov Institute, Moscow, Russia
"Equilibrium and Stability of 2D and 3D plasma configurations"

M. Mikhailov, A. Subbotin, V.D. Shafranov, M.Yu. Isaev, M. Samitov, Russian Research Centre Kurchatov Institute, Moscow, Russia; J**. Nuehrenberg**, Max Planck Institut fuer Plasma Physik, Greifswald *"Optimisation of Advanced Stellarator Systems"*

G. Moritz, GSI Darmstadt, Germany, and **V. Vysotsky**, All-Russia Scientific Cable R&D Institute, Moscow, Russian Fed., "Research and development of Novel-Cable-In-Conduit Conductors (N-CICC) for use in the fast ramping superconducting accelerators", INTAS Project 05-96-4889

V. Naulin, Risoe, Denmark (with S.Mueller), *"Adaptation of the ESEL fluid code for modelling of turbulence in the TORPEX device"*

J. Nührenberg, A. Koenies, V. Kornilov, A. Mishchenko, S. Sorge, IPP Greifswald, Germany, **A. Bottino, A. Peeters**, IPP Garching, Germany, **R. Hatzky**, Rechenzentrum MPG Garching, Germany
"Linear and nonlinear gyrokinetic code developments and simulations"

H.K.B. Pandya, Institute for Plasma Research, Bhat, Gandhinagar, India, *"Design of a vertical ECE diagnostic for TCV"*

L. Rossi, CERN, Switzerland, N4 - CARE " Coordination of studies and technical R&D for high energy high intensity hadron beams"

P. Savrukhin, A. Sushkov, RRC Kurchatov Institute, Moscow, Russian Federation, *"Planning of tangential X-ray measurements in TCV"*

V.D. Shafranov, M.Yu. Isaev, M. Mikhailov, A. Subbotin, Kurchatov Inst., Moscow, Russia, **J. Nuehrenberg**, IPP Greifswald, Germany, *"Advanced stellarator optimisation"*

J. Snipes, R. Parker, M. Porkolab, J. Freidberg, J.Sears, PFSC, MIT, USA, *"Fast particle physics, Alfven waves, and active MHD mode excitation on the Alcator C-Mod tokamak plasma"*

A. Sushkov, Nuclear Fusion Institute, Kurchatov, Moscow, Russia: 1) *"Electron heat transport at switch-off in sawtooth-less TCV discharges"*, 2) *"Development, commissioning and use of DMPX soft X-ray wire chamber towards Te measurements"*

E. Valeo, Princeton University, USA, and **R. Berger**, Lawrence Livermore National Laboratory, USA, *"Development of numerical methods for Vlasov simulations"*

E. Zapretilina, Efremov Research Institute of Electrophysical Apparatus (NIIEFA), St. Petersburg, Russian Fed., "Assessment of scaling laws for AC losses in ITER conductors"

Wendelstein Group, IPP Greifswald, Germany, "Test of conductor joint samples"

K. Yamazaki, K. Y. Watanabe, S. Okamura, T. Yamaguchi, Y. Narushima, H. Yamada, S. Sakakibara, C. Suzuki, National Institute for Fusion Science, Toki, Japan; S.P. Hirshman, Oak Ridge National Laboratory, USA, *"Model Anisotropic Pressure Equilibria in Stellarators with Tangential Neutral Beam Injection"*

J. Yu, Institute of Plasma Physics, Chinese Academy of Sciences, Hefei, P.R. China, 'Effects of irradiation in SINQ on the Chinese Low Activation Martensitic steel (CLAM)'.

4.8   Other collaborations within Switzerland

Nothing to report under our fusion activities.

5   The Educational Role of the CRPP

The CRPP plays a role in the education of undergraduate and postgraduate students, particularly in the Faculté des Sciences de Base (Faculty of Basic Sciences) of the EPFL. Advanced education and training in fusion physics and technlogy and plasma physics topics is carried out as part of the research activities of the Association. Section 5.1 presents the 5 courses given to physics undergraduates and to engineering undergraduates. In their fourth and final year, physics undergraduates spend time with a research group at the EPFL, typically 12 hours per week for the whole year. During this period, they perform experimental or theoretical studies alongside research staff, discovering the differences between formal laboratory experiments and the "real" world of research. After their final examination at the end of the 4th year, physics students are required to complete a "diploma" work with a research group, lasting a full semester. This diploma work is written up and defended in front of external experts. The CRPP plays a role in all of these phases of an undergraduate's education, detailed in Sections 5.2 and 5.3.

As an academic institution, the CRPP supervises many Ph.D. theses, also in the frame of the Physics Section of the EPFL. 8 PhDs were awarded in 2005. At the end of 2005 we have 34 PhD students supervised by CRPP members of staff, mostly in Lausanne but also 7 at the PSI site in Villigen. Their work is summarised in Section 5.4.

5.1   Undergraduate courses given by CRPP staff

S. Alberti, *Chargé de cours – "Plasma Physics I"*
This course is an introduction to plasma physics aimed at giving an overall view of the essential properties of a plasma and at presenting the approaches commonly used to describe its behaviour. We study single particle motion, the fluid description and the kinetic model. The relation between plasma physics and developing a thermonuclear reactor is presented and illustrated with examples.

N. Baluc, *Chargée de cours – "Material Physics"*
Basic course on materials physics, presented as an option to 3rd year Physics students. The course covers the theory of diffusion, dislocations and plasticity as well as the characterization of materials. Ways of production, structures, microstructures, physical and mechanical properties are presented for pure metals, intermetallic alloys, superalloys, shape memory alloys, steels, quasicrystals, glasses, gels, liquid crystals, aggregates, ceramics, composites, polymers, and nuclear materials for fission and fusion reactors.

A. Fasoli, Associate Professor – *"Plasma physics II"*
One semester option course presented to 4th year Physics students, introducing the theory of hot plasmas via the foundations of kinetic and magnetohydrodynamic theories and using them to describe simple collective phenomena. Coulomb collisions and elementary transport theory are also treated. The students also learn to use various theoretical techniques like perturbation theory, complex analysis, integral transforms and solution to differential equations.

A. Fasoli, Associate Professor – *"General Physics II"*
This course completes the introduction to mechanics provided in the first semester with the basic concepts of statics, oscillations and special relativity. It also covers the whole of thermodynamics, from the introduction to heat, temperature and kinetic theory to the first and second principles, including entropy and thermal

engines, ending with a treatment of transport and non-equilibrium phenomena in open systems.

J.B. Lister, *Maître d'Enseigenement et Rercherche (MER) – "Plasma Physics III"*
An introduction to controlled fusion, presented as a one semester option to 4th year Physics students. The course covers the basics of controlled fusion energy research. Inertial confinement is summarily treated and the course concentrates on magnetic confinement from the earliest linear experiments through to tokamaks and stellarators, leading to the open questions related to future large scale fusion experiments.

L. Villard, *Professeur Titulaire – "General Physics III-IV"*
Full year course given to students in their 2nd year Mechanical and Electrical Engineering. The course covers fluid dynamics, electromagnetism, waves and an introduction to quantum mechanics.

5.2   Undergraduate work performed at the CRPP

EPFL 4th year students (2005 Summer semester)

Mathieu BERNARD: *"Study of sawteeth in TCV"*
The student investigated the behaviour of sawteeth on TCV. He was able became familiar with the main diagnostics used, X-ray cameras and Electron Cyclotron Emission (ECE) radiometry. As a result of several experiments involving variation of toroidal field and plasma current, he showed that the sawtooth inversion radius correlates with the edge safety factor in qualitative agreement with very simple models. A discrepancy between X-ray and ECE measurements was solved by the introduction of paramagnetic corrections to the vacuum field. An attempt to identify the mixing radius was unsuccessful.

Loïc CURCHOD: *"Characterisation of electron temperature oscillations in off-axis ECRH X2 heat deposition experiments"*
Oscillations were measured on the high spatial resolution soft X-ray DMPX camera, with a characteristic time between energy confinement time and current redistribution time. With strong off-axis heating, sawteeth can be suppressed through loss of the $q=1$ surface, leaving only these long period oscillations. These oscillations can also co-exist with sawteeth, with a period of a few sawteeth, and in this case were already known under the name of "humpback sawteeth". The amplitude of the oscillations is typically larger than that of the sawteeth. The dependence of the oscillation period on the total power, radial deposition location and plasma density was studied. To analyse the radial oscillations, graphical programs were written and reveal that the oscillations are propagating towards the centre. These oscillations are similar the ones found earlier in lower hybrid heated Tore Supra discharges and interpreted as an interplay between the temperature and current profiles with a predator-prey cycle.

Mathias FERBER: *"Analysis of the ELMy operational regimes"*
The access to a stationary ELMy regime with the X3 EC wave heating was found difficult, most plasma discharges having ended in disruption. Multidimensional analysis of the operational trajectories of last year discharges showed only little difference between successful and non-successful discharges. Nevertheless, slight differences in the plasma shape could explain the phenomenon.

Christophe JAN: *"Measurement of the Mach number by probes of different size in the TORPEX plasma"*

The probe constructed in the first semester was used to characterise the plasma fows in different experimental conditions and in different directions. Mach numbers varying between 0 and 1 were observed, according to the plasma scenarios. A comparison of the results from probes of different sizes provided information on the influence of the probe geometry on the results.

Pierre JEAMBRUN: *"Experimental investigation of arc formation upon electrical contact separation in very small gaps"*
Arc formation during electrical contact opening is a key phenomenon which can limit the lifetime of switches and cause damage to various electrical components such as collectors. In this project, the arc formation in very small gaps (below 10 microns) is investigated experimentally on a specially designed set-up composed of two crossed wires. A current is passed through the contact between the wires and is interrupted by means of a piezo motor which allows precise movement of one of the wires. During separation, the electrical parameters of the circuit such as current and voltage are measured. In addition the light emitted by the arc when present is collected by an optical fibre and detected with a photomultiplier tube. Successive metal vapour arcs are observed at very small gaps (below 10 microns) due to the vaporisation of the liquid metal bridge formed during contact separation. At larger gaps gaseous arcs can be observed depending on the surrounding atmosphere. The effect of current, material, surface roughness and surrounding atmosphere on the formation and duration of arcs is investigated.

Martin JUCKER: *"Effect of anisotropic fast particles on axisymmetric equilibria"*
The anisotropic version of the fixed boundary version of the VMEC equilibrium code based on the variant of a bi-Maxwellian distribution function to model the effects of energetic particles was applied to a circular cross section tokamak of aspect ratio 3. Most calculations were carried out with a weak background plasma pressure, thus the beta obtained was dominantly from the hot particles. The anisotropy was controlled by the ratio of hot particle perpendicular to parallel temperature chosen mostly as 10 with central deposition. Comparison with analytic calculatutions valid at much larger aspect ratio revealed that basic plasma parameters such as the Shafranov shift, elongation and triangularity of internal flux surfaces failed to conform to expectations. This discrepancy may be due to profile effects.

Jacques VIERTL: *"Helium plasma spectroscopy"*
A study of the mechanisms leading to visible light emission in the TORPEX plasma and determining the width of the spectral lines was undertaken. An upper limit for the ion temperature was estimated by analysing the spectrum of the HeII 468.6nm line.

Nicolas SAGE: *"Three-dimensional magnetic probe"*
The construction of the magnetic probe and of the related electronics was improved. A measurement of the TORPEX confinement magnetic field was completed. First attempts at measuring the spectrum of the magnetic components of fluctuations in plasmas in which a current is induced by transformer effect were undertaken.

External students

Uma GUPTA, from the Indian Institute of Technology, Bombay (Metallurgical Engineering and Materials Science). Ms. Gupta joined the Superconductivity Group of CRPP for a summer training (May-June 2005) in the field of High Temperature Superconductivity. In the framework of this summer training an introduction to high current applications of high temperature superconductors (e.g. HTS current leads, HTS bus bars, HTS power cables) has been provided. In the experimental part of the work the current carrying capacity of an industrially fabricated

AgMg/Ag/Bi-2223 tape has been investigated by means of a temperature variable cryostat inserted in the bore of a 12 T superconducting laboratory magnet. The problems related to the measurement of low temperatures in the presence of high magnetic fields have been addressed. Some of the special features of the properties of high temperature superconductors (anisotropy with respect to the direction of the applied field, granularity, hysteresis of the critical current depending on whether the measurements are performed in increasing or decreasing field) have been considered in more detail.

Clément RECHATIN, from the Ecole Polytechnique (Paris, FR). Mr. Rechetin applied singular value decomposition (SVD) techniques to the study of turbulence in tokamak plasmas. Using this technique with the fast magnetic pickup coil, ECE and reflectometer diagnostics he was able to show that it is possible to determine the spatial structure and frequency distribution of the plasma instabilities. Clément has also applied the SVD technique to the study of turbulence at the H to L-mode transition. Clément has also applied other analysis to the turbulence at the H to L-mode transition showing that the turbulence has characteristic wave dispersion and power laws suggesting that this turbulence may be related to drift wave turbulence.

5.3   EPFL Diplomas awarded in 2005

Olivier PISATURO: *"Design and construction of a Mach probe for the TORPEX experiment"*
Following the work performed during the previous semester, in this laboratory work the student completed the implementation of the Mach probe diagnostic system for measuring plasma flows in TORPEX. A remote mechanical control system for positioning the probe has been installed and commissioned. A full calibration for estimating the absolute values of the flows was performed. In addition, a study of the feasibility of measurements of drift wave fluctuations in the TORPEX plasmas by optical emission diagnostics was performed. A two-channel system based on photomultiplier tubes is suitable for the detection of TORPEX fluctuations, the measurements of their spectra, their statistical properties and correlation functions. First calibrations of a one-channel prototype system were also performed.

Jonathan ROSSEL: *"Soft X-ray emissivity profile inversion in quasi-axisymmetric equilibria"*
A complete method of tomographic inversion accounting for the presence of magnetic islands and based on the measurements of a single pin-hole soft X-ray camera is presented. The method divides the signals into a low frequency component used for the determination of the stationary emissivity, and a high frequency component used for the parametric determination of the magnetic island emissivity. The magnetic islands are simulated by a simple model based on the concentration of a current perturbation on a resonance surface. A method of correction of the magnetic equilibrium using the tomographic inversion is also described. The inversion method results in a very accurate determination of the position of the resonance surface, as well as a precise estimation of the island width. Due to the high degree of automation of the method, only a minimal prior knowledge of the parameters of the magnetic islands is required. A possible application could be the assessment of models of the dynamics of the island growth.

Master studies presently underway (Winter semester 2005)

Mathieu BERNARD (H. Weisen)
Loïc CURCHOD (A. Pochelon)
Martin JUCKER (L. Villard)
Nicolas SAGE (A. Fasoli)

5.4 Postgraduate studies

Postgraduate courses given in 2005

Stefan BRUNNER, Jean-Marc MORET: "*Advanced theory of plasmas*" (course PY-08 of the EPFL doctoral school)
Objectives: complete the theoretical knowledge acquired before the post-graduate studies. Contents: kinetic theory of gas and plasma, relaxation processes in a fully ionised plasma, classical transport, waves in inhomogeneous plasmas, non linear phenomena

Nadine BALUC, Didier GAVILLET, Robin SCHAEUBLIN, Philippe SPAETIG: *"Effects of Radiation on Materials"*
This 28-hours course is given by three lecturers form the CRPP and one lecturer from the PSI (Dr. D. Gavillet). It is aimed at providing extensive information on the effects of radiation (neutrons, protons, ions) on the structure, microstructure and mechanical properties of materials for nuclear installations. It is divided into five chapters: 1) introduction to radiation damage and radiation effects, 2) radiation damage and analysis tools, 3) radiation damage and fracture mechanics, 4) radiation effects on materials for fusion reactors, 5) radiation effects on materials for fission reactors.

Christoph HOLLENSTEIN, Alan HOWLING: *"Plasma in industry: physics basis and applications"* (course PY-10 of the EPFL doctoral school)
The course provides the basis necessary for R&D in the field of plasma processing in industry, outlining the applications and related issues. Contents: Introduction to the physics and chemistry of plasma used in industry; introduction to modelling of plasma in equilibrium and non-equilibrium; plasma sources used in industry.

André JAUN, *prof KTH Stockholm,* **Laurent VILLARD**: "*Numerical Methods for Partial Differential Equations*"
Course of the EPFL Doctoral School given on the web to KTH and EPFL PhD students in science and engineering.

Doctorate degrees awarded during 2005

Gilles ARNOUX: *"Plasma EC heating at the 3rd harmonic of the electron cyclotron frequency"* (EPFL thesis No. 3401(05))
The TCV electron cyclotron heating (ECH) system is composed of 3 gyrotrons (0.5MW, 118GHz, 2s. pulse length in TCV) for the 3rd harmonic X-mode (X3) EC heating. This system has allowed the first detailed study of the X3 absorption properties in a top-launch configuration, based on experiment and simulations.
The X3 absorption is shown to mainly depend on the injection conditions and the electron temperature. Full single-pass absorption has been measured increasing

the central temperature nearly by a factor three (1keV -> 2.7keV) when 1.35 MW was injected in low confinement regime plasmas (L-mode).

An absorption level of 85% has been measured increasing the central temperature by a factor three (0.9keV -> 2.7keV) by injecting 1.35MW in H-mode plasmas. A new ELM dynamic has been observed for the first time in TCV in these experiments.

The X3 absorption was shown to depend strongly on the wave injection angle. In order to maximize the absorption during a plasma discharge by optimizing the injection angle, a real time feedback control has been developed and used in L-mode plasmas. The system is based on the synchronous demodulation technique and uses a PI controller.

In order to simulate the X3 wave propagation and absorption, the linear ray-tracing code TORAY-GA has been used. The simulations predict an absorption dependence on the temperature and the injection conditions in agreement with the experimental results. Since TORAY-GA does not take into account the diffraction effects on the beam propagation, a comparison with the beam tracing code ECWGB that includes diffraction has been performed. This comparison has been performed in collaboration with the CNR in Milano (Istituto di Fisica del Plasma).

The present work on X3 absorption properties has demonstrated the efficiency of the X3 heating system on TCV, therefore extending the beta limits study capabilities in elongated plasmas.

Raul BONADÉ: *"Constitutive behaviour and fracture properties of tempered martensitic steels for nuclear applications: Experiments and modelling"* (EPFL thesis 4460(05))

A detailed microstructural analysis of the tempered martensitic Eurofer97 steel has been undertaken. The main microstructural features of this steel were identified and discussed, including prior austenitic grain size, internal structure of the prior austenitic grains, analysis of second phase particles and description of the dislocation structure in the as-received condition. A high purity Fe-9wt%Cr ferritic model alloy has been developed and its microstructure has also been analyzed in detail.

The plasticity of the Eurofer97 steel and of the ferritic model alloy was studied by means of tensile test, which were carried out over a broad range of temperatures (77 K-473 K) and strain rates. The plastic flow of these alloys has been modelled using the one-microstructural parameter model (dislocation density). As expected for the body-centered cubic metals and alloys, two different temperature regions on temperature were identified; these regions are characterized by different temperature dependences of the yield stress and of the plastic strain-hardening. The, first region, at $T > 200K$ was modelled based on the Kocks model originally developed for single phase face-centered metals and alloys. This model provided a successful description of the hardening behavior for the Eurofer97 steel. For the ferritic alloy, the one parameter model was applied successful only in a small range of plastic deformation. The formation of elongated dislocation cells has been identified as the microstructural feature responsible for the departure of the model predictions. In the low temperature regime $T < 200K$, the lattice friction on the screw segments strongly influences the dislocation dynamics. We have modified a model originally proposed by Rauch to account for the effect of the lattice friction. A general constitutive law has been developed for the Eurofer97 at low temperatures. The modified model described properly the experimental data with parameters consistent with the characteristics of the microstructure. Finally, the analysis of the effect of temperature on the parameters of the two models was consistent with the expected trends of the physical phenomena associated to it.

It has been clearly demonstrated that the toughness master curve of the reactor pressure vessel (RPV) steels, does not describe properly the temperature dependence of the fracture toughness in the case of the tempered martensitic steel Eurofer97. Based on our extensive experimental data obtained with well

constrained C(T) specimens of the 25 mm thick plate, a new master curve has been proposed:

$$K_{Jc(med)} = 30 + 70\,exp\left[0.04(\,T - T_0\,)\right]$$

A possible variation in fracture toughness through the thickness of the 25 mm plate has been investigated using small 0.2 T C(T) specimens. No variation in fracture toughness has been observed.

Size effects in fracture toughness has been studied by comparing 0.2 T C(T) and 0.4 T C(T). We have demonstrated that the censoring limits determined from the ASTM E1921 procedure (M=30) is too lenient. Based on detailed statistical analysis of the fracture data, a new M value of 80 is proposed for the C(T) specimens.

A comparison between our data and data from other authors revealed an important difference in fracture toughness between the 14 mm and the 25 mm plates of Eurofer97. This difference has been assessed by determining the transition temperature T_0 using the procedure described in the ASTM E-1921 standard combined to the new expression for the master curve.

We have compiled a fracture toughness C(T) database for the F82H mod. The results have been compared to the Eurofer97 database. We have demonstrated that both datasets share a common lower bound curve for fracture toughness. However, the upper bounds defined by the extension of the scatter at different temperatures are very different. Indeed the F82H mod. steel features a larger scatter band for all the temperatures analyzed. The differences in fracture toughness were correlated to those observed on Charpy tests with KLST specimens.

A local model for cleavage fracture has been used to predict correctly the lower bound fracture toughness curve for Eurofer97. The model assumes that cleavage fracture occurs when a critical condition is attained. This critical condition is defined by a critical stress σ^* acting on a critical area A^*. Detailed 2D finite element modelling of C(T) specimens has been undertaken to calibrate the parameter of the model for the Eurofer97 steel. We have demonstrated that the calibration of the model strongly depend on the particular specimen geometry used. In this sense, the use of general Area-K_{Jc} correlations as obtained from small scale yielding conditions cannot be used in the context of the σ^*-A^* model.

Emiliano CAMPITELLI: "*Study of the relation between irradiation-induced microstructure and mechanical properties in Zircaloy*" (EPFL thesis No. 3304(05))
In the framework of a fission materials surveillance programme, the need has arisen to design experimental methods to be used with a limited amount of material for Post Irradiation Examination of Zr alloys reactor components. Having to deal with radioactive material, it was particularly important to devise experimental testing procedures as simple as possible but from which reliable information could be drawn. Also, within fusion materials development programme, irradiations have continuously been performed either in reactors or with particle accelerators. In both cases, the irradiation volumes are usually limited. The concern here is to optimize the volume of the irradiated samples and to have a very definite and homogeneous damage dose and irradiation temperature. The goal of this work was to implement finite element models for non-standard tests to ultimately study the mechanical properties of Zircaloy cladding tubes for fission applications and tempered martensitic steels for fusion applications in the unirradiated and irradiated condition. One model was developed for a proposed, new kind of ring tensile tests. Another model was developed for the so-called small ball punch test. In both cases the use of non-standard tests was validated by performing standard tests on alloys with well-defined mechanical constitutive behaviour and by using it as an input in the finite element models of the non-standard tests. In this way, the irradiation hardening of the irradiated condition in both materials was assessed giving results in excellent agreement with literature. In addition, the anisotropic mechanical

properties of the Zr alloy were characterized and the strain hardening behaviour of the irradiated and unirradiated tempered martensitic steel was characterized at strain levels for which tensile tests would have been inappropriate.

Sergi FERRANDO i Margalet: *"Bootstrap Current and Stability in the Asymptotic Regime in Quasi-Symmetric Configurations" (EPFL thesis 3379(05))*
This thesis has been divided into two parts. In the first part, we present a self-consistent method to calculate the BC and assess its effect on equilibrium and stability in general 3D configurations. This procedure is applied to two reactor-size prototypes: a quasi-axisymmetric (QAS) system
and a quasi helically symmetric (QHS) system with magnetic structures that develop BC in opposite directions. The BC increases with the plasma pressure, therefore its relevance is
enhanced when dealing with reactor-level scenarios. The behaviour of both prototypes at reactor level values of beta is assessed, as well as its alteration of the equilibrium and stability. In the QAS prototype, BC-consistent equilibria have been computed up to beta=6.7% and the configuration is shown to be stable up to beta=6.4%. Convergence of self-consistent BC calculations for the QHS case is achieved only up to beta =3.5%, but the configuration is unstable for beta> 0.6%. The relevance of symmetry breaking modes of the Fourier expansion of the confining magnetic field on the generation of BC is studied for each prototype. This proves the close relationship between magnetic structure and BC. Having established the potentially dangerous implication of the BC, principally, in reactor prototypes, a method to compensate its harmful effects is proposed in the second part of the thesis. It consists of the modelling of the current driven by externally launched ECWs within the plasma to compensate the effects of the BC. This method is flexible enough to allow the identification of the appropriate scenarios in which to generate the required CD depending on the nature of the confining magnetic field and the specific plasma parameters of the configuration. Both the BC and the CD calculations are included in a self-consistent scheme which leads to the computation of a stable BC+CD-consistent MHD equilibrium.

Andrei MARTYNOV: *"Ideal MHD stability of tokamak with moderate and low aspect ratio"* (EPFL thesis No. 3218(05))
The thesis has studied the instabilities occurring in plasmas in tokamak configurations, within the framework of ideal magnetohydrodynamics. Particular emphasis was given to the instability caused by the internal kink modes which, in configurations with low aspect ratio, are studied both within a standard analytical approach and using numerical simulations. The results showed the invalidity of the analytical approach in these configurations and proposed a parameterization based on numerical results. An easy-to-use scaling formula has been derived which should be useful for many applications, in particular transport simulations with a self-consistent sawtooth model. The thesis has also studied in details the instabilities occurring with reverse magnetic shear profiles and relatively large local gradients. External kink modes and infernal modes can become unstable even at relatively low values of the normalized beta, $\beta_N \sim 1$. The dependence of the stability limits on the value of the minimum q, its radial location and the pressure gradient have been analysed. A comparison with experimental results has shown that these modes are responsible for the disruptions or minor disruptions observed in electron internal transport barriers scenarios in TCV.

Lukas STINGELIN: *"Beam Cavity Interactions in High Power Cyclotrons"* (EPFL thesis No. 3169(05)*)*

The ring cyclotron of the Paul Scherrer Institute (PSI) accelerates an intense proton beam from 72MeV up to 590MeV. This beam can excite parasitic electromagnetic oscillation modes (HOMs), because of its time structure.

Until now, there was no tool available to predict the potentially harmful effect of these HOMs onto the beam operation of the cyclotron. It is foreseeable that these effects might play a role if even higher beam currents have to be accelerated. This dissertation investigated therefore beam-cavity interactions by numerical analysis and measurement.

A simplified computation method is developed since a self-consistent simulation is impossible on today's computers: The parallel eigensolver Omega3P of the Stanford Linear Accelerator Center (SLAC) allowed us to calculate eigenmodes of the entire ring cyclotron for the first time ever. The rf fields are expanded onto a superposition of these modes and the excitation is calculated in frequency domain. Trajectories of the particles in the static magnetic field, superposed with the space charge fields and the beam excited HOMs, are then simulated.

The simulation results confirm that up to proton beam currents of 2mA, corresponding to the routinely accelerated beam intensities, only a small deformation of the charge distribution appears. This thesis leads to a new simulation tool for further studies of intensity increases in high power cyclotrons.

Raluca STOENESCU: *"Effects of neutron irradiation on the microstructure and mechanical properties of the heat affected zone (HAZ) of stainless steel welds"* (EPFL thesis No. 3326(05)*)*

Multiscale modelling appears now as a major tool for the description of plasticity of materials. This work is aimed at determining the amplitude of plasticity mechanisms influenced by radiation induced effects at the mesoscale level (μm) by computational simulation. It is proposed to perform dislocation dynamics simulations of the plasticity of Fe and Fe-Cr samples containing given densities of irradiation-induced defects (dislocation loops, voids, He bubbles) at temperatures below 400°C. Eventually, a model alloy containing the unshearable hardening features representing the defects shall be established. In this work the microMegas code is used for applying the Discrete Dislocation Dynamics model for simulating and visualizing dislocation-based plastic deformation in crystals. Preliminary results of the simulation, performed for low strains, showed a serration behavior of the stress versus strain. Also it has been observed that in the presence of obstacles in the matrix, deformation occurs by junction formation and cross slip events at the beginning of deformation and then by increase in the dislocation density as a result from forest hardening.

Marco WISCHMEIER: *"Divertor detachment in the TCV and JET tokamaks"* (EPFL thesis No. 3176(05)*)*

Divertor detachment is currently assumed to be a fundamental pre-requisite for the successful operation of future fusion reactors. Only by partially detaching the divertor in the regions of highest power flux density can high performance tokamak operation be made compatible with the technological limits set by the thermo-mechanical properties of surfaces in contact with the plasma. Although the various physics components of the detachment process are thought to be well known, their relative importance and the degree to which each may affect the others, thus determining the final detached state, cannot in general be deduced from any simple analytic approach. Instead, sophisticated two and three dimensional interpretative and predictive code packages have been developed within the fusion community to model the scrape-off layer (SOL) and divertor plasmas of magnetic confinement devices. One of these, the SOLPS code, has for some time been employed as a tool for the design of the divertor in the next step tokamak reactor, ITER. In reality,

however, these codes have not, in general, been fully validated against experimental observations from current tokamaks, in particular with regard to divertor detachment.

This thesis aims to contribute to such validation by thorough comparisons between numerical simulations, using the SOLPS5 (plasma fluid, Monte Carlo neutral) code package and experimental characterization of the detachment process in two very different tokamaks, TCV and JET. The approach taken has been to test the code against experiment, not only for two machines with a vast difference in size and divertor geometry, but also for plasma operation with either deuterium or helium fuel. Changing the fuel species in a tokamak containing significant graphite first wall components as do TCV and JET, dramatically modifies the impurity production mechanism but also the important atomic physics processes at work, both of which influence the detachment threshold. In TCV, divertor detachment in the simplest of situations is experimentally observed to be anomalous and could not be explained by the first attempts at code modelling prior to this thesis. Evidence is presented for the detachment anomaly being directly linked to enhanced interaction between the graphite main chamber walls at high plasma density due to anomalous convective radial transport. Such interaction is not well modelled by the code and the results presented in this thesis highlight an important area in which the complexities of the real situation are inadequately represented in the numerical model. This work also constitutes the first known application of the SOLPS code to tokamak simulation with consistent modeling of molecular hydrocarbons. Indeed, they are found to be important in producing high degrees of numerical detachment.

In JET, experimental data from high density helium plasma operation have been successfully modelled, constituting the first ever simulations of pure He discharges on this machine. Helium detachment is very different to that in deuterium, due in large part to the absence of carbon chemistry. The simulation results demonstrate this together with strong evidence for conclusions to be drawn concerning the principal mechanisms driving the detachment. Similar good agreement is obtained between code and experiment for helium operation on TCV and a comparison of code results between the two devices demonstrates how divertor geometry can have a significant impact on the detachment behaviour.

Alexei ZABOLOTSKY: *"Particle transport in tokamak plasmas"* (EPFL thesis No. 3252(05)*)*

The aim of this thesis was to document and tentatively interpret the experimental density profile behaviour in the TCV and JET (Joint European Torus) tokamaks in the framework of different theoretical and semi-empirical models. A detailed analysis of the particle sources showed that edge fuelling in TCV and JET cannot be responsible for density gradient in the plasma bulk, confirming the presence of particle convection or a 'pinch'. The existence of an anomalous pinch was unambiguously demonstrated both on JET and on TCV by the observation of peaked density profiles in stationary, fully relaxed, fully current driven discharges and hence in the absence of the neoclassical Ware pinch. In TCV and JET, density gradient lengths (or profile peaking parameters) in L-mode were found to depend on magnetic shear with no dependence on collisionality. H-mode density profiles in JET, on the other hand, are clearly dependent on collisionality in agreement with theory and a prior observation on ASDEXUpgrade, while exhibiting only a weak or no dependence on shear and temperature profiles.

Ph.D. Theses supervised by CRPP staff at the end of 2005

Paolo ANGELINO: *"Gyrokinetic model for electron and ion dynamics in axisymmetric plasma configurations"*
The global nonlinear electrostatic PIC code ORB5 solves the gyrokinetic Vlasov-Possion system assuming adiabatic electrons in tokamak magnetohydrodynamic (MHD) equilibria. The present version of ORB5 shows remarkable particle and energy conservation properties and can be used for physics studies in toroidal geometry. In particular, the optimized tracer loading method has been adapted to tokamak geometry and implemented in ORB5 together with a new adaptive gyro-average algorithm. The recently implemented cache sorting speeds up elaboration time on the most widely used family of processors. Beside the original standard-δf method, a direct-δf method has been implemented. Advantages and drawbacks of each scheme, applied to tokamak equilibria, have been investigated. The problem of using a local versus canonical Maxwellian distribution functions has been addressed. The mutual interactions of ion temperature gradient (ITG) driven modes, zonal flows and geodesic acoustic modes (GAM) in tokamak plasmas have been investigated. A series of numerical simulations with the same initial temperature, density and magnetic shear profiles has been performed using a sequence of ideal MHD equilibria differing only in the value of the total plasma current. The turbulence-driven volume-averaged radial heat transport is found to scale inversely to the total plasma current.

Alessandro BORTOLON: *"Charge eXchange Recombination Spectroscopy"*
In TCV ion temperature and toroidal velocity are measured by the horizontal Charge eXchange Recombination Spectroscopy diagnostic. In 2005 the installation of the vertical CXRS system has been completed, with the upgrade of the observation head together with spectrometer and CCD detector setup. The system observation head is located in the bottom part of the vessel, providing up to 40 vertical measurements points along the plasma minor radius. This configuration permitted the first measurements of the poloidal component of plasma rotation.
Various experiments continued the study of rotation in L-mode plasmas in limiter configuration. In particular, a transition a new regime in which central v_{tor} is positive was observed and extensively studied. Transition to this regime is very reproductible along density ramps, occurring at a central density $n_{e0} \sim 6 \times 10^{19}$ m^{-3}. After the transition the rotation profile inverts direction inside $\rho = 0.7$, keeping similar absolute values. The edge rotation is unaffected. The collected observations suggest that the quantity determining the transition is at least a combination of n_e and T_e: a parameter such as collisionality provided primary interpretation of the observed trends.
During the TCV opening, absolute intensity calibration was performed by means of a calibrated spectral lamp positioned inside the vessel along the diagnostic chords. The density profile of the observed species can now be deduced and used to estimate the Z_{eff} profile. Experiments were made observing CX emission of CV and CIV ions, in order to reconstruct the ionsisation equilibrium distribution along the plasma radius, and deduce the impurity transport coefficients.

Yann CAMENEN: *"Confinement studies in shaped and extremely shaped plasmas heated by electron cyclotron waves"*
During the present year, experiments have been carried out in TCV to separate the influence of plasma triangularity and plasma collisionality on core electron heat transport. The plasma triangularity was varied from negative to positive values, $\delta = -0.4$ to $\delta = +0.4$, at constant plasma collisionality, to complement the previous experiments where these two parameters were coupled. The electron heat diffusivity, calculated from power balance and heat pulse propagation

measurement, is shown to decrease with decreasing plasma triangularity. As a consequence, the plasma energy confinement increases strongly at negative plasma triangularity and only half of the electron cyclotron heating (ECH) power is required at δ=−0.4 as compared to δ=+0.4 to obtain the same temperature profile. Concerning the effect of plasma collisionality, an increase of this parameter leads to a decrease of the experimental electron heat diffusivity, which is in qualitative agreement with the prediction of trapped electron mode (TEM) simulations. This supports the fact that TEM, predicted to be the most unstable mode by local gyro-fluid (GLF23) and global collisionless gyro-kinetic (LORB5) linear simulations in these strongly ECH heated plasmas, plays a crucial role in the transport of electron heat. Moreover, the Duplex Multiwire Proportional X-ray detector (DMPX) has been used to observe the plasma soft X-ray emission in two energy ranges simultaneously, allowing for the determination of the plasma electron temperature. This method allows for the first time in TCV retrieving the electron temperature profile with both high spatial and temporal resolution for the wide range of TCV plasmas, including high density plasmas overdense to ECE radiation, and will be of use for future EC power absorption and electron heat transport studies.

Lukas DERENDINGER: *"Design of low-energy plasma sources"*
At the beginning of 2005, preliminary measurements were made with single and double Langmuir probes in the DC arc column using the vacuum chamber as anode. Silane gas is used in the industrial reactor for epitaxial deposition of silicon, but argon gas was used here to characterise the plasma properties. Electron temperature, density, floating potential and plasma potential profiles are compared with numerical simulations made with Femlab. In a second step a circular anode was added to obtain a system more similar to the industrial version. Studies of the noise frequencies and plasma flickering due to instabilities were also carried out. Some problems were discovered and solved: a strong high frequency noise from the power source is now filtered by a built-in capacitor and deposition on the filament insulator was found to cause an important change in voltage distribution.
During the summer a multi-Langmuir probe containing 59 single surface probes was installed at the position of the silicon wafer substrate in order to efficiently analyse any configuration changes (geometry of anode and source, magnetic confinement, different pressures and currents). A multiplexer and a digital multimeter controlled by Labview software reads out the probes and enables instantaneous monitoring of plasma uniformity and stability at the substrate surface. After an unintended revision of the turbo pump, first measurements with these new probes were made. A transport barrier of a permanent magnet cusp field at the reactor circumference will be tested for reducing plasma radial gradients.

Antoine DESCOEUDRES: *"Experimental characterization of electrical discharge machining plasmas"* (Top Nano 21 project n° 5768.2)
Electrical Discharge Machining (EDM) has been a well known machining technique for more than fifty years. Nowadays it is widely used in a large number of industrial areas. However, to improve on the performance of EDM, it is necessary to understand the electrical discharge in detail. Optical emission spectroscopy and imaging are used to diagnose the plasma created during the machining process. The analysis of emission spectra shows that the plasma is cold (electron temperature 0.7eV) and extremely dense (electron density up to $2\cdot10^{18}cm^{-3}$ at the beginning of the discharge). Time-resolved spectroscopy shows that the density is decreasing afterwards with time. The low temperature and the high density measured prove that the EDM plasma is weakly non-ideal. In addition, an endoscope has been used to perform spatially resolved spectroscopy and imaging of the plasma. Profiles between the electrodes of electron density and of electron temperature have been estimated. The density is found to slightly increase towards the plasma center, whereas the temperature is quite constant across the plasma. The plasma contamination from the electrodes is found to be concentrated in their

vicinity. Imaging shows that the plasma develops very fast after the breakdown (<50ns), and then remains stable during the whole discharge. After the discharge, light is still emitted by incandescent metallic particles coming from erosion of the workpiece.

Emiliano FABLE: *"Simulation of plasma transport"*
The study of the behaviour of particle transport in the presence of an eITB (electron Internal Transport Barrier), and more generally in the presence of electron cyclotron radiofrequency heating (ECRF heating), has been started, with emphasis on the dependence of density profile tailoring on the local characteristics of current profile and power deposition. Respect to this topic, and in collaboration with the ASDEX Upgrade staff, experiments with off-axis ECRF heating in Ohmic L-mode plasmas have been performed, showing a strong dependence of density gradient on the local shear independently of the collisionality. As regard eITBs, an interesting result has been found that density and temperature are strongly coupled for the steady state fully developed eITB. Now the work is in progress on several topics, apart from particle transport with ECH and in ITB scenarios: the behaviour of electron heat transport during collisionality scans in Ohmic L-modes; the development of a Fortran90 module to simulate sawtooth crash in tokamak plasmas, module to be coupled to transport codes.

Barbora GULEJOVA: *"Exploitation of the new AXUV diagnostic"*
The new system of 7 AXUV diode pinhole cameras installed on TCV in late 2004 has been equipped with a complete fast acquisition system with 288 channels, allowing all 280 AXUV chords to be acquired at (variable) rates up to 100 kHz for all TCV shots. At the time of writing the system is 50% functional, with the 140 bolometer channels operational and providing high quality data, but with most of the 140 Ly-alpha filtered diodes presently experiencing some problems, which are the subject of ongoing investigation. These cameras will be used to investigate transient phenomena and to study the contribution of charge exchange neutrals to the total plasma radiation. The latter can be derived through comparison of tomographic inversion of total radiation derived from the tradiational foil bolometry system alos installed on TCV and the AXUVcameras. Work has begun on the details of tomographic reconstruction of data from both systems in collaboration with colleagues from the Hungarian Association. In parallel, considerable effort is being devoted to learning the use of the SOLPS5 fluid-Monte-Carlo edge code which will be the principal interpretive tool to be used in conjunction with the AXUV system. Simulations have begun for the first time of the TCV H-mode edge plasma using experimental data to contrain the code and with the ultimate aim of simulating an ELM event. In this respect, special input files will be required to reproduce the poloidal distribution of enhanced transport coefficients that characterise the ELM. A two-week Euratom mobility visit is planned in November 2005 to IPP Garching, the centre for SOLPS5 development, in order to seek assistance in developing these files.

Seyed Masood HAFEZ HAGHIGHAT: *"Dislocation dynamic modeling of irradiation induced effects in Fe and Fe alloys"*
Multiscale modelling appears now as a major tool for the description of plasticity of materials. This work is aimed at determining the amplitude of plasticity mechanisms influenced by radiation induced effects at the mesoscale level (μm) by computational simulation. It is proposed to perform dislocation dynamics simulations of the plasticity of Fe and Fe-Cr samples containing given densities of irradiation-induced defects (dislocation loops, voids, He bubbles) at temperatures below 400°C. Eventually, a model alloy containing the unshearable hardening features representing the defects shall be established. In this work the microMegas code is used for applying the Discrete Dislocation Dynamics model for simulating

and visualizing dislocation-based plastic deformation in crystals. Preliminary results of the simulation, performed for low strains, showed a serration behaviour of the stress versus strain. Also it has been observed that in the presence of obstacles in the matrix, deformation occurs by junction formation and cross slip events at the beginning of deformation and then by increase in the dislocation density as a result from forest hardening.

Jan HORACEK: *"Measurement of edge electrostatic turbulence in the TCV tokamak plasma boundary"*
Following on from the demonstration, in 2004, of universality in the statistical behaviour of particle density and flux fluctuations measured in the TCV scrape-off layer, a collaboration has been established with the Risoe National Laboratory in an attempt to understand, by detailed theory-experiment comparison, more about the physical mechanisms driving the turbulence. The Danish group have developed a two dimensional fluid turbulence model solving
reduced equations in a local slab equiibrium with inhomogenous magnetic field and a steep pressure gradient driving turbulence in the edge region. In the SOL, disspation terms describing collisional diffusion and parallel losses are prescribed on a physics basis, adapted to TCV dimensions and plasma parameters. Direct comparison of experiment with the results of a simulation closely matching the edge conditions of a high density TCV diverted discharge has yielded a remarkable level of agreement both across a large variety of statistical parameters characterising the turbulence and the magnitude of the fluctuation driven cross-field flux itself. This constitutes extremely strong evidence for interchange motions being at the origin of the anomalous particle transport and is the first known demonstration of quantitative agreement between turbulence simulations and experiment in the tokamak SOL.

Sudheer Kumar JAWLA: "Gyrotron development"
This thesis started recently is aimed towards the developments in Gyrotrons. The first phase would be to find a suitable method for the phase retrieval of a microwave beam and to test the recently designed X3 top launcher mirror to be installed on TCV. The second phase would focus on the upgrade of the 118GHz tube, presently 500kW / 2s / Sapphire window; to be upgraded to 600-700kW / 2s /Diamond window.

Sébastien JOLLIET: *"Non-linear gyrokinetic simulations"*
Gyrokinetic theory is a useful tool for studying microinstabilities, such as ITG and TEM modes, which are commonly held responsible for anomalous transport observed in tokamaks. From a numerical point of view, simulating TEM and ITG simultaneously is a difficult task due to disparate spatial and time scales. The aim of this work is the implementation of kinetic electrons in the nonlinear, global PIC code ORB5. The PIC method unavoidably suffers from numerical noise and leads to the loss of energy conservation for long simulations. Therefore several numerical algorithms have been developed and implemented in the code. The ORB5 code has been entirely rewritten in magnetic coordinates. The use of the straight-field-line coordinate allows a gain of CPU and will be appropriate for solving the fast parallel motion of electrons. A new field line following Fourier filter has been implemented, which strongly decreases numerical noise caused by unphysical high-$k_{//}$ modes. A new initialisation of the perturbed density has been added to suppress the long, unwanted early simulation phase when using many markers. A parallel solver using SCALAPACK has been developed, reducing memory requirements by up to one order of magnitude. All these improvements are helpful to accurately simulate large plasmas, which has now become possible thanks to the BlueGene cluster at EPFL, on which the ORB5 code was ported.

Sun Hee KIM: *"Full tokamak discharge simulations using DINA-CH"*
Full non-linear tokamak simulations using DINA-CH free boundary evolution code require more complete transport and heat source modeling. For this, DINA-CH has been combined with an integrated modeling code CRONOS on the Simulink environment. This first attempt has revealed not only the possibility of combined calculation, but also several difficulties. After resolving these difficulties, free-boundary features of tokamak modeling which have been inadequately described by fixed-boundary or prescribed boundary transport simulations will be studied.
Initial study on the ELM triggering in TCV and ASDEX Upgrade has done by virtue of the capability of DINA-CH simulator in which plasma response by external triggering signal can be simulated. The opposite ELM behaviour with respect to the vertical plasma motion in two devices has been studied. The passive stabiliser in ASDEX Upgrade has the same effect as the G-coil in TCV and this causes the opposite ELM behaviour. The flux surface deformation caused by the vertical plasma movement and externally perturbed PF currents seems to trigger ELMs. For the validation of this result, experiments with a radial plasma movement which can generate bigger flux surface deformation have been proposed for ASDEX Upgrade.

Igor KLIMANOV: *" Reconstruction of the electron distribution function during ECRH/ECCD*
and magnetic reconnection events in a tokamak plasma"
The study required the development of a new diagnostics and related analysis tools. A new 24-channel Low Field Side (LFS) radiometer was built. Two antennas (at Z=0 cm and Z=21 cm) were installed and now are routinely used for conventional Electron Cyclotron Emission (ECE) measurements on TCV. A third ECE LFS line was connected to the steerable launcher. Oblique ECE and electron Bernstein emission measurements have been performed. Poloidal and toroidal angle sweeps were performed during individual shots, which allowed ECE tomography reconstruction and analysis of the Doppler shifted ECE. A numerical module to simulate the ECE emission spectra at any angle for any distribution function has been developed. The code is combined with the plasma ray-tracing code TORAY-GA and can be used with the Fokker-Plank code CQL3D. Experiments dedicated to the study of the electron distribution function during ECCD and during magnetic reconnection events, such as sawteeth, have been carried out on TCV. The non-thermal ECE in these regimes has been analyzed, and energy spectra of the suprathermal electrons and their density have been reconstructed. The dynamics of fast electrons generated by reconnection has also been studied.

Xavier LAPILLONNE: *"Gyrokinetic Simulations using Eulerian Approach"*

Bin LONG: *"Investigations of Liquid Lead-Bismuth Embrittlement Effects on both Unirradiated and Irradiated Ferritic/Martensitic Steels"*
spallation targets such as the MEGAPIE (the megawatt pilot experiment) target and the future ADS (accelerator driven system) spallation targets which utilize liquid lead-bismuth eutectic (LBE) as target material, liquid metal embrittlement (LME) effects on the performance of target structural materials is one of critical issues that determine the lifetime of the targets. LBE embrittlement effects have not been well understood at present. The aim of this study is to carry out a series of mechanical tests on both unirradiated and irradiated ferritic/martensitic steels in LBE environments to quantify the degradation effects by LBE on the fracture properties of these steels.
The preliminary results have been obtained by performing slow-strain-rate tensile (SSRT) tests in static LBE with saturated oxygen at temperatures ranging from 250°C to 425°C. The tested material is the martensitic steel T91 that will be used as structural material in MEGAPIE. Two groups of samples are being used. Group-I

samples with microcracks on surfaces indicate clearly that the LBE embrittlement effect starts to occur when temperature reaches 300°C, while Group-II samples without microcracks do not show this effect. LBE embrittlement effect occurs after the onset of necking of the specimens. SEM observations show that specimens rupture in a brittle mode when embrittlement occurs. It is concluded that the requirements for the susceptibility to LBE embrittlement effect of the T91 steel are: surface cracks or flaws, wetting, and a high level of stress concentration at crack tips.

Alessandro MARINONI: *"Experimental study of plasma fluctuations in tokamaks"*
The aim of this work is to investigate plasma density fluctuations in the edge region of the tokamak JET and in the core region of the tokamak TCV.
The first project relies on the microwave reflectometry diagnostic, mainly on the X-mode correlation reflectometer, which should be able to yield the fine scale spatial correlation structure of the turbulence. Software for data analysis, which includes advanced techniques such as wavelets and coherent averaging, has been developed in order to analyze spectral and correlation properties of density fluctuations. Even if the signal to noise ratio of past data was found out to be insufficient to give any appreciable information, the recent upgrade of the diagnostic is expected to increase considerably the quality of future measurements.
The second project included a complete feasibility study of core turbulence diagnostics, whose result has been the identification of the tangential Phase Contrast Imaging technique as the best available option. Part of the already performed design has been based on a set of gyrokinetic simulations performed with the codes GS2 and KINEZERO, recently installed on PLEIADES and graphically interfaced with MATLAB. The design of the optimal geometrical configuration of the imaging optics is ongoing.

Janos MARKI: *"TCV divertor infrared measurements"*
Infra-red camera data from the two micro-bolometer systems viewing the TCV divertor target regions are being analysed in an attempt to extract values for the sheath heat transmission factors by combining the IR surface power measurements with those of local divertor plasma parameters. The IR power is being deduced from the measured surface temperature by solving the inverse heat conduction problem using the THEODOR finite difference code supplied by IPP Garching and in wide use throughout the Fusion community for IR data analysis. In the first instance effort has concentrated on the vertically viewing system, for which the temperature calibration has been checked using a dedicated in-vessel heated tile. This has revealed some problems with the initial bench-top calibration and has required some modifications to the method of converting IR intensities to temperatures. In addition to this analysis effort, work has begun on the preparation of a new, high speed IR camera system using a cooled CMT detector operating in the 3-5 micron waveband which will be the core diagnostic tool for the thesis research. The camera (Thermosensorik) has been purchased, with delivery expected in early 2006. Work now proceeds on relay optics design and mechanical support systems.

Mikhail MASLOV: *"Particle transport and confinement in TCV and JET"*
This work is connected with experimental data analysis of particle transport experiments on the TCV and JET tokamaks. It involves physics data analysis as well as contributions to Thomson scattering (TS) as a key diagnostic for this project.
The divertor TS spectrometers for TCV were modified, calibrated and installed on TCV. An automatic data validation program for TS on TCV is under development. Mr Maslov also visited JET under mobility to produce a code for modeling the processing of LIDAR TS raw data. The code was used to identify the origin of systematic inconsistencies of density profiles measured using LIDAR TS and FIR

interferometer at JET, suggesting alternative processing algorithms for removing perturbations due to stray light.

Nicolas MELLET: *"Extension of the LEMAN code to include finite temperature effects in the dielectric tensor to resolve singular mode structures and study effects of mode conversion without having to include gyroradius effects as in the PENN code"*
A new warm formulation was applied for the calculation of the dielectric tensor in the LEMan code. This permits to obtain Landau damping and to model the Kinetic Alfven Wave (KAW). One of the main properties of this wave is the direction of its propagation which is opposite to the cold Surface Quasi-Electrostatic Wave (SQEW). The extended version of the code was successfully benchmarked against the 1D code ISMENE. Several other geometries in 2D (circular cross section torus and bumpy mirror) and 3D (straight helix) were investigated and showed good agreement with the dispersion relation. Convergence was also verified through the analysis of Coulomb Gauge, integrated local and global power balance. Parallelisation has been performed using the BABE (Burn At Both Ends) algorithm for the solver and allowed computing of 3D cases in the ICRF domain which was impossible due to memory requirements, even in the cold model. In this range of frequencies the magnetic beach scenario was reproduced in a bumpy mirror with toroidal effects. The results exhibit displacement of the resonant surface and corresponding absorption.

Pablo MUELLER *"Finite element simulation of fracture specimens in the transition of tempered martensitic steels"*
In order to model the fracture toughness-temperature curve in the low transition of the tempered martensitic steel Eurofer97 based upon a local approach of cleavage, 3D simulations of Compact Tension specimens (CT), containing a blunting crack were performed using the ABAQUS package. The material properties are introduced in the simulations through the tensile curves. Simulations were performed at low temperatures corresponding to the lower transition and the stress field at the crack tip was characterized. A Fortran program was developed to extract the maximum principal stress (or any component of the stress) at every node and to calculate the volume of material encompassing a critical value of a given component of the stress tensor. The effect of the plastic flow strain-rate dependence on the size of the critical area at a given applied stress intensity factor has been investigated and was shown to be not negligible for large value of the critical stress, above 2000MPa.

Stefan MUELLER: *"Basic investigation of turbulence and transport in toroidal plasmas"*
Two major lines of development have been followed in 2005. First, a method was developed to visualize and analyze statistically the spatiotemporal behavior of the turbulence, measured by the HEXTIP probe array. This method provides us now with a quantitative basis for comparisons (theory-theory, experiment-experiment, theory-experiment) in terms of the spatiotemporal properties of the turbulence. Second, the development of a 3D variant of the ESEL code was started, dedicated to global simulations of the TORPEX device. The code was restructured and parallel dynamics were implemented. The important questions of conservation properties and parallel boundary conditions were addressed.

Gennady PLYUSHCHEV: *"Turbulence studies in TORPEX"*
This work, within the TORPEX basic experimental plasma group, was focused on the new experiments that involve induced longitudinal electrical field. Calculation of expected plasma current for equilibrium cases has been done. Supplementary diagnostics (poloidal flux loop and rogowskii coils) have been developed, calibrated and installed on the TORPEX device. The possibility to use AXUV detectors for soft

X-ray measurements under conditions of the regime has been analyzed. The entire ohmic system has been tested using a copper wire loop instead of plasma column. An optimization of ohmic transformer coils system to maintain the plasma equilibrium via poloidal 'parasitic' magnetic field has been started. Non-equilibrium plasma current has been experimentally obtained. To close flux surfaces it is necessary to make further optimization in order to decrease parasitic vertical magnetic field and achieve the plasma equilibrium.

Mario PODESTA: *"Experimental studies of transport properties in toroidal plasmas"*
The knowledge of particle source and loss mechanisms is a fundamental aspect for the characterisation of magnetically confined plasmas. In the last year these two aspects have been extensively investigated in TORPEX, a toroidal device where plasmas of Argon and Hydrogen are generated and heated by microwaves in the electron cyclotron range of frequencies. Techniques based on the Fourier and Laplace analysis of the plasma response to a modulation of the plasma source have been applied to obtain spatially resolved profiles of the particle sources. By means of the same techniques the time-scales characterising the plasma dynamics can be deduced, and a global loss rate estimated. The dominant loss mechanisms and their dependence upon the plasma properties are then studied. For example, the link between the local particle losses across B and the spectral features of the plasma instabilities observed in TORPEX are investigated by measuring the frequency-resolved particle flux. The first results indicate a correlation between fluctuation-induced fluxes, spectral features of the instabilities and resulting density profiles.

Francesca Maria POLI: *"Study of fluctuations and turbulence in toroidal plasma"*
Fluctuations in the fundamental parameters of the plasma, such as density and potential, are present in most plasma experiments. Electrostatic probes provide a localised measurement of these fluctuating quantities. On TORPEX, different sets of Langmuir probes, more than 100 in total, allow the direct measurement of frequency spectra up to 125 kHz, and a local estimate of wave-number spectra, through the application of statistical techniques based on two-point measurements. The wave dispersion relation can be then reconstructed in both linear and non-linear regimes. A four-tip probe, developed and installed on TORPEX during summer 2005, allows the measurement of particle spectral flux along the radial direction, up to 1MHz. Experiments have been run on TORPEX with different neutral gas pressure to investigate the effect of collisions on the saturation of instabilities into a non-linear state. The mutual effect of density gradient, magnetic field strength and electric field on the onset, nature and evolution of instabilites is still under study.

Amuthan RAMAR: *"Development and Characterization of Oxide Dispersion Strengthened (ODS) Reduced Activation Ferritic/Martensitic (RAFM) Steels"*
Effects of irradiation on two ODS RAFM steels, with the EUROFER 97 RAFM steel as matrix material and 0.3wt.% Y_2O_3 particles as reinforcement material have been investigated. Following irradiation with 590MeV protons to 0.3 and 1.0dpa at room temperature and 350°C, tit was found that the mechanical properties of the materials are only slightly altered, with a raise in the yield strength but no significant decrease of the total elongation, relatively to the base material. Samples irradiated at room temperature contain irradiation-induced defects in the form of blacks dots with sizes ranging between 2 and 3nm, while after irradiation at 350°C irradiation-induced a_0 <100>{100} dislocation loops are clearly visible along with nano-sized cavities. The dispersed yttria particles are stable for all irradiation conditions. The density of the irradiation-induced defects and the dispersoids are about $2.3 \times 10^{22} m^{-3}$ and $6.2 \times 10^{22} m^{-3}$, respectively. Thus, the weak impact of

irradiation on the mechanical properties of ODS RAFM steels is explained by a lower density of irradiation-induced defects relatively to the density of the reinforcing particles.

Andrea SCARABOSIO: *"Studies on MHD activity as a function of plasma shape in standard TCV scenarios and MHD phenomena in advanced scenarios"*
The last part of this thesis focuses on momentum transport phenomena associated with MHD activity. MHD modes are observed to induce a large loss of total momentum by flattening the rotation profile inside the most unstable resonant surface typically the q=2 surface, as measured by active Charge eXchange Recombination Spectroscopy,. The rotation frequency of large MHD mode derived from magnetic measurement agrees well with the core toroidal rotation frequency from CXRS. Plasma acceleration, or spin-up, following the global loss of confinement due to MHD modes, is observed in TCV. The toroidal rotation profile evolves on a slower time scale (τ_ϕ=100÷150 ms) than the other main plasma parameters such as the electron density and temperature. The time evolution of the velocity profiles during plasma spin-up is well reproduced by a 1D diffusion-advection momentum transport model with an ad hoc momentum source. The momentum diffusion coefficient was found to range from 10 to 40 times the value calculated from collision theory, depending on the momentum source model used in the simulation. The frequency of the sawtooth precursor oscillation systematically exceeds the angular rotation frequency of the carbon impurity. Preliminary results indicate that the measured sawtooth precursor frequency is consistent with the angular velocity associated with the E×B flow calculated from neoclassical theory.

Christian SCHLATTER: *"Neutralisation of fast ions"*
The neutralization of ions in thermal TCV tokamak plasmas was modeled using transport codes (KN1D, a kinetic transport algorithm and DOUBLE-TCV, a Monte Carlo code) and compared to measurements of the neutral charge-exchange flux detected with TCVs neutral particle analyzers (one with vertical line of sight, and a Compact NPA installed in 2004 with horizontal chord, measuring two particle species simultaneously). It is found that neutrals of different energies emerge from well different plasma radii, therefore the ion temperature inferred at different energies of the corresponding charge exchange flux energy spectrum was used to reconstruct an ion temperature profile derived from NPA measurements. The temperature profile coincides with the profile obtained from charge exchange recombination spectroscopy (CXRS). Further, the combination of simulation and experiment recovers absolute profiles of neutral particle density profiles for the hydrogenic species and the isotopic plasma composition.
The analysis of the creation and behavior of suprathermal ion populations on TCV in discharges with ECH and ECCD phases will continue as soon as a shielding of the NPA against X-rays (produced by runaway electrons) is installed.
The high energy NPA at the Joint European Torus (JET) was recalibrated by the end of 2005 to bring the diagnostic back to operation after the long shutdown.

Hannes SCHMIDT: *"Characterisation of a high density, large-area VHF plasma source"*
The objective of this project is a feasibility study of a novel, large-area plasma-based thin film production technique. The successful "proof of principle" for a shaped electrode based on a cylindrical reactor design was given in 2003, for an industrial-type rectangular reactor the proof followed in 2005.
The reactor was converted to the novel electrode design intended to suppress the standing wave effect at 67.80MHz. Modification of the differential pumping system was necessary in order to find a more favourable process window to avoid parasitic discharges. Plasma with the built-in shaped electrode turned out to be much less

stable and the proof was made for selected process conditions only. A comprehensive electrical characterization of the system at the typical industrial frequencies (13.56MHz, 27.12MHz, 40.68MHz, 67.80MHz, and 100MHz) was performed including DC and peak-to-peak voltages on the RF electrode. An extensive impedance characterization and analysis of the system closed the measurement series.

Experimental work is finished; data analysis and thesis writing are ongoing.

The project was performed in collaboration with UNAXIS Displays.

Benjamin STRAHM: *"Thin film technology for solar cells"*

Micro-crystalline silicon has some advantages compared to amorphous silicon in the domain of thin film solar cells, as it shows greater efficiencies and stability during long term exposure to light. Even if these two materials are processed with the same plasma enhanced chemical vapor deposition (PE-CVD) technique, the plasma parameters are quite different to obtain one or the other of these microstructures. The process parameter space has 7 dimensions (power density, pressure, temperature, total gas flow rate, excitation frequency, gas composition and interelectrode gap), thus it is very difficult to define a boundary between the two regimes of deposition. An analytical model based on a set of chemical reactions that take place in the plasma (gas phase and surface reactions) has been developed. With this model, the parameter space has been reduced to only two dimensions: gas composition and fraction of dissociated silane in the plasma. The installation of a Fourier Transform Infrared (FTIR) absorption spectroscopy measurement in the pumping line of a large area PE-CVD reactor has allowed a confrontation between the model and experimental data. Results show that the model is in good agreement with experimental data at low silane concentration, corresponding to a powder free plasma regime.

Alban SUBLET: *"Study of Atmospheric and Near Atmospheric Pressure Dielectric Barrier Discharges for SiOx deposition on polymer films"*

A preliminary study of SiOx deposition has been done to determine the key parameters and their influence on the coating quality: pressure (from 5 to 1000mbar), power, gas flow and gas mixture ($N_2/O_2/HMDSO$). At high pressures, reactions are governed by gas-phase chemistry, which, for SiOx deposition processes, results in the production of particles and powders. Ex-situ characterizations of the deposited layer obtained in these different conditions have been done by FTIR, AFM and XPS measurements. FTIR profiles of the deposited layer reveal a decarbonification of the layer along the gas flow. This could be due to the progressive decomposition of HMDSO along the gas flow. AFM measurement reveals the presence of a powdery layer with particles of about 100nm in diameter at the end of the substrate in the gas flow direction. These results have been confirmed by in-situ laser light scattering (LLS) measurements with an Ar^+ ion laser. According to our electrode geometry (60*60 mm^2 and 2mm gap), at 500mar, we obtain a very smooth layer of non stoichiometric composition at the entrance of the discharge and a rough layer, mainly composed of particle accumulation with a quasi stoichiometric composition, at the exit.

These results have been presented at the workshop on Cold Atmospheric Pressure Plasmas (CAPPSA 2005) in Bruges in September.

LLS measurements are still under investigation to determine Rayleigh domains and polarization degree, however it is hard to achieve because powder formation is pulsed (powder burst every ~ 2s) and non reproducible. Laser absorption measurements are planned to quantify the powder density according to the position in the discharge, the pressure and the power.

Gang YU: *"Investigation of the irradiation-induced defects in reduced activation ferritic/martensitic (RAFM) steels"*

The reduced activation ferritic/martensitic (RAFM) steel EUROFER97 is presently considered as a promising structural material for first wall and breeding blanket applications in fusion reactors. SANS measurements will be performed on series of specimens of the EUROFER97 irradiated with protons in the PIREX facility and in the SINQ Target station, at the Paul Scherrer Institute.

SANS measurements were carried out on various unirradiated and irradiated bcc materials, namely RAFM steels, the EUROFER97. Different irradiation temperatures and doses were investigated, ranging from 50°C to 350°C and from 0.3 to 2 dpa respectively. Of particular interest are the results of the irradiation at/or less 250¡C for EUROFER97, where only a high density of small black dots was observed in TEM, resolution limit 3 1nm. By using a magnetic field during the SANS measurements, the nuclear and magnetic contrasts were determined, as well as a cluster size distribution (peak at 0.6 nm) for the irradiation induced defects. The ratio between the nuclear plus magnetic scattering intensity and the nuclear scattering intensity, A, was found higher than that calculated for He bubbles, for instance. Based on the theory of small angle scattering of small dislocation loops [J. Henry, M.-H. Mathon, P. Jung, J. Nucl. Mat. 318 (2003) 249], the contribution of small dislocation loops, as detected by TEM, is three orders of magnitude smaller than the measured the scattering intensities. Therefore, it must be concluded that the scattered intensity may be due to helium clusters that may grow to helium bubble for temperatures higher than 350¡C.The atomic volumes of the helium is a key point in the analysis of experimental data. If helium in the cluster is in the lattice form or in the interstitial form, its atomic volume is much less than the atomic volume in bubbles. A have been calculated for a void, a substitutional helium cluster, an interstitial helium cluster and a bubble that equal to 1.36, 1.90, 2.24 and 1.45 respectively.

If helium clusters form in samples irradiated at temperatures < 250°C, they will evolve to become bubbles when the sample temperature is increased to 400°C. In this case A decreases from 2.24 to 1.45.

The present proposal has several aims:

1.SANS measurements will be performed on specimens of pure iron irradiated at temperature 50°C to 1 dpa with 590MeV protons in the PIREX facility at the Paul Scherrer Institute, the helium production rate is about 50-100 appm He/dpa. SANS measurement are under a saturating magnetic field to identify the helium cluster size, distribution, as a link the TEM observations. A will be determined. As there is no carbide interference, A only characterize the type of helium cluster.

2.SANS measurements will be performed on specimens of EUROFER97 steel specimens irradiated with the SINQ target station to 7.9, 17.9 and 19.3 dpa at temperatures of 150-350°C, the helium production rate about 300-1000 appm He/dpa. SANS measurement are under a saturating magnetic field to identify the helium cluster size, distribution, as a link the TEM observations.

3.SANS measurements to EUROFER97 steel specimens irradiated with the 590MeV proton irradiation to 0.3, 1 and 2 dpa at temperatures of 250¡C, the helium production rate about 100 appm He/dpa and measured by the SANS technique under a saturating magnetic fields to detect the helium cluster size, distribution, as well as link the TEM observation.

4.Annealed specimens of EUROFER97 steel irradiated at 250¡C to 2.0 dpa will be measured by the SANS technique under a saturating magnetic fields to compare the obtained results to the results obtained under point 2. above to address the helium cluster evolution, including the mean size, number density and size distribution,as a link the TEM observation. A will be determined. The annealing temperatures will be 400°C, 550°C and 650°C respectively.

Alexandra ZHUCHKOVA: *"Heavy Ion Beam Probe experiment and Polarimetry"*

Two new diagnostics are planned to be installed on TCV: HIBP and Polarimetry. HIBP will give opportunity to measure plasma potential, density and potential

fluctuations, poloidal flux. The work of adapting of the simulation program for HIBP, which was developed in Kurchatov Institute, to using for TCV was carried out. It was installed on Hal and some calculation was made using it. Polarimetry diagnostics will allow to carry out measurements of q profile on low density plasma based on Farady rotation, which is a very

important quantity for plasma studying. The work under hardware for Polarimetry was started. Schootky diode detectors were tested. Designing of the new optic system for Polarimetry is started.

Costanza ZUCCA: *"Current profile simulations during electron Internal Transport Barrier formation in TCV"*

Plasma advanced scenarios characterized by a rapid drop in the central electron heat transport coefficient and thus improved electron energy confinement have been obtained in many tokamaks and are usually related to the appearance of an Internal Transport Barrier (ITB). Experiments have been conducted in TCV to elucidate the role of the plasma current density (j_p) profile evolution from peaked to hollow in the electron ITB (eITB) formation, in particular the importance of the occurrence of a zero-shear surface for triggering the barrier. A systematic study of TCV eITB discharges has been carried out with the use of the ASTRA transport code, suggesting a correlation between the barrier formation and the safety factor (q) profile inversion, i.e. that the radial location and time of the eITB triggering are consistent with the spatial and temporal appearance of a minimum in the q profile. In this context ASTRA has been employed in an interpretative mode, constrained by experimentally measured density and temperature profiles, to provide modelling of the q and j_p evolutions, of which there exists no direct measurement. An accurate modelling of the current density profile in both steady-state and transient simulations has been provided and comparisons of the numerical results with the experimental profiles have also been discussed. In addition, a study of the sensitivity of the j_p profile on the various actuators such as, for instance, the bootstrap current density, the driven electron cyclotron current density or the loop voltage, has started. Further investigation will be performed to better understand the interplay between the extension of the negative shear region and the degree of improved confinement.

6 Public relations activities in 2005

6.1 General outreach activities

An outreach activity presenting the progress in fusion and plasma science and their related activities was set-up for different levels of education: undergraduates, high school students, elementary school students, teachers at all levels, the general public and government officials. We have been active via public colloquia, "round tables" and talks on energy issues especially on fusion energy.

EPS13 : WYP 2005 (World Year of Physics) in July in Bern

A special edition of the European Physical Society (EPS13: "100 years anniversary of the theory of relativity") took place in July at the University of Bern, where Albert Einstein worked in 1905, when he published his theory of relativity. The European and Swiss Fusion research programme was presented as an exhibition, with the help of the European Commission. Mr Hugues Desmedt (CEA) was present during the exhibition and actively participated in the composition and the design of the posters which were presented on this occasion. This represents an upgrade of the usual European exhibition which is now under the responsibility of the CNR Padova – Italian Association. The "Starmakers" movie was shown in 3D, with the Barco system lent by the Italian Association. The large model of ITER was also shown. Several scientists from CRPP participated as guides to this expo. The success was good with about 700 visitors, especially considering that the event was in July, addressed to mainly a High Energy Physics audience, and when the universities were on vacation.

Organised visits to the CRPP

We welcomed about 1200 visitors to the CRPP in Lausanne, mostly in groups of about 20 to 80 people. About 50% of the visitors came from schools, high schools or universities, 85% of the visitors were from Switzerland, the rest from various countries. Among this multitude of visits, we welcomed the so-called "Passeports-Vacances" for 42 young people 13 -15 years old who were able to visit different laboratories at the EPFL in the summer, the traditional visit of UNI-3 Geneva to tour TCV attracted more than 80 people in spring. Many firms organised special visits to CRPP for their members or customers, to see the fusion as well as the industrial plasma processing activities.

A tour of CRPP was organised for Dr Janoz Potocnik, European Commissioner during his official visit to Switzerland on November 16th; arrangements were made by the SER, the Federal Office for Science & Research. Dr. Potocnik was impressed by the diversity and the high level of science and technology visible in the CRPP activities. He made a comment on the positive impact of the ITER site selection of Cadarache, on the European Scientific research and on boosting the European industries. This impact will be maintained during the construction of ITER but should also be kept alive to stimulate the effort for the Demo phase, which is already in the starting blocks.

Web activities on http://crppwww.epfl.ch

The main CRPP website is regularly kept up to date, including links to other sites, mainly fusion oriented

6.2 Activities linked to the ITER siting decision

With the announcement of ITER site on the 28th June 2005, we maintained close contact with the media, through press releases and interviews, as well by participating in radio and TV broadcasts. Many people were involved in these contacts and different performances in special programmes as well as news programmes. Many members of the CRPP appeared on TV and radio broadcasts.

6.3 Organisation of meetings and conferences

The 10th International Conference on Accelerator and Large Experimental Physics Control Systems (ICALEPCS 2005) was co-chaired by Jo Lister and Bertrand Frammery (CERN). The presence of the magnetic fusion community was enhanced with presentations from JET, Tore Supra, RFX, MIT, ASDEX Upgrade. A round table discussion was organised on the issues of multinational in-kind procurement for large physics experiments, such as High Energy Physics and fusion. Nearly 100 of the delegates visited TCV on the Saturday following the conference.

6.4 External courses to generalist audiences

In May and June, five 1 hour seminars were presented at CERN as part of their academic training programme. The first two on "The ITER Project - Its aims and design challenges" and "The ITER Project - The challenges of controlling and operating ITER" were given by Jo Lister. The last three on "The ITER Project - Procurement and Quality Assurance issues for ITER magnets", "The ITER Project - The performance prediction from a single strand to large size conductors ", "The ITER Project - The evolution of design and manufacture of fusion conductors" were given by Pierluigi Bruzzone.

Christoph Hollenstein presented a "Vakuum Kurs" at CERN to the Swiss Vacuum Society on 12-13 May and 23-24 June.

A presentation was made by Jo Lister to the Association Vaudoise des Chercheurs en Physique on "The ITER challenges" in June.

Among the many presentations of fusion in different places, a talk by Pierre Paris was made on 21 October in Arles (France), in the frame of the Forum Rhodanien "La fusion thermonucléaire: une option énergétique pour le futur", where Dr Michel Chatelier (Head of Unit, CEA Cadarache, F) also presented "De Tore Supra à ITER".

Prof. M.Q. Tran gave several talks on fusion in Switzerland and in gymnasiums.

In November, Pierre Paris presented « Fusion nucléaire et coopération internationale ITER », in the frame of the Forum France-Suisse for the 100 years anniversary of AIESME " Energie et transport".

Christoph Hollenstein gave an introduction to plasma physics and its applications in industry as a Course for the Swiss Vacuum Society in Le Locle in November.

6.5   Starmakers

"The Starmakers" movie is now available in 19 languages: English, French, German, Italian, Portuguese, Spanish, Danish, Finns, Basque, Hungarian, Korean, Japanese, Russian, Chinese, Dutch, Slovenian, Czech, Rumanian, Polish. And a version is now being made on DVD. This work was possible due to a special effort by the Audiovisual service of the EPFL, especially Edgar Bastian and his team. Moreover the help in translation by the international CRPP team allowed the different national languages to be rapidly recorded. The compilation of the DVD is attributable to Mr Hugues Desmedt.

APPENDICES

APPENDIX A Articles Published in Refereed Scientific Reviews During 2005

(see CRPP archives at http://crppwww.epfl.ch/archives)

Alberti S., Arnoux G., Porte L. Hogge J.-P., Marletaz B., Marmillod P., Martin Y., Nowak S. and TCV Team, *"Third-harmonic, top-launch, ECRH experiments on TCV tokamak"*, Nucl. Fusion 45, 1224-1231 (2005)

Anghel A., Bruzzone P., *"Measurement of contact resistance distribution in typicl ITER size conductor termination",* Fusion Eng. & Design, in press (2005)

Arnoux G., Alberti S., Porte L., Nowak S., Marletaz B., Marmillod P., Martin Y., and TCV team, *"Third harmonic X-mode top-launch on the TCV tokamak"*, Plasma Phys. & Contr. Fusion, 47, 295-314 (2005)

Baluc N., Schaeublin R., Spaetig P., Victoria M., *"Hardening mechanisms in ferritic/martensitic steels",* Effects of Radiation on Materials, edited by M.L. Grossbeck et al., ASTM International (PA), 341-351 (2004)

Blais A., Jodoin B., Dorier J.-L., Gindrat M., Hollenstein Ch., *"Inclusion of aerodynamic non-equilibrium effects in supersonic plasma jet enthalpy probe measurements",* J. of Thermal Spray Technol. 14(3), 342-353 (2005)

Bruzzone P., Stepanov B., Zapretilina E., *"Anomalies on V-I characteristics of bumps in thecable-in-conduit conductors",* Fusion Eng. & Design, 75-79, 111-115 (2005)

Bruzzone P., Bagnasco M., Bessette D., et al., Stepanov B., Wesche R., *"Test results of the ITER PF insert conductor short sample in SULTAN"*, IEEE Trans. Appl. Supercond. 15, 1351-1354 (2005)

Camenen Y., Pochelon A., Bottino A., Coda S., Ryter F., Sauter O., Behn R., Goodman T.P., Henderson M.A., Karpushov A., Porte L., Zhuang G., *"Electron heat transport in shaped TCV L-mode plasmas"*, Plasma Phys. & Contr. Fusion 47, 1971-1987 (2005)

Chavan R., Henderson M.A., Sanchez F., *"A frictionless steering mechanism for the front steering ECCD ITER upper port launcher"*, Third IAEA Technical Meeting on "ECRH Physics and Technology for ITER", Como, Italy, May 2005, J. of Physics: Conference Series 25, 151-157 (2005)

Ciazynski D., Bessette D., Bruzzone P., Martovetsky N., Stepanov B., Wesche R., Zani L., Zanoni R., Zapretilina E., *"DC performances of ITER NbTi conductors: models vs. measurements",* IEEE Trans. Appl. Supercond. 15, 1355-1358 (2005)

Coda S., Goodman T.P., Henderson M.A., Sauter O., Behn R., Bottino A., Camenen Y., Fable E., Martynov An., Nikkola P., Scarabosio A., Zhuang G., Zucca C., and TCV Team, *"High-bootstrap, noninductively sustained electron internal transport barriers in the Tokamak a Configuration Variable"*, Phys. of Plasmas, 12(5), part 2, 056124 (2005)

Cooper W.A., Hirshman S.P., Yamaguchi T., et al., *"3D anisotropic pressure equilibria that model balanced tangential neutral beam injection effects",* Plasma Phys. & Contr. Fusion 47, 561-567 (2005)

Descoeudres A., Hollenstein Ch., Waelder G., Perez R., *"Time-resolved imaging and spatially-resolved spectroscopy of electrical discharge machining plasma",* J. of Physics D: Applied Physics 38, 4066-4073 (2005)

Egedal J., Fox W., Porkolab M., Fasoli A., *"Eigenmode response to driven magnetic reconnection in collisionless plasma",* Phys. of Plasmas 12, 052107 (2005)

Favez J.-Y., Lister J.B., Mullhaupt Ph., Srinivasan B., *"Improving tokamak vertical position control in the presence of power supply voltage saturation",* Plasma Phys. & Contr. Fusion 47(10, 1709 (2005)

Fietz W.R., Fink S., Heller R., et al., Pasztor G., Wesche R., *"High temperature superconductors for the ITER magnet system and beyond",* Fuion Eng. & Design, 75-79, 105-109 (2005)

Fikar J., Schaller R., Baluc N., *"Mechanical spectroscopy of decagonal Al-Cu-Fe-Cr quasicrystalline coatings",* Phil. Mag. 84, 3571 (2004)

Fikar J., Schaller R., Baluc N., *"Mechanical spectroscopy of Al-Cu-Fe quasicrystalline coatings",* Mater. Sci. Engin. A370, 524 (2004)

Furd F., Ilyin Yu, Komarek P., et al., Marinucci C., *"The ITER toroidal field model coil project",* Fusion Eng. and Design, in press (2005)

Ganesh R., Vaclavik J., *"Global gyrokinetic stability of pressure-gradient-driven electromagnetic modes in tokamaks with regions of low shear",* Phys. Rev. Letters 94, 145002 (2005)

Garcia O.E., Horacek J., Pitts R.A., Nielsen A.H., Fundamenski W., Graves J.P., Naulin V., J. Juul Rasmussen, *"Evidence for interchange turbulence in the TCV scrape-off layer",* accepted in Plasma Phys. & Contr. Fusion

Goodman T.P., and TCV Team, *"Safety factor profile requirements for electron ITB formation in TCV",* Plasma Phys. & Contr. Fusion 47, B107 (2005)

Graves J.P., Angioni C., Budny R.V., et al., Coda S., Goodman T.P., Henderson M.A., Mueck A., Sauter O., and JET-EFDA contributors, *"Sawtooth control in fusion plasmas",* Plasma Phys. & Contr. Fusion 47, B121 (2005)

Graves J.P., Horacek J., Pitts R.A., Hopcraft K.I., *"Self-similar density turbulence in the TCV tokamak scrape-off layer",* Plasma Phys. & Contr. Fusion 47, L1-L9 (2005) (Letter to the Editor)

Graves J.P., *"Internal kinkmodestabilizationandthe properties of auxiliary heated ions",* Phys. Plasmas 12, 090908-1 - 090908-9 (2005)

Guittienne Ph., Chevalier E., Hollenstein Ch., *"Towards an optimal antenna for Helicon waves excitation",* J. Appl. Phys. 98, 083304 (2005)

Heidinger R., Fischer U., Hailfiner G., et al., Henderson M., *"Structural integration studies for the ITER ECRH Upper Launcher",* J. of Physics: Conference Series 25, 234-242 (2005)

Heller R., Darweschsad M.S., Dittrich G., et al., Wesche R., *"Experimental results of a 70kA high temperature superconductor current lead demonstrator for the ITER magnet system",* IEEE Trans. Appl. Supercond. 15, 1496-1499 (2005)

Henderson M.A., Chavan R., Heidinger R., Nikkola P., Ramponi G., Saibene G., Sanchez F., Sauter O., Serikov A., Zohm H., *"The front steering launcher design for the ITER ECRH upper port",* Third IAEA Technical Meeting on "ECRH Physics and Technology for ITER", Como, Italy, May 2005, J. of Physics: Conference Series 25, 143-150 (2005)

Henderson M.A., Camenen Y., Coda S., Goodman T.P., Nikkola P., Pochelon A., Sauter O., and TCV Team, *"Rapid and localized eITB (Electron Internal-Transport-Barrier) formation during shear inversion in fully non-inductive TCV discharges",* Phys. Rev. Letters 93(21), 215001 (2004)

Horacek J., Pitts R.A., Graves J.P., *"Overview of edge electrostatic turbulence experiments on TCV",* Czechoslovak Journal of Physics, 55(3), 271-283 (2005)

Howling A.A., Sansonnens L., Schmidt H., Hollenstein Ch., *"Comment on "Ion energy uniformity in high-frequency capacitive discharges" [Appl. Phys. Lett. 86, 021501 (2005)]",* Appl. Phys. Lett. 87, 076101 (2005)

Howling A.A., Derendinger L., Sansonnens L., Schmidt H., Hollenstein Ch., Sakanaka E., Schmitt J.P.M., *"Probe measurements of plasma potential nonuniformity due to edge asymmetry in large-area radio-frequency reactors: the telegraph effect",* J. Appl. Phys. 97, 123308 (2005)

Hurd F., Sborchia C., Salpietro E., et al., Bruzzone P., *"Design and manufacture of a full size joint sample (FSJS) for the qualification of the poloidal field (PF) insert coil",* IEEE Trans. Appl. Supercond. 15, 1379-1382 (2005)

Ilyin Y., Nijhuis A., Abbas W., Bruzzone P., Stepanov B., *"Reconstruction of the current unbalance in full-size ITEr NbTi CICC by self field measurements",* IEEE Trans. Appl. Supercond. 15, 1391-1394 (2005)

Klimanov I., Porte L., Alberti S., Blanchard P., Fasoli A., Goodman T.P., *"Electron cyclotron emission spectrometry on TCV",* Rev. Sci. Insrum 76, 093504 (2005)

Lister J.B., Dokuka V.N., Khayrutdinov R.R., Lukash V.E., Duval B.P., Moret J.-M., Artaud J.-F., Baziuk V., Cavinato M., *"Evolution of the DINA-CH tokamak full discharge simulator",* Fus. Engin. & Design 74, 633-637 (2005)

Marinucci C., Bruzzone P., Della Corte A., Savoldi Richard L., Zanino R., *"Pressure drop in the ITER PFI cable-in-conduit conductor",* IEEE Trans. Appl. Supercond. 15, 1383-1386 (2005)

Martovetsky N., Bruzzone P., Stepanov B., Wesche R., et al., *"Effect of the conduit material on CICC performance under high cycling loads",* IEEE Trans. Appl. Supercond. 15, 1367-1370 (2005)

Martynov An., Graves J., Sauter O., *"The stability of the ideal internal kink mode in realistic tokamak geometry",* Plasma Phys. & Contr. Fusion, 47, 1743-1762 (2005)

Moret J.-M., *"A software package to manipulate space dependencies and geometry in magnetic confinement fusion",* Rev. Sci. Instrum 76, 073507 (2005)

Mueck A., Goodman T.P., Maraschek M., Pereverzev g., Ryter F., Zohm H., and ASDEX Upgrade Team, *"Sawtooth control experiments on ASDEX Upgrade",* Plasma Phys. & Contr. Fusion 47(10), 1633 (2005)

Mueller S.H., Fasoli A., Labit B., McGrath M., Pisaturo O., Plyushchev G., Podesta M., Poli F.M., *"Basic turbulence studies on TORPEX and challenges in the theory-experiment comparison",* Physics of Plasmas 12, 090906 (2005)

Murari A., et al., Testa D., Fasoli A., *"Burning plasma diagnostics for the physics of JET and ITER",* Plasma Phys. & Contr. Fusion 47(12B), B249 (2005)

Pitts R.A., Coad J.P., Coster D.P., et al., Horacek J., and JET EFDA contributors, *"Material erosion and migration in tokamaks",* Plasma Phys. & Contr. Fusion 47(12B), B303 (2005)

Pitts R.A., Andrew P., Bonnin X., Chankin A.V., et al., *"Edge and Divertor Physics with reversed toroidal field in JET",* Invited paper to 16th Int. Conf. on Plasma Surface Interactions in Controlled Fusion Devices, Portland Maine, U.S.A., May 24-28, 2004, J. Nucl. Mater. 337-339, pp 146-153 (2005)

Podesta M., Fasoli A., Labit B., McGrath M., Mueller S.H., Poli F.M., *"Plasma production by low-field side injection of electron cyclotron waves in a simple magnetized torus",* Plasma Phys. & Contr. Fusion 47, 1989-2002 (2005)

Sansonnens L., *"Calculation of the electrode shape for suppression of the standing wave effect in large area rectangular capacitively-coupled reactors",* J. Appl. Phys. 97, 063304 (2005)

Sansonnens L., Strahm B., Derendinger L., Howling A.A., Hollenstein Ch., Ellert Ch., Schmitt J.P.M., *"Measurements and consequences of non-uniform RF plasma potential due to surface asymmetry in large area RF capacitive reactors",* AVS 51st Int.Symposium & Exhibition, Anaheim, USA, November 2004, J. Vacuum Sci. and Technol. A 23(4), 922-926 (2005)

Sauter O., Coda S., Goodman T.P., Henderson M.A., Behn R., Bottino A., Fable E., Martynov An., Nikkola P., Zucca C., and TCV Team, *"Inductive current density perturbations to probe electron internal transport barriers in tokamaks",* Phys. Rev. Lett. 94, 105002 (2005)

Schaeublin R., Yao Z., Baluc N., Victoria M., *"Irradiation induced stacking fault tetrahedra in fcc metals",* Phil. Mag. 85, 769 (2005)

Sharapov S., et al., Fasoli A., Testa D., *"Experimental studies of instabilities and confinement of energetic particles on JET and on MAST",* Nucl. Fusion 45, 1168-1177 (2005)

Sharma A.S., Limebeer D.J.N., Jaimoukha I.M., Lister J.B., *"Modelling and control of TCV",* IEEE Transactions on control system technology, 13(3) (2005)

Snipes J., et al., Fasoli A., *"Active and fast particle driven Alfven eigenmodes in Alcator C-Mod",* Phys. of Plasmas 12, 056102 (2005)

Sobbia R., Sansonnens L., Bondkowski J., *"Uniformity study in large-area showerhead reactors",* AVS 51st Int.Symposium & Exhibition, Anaheim, USA, November 2004, J. Vacuum Sci. and Technol. A23(4), 927-932 (2005))

Spaetig P., Schaeublin R., Baluc N., Kohlbrecher J., Victoria M., *"SANS investigation of proton-irradiated EUROFER97",* J. Nucl. Mater. 329-333, 289 (2004)

Spaetig P., Campitelli E.N., Bonade R., Baluc N., *"Assessment of plastic flow and fracture properties with small specimen test techniques for IFMIF-designed speciments",* Nucl. Fusion 45, 635 (2005)

Stepanov B., Bruzzone P., Vogel M., *"A low cost joint for the ITER PF coils, design and test results",* Fusion Eng. & Design, 75-79, 259-263 (2005)

Testa D., Boswell C., Fasoli A., and JET-EFDA contributors, *"Experimental study of the dependence of the damping rate of n=1 TAEs on the on-axis safety factor and toroidal rotation shear",* Nucl. Fusion 45, 907-917 (2005)

Testa D., Bigi M., *"Current losses induced by edge localised modes in JET tokamak plasmas",* Plasma Phys. & Contr. Fusion 47, 733-744 (2005)

Ulbricht A., Duchateau J.L., Fietz W.H., et al., Bruzzone P., Marinucci C., *"The ITER toroidal field model coil project",* Fusion Eng. and Design 73, 189-327 (2005)

Watanabe K.Y., Sakakibara S., Narushima Y., et al., Cooper W.A., *"Effects of global MHD instability on operational high-beta regime in LHD",* Nucl. Fusion 45, 1247-1254 (2005)

Weisen H., Zabolostky A., et al., *"Collisionality and shear dependences of density peaking in JET and extrapolation to ITER",* Nucl. Fusion 45, L1-L4 (2005)

Wesche R., Anghel A., Bruzzone P., Gislon P., Muzzi L., *"Analyses and implications of V-I characteristic of PF insert conductor sample",* Fusion Eng. and Design 75-79, 229-233 (2005)

Zhuang G., Behn R., Klimanov I., Nikkola P., Sauter O., *"Influence of non-Maxwellian velocity distributions during ECRH and ECCD on electron temperature measurements by Thomson scattering",* Plasma Phys. and Contr. Fusion 47, 1539-1558 (2005)

Zohm H., Heidinger R., Henderson M., Poli E., Ramponi G., Saibene G., Verhoeven A.G.A., *"Comparison of the performance of different options for the ITER ECRH Upper Launcher",* J. of Physics: Conference Series 25, 234-242 (2005)

APPENDIX B Conferences and Seminars

(see CRPP archives at http://crppwww.epfl.ch/archives)

B.1 Conference and conference proceedings published in 2005

Alberti S., Arnoux G., Porte L., Bortolon A., Karpushov A., Martin Y., Nowak S., Pitts R., and the TCV team, *"Third-harmonic X-mode, real-time controlled top-launch ECW experiments on TCV tokamak",* Third IAEA Technical Meeting on "ECRH Physics and Technology for ITER", Como, Italy, May 2005

Alfier A., Behn R., Nielsen P., Pasqualotto R., Zhuang G., Martin Y., Schombourg K., *"Influence of ELMs on Edge Temperature and Density Profiles in TCV",* 32nd EPS Conference on Plasma Physics, Tarragona, Spain, June 2005

Angelino P., Bottino A., Hatzky R., Jolliet S., Sauter O., Tran T.M., Villard L., *"Effects of plasma current on nonlinerar interactions of ITG turbulence, zonal flows and geodesic acoustic modes",* 11th European Fusion Theory Conference, September 2005, Aix-en-Provence, France, September 2005 (invited paper)

Anghel A., Bruzzone P., *"Results of contact resistance distribution in ITER conductor termination",* Proc. 19th Int. Magnet Technology Conference, MT-19, Genoa, Italy, 18-23 September 2005

Arnoux G., Alberti S., Porte L., Nowak S., Marletaz B., Marmillod Ph., Martin Y., and TCV Team, *"Third Harmonic X-mode ECHTop-launch In the TCV Tokamak",* Proc. in 16th topical conference on RF power in plasmas

Baluc N., *"Effects of radiation on metals and alloys",* EUROMAT 2005, Prague, Czech Republic (2005)

Bondkowski J., Sobbia R., Sansonnens L., *"3D numerical simulation of plasma enhanced chemical vapour deposition (PPECVD) applied to large-area showerhead reactors",* Proc. AM-LCD04 Conference, Tokyo, 25 August 2004 (2005)

Bruzzone P., *"30 Years of conductors for fusion. A summary and perspective",* Proc. 19th Int. Magnet Technology Conference, MT-19, Genoa, Italy, 18-23 September 2005

Bruzzone P., Stepanov B., Wesche R., Portone A., Salpietro E, Vostner A., DellaCorte A., *"Test results of a small size CICC with advanced Nb3Sn strands",* Proc. 19th Int. Magnet Technology Conference, MT-19, Genoa, Italy, 18-23 September 2005

Bruzzone P., Stepanov B., Zapretilina E., *"A critical review of coupling current losses for cable-in-conduct conductors",* Proc. 19th Int. Magnet Technology Conference, MT-19, Genoa, Italy, 18-23 September 2005

Bruzzone P., Stepanov B., Wesche R., *"Transverse load degradation in Nb3Sn cable-in-conduct conductors with different cable pattern",* Proc. of Cryogenic Engineering Conference / Int. Cryogenic Materials Conference, CEC/ICMC, Keystone, CO, USA, 29 August - 2 September 2005

Bruzzone P., Stepanov B., Zanino R., Savoldi Richard L., *"Results of thermo-siphon occurence in ITER cable-in-conduct conductor with dual channel",* Proc. of Cryogenic Engineering Conference / Int. Cryogenic Materials Conference, CEC/ICMC, Keystone, CO, USA, 29 August - 2 September 2005

Camenen Y., Pochelon A., Bottino A., Pavlov I., Behn R., Coda S., Goodman T.P., Henderson M.A., Moret J.-M., Porte L., Sauter O., Zhuang G., *"Electron heat transport dependence on plasma shape and collisionality in EC heated L-mode TCV plasmas",* 32nd EPS Conference on Controlled Fusion and Plasma Physics, Tarragona, Spain, 27 June - 01 July 2005, Europhys. Conf. Abstract 29C (2005) P-1.052

Campbell D.J., Saibene G., and contributors to the EFDA ECRH Upper Launcher Tasks, Henderson M., *"The ITER ECRH Upper Launcher - Status of EU Design and R&D activities",* 3rd IAEA Technical Meeting on "ECRH Physics and Technology for ITER", Como, Italy, May 2005

Chavan R., Henderson M.A., Sanchez F., *"A frictionless steering mechanism for the front steering ECCD ITER upper port launcher",* Third IAEA Technical Meeting on "ECRH Physics and Technology for ITER", Como, Italy, May 2005

Cooper W.A., Graves J.P., Yamaguchi T., Narushima Y., Okamura S., Sakakibara S., Suzuki C., Watanabe K.Y., Yamada H., Yamazaki K., *"Stability Properties of Anisotropic Pressure Stellarator Plasmas with Fluid and Noniteractive Energetic Particles",* 15th International Stellarator Workshop

Fable E., Sauter O., Zabolotsky A., Weisen H., Marinoni A., *"Density behavior during electron internal transport barriers in TCV fully non inductive discharges",* 32nd EPS Conference on Plasma Physics, Tarragona, Spain, June 2005

Fasoli A., Labit B., McGrath M., Mueller S.H., Plyushchev G., Podesta M., Poli F.M., *"Energetic ion physics for burning plasmas",* Annual Meeting of the German Physical Society, Berlin, Germany, 2005 (invited paper)

Fietz W.H., Heller R., Lietzow R, et al., Wesche R., *"High temperature superconductor current leads proposal for ITER",* Proc. of the IEEE Symposium on Fusion Engineering, SOFE 2005, Knoxville, TN, USA, 26-29 September 2005

Graves J.P., *"Sawtooth control in fusion plasmas",* 32nd EPS Conference on Controlled Fusion and Plasma Physics, Tarragona, Spain, 27 June - 01 July 2005

Graves J.P., *"Internal kink stabilisation and the properties of auxiliary heated ions and alpha particles",* 2nd IAEA Technical Meeting on the Theory of Plasma Instabilities: Transport, stability and their interaction, 2 - 4 March 2005, Trieste, Italy

Heidinger R., Fischer U., Hailfiner G., et al., Henderson M., *"Structural integration studies for the ITER ECRH Upper Launcher",* 3rd IAEA Technical Meeting on "ECRH Physics and Technology for ITER", Como, Italy, May 2005

Heller R., Fietz W.H., Lietzow R., et al., Wesche R., *"70kA high temperature superconductor current lead operation at 80K",* Proc. 19th Int. Magnet Technology Conference, MT-19, Genoa, Italy, 18-23 September 2005

Henderson M.A., Chavan R., Heidinger R., Nikkola P., Ramponi G., Saibene G., Sanchez F., Sauter O., Serikov A., Zohm H., *"The front steering launcher design*

for the ITER ECRH upper port", Third IAEA Technical Meeting on "ECRH Physics and Technology for ITER", Como, Italy, May 2005

Henderson M., Chavan R., Heidinger R., Ramponi G., Saibene G., Sanchez F., Shidara H., Zohm H., *"The design and physics performance of the ITER upper port ECH front steering launcher"*, SOFE 2005, 21st IEEE/NPSS Symposium on Fusion Engineering

Henderson M.A., Chavan R., Nikkola P., Ramponi G., Saibene G., Sanchez F., Sauter O., Shidara H., Zohm H., *"The physics performance of the front steering launcher for the ITER ECRH upper port"*, 16th Topical Conference on RF power in plasmas, Park City, Utah, April 2005

Henderson M.A., Behn R., Bottino A., Camenen Y., Coda S., Fable E., Goodman T.P., Marynov An.,, Nikkola P., Pochelon A., Sauter O., Zucca C., *"Control of the eITB formation and performance in fully non-inductively sustained ECCD discharges in TCV"*, 16th Topical Conference on RF power in Plasmas, Park City, Utah, USA, April 2005, AIP Conf. Proc. 787, 399 (2005)

Hogge J.-P., Alberti S., Arnold A., et al., Chavan R., Fasel D., Goodman T., Henderson M.A., Marmillod P., Perez A., Porte L., Tran M.Q., Yovchev I., *"Development of a 2MW, CW coaxial gyrotron at 170GHz and test facility for ITER"*, Third IAEA Technical Meeting on "ECRH Physics and Technology for ITER", Como, Italy, May 2005

Horacek J., Garcia O.E., Graves J.P., Pitts R.A., Nielsen A.H., Naulin V., Rasmussen J.J., *"Plasma electrostatic turbulence in TCV tokamak edge: direct comparison of experiment with 2D simulation"*, 32nd EPS Conference on Plasma Physics, Tarragona, Spain, June 2005

Howling A.A., Sansonnens L., Hollenstein Ch., *"Electromagnetic sources of nonuniformity in large area capacitive reactors"*, 27th Dry Process Symposiu, DPS2005, Jeju, Korea (invited paper)

Jolliet S., Angelino P., Bottino A., Hatzky R., Sauter O., Tran T.M., Villard L., *"Recent advances in non-linear PIC simulaions in magnetic coordinates"*, 11th European Fusion Theory Conference, September 2005, Aix-en-Provence, France, September 2005

Karpushov A.N., Duval B.P., Schlatter Ch., Weisen H., Afanasyev V.I., Chemyshev F.V., Mirnov M.I., *"Determination of the Radial Profile of Hydrogen Isotope Composition in TCV plasmas"*, 32nd EPS Conference on Plasma Physics, Tarragona, Spain, June 2005

Kim S.H., Artaud J.-F., Basiuk V., Khayrutdinov R.R., Dokuka V., Lister J.B., Lukash V.E., *"Combined DINA-CH and CRONOS Simulations of ITER"*, 32nd EPS Conference on Plasma Physics, Tarragona, Spain, June 2005

Kim S.H., Cavinato M., Dokuka V., Khayrutdinov R.R., Lang P.T., Lister J.B., Lukash V.E., Martin Y.R., Villard L., *"Comparing magnetic triggering of ELMs in ASDEX Upgrade and TCV with the DINA-CH tokamak simulator"*, 32nd EPS Conference on Plasma Physics, Tarragona, Spain, June 2005

Labit B., Fasoli A., McGrath M., Mueller S.H., Plyushchev G., Podesta M., Poli F.M., *"Drift waves in the TORPEX toroidal plasma device"*, 32nd EPS Conference on Plasma Physics, Tarragona, Spain, June 2005

Lindau R., Moeslang A., Rieth M., et al., Baluc N., *"Present development status of EUROFER and ODS for application in blanket concepts",* Proc. 23rd SOFT Conference, Venice, Italy (2004)

Lister J.B., Appel L., Huysmans G., Schlatter G., Suttrop W., *"Creating an XML Driven Data Bus between Fusion Experiments",* ICALEPCS 2005, Geneva, Switzerland, October 2005

Martin Y., Porte L., Alberti S., Pitts R.A., *"Third harmonic EC heating of ELMy H-mode in TCV",* 10th IAEA Technical Meeting on H-mode Physics and Transport Barriers

Martin Y.R., Coda S., Duval B.P., Llobet X., Moret J.-M., *"A new plant control software for the TCV tokamak",* Conference on Accelerator and Large Experimental Physics Control Systems, ICALEPCS 2005, Geneva, Switzerland, October 2005, Europhys. Conf. Abstr. 29J, P-01.083-7 (2005)

Martynov A.A., Galkin S.A., Medvedev S. Yu., Villard L., *"Reversed current density in tokamaks - equilibrium and stability issues",* 32nd EPS Conference on Plasma Physics, Tarragona, Spain, June 2005, P5.065

Medvedev S. Yu., Ivanov A.A., Martynov A.A., Poshkhonov Yu. Yu., Lister J.B., Martin Y., Sauter O., Villard L., *"Reversed current density in tokamaks - equilibrium and stability issues",* 32nd EPS Conference on Plasma Physics, Tarragona, Spain, June 2005, P5.064

Moeller C., Henderson M.A., *"Focusing a remotely steered wave beam",* 7th Biennial Transmission Line Workshop, Virginia Beach, Virginia, USA, September 2005

Mueck A., Laqua H.P., Coda S., Duval B., Goodman T.P., Klimanov I., Martin Y., Pochelon A., Porte L., *"O-X-B Mode Conversion in the TCV Tokamak",* 32nd EPS Conference on Plasma Physics, Tarragona, Spain, June 2005, Europhys. conf. Abstr. 29C, P-4.110 (2005)

Mueller S., Fasoli A., Labit B., McGrath M., Plyushchev G., Podesta M., Poli F.M., *"Basic turbulence studies on TORPEX and challenges in the theory-experiment comparisons",* 2nd IAEA Technical Meeting on Theory of Plasma Instabilities, Triest, Italy, 2005 (invited paper)

Murari A., et al., Testa D., Fasoli A., *"Burning plasma diagnostics",* 32nd EPS Conference on Controlled Fusion and Plasma Physics, Tarragona, Spain, June - July 2005

Narushima Y., Sakakibara S., Watanabe K.Y., et al., Cooper W.A., *"Experimental study of current driven MHD mode in LHD",* EPS conference Tarragona, Spain, June-July 2005

Nelson-Melby E., Harvey R.W., Smirnov A.P., Ram A.K., Coda S., *"Fully relativistic ray-tracing and dispersion relations of electron Bernstein waves",* 16th Topical Conf. on Radio Frequency Power in Plasmas, Park City, Utah, USA, 2005, AIP Conf. Proc. 787, 357 (2005)

Piosczyk B., Alberti S., Bariou D, et al., Goodman T., Henderson M., Hogge J.–P., Porte L., Tran M.Q., Yovchev I., *"Progress in the development of the 170GHz coaxial cavity gyrotron for ITER",* SMP 2005 Conference on the Volga Boat in Russia

Pitts R.A., Coad J.P., Coster D.P., et al., Horacek J., and JET EFDA contributors, *"Material erosion and migration in tokamaks",* 32nd EPS Conference on Plasma Physics, Tarragona, Spain, June 2005 (Invited talk)

Pochelon A., Alberti S., Arnoux G., Camenen Y., Fable E., Mueck A., Porte L., and the TCV Team, *"Recent physics results with electron cyclotron heating in TCV",* 6th Int. Workshop on "Strong Microwaves in Plasmas, July 25 - August 1, 2005, Nizhny Novgorod, Russia (invited plenary lecture)

Podesta M., Fasoli A., Labit B., McGrath M., Mueller S.H., Plyushchev G., Poli F.M., *"Experimental studies of plasma production and transport mechanisms in the toroidal device TORPEX",* 32nd EPS Conference on Plasma Physics, Tarragona, Spain, June 2005

Poli F.M., Fasoli A., Labit B., McGrath M., Mueller S.H., Plyushchev G., Podesta M., *"Investigatin of turbulence and transport in the toroidal device TORPEX",* Transport Task Force Meeting, Napa Valley, USA, April 2005

Portone A., Salpietro E., Bottura L., Bruzzone P., et al., *"Conceptual design of the 12.5T superconducting EFDA dipole",* Proc. 19th Int. Magnet Technology Conference, MT-19, Genoa, Italy, 18-23 September 2005

Ramar A., Leguey T., Munoz A., Baluc N., Schaeublin R., *"Ti influence on the microstructure and the mechanical behaviour of an EDS ferritic/martensitic EUROFER 97 steel",* EUROMAT 2005, Prague, Czech Republic (2005)

Sanchez F.,, Bertizzolo R., Chavan R., Henderson M., Landis J.-D., *"A frictionless steering mechanism for the Front Steering ECCD ITER Upper Port Launcher",* SOFE 2005, 21st IEEE/NPSS Symposium on Fusion Engineering

Sansonnens L., Hollenstein Ch., Feitknecht L., Shah A., Ballif Ch., Kroll U., *"High-rate large-area silicon deposition by VHF plasma",* Technical Symposium on "CSEM, EPFL & IMT collaboration day, Micro and Nano Technology", Neuchatel, 17 October 2005

Sansonnens L., Schmidt H., Howling A.A., Hollenstein Ch., Ellert C., Buechel A., *"Application of the shaped electrode technique to a large area rectangular capacitively-coupled plasma reactor to suppress standing wave nonuniformity",* AVS 52st Int. Symposium & Exhibition, Boston, USA, October 30 - November 1, 2005

Sauter O., Zohm H., *"Partial Stabilisation of NTMs with ECCD for standard scenarios in ITER",* 32nd EPS Conference on Plasma Physics, Tarragona, Spain, June 2005

Sauter O., Behn R., Bottino A., Camenen Y., Coda S., Fable E., Goodman T.P., Henderson M.A., Martynov An., Nikkola P., Zhuang G., Zucca C., *"Physics of steady-state electron internal transport barriers on TCV",* 10th IAEA Technical Meeting on H-mode Physics and Transport Barriers, St. Petersburg, September 2005

Sauter O., *"Particle transport in TCV electron internal transport barriers (eITBs)",* ITPA topical Group on Transport Physics meeting, St. Petersburgh, 2005

Sauter O., *"Spontaneous rotation, spin-up and sign flip in TCV ohmic discharges",* ITPA topical Group on Transport Physics meeting, St. Petersburgh, 2005

Scarabosio A., Bortolon A., Duval B.P., Karpushov A., Pochelon A., *"Momentum transport and plasma rotation spin up in TCV",* 32nd EPS Conference on Plasma Physics, Tarragona, Spain, June 2005, Vol 29C, P1.049

Schlatter Ch., Duval B.P., Karpushov A.N., *"Reconstruction of Hydrogenic Ion Temperature Profiles on TCV",* 32nd EPS Conference on Plasma Physics, Tarragona, Spain, June 2005

Schombourg K., Lister J.B., Martin Y., *"Synchronisation of ELMs within magnetic perturbation bursts in TCV",* 32nd EPS Conference on Plasma Physics, Tarragona, Spain, June 2005

Siegrist M.R., Tonetti G., Weisen H., Melnikov A., Perfilov S., *"The Heavy ion beam diagnostic project for the TCV tokamak",* SOFE 2005, 21st IEEE/NPSS Symposium on Fusion Engineering

Tanna V.L., Fietz W.H., Heller R., et al., Wesche R., *"Conceptual design of a high temperature superconductor current feeder system for ITER",* Proc. of the 7th European Conference on Applied Supreconductivity, EUCAS 2005, Vienna, Austria, 11-15 September 2005

Testa D., Fasoli A., Boswell C., *"Measurement of the instability threshold for Toroidal Alfven Eigenmodes as function of the ion grad B-drift direction in JET tokamak plasmas",* 32nd EPS Conference on Controlled Fusion and Plasma Physics, Tarragona, Spain, June - July 2005

Thumm M., Alberti S., Arnold A., et al., Hogge J.-P., Tran M.Q., *"Status of 1MW, 140GHz, CW gyrotron for W7-X",* SMP 2005 Conference on the Volga Boat in Russia (invited talk)

Tran M.Q., *"Fusion: a sustainable energy source",* Tutorial: Future energy sources and technolgoies for electricity systems, 22 August 2005, PSCC 2005, Lige, Belgium (invited talk)

Tran M.Q., *"ITER and the road map towards fusion energy",* Int. Conf. on Nuclear Energy for New Europe 2005, Bled, Slovenia (Invited paper)

Tran M.Q., *"Les enjeux du projet ITER: Enjeux technologiques",* Journe ECRIN, "ITER - Enjeux scientifiques, technologiques et socio-économiques", Assemblée Nationale, Paris, France, 11 octobre 2005

Tran M.Q., *"Material science and technology in the roadmap towards a fusion reactor",* 12th Int. Conference on Fusion Reactor Materials ICFRM-12, Santa Barbara, CA, USA, 4-9 December 2005 (plenary invited talk)

Villard L., Angelino P., Bottino A., Hatzky R., Jolliet S., Sauter O., Tran T.M., *"Gyrokinetic particle simulations of ITG modes and zonal flows with canonical and local equilibrium distributions",* 11th European Fusion Theory Conference, September 2005, Aix-en-Provence, France, September 2005

Weisen H., Zabolotsky A., Maslov M., Giroud C., and JET EFDA contributors, *"Scaling of density peaking in JET H-modes",* 10th IAEA Technical Meeting on H-mode Physics and Transport Barriers, St. Petersburg, 28-30 September 2005

Wesche R., Stepanov B., Bruzzone P., *"Comparison of the DC performance of full- and sub-size NbTi cable-in-conduit conductors",* Proc. 19th Int. Magnet Technology Conference, MT-19, Genoa, Italy, September 2005

Wischmeier M., Pitts R.A., Horacek J., Coster D., Reiter D., *"Enhanced main chamber wall interaction as an explanation for anomalous divertor detachment on TCV",* 32nd EPS Conference on Plasma Physics, Tarragona, Spain, June 2005

Yu G., Nita N., Baluc N., *"Thermal creep behaviour of the EUROFER 97 RAFM steel and two european ODS EUROFER 97 steels",* Proc. 23rd SOFT Conference, Venice, Italy 2004

Yu G., Schaeublin R., Baluc N., *"Small angle neutron scattering (SANS) signal pattern simultion",* EUROMAT 2005, Prague, Czech Republic (2005)

Zanino R., Savoldi Richard L., Salpietro E., et al., Bruzzone P., *"Implications of NbTi short-sample test results and analysis for the ITER poloidal field conductor insert",* Proc. 19th Int. Magnet Technology Conference, MT-19, Genoa, Italy, 18-23 September 2005

Zanino R., Savoldi Richard L., Bruzzone P., *"A critical assessment of pressure drop design criteria for the ITER conductors",* Proc. of Cryogenic Engineering Conference / Int. Cryogenic Materials Conference, CEC/ICMC, Keystone, CO, USA, 29 August - 2 September 2005

Zohm H., Heidinger R., Henderson M., Poli E., Ramponi G., Saibene G., Verhoeven A.G.A., *"Comparison of the performance of different options for the ITER ECRH upper launcher",* 3rd IAEA Technical Meeting on "ECRH physics and technology for ITER", Como, Italy, May 2005

American Physical Society (APS)

Angelino P., Bottino A., Hatzky R., Jolliet S., Sauter O., Tran T.M., Villard L., *"Coupling of zonal flows and geodesic acoustic modes: effects on turbulent transport",* 47th APS-DPP meeting, Denver, Colorado, USA, October 2005

Fasoli A., Labit B., McGrath M., Müller S.H., Plyushchev G., Podesta M., Poli F., *"Electrostatic turbulence and transport in a simple magnetized plasma",* 47th Annual Meeting APS, Division of Plasma Physics, Denver, USA 2005 (invited paper)

Fasoli A., Labit B., McGrath M., Mueller S.H., Plyushchev G., Podesta M., Poli F.M., *"Electrostatic turbulence and transport in a simple magnetized plasma",* 47th Annual Meeting APS, Division of Plasma Physics, Denver, USA 2005 (invited paper), submitted to Phys. of Plasmas

Harvey R.W., Smirnov A.P., Ershov N.M., et al., Coda S., *"Electron cyclotron emission from nonthermal distributions,* 47th Annual Meeting APS, Division of Plasma Physics, Denver, USA 2005, Bull. Am. Phys. Soc. 50, QP1.00052 (2005)

Mueck A., Laqua H.P., Coda S., Duval B., Goodman T.P., Klimanov I., Martin Y., **Pochelon A., Porte L.**, *"Electron Bernstein wave heating in the TCV tokamak",* 47th Meeting of the Division of Plasma Physics of the APS, Denver, CO, 2005, Bull. Am. Phys. Soc. 50, FP1.00062 (2005)

Mueller S.H., Fasoli A., Labit B., McGrath M., Plyushchev G., Podesta M., Poli F.M., *"Investigation on turbulent structures on the TORPEX device",* 47th Annual Meeting APS, Division of Plasma Physics, Denver, USA 2005

Workshop

Angelino P., Bottino A., Allfrey S.J., Hatzky R., Sauter O., Tran T.M., Villard L., *"Global nonlinear simulations of electrostatic ITG modes in tokamaks",* SciDAC workshop on plasma turubulence,laguna Beach, CA, US, February 2005

Henderson M.A., Hogge J.-P., Chavan R., et al., Nikkola P., Sanchez F., Sauter O., Shidara H., *"The front steering launcher design for the ITER ECRH upper port",* US-Japan-EU RF Technology Workshop, Santa Cruz, California, June 2005

Moeller C., Henderson M.A., *"The prospects of remotely focusing wave beam",* US-Japan-EU RF Technology Workshop, Santa Cruz, California, June 2005

Mueller S.H., Fasoli A., Labit B., McGrath M., Plyushchev G., Podesta M., Poli F.M., *"Turbulence studies on TORPEX and perspectives for Theory-Experiment comparison",* Int. Workshop on Turbulence and Transport at the Plasma Edge of Tokamaks, University of Innsbruck, Austria, April 2005

Sublet A., Dorier J.-L., Hollenstein Ch., *"Sub-atmospheric pressure barrier discharge for SiOx deposition: plasma diagnostics and coating characterization",* 2nd Int. Workshop on Cold Atmospheric Preesure Plasmas: Sources and Applications, CAPPSA 2005, Bruges, Belgium, 30 August - 2 September 2005

B.2 *Seminars presented at the CRPP in 2005*

Dr. M. Campbell, PH Deparment, CERN. Spokesman, Medix2 Collaboration, *"Medipix2, a single photon counting pixel readout system aimed at spectroscopic X-ray imaging"*

J. Decker, MIT, PSFC, Cambridge, USA, *"Current drive calculations in tokamak plasmas"*

S. Gnesin, Padova, Italy, *"Characterization of an ion beam for the development of an electric field diagnostic in a plasma"*

Dr. S. Ratynskaia, Max-Planck-Institute for extraterrestrial physics, Garching, Germany, *"Experimental studies of waves and anomalous transport in dusty and low-temperature magnetized plasma"*

Dr. S. Coda, CRPP-EPFL, *"High-bootstrap, non-inductively sustained electron internal transport barriers in TCV"*

Dr. V.S. Udintsev, CEA/DSM/DRFC, CEA/Cadarache, France, *"Progress in Studies of Non-linear Temperature Oscillations in the Plasma Core and their Interplay with MHD on Tore Supra"*

Dr. A. Bottino, CRPP-EPFL, *"On the physics of the ion temperature gradient (ITG) mode"*

Dr. M. Gindrat, CRPP-EPFL, *"Characterization of supersonic low-pressure plasma jets"*

S.K. Jawla, Department of Physics, ITT Dehli, India, *"Evaluation of mode fields and electron acceleration in waveguides using microwaves"*

C. Le Drian, Section de Physique, EPFL, *"Caractérisation d'amplificateurs à boîtes quantiques"*

Dr. P. Nikkola, CRPP-EPFL, *"The effect of electron transport on electron cyclotron current drive in tokamak plasmas"*

Prof. J. Yu, China Institute of Atomic Energy (CIAE), Beijing, P.R. China, *"Nuclear power strategy and fusion energy research in China"*

Dr. P. Popovitch, CRPP-EPFL, *"Low-frequency electromagnetic wave propagation in 3D plasma configurations"*

Prof. J. Yu, China Institute of atomic Energy (CIAE), Beijing, P.R. China, *"Nuclear power strategy and fusion energy research in China"*

Dr. P. Popovitch, CRPP-EPFL, *"Low-frequency electromagnetic wave propagation in 3D plasma configurations"*

E. Asp, DRFC, CEA-Cadarache, France, *"Energy confinement and stiffness of the Weiland model in the hot electron mode"*

Dr. H. Igami, RF plasma heating division, National Institute for Fusion Science, Toki City, Japan, *"Recent results of ECRH experiment on LHD"*

G. Turri, UKAEA Fusion Association, Imperial College, London, UK, *"Magnetic reconnections in MAST"*

J. Paley, Imperial College, London, UK, *"Energy flow during disruptions"*

G. Turri, Imperial College, London, UK, *"Magnetic reconnections in MAST"*

Dr. R. Kamendje, Inst. für Theoretische Physik, Technische Univ. Graz, Austria, *"Kinetic modeling of ECRH/ECCD in a tokamak with the Monte Carlo code ECNL"*

J. Rossel, CRPP-EPFL, *"Soft X-ray emissivity profile inversion in quasi-axisymmetric equilibria"*

Dr. M. Wischmeier, CRPP-EPFL, *"Simulating divertor detachment in the TCV and JET tokamaks"*

Dr. X. Garbet, DRFC, CEA Cadarache, France, *"Turbulent fluxes and entropy production rate"*

Prof. D. Bora, Inst. For Plasma Research, *"Basic experiments in toroidal assembly"*

X. Lapillonne, Imperial College London, *"The linear delta expansion applied to the quantum anharmonic oscillator"*

Dr. V.S. Udintsev, DRFC, CEA Cadarache, France, *"Correlation ECE on Tore Supra: recent results and future plans"*

M. Kibalchenko, Imperial College London & CRPP-EPFL, *"Statistical study of the errors arising from plasma reconstruction using inverse equilibrium for the TCV tokamak"*

Dr. K. Hamamatsu, JAERI, Japan, *"Optimum EC beam injection for stabilization of NTM"*

Prof. A.H. Glasser, Los Alamos National Lab., USA, *"Spectral element simulation and adaptive grid generation for magnetically confined plasmas"*

A. Diallo, Univ. of Iowa, USA, *"On the phase-space resolution of ion density fluctuations"*

Dr. Y. Idomura, JAERI, Naka, Ibaraki, Japan, *"Gyrokinetic simulations of ETG turbulence and zonal flows"*

Prof. B.A. Trubnikov, Kurchatov Inst., Moscow, Russia, *"Theory of competition"*

Dr. P. Popovitch, CRPP-EPFL, *"VTK: powerful tool for (aesthetically pleasing) 3D data visualization"*

Dr. G. Conway, IPP Garching, Germany, *"Turbulence and Er characterisation in ASDEX Upgrade using Doppler reflectometry"*

M. Biel, AGH-Univ. of Science and Technology, Faculty of Metallurgy and Materials science, Krakow, Poland, *"Microstructure and properties of titanium biomaterials after surface treatment"*

A. Pitzschke, Inst. Für Medizinische Physik und Biophysik, Univ. Leipzig, Germany, *"Investigations of the interaction between beta-amyloid peptides with lipid membranes using atomic force microscopy and fluorescence spectroscopy"*

Dr. Y. Nakamura, JAERI, Ibaraki, Japan, *"Numerical simulation of fully non-inductive current buildup and external control of ITB profile with Slim Center Solenoid"*

Dr. J.M. Fontdecaba Climent, CIEMAT, Madrid, Spain, *"CX-NPA diagnostics in TJ-II"*

M. Priego Wood, Facultad de Ciencias Matematicas, Univ. Complutense de Madrid, Spain, *"Anomalous diffusion, clustering and pinch of impurities in plasma edge turubulence"*

Dr. T. Dannert, Max-Planck-Inst. Für Plasmaphysik, Garching, D., *"Particle transport in ITG-TEM gyrokinetic turbulence"*

Dr. M. Greenwald, MIT Boston, USA, *"Vision for data management and remote collaboration for ITER"*

Dr. V.F. Shevchenko, Culham Science Centre, Abingdon, UK, *"EBW studies on MAST"*

Dr. F. Castejon, Lab. Nacional de Fusion, CIEMAT, Spain, *"Influence of magnetic topology on transport and stability in Stellarators"*

Prof. P. Wurz, Space Research & Planetary Sciences, Univ. Bern, Switzerland, *"Investigation of the interstellar neighborhood of our solar system: present and future research"*

A. Bousquet, Lab. Des Plasmas et des Couches Minces, Inst. Des Matériaux Jean Rouxel UMR 6502, Nantes, France, *"Thin film deposition by radiofrequency low pressure pulsed plasma in hexamethyldisiloxane/oxygen mixture"*

Dr. R. Herzog, CERN, Genève, Switzerland, *"Protecting the superconducting elements of the LHC accelerator"*

Dr. G. Arnoux, CRPP-EPFL, *"Chauffage de plasmas par ondes électromagnétiques à la troisième harmonique de la fréquence cyclotron des électrons dans le tokamak TCV"*

Dr. M. Henderson, CRPP-EPFL, *"Physics Performance of the ITER ECH Upper Launcher2*

B.3 *Other external presentations in 2005*

Angelino P., *CEA Cadarache, France, September 2005,* "Coupling of zonal flows and geodesic acoustic modes: effects on turbulent transport"

Appert K., *Nuklearforum Schweiz, Olten, Switzerland, 22 November 2005,* "ITER: Ein Meilenstein auf dem Weg zum Fusionsreaktor"

Baluc N., *Max-Planck-Institut fuer Plasmaphysik, Garching, Germany, April 2005,* "On the use of RAFM stees and their ODS variants as structural materials for fusion reactors"

Baluc N., *Southwestern Institute of Physics, Chengdu, P.R. China, June 2005,* "Status of R&D on materials for fusion reactors"

Baluc N., *Institute of Plasma Physics, Chinese academy of Sciences, Hefei, P.R. China, June 2005,* "Status of R&D on materials for fusion reactors"

Baluc N., *China Institute of Atomic Energy (CIAE), Beijing, P.R. China, July 2005,* "Status of R&D on materials for fusion reactors"

Bruzzone P., *Max-Planck-Institut fuer Plasmaphysik, Garching, Germany, 19 January 2005,* "CRPP conceptual design activities for high field dipole"

Bruzzone P., *Max-Planck-Institut fuer Plasmaphysik, Garching, Germany, 3 March 2005,* "Progress on CRPP conceptual design activities for high field dipole"

Bruzzone P., *CEA Cadarache, France, 4 July 2005,* "Schedule items at CRPP"

Bruzzone P., *CERN Academic Training, May 2005,* "The ITER project - The evolution of design and manufacture of fusion conductors"

Bruzzone P., *CERN Academic Training, May 2005,* "The performance prediction from a single strand to large size conductors"

Bruzzone P., *CERN Academic Training, May 2005,* "Procurement and quality assurance issues for the ITER magnets"

Bruzzone P., *ECOMAG-05 Lecture, Frascati, Italy, October 2005,* "Configurations and properties of low losses superconducting cables"

Cooper W.A., *Seminar given at CSCS, Manno, CH, 27 September 2005,* "Stability properties of anisoropic pressure stellarator plasmas with fluid and non-interacting energetic particles"

Cooper W.A., *Leysin American School, Switzerland, 17 November 2005,* "Les forces de la nature"

Fasoli A., Podesta M., *CNR-Milano, Italy, 12 December 2005,* "Plasma production and electrostatic turbulence studies in a simple toroidal plasma"

Henderson M.A., *Auburn University, Physics Department, Auburn, Alabama, USA, April 2005,* "Control of the eITB formation and performance in fully non-inductively sustained ECCD discharges in TCV"

Henderson M.A., *General Atomic, ECH Group, San Diego, USA, April 2005,* "The physics performance of the front steering launcher for the ITER ECRH upper port"

Henderson M.A., *ADEX Upgrade, ECH Group, Garching, Germany, November 2005,* "The front steering launcher"

Hollenstein Ch., , "Seminar at Leibniz-Institute for Surface Modification (IOM) and applied Physics / Materials Research University Leipzig, December 2005"

Lister J.B., *University of Greifswald, Germany, 20 January 2005,* "TCV - The challenge of shaping"

Lister J.B., *EPF Lausanne, 28 April 2005 (presented to the EPFL Physics Students),* "La fusion contrôlée - Toison d'or des physiciens et espoir pour l'avenir"

Lister J.B., *CERN Academic Training, May 2005,* "The ITER Project - Its aims and design challenges"

Lister J.B., *CERN Academic Training, May 2005,* "The ITER Project - The challenges of controlling and operating ITER"

Mueller S., *Univ. of California at San Diego (UCSD), Engineering Department, San Diego, USA, 31 October 2005,* "Investigation of turbulent structures on the TORPEX experiment"

Mueller S., *Univ. of California at San Diego (UCSD), Physics Department San Diego, USA, 2 November 2005,* "Investigation of turbulent structures on the TORPEX experiment"

Mueller S., *Univ. of California at Irvine (UCI), Physics Department San Diego, USA, 3 November 2005,* "Investigation of turbulent structures on the TORPEX experiment"

Mueller S., *Univ. of California at Los Angeles (UCLA), Physics Department San Diego, USA, 4 November 2005,* "Investigation of turbulent structures on the TORPEX experiment"

Pitts R.A., *Dept. of Physics, University of Basel, Switzerland, 7 November 2005,* "Material erosion and migration in tokamaks"

Sauter O., *10th course on global and local control of tokamak plasmas, Erice, Italy, 2005,* "Bootstrap current: control of current and pressure profiles"

Sauter O., *10th course on global and local control of tokamak plasmas, Erice, Italy, 2005,* "Neoclassical tearing modes"

Strahm B., *Univ. Neuchatel, Institut de Microtechnique, 28 octobre 2005,* "An analytical model for deposition of amorphous and microcrystalline silicon"

Tran M.Q., *Seminar given at the EMPA, Duebendorf, Switzerland, 26.08.05,* "ITER and the road map towards fusion energy"

Tran M.Q., *Physics Colloquium, Univ. of Neuchâtel, Switzerland, October 2005*, "ITER and the European strategy towards fusion energy"

APPENDIX C   External activities of CRPP Staff during 2005

C.1   National and international committees and ad-hoc groups

MEMBERSHIP

K. Appert   Member of the EFDA Steering Committee
                   Member of the CCE-FU committee

N. Baluc   Scientific and Technical Advisory Committee, Euratom
                   International Organizing Committee of the SOFT (Symposium on Fusion Technology) Conference
                   IEA Annex II Executive Committee
                   IEA Fusion Materials Agreement Executive Committee
                   Steering Committee Association Euratom-Confederation Suisse
                   Steering Committee CRPP-PSI
                   Steering Committee PSI-CRPP on Materials for Nuclear Applications (SCMATNUC).
                   Member of the Swiss Society for Optics and Microscopy (SSOM)
                   Task Coordinator of the Euratom Task TTMS-003 entitled 'Compatibility of Steels with Hydrogen and Liquids' of the Tritium Breeding and Materials Programme of EFDA
                   Task Coordinator of the subproject entitled 'Radiation-Resistant Materials' of the EXTREMAT Integrated Project (IP) of the 6th European Framework Programme

P. Bruzzone   International Magnet Technology Conference Organizing Committee
                   ITER Magnet Expert Group
                   Wendelstein 7-X Magnet Advisory Board
                   GSI Magnet Advisory Group

W.A. Cooper   Chairman, CSCS Large users assembly, Switzerland

A. Fasoli   Scientific and Technical Advisory Committee, Euratom
                   ASDEX Upgrade Programme Committee, Germany
                   Scientific Expert for Switzerland at Fusion Power Coordination Committee of the International Energy Agency
                   International Tokamak Physics Activities: Steady-State Operation and Energetic Particles Topical Group
                   Member of ad-hoc group of STAC for the monitoring of 2003 activities and 2005 work program of JET
                   Member of ad-hoc group of STAC for assessment of the progress in Research and Development of Lower Hybrid Current Drive.
                   Chairman of ad-hoc group of STAC for the monitoring of 2004 activities and 2006 work program of JET
                   Member of ad-hoc group of STAC for assessment of the progress in Control and Steady-state, 2005
                   Scientific Committee, 9th IAEA Technical Meeting on Energetic Particles in Magnetic Confinement Systems, 2005
                   Committee for 'Bourses Ecole Doctorale, EPFL

Ch. Hollenstein   Member of the Scientific committee of the department STI of the CNRS.
                   Expert for Deutschen Forschungsgemeinschaft (DFG) for the proposal of the establishment and funding of a transregional collaborative research centre (University and IPP Greifswald/University of Kiel)
                   Vice president Swiss Vacuum society
                   Member of the IUVSTA Plasma Division
                   Member of the Wissenschaftlicher Beirat Leibniz-Institut für Oberflächenmodifizierung Leipzig

Nomination as expert for the Deutschen Wissenschaftsrat (WR) for the audit of the Bundesanstalt fuer Materialforschung und -pruefung (BAM) in Berlin

J.B. Lister   International Tokamak Physics Activities: MHD, Disruption and Control Topical Group
EPS-13, Bern 2005, International Core Programme Committee
31st EPS Conference Programme Committee, London 2004
32nd EPS Conference Programme Committee, Tarragona 2005
33rd EPS Conference Programme Committee, Roma 2006
International Scientific Advisory Committee and co-chairman of the Local Organising Committee for ICALEPCS, Geneva 2005
Member of the STAC working group on Real Time Monitoring and Control

C. Marinucci   CHATS, Scientific Programme Committee

R.A. Pitts   International Tokamak Physics Activities: SOL + Divertor Topical Group
Leader of the EFDA Plasma Edge Task Force

A. Pochelon   Member of the Committee of the Swiss Nuclear Forum

O.Sauter   Scientific Committee of the 11th European Fusion Theory Conference

R. Schäublin   Member of the board of the Swiss Society for optics and microscopy

P. Spätig   Member of an ad hoc expert group to evaluate the IFMIF Comprehensive Design Report

M.Q. Tran   EFDA Leader, Director of the Inst. of Physics of Energy and Particle, EPFL
Electron Cyclotron Wave Task Area Leader
Chairman of the Electron cyclotron Wave-Coordinating Committee
Consultative Committee for the Euratom Specific Research and Training Programme in the field of Nuclear Energy, Fusion (CCE-FU), in his role of EFDA Leader
CCE-FU Special Working Group on "The accompanying programme"
Scientific and Technical Advisory Committee, Euratom, in his role of EFDA Leader
Standing Committee of the International Symposium on Fusion Nuclear Technology
Scientific Committee of the IAEA Technical Meeting on ECRH Physics and Technology for ITER
Expert on the IAEA International Fusion Research Council
Chairman of the Fusion Staffing Committee created by the CCE-FU
Member of the Steering Committee of the Center of Competence on Energy and Mobility of the the CEPF
Member of the Steering Committee for the 2008 Fusion Energy Conference
Member of co-chair of Selection Committee for professorship (Max-Planck-Geselschaft, ETH-Z, EPF-L)
Swiss delegate at the Fusion Power Coordinating Committee

L. Villard   Scientific and Technical Advisory Committee, Euratom
Conseil Scientifique du Département de Recherche sur la Fusion Contrôlée – CEA, France
Referee, PhD thesis, Oleksiy Mishchenko, Ernst Moritz Arndt Universität Greifswald and Max-Planck Gesellschaft, Institut für Plasmaphysik, Greifswald – *New methods in gyrokinetic particle-in-cell simulations*
Chair, ad-hoc group of STAC for the assessment of an application for a Cost-Sharing Action by the Comenius University, Bratislava, Slovakia

H. Weisen   Member of the International Advisory Board of IPP Prague.
Member of the Diagnostic Working Group for JET EPII diagnostics.

Member of the jury of the thesis of Laure Vermare, Université de Provence, Aix-Marseille I, on 'Mesures de l'activité magnétohydrodynamique et de la micro-turbulence par réflectométrie à balayage`.

PARTICIPATION

B. Duval ICALEPCS 2005 Local Organising Committee
Remote Participation Users Group, EFDA-JET
32nd EPS Local Organising Committee

C. Marinucci ITER TFMC Test and Analysis Group

Y.R. Martin International Tokamak Physics Activity: Confinement Database and Modelling Topical Group

L. Villard Ad-Hoc Group for the assessment of an application for a Cost-Sharing Action by the Bulgarian Academy of Sciences

C.2   Editorial and society boards

A. Fasoli International Tokamak Physics Activities group on Steady-State Operation and Energetic Particles

Ch. Hollenstein Editorial Board Plasma Chemistry and Plasma Processing Kluwer Academic/Plenum Publisher

J.B. Lister Chairman of the European Physical Society Plasma Physics Division
Deputy Editor of Plasma Physics and Controlled Fusion

Y.R. Martin Chairman of the Association Vaudoise des Chercheurs en Physique

P.J. Paris Fusion Expo Consortium Committee
EFDA Information Network
"Fédération Romande de l'Energie" Committee
Chairman of the "International Association of Specialists in Energy" (AISEN)

A. Pochelon Member of the Swiss Physical Society Committee, as auditor

L. Sansonnens Committee of the Swiss Physical Society, Responsible for Applied Physics

M.Q. Tran Board of Editors of Nuclear Fusion

C.3   EPFL committees and commissions

N. Baluc Commission Ecole Doctorale en Science et Génie des Matériaux

J-L. Dorier Commission du Doctorat de la Section de Physique, FSB-EPFL

A. Fasoli Commission d'Enseignement de la Section de Physique, FSB-EPFL

Ch. Guillemin Assemblée d'Ecole, EPFL

J-Ph. Hogge Commission du Doctorat de la Section de Physique, FSB-EPFL

O. Sauter Commission d'Informatique, FSB-EPFL

M.Q. Tran Commission du Doctorat de la Section de Physique, FSB-EPFL

Conseiller d'Etudes, Section de Physique, EPFL
Commission stratégique de la Section de Physique, EPFL
Membre du Comité de Sélection du Prix de la meilleure thèse EPFL

T.M. Tran Groupe de travail technique du Comité de Pilotage HPC/MPC, EPFL

L. Villard Délégué à la mobilité, Section de physique, FSB-EPFL
Conseiller d'Etudes, Section de physique, FSB-EPFL
Commission d'Enseignement de la Section de Physique, FSB-EPFL
Groupe de travail Informatique et Numérique, Section de Physique, FSB-EPFL
Groupe de travail technique HPC (High Performance Computing) – EPFL
Steering Committee, HPC (High Performance Computing) – EPFL
Steering Committee, Blue Gene Project - EPFL

APPENDIX D   Lausanne Reports (LRP)

(see CRPP archives at http://crppwww.epfl.ch/archives)

Wischmeier M., *"Simulating divertor detachment in the TCV and JET tokamaks (EPFL Thesis 3176(04))",* LRP 799/05

Moret J.-M., *"A software package to manipulate space dependencies and geometry in magnetic confinement fusion",* LRP 800/05

Howling A.A., Derendinger L., Sansonnens L., Schmidt H., Hollenstein Ch., Sakanaka E., Schmitt J.P.M., *"Probe measurements of plasma potential nonuniformity due to edge asymmetry in large-area radio-frequency reactors: the telegraph effect",* LRP 801/05

Marmy P., *"Creep-fatigue of CuCrZr: A review of the existing fatigue, creep and creep-fatigue data base and a life prediction analysis using a time based damage evaluation",* LRP 802/05

Martynov A., *"Ideal MHD stability of tokamak plasmas with moderate and low aspect ratio (EPFL thesis 3218(05) 2005)",* LRP 803/05

IAEA TCM Participants, *"Papers presented at the 20th IAEA Fusion energy conference, held in Vilamoura Portugal, Nov. 1-6, 2004",* LRP 804/05

Wesche R., Heller R., Fietz W.H., Tanna V.L., Zahn G., *"Report on the conceptual design of external HTS bus bars - EFDA Reference TW4-TMSF-HTSCOM, Deliverable 2",* LRP 805/05

IAEA Participants, *"Papers presented at theThird IAEA Technical Meeting on "ECRH Physics and Technology for ITER", 2-4.05.2005, Como, Italy",* LRP 806/05

Alberti S., Arnoux G., Porte L., Hogge J.-P., Marletaz B., Marmillod Ph., Martin Y., Nowak S., and TCV Team, *"Third-harmonic, top-launch, ECRH experiments on TCV tokamak",* LRP 807/05

Descoeudres A., Hollenstein Ch., Waelder G., Perez R., *"Time-resolved imaging and spatially-resolved spectroscopy of electrical discharge machining plasma",* LRP 808/05

Camenen Y., Pochelon A., Bottino A., Coda S., Ryter F., Sauter O., Behn R., Goodman T.P., Henderson M.A., Karpushov A., Porte L., Zhuang G., *"Electron heat transport in shaped TCV L-mode plasmas",* LRP 809/05

Ferrando i Margalet S., *"Bootstrap current compensation with electron-cyclotron waves in 3D reactor-size configurations (Thse EPFL No. 3379(2005))",* LRP 810/05

Pochelon A., Alberti S., Arnoux G., Camenen Y., Fable E., Mueck A., Porte L., and the TCV Team, *"Recent physics results with electron cyclotron heating in TCV",* LRP 811/05

APPENDIX E   The basis of controlled fusion

E.1   Fusion as a sustainable energy source

Research into controlled fusion aims to demonstrate that it is a valid option for generating power in the long term future in an environmentally, politically and economically acceptable way. Controlled fusion is a process in which light nuclei fuse together to form heavier ones: during this process a very large amount of energy is released. For a fusion reactor it is planned to use the two isotopes of hydrogen: deuterium (D) and tritium (T), which fuse together much more readily than any other combination of light nuclei according to the following reaction:

$$D^2 + T^3 \rightarrow He^4 + n + 17.6MeV$$
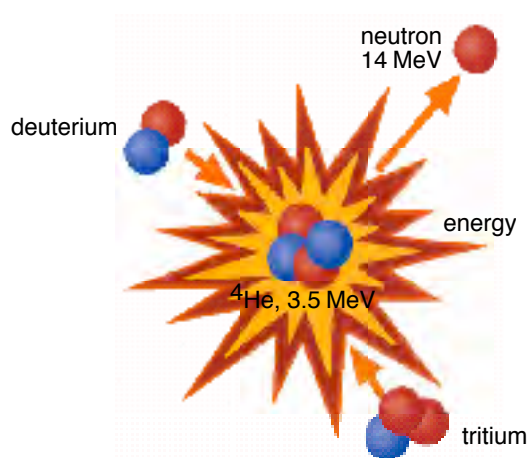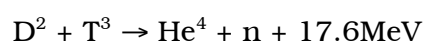
Fig. E.1   *Schematic of a fusion reaction between deuterium and tritium nuclei. The products are 3.5MeV ^{4}He, the common isotope of helium, and a 14MeV free neutron.*

The end products are helium and neutrons (n). The total energy liberated by fusing one gram of a 50:50% mixture of deuterium and tritium is 94000kWh, which is 10 million times more than from the same mass of oil. 80% of this energy is carried by the neutrons with an energy of 14MeV while the remaining 20% is carried by the helium nucleus. All this energy eventually becomes heat to be stored or converted by conventional means into electricity.

The temperature at which fusion reactions start to become significant are above a few tens of millions of degrees. For the D-T reaction, the optimal temperature is of the order of 70-200 million degrees. At such temperatures the D-T fuel is in the plasma state.

Deuterium is very abundant on the earth and can be extracted from water (0.034g/l). Tritium does not occur naturally, since its half-life is only 12.3 years, but it can be regenerated from lithium using the neutrons produced by the D-T fusion reactions. The two isotopes of natural lithium contribute to this breeding of tritium according to the reactions:

$$Li^6 + n \rightarrow He^4 + T^3 + 4.8MeV$$

$$Li^7 + n \rightarrow He^4 + T^3 + n - 2.5MeV$$
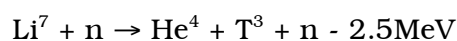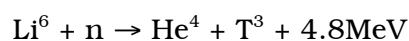
The relative abundance of the two lithium isotopes Li^6 and Li^7 are 7.4% and 92.6%, respectively. The known geological resources of lithium both in the earth and in the sea water are large enough to provide energy in an unlimited time.

E.2   Attractiveness of fusion as an energy source

The inherent advantages of fusion as an energy source are:

- The fuels are plentiful and their costs are negligible because of the enormous energy yield of the reaction;
- The end product of the reaction is helium, an inert gas;
- No chain reaction is possible; at any time only a very small amount of fuel is in the reacting chamber and any malfunction would cause an immediate drop of temperature and the reaction would stop;
- No after-heat problem can lead to thermal runaway;
- None of the materials required by a fusion power plant are subject to the provisions of the non-proliferation treaties.

Its further potential advantages are:

- Radioactivity of the reactor structure, caused by neutrons, can be minimised by careful selection of low-activation materials resulting in a manageable quantity of long lived radioactive waste;
- The release of tritium in normal operation can be kept to a very low level. The inventory of tritium in the breeding section of the reactor and on the site can be sufficiently small so that the worst possible accident could not lead to a harmful release to the environment requiring evacuation of the nearby population.

APPENDIX F   Glossary

The following is a general purpose glossary for the field of controlled fusion and plasma physics.

Additional heating: Usually with reference to a plasma which is initially heated by a toroidal current induced in the plasma (ohmic heating), additional heating designates other means of heating a plasma (absorption of electromagnetic waves or of injected fast neutral particles).

Advanced Tokamak Scenarios: Tokamaks normally generate natural profiles of plasma current and plasma pressure. External non-inductive current drive and local control of the current and pressure profiles can allow access to enhanced regimes and even steady state operation, generally referred to as Advanced Tokamak Scenarios.

ALCATOR C-MOD: High field, high density tokamak at MIT (USA) with an elongated, diverted plasma and metallic walls.

Alfvén gap modes: The toroidal nature of tokamak plasmas produces gaps in the otherwise continuous spectrum of Alfvén waves, populated by discrete, weakly damped Alfvén gap modes. Under certain conditions these modes can be destabilised by resonant energy transfer from energetic particles, e.g. α-particles from fusion reactions.

Alfvén waves: A fundamental plasma wave, which is primarily magneto-hydrodynamic in character with an oscillation of the magnetic field and, in some cases, plasma pressure. In tokamaks, these waves are typically strongly damped. See also fast Alfvén wave.

Alfvén velocity: The velocity of propagation of Alfvén waves in the direction of the magnetic field; it is proportional to the magnetic field strength, and inversely proportional to the square root of the mass density.

alpha particle, or α-particle He^4: The nucleus of the helium atom, composed of two protons and two neutrons, is one of the two products of the DT fusion reaction (the other one is a neutron). The α-particles, being electrically charged, are trapped by the magnetic confinement field and therefore can release their energy to the plasma contrary to the neutrons which escape from the plasma and transfer their energy in the blanket surrounding the plasma core. The plasma

heating which is provided by these α-particles as they slow down due to collisions is essential for achieving ignition.

Alternative lines: Magnetic confinement development other than the tokamak.

Analytic/Computational modelling: Analytic: algebraic solution of basic equations. Computational: numerical solution of basic equations.

Anomalous transport: Measured heat and particle loss is anomalously large compared with collisional theory of heat transport in toroidal plasmas.

ASDEX-Upgrade: Medium-sized Tokamak at Garching (Association Euratom-IPP, Germany) with an elongated, diverted plasma.

Aspect ratio: The ratio between the large radius and the small radius of a torus.

Auxiliary heating: See additional heating.

Ballooning instability: A local instability which can develop in the tokamak when the plasma pressure exceeds a critical value; it therefore constrains the maximum β that can be achieved. It is analogous to the unstable bulge which develops on an over-inflated tyre.

Beta (β): Ratio of plasma pressure to magnetic field pressure. One of the figures of merit for magnetic confinement: the magnitude of the magnetic field pressure determine the cost of the field coil that generates it; since fusion reactivity increases with the square of the plasma pressure, a high value of ß indicates good performance. The highest values achieved in tokamaks reach 40% (START).

Beta-normalised (β_N): The ratio of plasma current (in MA) to the product of minor radius (in m) and magnetic field (in T) characterises the limit to the achievable β imposed by ideal MHD. β-normalised is the ratio of β (as a percentage) to the above ideal MHD parameter. Generally β_N ~3 should be achievable, but techniques for obtaining higher values have been found experimentally.

Blanket: A structure containing lithium or lithium compounds surrounding the plasma core of a fusion reactor. Its functions are to breed tritium, via lithium-neutron reactions, and to absorb most of

the fusion energy to be used for electricity generation.

Bootstrap current: Theory developed in 1970 predicted that a toroidal electric current will flow in a tokamak which is fuelled by energy and particle sources that replace diffusive losses. This diffusion driven "Bootstrap current", which is proportional to β and flows even in the absence of an applied voltage, could be used to provide the poloidal magnetic field: hence the concept of a Bootstrap tokamak, which has no toroidal voltage. A Bootstrap current consistent with theory was observed many years later on JET and TFTR; it now plays a role in optimising advanced tokamaks.

Breakeven: The fusion performance of a power plant is denoted by Q, which is the ratio of the power released by fusion reactions to that used to heat the plasma. As a convention, scientific breakeven corresponds to Q=1 and ignition to Q=infinity. A fusion power plant would operate at Q~50.

Breeding ratio: The number of tritium atoms produced in the blanket of a fusion power station per tritium nucleus burned in the fusion plasma.

Burn: The fusion process of consuming DT fuel in a reactor, releasing energy.

CCE-FU: The Consultative Committee for the Euratom Specific Research and Training Programme in the field of Nuclear Energy, Fusion. Formerly the CCFP.

CEA: Commissariat à l'Energie Atomique, France. Partner in the Association EURATOM-CEA which operates the TORE SUPRA tokamak.

CFI: Committee on Fusion-Industry.

Charge exchange measurement: Measures the plasma ion temperature. Neutral atoms in the plasma (for example from a neutral beam) donate electrons to hot plasma ions, which are thereby neutralised. These hot atoms are no longer confined by the magnetic field and leave the plasma. Their energy is measured by a neutral particle analyser.

CIEMAT: Centro de Investigaciones Energéticas Medioambientales y Tecnológicas, Spain. Partner in the Association EURATOM-CIEMAT. Operates the flexible heliac stellarator TJ-II.

Classical transport: Collisions between the individual particles of a plasma allow them to move across the magnetic field. Theories which describe this mechanism are called "classical" (or "neo-classical" when additional effects due to the toroidal geometry are included). The measured heat and particle transport is usually higher than predicted by these theories.

Collisionality: Non-dimensional parameter, which is the inverse ratio of the mean free path of plasma particles between collisions to a characteristic length of the magnetic field configuration.

Compact torus: Class of closed magnetic configurations in which no material elements (coils, conductors or walls) need to link through the bore of the plasma torus. Thus the vessel of compact tori can be spherical or cylindrical.

COMPASS: COMPact ASSembly, a tokamak for studies of plasma stability, at Culham, UK (Association EURATOM-UKAEA). Originally with circular vessel (COMPASS-C), later with D-shaped vessel (COMPASS-D).

Confinement time: In a fusion plasma neither particles nor energy are perfectly confined. Particle confinement time is the time during which the particles, on average, stay confined. The energy confinement time, which is usually shorter than the particle confinement time, is defined in steady state as the ratio of the plasma energy content to the total power input to the plasma and is a measure of how fast a plasma would cool if there were no heating.

CRPP: Centre de Recherches en Physique des Plasmas. Fusion laboratories of the Association EURATOM-Swiss Confederation at the Ecole Polytechnique Fédérale de Lausanne and the Paul-Scherrer Institute, Villigen (CRPP-Fusion Technology).

Current drive (non-inductive): In a tokamak, plasma current can be driven inductively, with the toroidal plasma acting as a secondary winding of a transformer whose primary coil is at the central column of the device. Continuous current cannot be driven by transformer action. 'Non-inductive' current drive methods are applied either by injecting particles with directed momentum into the plasma or by accelerating electrons by electromagnetic waves so that they carry the current. Also being applied to control instabilities and to optimise confinement by modifying the current profile. The bootstrap effect also drives current.

Current profile (current distribution): The distribution of current density across the minor radius of the plasma.

Current ramp-up (down): The increase (decrease) of plasma current either at the start of operation or during operation.

Cyclotron frequency: Charged particles in a magnetic field have a natural frequency of gyration in the plane perpendicular to the magnetic field - the cyclotron frequency. For electrons in a tokamak, the cyclotron frequency is typically a few tens of GHz (28GHz per Tesla), and for ions, a few tens of MHz (7.5MHz per Tesla for deuterium).

Cylindrical approximation: An approximation to the true tokamak geometry in which the torus is straightened, so that the toroidal direction becomes the cylinder axis. There are two directions of symmetry: along the axis (the 'toroidal' direction) and about the axis (the 'poloidal' direction).

DCU: Dublin City University, Ireland. Partner in the Association EURATOM-DCU.

DEMO: Demonstration Reactor (the first device in the European fusion strategy intended to produce significant amounts of electricity).

Deuterium: A stable isotope of hydrogen, whose nucleus contains one proton and one neutron. In heavy water, normal hydrogen is replaced by deuterium. Sea water contains, on average, 34g deuterium per m^3. Deuterium plasmas are used routinely in present-day experiments; in a fusion power plant the plasma will consist of a mixture of deuterium and tritium which fuse more readily then two deuterium nuclei.

DG Research (DG RTD): The Directorate-General of the European Commission, Brussels, responsible for Research and Development. Formerly DG XII.

Diagnostic: Apparatus used for measuring one or more plasma quantities (temperature, density, current, etc.).

DIII-D: The largest operating US tokamak, run by General Atomics, San Diego. It has a flexible configuration and studies core and divertor physics with intense additional heating.

Diffusion, thermal (or particle): The random flow of heat (or particles) in the presence of a thermal (or density) gradient.

D-He³: Deuterium-³Helium: A potential fuel mix for fusion with low release of neutrons, but which would require a much higher fusion triple product (nTτ) than DT to reach ignition. ³Helium is an isotope of helium which is not available in appreciable quantities on Earth.

Disruption, Disruptive instability: A complex phenomenon involving MHD instability which results in a rapid release of energy to the wall and strong electromechanical forces in a tokamak. Plasma control may be lost, triggering a VDE (q.v.). This phenomenon places a limit on the maximum density, pressure and current in a tokamak.

Distribution function: Describes both the space and velocity distribution of plasma particles.

Divertor: A magnetic field configuration with a separatrix, affecting the edge of the confinement region, designed to remove heat and particles from the plasma, i.e. divert impurities and helium ash to divertor plates in a target chamber. Alternative to using a limiter to define the plasma edge.

Double null: See Single/double null divertors.

Drift kinetic theory: Kinetic theory which describes plasma processes which have spatial scales much greater than the particle Larmor radii.

Drift orbits: Particle motion is tied to straight magnetic field lines. However, electric fields and gradients of the magnetic field give an additional drift perpendicular to the magnetic field creating drift surfaces displaced from the magnetic surfaces.

Driven current: Plasma current produced by a means external to the plasma, inductively or non-inductively.

Driver: In inertial confinement fusion, the laser or particle beam system used to compress a target pellet.

DTE: The deuterium-tritium experiment at JET which in 1997 set new records for fusion power production. Followed the Preliminary Tritium Experiment of 1991.

ECCD: Electron Cyclotron Current Drive. Non-inductive current drive technique using directed electron cyclotron resonance waves.

ECE: Electron Cyclotron Emission. Radiation emitted by electrons as a result of their cyclotron motion around magnetic field lines. Used to measure electron temperature.

ECH: Electron-Cyclotron Heating. Radio wave heating near the resonance frequency (or its multiple) of the electron gyration in a magnetic field. In present and future machines ECH is at typically 60-170GHz, depending on the magnetic field strength in a machine.

EFDA: European Fusion Development Agreement. The organisational framework of the EU fusion activities for the exploitation of the JET Facilities, international collaboration (including ITER) and supporting technology.

EFET: European Fusion Engineering & Technology: a fusion technology oriented European Economic Interest Grouping.

Electron temperature: A measure of electron thermal energy in units of degrees or electron volts (1eV ~ 10^4 degrees Kelvin).

ELM: Edge localised mode. An instability which occurs in short periodic bursts during the H-mode in divertor tokamaks. It modulates and enhances the energy and particle transport at the plasma edge. These transient heat and particle losses could be damaging in a reactor.

ENEA: Ente per le Nuove Tecnologie, l'Energia e l'Ambiente, Italy. Partner in the Association EURATOM-ENEA.

Energetic particle: In terms of energy, the particles in a plasma can be divided into two classes. The more numerous thermal particles are characterised by a temperature typically in the range 1–30keV for modern tokamaks. The less numerous class of energetic particles has significantly higher energy up to several MeV. Energetic particles can be created by electric fields, fusion reactions, neutral beam injection or RF heating.

EPS: European Physical Society. Its Plasma Physics Division hosts the major European annual conference on Plasma Physics.

Error fields: The magnetic coils of a tokamak are designed to give the desired magnetic field configuration. The finite number of coils and imperfections in their construction lead to unwanted deviations from this configuration known as error fields. These could lead to disruptions and are of particular concern for larger tokamaks.

EXTRAP T-II: External Trap II, a medium-sized reversed field pinch (RFP) at the Royal Institute of Technology, Stockholm (Association EURATOM-NFR),

built for RFP transport and shell stabilisation studies in support of RFX.

EURATOM: European Atomic Energy Community.

Faraday rotation: The rotation of the plane of polarisation of light passing through a magnetised plasma.

Fast Alfvén wave: The fast Alfvén wave exists over a broad frequency spectrum, from the ion cyclotron range of frequencies (ICRF) where its character is electromagnetic, down to magnetohydrodynamic frequencies. Its velocity is comparable to the Alfvén velocity. The fast Alfvén wave is used routinely for high-power (~20MW) ICRF heating on JET, as it is efficiently absorbed in the plasma by the mechanism of ion cyclotron resonance. Although usually stable in tokamaks, the wave can be excited by energetic ion populations.

Fast wave current drive: Current drive produced by a fast wave. The wave can penetrate the plasma more easily than a lower hybrid wave.

Feedback: Use of measurements of plasma parameters to control the parameters, shape or profiles of the plasma to obtain desired conditions.

Field lines, Flux surfaces: Imaginary lines marking the direction of a force field. In a tokamak these define a set of nested toroidal surfaces, to which particles are approximately constrained, known as flux surfaces.

Field reversed configuration: A compact torus with a strongly elongated plasma. The plasma is contained in a cylindrical vessel inside a straight solenoid. The confining magnetic field usually has only a poloidal component. Not to be confused with reversed field pinch.

FIR: Far infra-red (e.g. wavelength ~ 0.2 to 1mm). FIR lasers are used to measure the magnetic field and plasma density.

"Fishbones": Rapid bursts of MHD activity sometimes observed when neutral beam heating is used in tokamaks (fishbone refers to the shape of the bursts in oscillating magnetic field when plotted as a function of time).

First wall: The first material boundary that surrounds the plasma. Today, the first wall in many machines is protected by low-Z materials (such as carbon tiles, boron or beryllium coating). Future tokamaks will require metallic walls.

Flat-top current: Constant current during quasi-stationary operating conditions.

Fokker-Planck Code: A computer code to calculate the velocity distribution of plasma particles allowing for collisional relaxation and plasma heating. Calculates distribution functions (q.v.).

FOM: Stichting voor Fundamenteel Onderzoek der Materie (Foundation for basic investigations of matter), The Netherlands. Partner in the Association EURATOM-FOM.

FTU: Frascati Tokamak Upgrade, a high density, high current tokamak at Frascati, Italy (Association EURATOM-ENEA).

Fusion triple product: Product of (ion) density, (ion) temperature and energy confinement time. A measure of the proximity to break-even and ignition.

Fusion product: The product of a fusion reaction, for example an α-particle or neutron in a deuterium-tritium plasma.

Fusion reactivity: Fusion reaction rate. For present typical tokamak conditions, it increases with the square of the density and the ion temperature of the plasma.

Full wave theory: Wave theory which includes complete accounting of wave energy (transmitted, reflected and absorbed, including energy transferred to other waves) for studying RF heating.

FZK: Forschungszentrum Karlsruhe, Germany. Partner in the Association EURATOM-FZK, active in fusion technology and, with the development of gyrotrons, in plasma engineering.

FZJ: Forschungszentrum Jülich GmbH, Germany. Partner in the Association EURATOM-FZJ, operating the tokamak TEXTOR.

GSI: Gesellschaft fuer Schwerionenforschung, Darmstadt, Germany. Studying heavy-ion physics, and driver physics with possible application for inertial confinement fusion.

Gyro-kinetic theory: Version of kinetic theory in which the Larmor radius is not assumed to be small. An essential theory for investigating fine-scale instabilities which might be responsible for driving turbulence, which may in turn be responsible for anomalous transport.

Gyrotron: Device used for generating high power microwaves in the electron cyclotron range of frequencies (50 - 200GHz). This UHF wave is mostly used to heat the plasma at the electron cyclotron resonance frequency. It also could be used to diagnose the plasma.

Heliac: Stellarator configuration with a central toroidal coil around which the plasma column is wound helically. Because of its high capability of investigating a wide range of stellarator configurations, it is used for TJ-II.

Helias: Optimised stellarator configuration, used with modular coils for Wendelstein VII-X (Germany) and SHEILA (Australia).

H-mode: A High confinement regime that has been observed in tokamak plasmas. It develops when a tokamak plasma is heated above a characteristic power threshold, which increases with density, magnetic field and machine size. It is characterised by a sharp temperature gradient near the edge (resulting in an edge "temperature pedestal"), ELMs and typically a doubling of the energy confinement time compared to the normal "L" regime. Today, a variety of high confinement modes have been identified in divertor and in limiter configurations (e.g. the I-mode), which, in part, have been obtained by special tailoring of the radial plasma current profile.

H-transition (or L-to-H transition): Transition into the H-regime from the L-regime, usually quite sudden, at a certain threshold power of additional heating and specific plasma parameters.

Halo currents: See Vertical Displacement Event.

Helicity injection: The helicity of a toroidal plasma is related to a linkage of toroidal and poloidal magnetic fluxes, and is approximately conserved throughout a discharge. If additional helicity can be injected, the plasma current could be sustained or even increased.

Helium ash: Fusion reactions in a deuterium-tritium plasma produce energetic α-particles (helium nuclei), which heat the plasma as they slow down. Once this has happened, the α-particles have no further use: they constitute helium ash, which dilutes the fuel and must be removed to maintain a burning plasma.

High beta (β): Condition in which the plasma energy is a significant fraction of the energy in the magnetic field. An alternative measure is the ratio between the

plasma energy and the energy in the poloidal magnetic field, the poloidal β.

High field ECH launch: Electron cyclotron waves can be launched from the inside of the plasma torus. This allows higher density plasma to be heated.

Hydrogen: The lightest element; the nucleus consists of only one proton, the atomic shell of one electron. Isotopes of hydrogen, with one or two additional neutrons in the nucleus, are deuterium and tritium respectively.

IAEA: International Atomic Energy Agency (of the United Nations), Vienna, Austria. The ITER-EDA is undertaken under the auspices of the IAEA.

ICE: Ion Cyclotron Emission. Observed in JET and TFTR as a suprathermal signal, apparently driven by collective instability of energetic ion populations such as fusion products and injected beam ions.

ICF: Inertial Confinement Fusion. Intense beams of laser light or light or heavy ion beams are used to compress very rapidly and heat tiny target pellets of fusion fuel to initiate fusion burn in the centre. Sufficient fusion reactions must occur in the very short time before the fuel expands under its own pressure. The inertia of the pellet's own mass determines the time scale during which fusion reactions occur, hence the name inertial confinement.

Ideal: In the context of MHD, 'ideal' implies that the magnetic field and the plasma always move together. For this to occur, the electrical resistivity of the plasma must be negligible.

Ideal internal kink modes: An MHD instability of the central region of a tokamak. This, or its close relative the resistive internal kink mode, may be involved in the Sawtooth disruptions which occur in most Tokamaks.

IEA: International Energy Agency (of the OECD), Paris, France. Implementing agreements for international collaboration on specific topics in fusion have been set up in the frame of the IEA.

Ignition condition: Condition for self-sustaining fusion reactions: heat provided by fusion α-particles replaces the total heat losses. External sources of plasma heating are no longer necessary and the fusion reaction is self-sustaining. Ignition is not required for energy gain in a power station. Retaining a level of external heating or current drive will be required

to control the plasma pressure and current profiles, to optimise the performance, leading to a so-called "driven burn".

Impurities: Ions, other than the basic plasma ion species, which are unwanted as they lose energy by radiation and dilute the plasma.

Impurity screening: The prevention of impurities from entering the plasma.

Internal kink: A type of MHD instability that can occur within the central region of the plasma (where q < 1) reducing the peak temperature and density.

Internal Reconnection Event (IRE): An instability which breaks magnetic field lines and reconnects them with a different topology to reduce the system to a lower energy state - associated with the operating limits of spherical tokamaks.

Ion Bernstein wave: A wave which only exists in a hot plasma and is supported by the ions. It propagates at right angles to the magnetic field, when it is undamped, at harmonics of the ion cyclotron frequency. There is also an electron Bernstein wave which propagates at harmonics of the electron cyclotron frequency.

Ion Cyclotron Current Drive (ICCD): Non-inductive current drive using ICRH.

Ion Cyclotron Resonance Heating (ICRH)/Ion Cyclotron Resonance Frequencies (ICRF): Additional heating method using RF waves at frequencies ($\sim$ 20-50MHz) matching the frequency at which ions gyrate around the magnetic field lines.

IPP: Max-Planck-Institut fuer Plasmaphysik, Garching, Germany. Partner in the Association EURATOM-IPP, operating the tokamak ASDEX-Upgrade and the stellarator Wendelstein VII-AS. Also has sites in Berlin and in Greifswald, where the construction of the large superconducting stellarator Wendelstein VII-X is in progress. The name is also used for the Czech Republic Association.

IR: Infra Red part of the electromagnetic spectrum.

IRE: Internal Reconnection Event.

IST: Instituto Superior Técnico, Portugal. Partner in the Association EURATOM-IST.

ISTTOK: Tokamak, for study of non-inductive current drive, at the Instituto Superior Técnico (IST), Lisbon, Portugal.

ITER: International Thermonuclear Experimental Reactor (the next step as a

collaboration between EURATOM, Japan, China, India, Korea, the Russian Federation and the USA, under the auspices of the IAEA). After a conceptual design phase - CDA (1988-1990), and engineering design activities (ITER-EDA, 1992-2001), now under the Coordinated Technical Activities (CTA).

JAEC: Japan Atomic Energy Commission, Tokyo, Japan.

JAEA: Japan Atomic Energy Agency. Headquarters in Tokyo, Japan.

JET: Joint European Torus. The largest tokamak in the world, sited at Abingdon, UK. Operated as a Joint Undertaking (JET Joint Undertaking), until the end of 1999. The scientific exploitation of the JET facilities is now guaranteed by the Euratom fusion Associations within the EFDA framework. The operation of the facility is the responsibility of the Association Euratom-UKAEA.

JT-60U: Japanese tokamak at Naka. The largest Japanese tokamak and second largest operating experiment after JET, but not designed for use with D-T fuel.

keV: Kilo-electronvolt. Energy which an electron acquires passing a voltage difference of 1000 volts. Also used to measure the temperature of a plasma (1 keV corresponds to 11.8 million degrees Kelvin).

Kinetic instability: Oscillation which is unstable as a result of the energy distribution of ions or electrons.

Kinetic theory: A detailed mathematical model of a plasma in which trajectories of electrons and ions are described. More complex than fluid and two-fluid theories, it is necessary in the study of RF heating and some instabilities, particularly when energetic particles are involved.

L-H transition: Change from L regime to H regime (usually quite sudden).

L-mode: As opposed to the H mode. Regime with degradation of confinement, in additionally heated plasmas, with respect to plasmas heated ohmically by the plasma current.

Langmuir probe: Electrical probe inserted into the edge of a plasma for measurements of density, temperature and electric potential.

Larmor radius: Radius of the gyratory motion of particles around magnetic field lines.

Large scale ideal modes: A large scale mode has a wavelength which is a significant fraction of the plasma dimensions and assumes ideal MHD.

Laser ablation: Use of lasers to produce a sudden influx of impurities into the plasma from a solid surface.

Last closed flux surface: The boundary separating those magnetic field lines that intersect the wall (open lines) from the magnetic field lines that never intersect the wall (closed lines).

Lawson criterion: The value of the confinement time multiplied by the ion density (at the required temperature) which must be exceeded in a fusion reactor to reach ignition.

Limiter: A material surface within the tokamak vessel which defines the edge of the plasma and thus avoids contact between the plasma and the vessel. A pumped limiter can also be used to remove heat and particles and is an alternative exhaust system to the divertor.

LLNL: Lawrence Livermore National Laboratory, Livermore, USA.

Locked modes: MHD modes that cease rotating (though they can still grow).

Low-activation materials: Materials which do not develop high, long-lived radioactivity under neutron irradiation.

Low aspect ratio: Low ratio of major to minor radius of the torus.

Lower hybrid current drive (LHCD): Non-inductive current drive using lower hybrid waves.

Lower hybrid heating (LHRH): Plasma heating by radio frequency waves at the "lower hybrid" resonance frequency in the plasma. Typical frequencies are a few GHz.

Lower hybrid (LH) wave: A plasma wave of frequency between the ion and electron cyclotron frequencies. It has a component of electric field parallel to the magnetic field, so it can accelerate electrons moving along the field lines.

Magnetic axis: The magnetic surfaces of a tokamak form a series of nested tori. The central 'torus' defines the magnetic axis.

Magnetic Confinement Fusion (MCF): Confinement and thermal insulation of a plasma within the reactor core volume by the action of magnetic fields. In toroidal magnetic confinement, usually both toroidal and poloidal components of the magnetic field are needed (the field lines are

threaded like the filaments of a cable which is bent into a ring).

Magnetic islands: Islands in the magnetic field structure caused either by externally applied fields or internally by unstable current or pressure gradients. See tearing magnetic islands.

Magnetic surfaces (flux surfaces): In toroidal magnetic confinement, the magnetic field lines lie on nested toroidal surfaces. The plasma pressure, but not the amplitude of the magnetic field, is a constant on each magnetic surface.

Magneto-acoustic cyclotron instability: This instability results from an exchange of energy between the fast Alfvén wave (or magneto-acoustic wave) and an ion Bernstein wave which has a source of free energy through the presence of a population of energetic (non-thermal) ions, e.g. fusion products. The instability occurs for propagation perpendicular to the equilibrium magnetic field.

Major radius: The distance from the tokamak symmetry axis to the plasma centre.

Marfe: A localised and radiating thermal instability sometimes observed near the edge of tokamak plasmas.

Marginal Stability: Close to the transition from stability to instability.

MAST: Mega Amp Spherical Tokamak at Culham (Association EURATOM-UKAEA), twice as big as START. Began operation in 1999.

MeV: Mega-electronvolt, unit for nuclear energies. Energy which an electron acquires passing a voltage difference of 1 million volts.

MHD (Magnetohydrodynamics): A mathematical description of the plasma and magnetic field, which treats the plasma as an electrically conducting fluid. Often used to describe the bulk, relatively large-scale, properties of a plasma.

MHD instabilities: Unstable distortions of the shape of the plasma/magnetic field system.

Microinstabilities: Instabilities with characteristic wave-lengths similar to the ion Larmor radii, rather than to the tokamak dimensions. These are thought to be responsible for the fine scale turbulence in tokamaks, and hence anomalous transport.

Minor radius: Half the small diameter of the tyre-shaped toroid.

Mirnov coils: Pick-up coils at the edge of the plasma for measuring the time variation of magnetic fields arising from instabilities.

Mirror: A linear magnetic confinement concept with a weaker magnetic field in a central region and with strong fields at both ends which reflect contained particles by the mirror effect. Some variants exist to increase the magnetic field in all directions from the centre or to improve the closure of the bottlenecks. The Tandem Mirror confinement concept also involves electrostatic fields.

MIT: Massachusetts Institute of Technology, Boston, USA. Operates the high-field divertor tokamak ALCATOR C-MOD.

Mode: A resonant wave or oscillation in a plasma. Also used as a synonym for an operating regime.

Mode number: Characterises the wavelength of a mode normalised to the device size.

Monte Carlo code: A statistical technique used in numerical calculations where events may occur many times, each with a certain probability.

Motional Start Effect (MSE): The measurement of shifts and splitting of spectral lines emitted from particles moving in a local electric field. This can be interpreted to give the local magnetic field inside the tokamak if the particle velocity is known, and is a major diagnostic on some tokamaks to deduce the current profile.

MPQ: Max-Planck-Institut fuer Quantenoptik, Garching, Germany. Active, within its programme, in ICF (laser fusion) related physics. Partially supported by Euratom, for a "keep in touch activity" in ICF.

Negative ion beam: To produce neutral beams, negative ions (obtained by the addition of electrons to neutral atoms) are accelerated and then neutralised before entering the plasma. The efficiency of creating neutral beams from positive ions is too low at the beam energy required for a fusion power station, of the order of 1 MeV.

Neo-classical theory: Classical collisional plasma transport theory, corrected for toroidal effects. The neoclassical theory predicts the existence of the bootstrap current.

Neo-classical tearing mode: The magnetic island produced by a tearing mode perturbs the bootstrap current which further amplifies the island and degrades confinement or leads to a disruption.

NET: Next European Torus, a design for the Next Step which had been prepared by the NET team (located at the Association EURATOM- IPP in Garching) and which largely influenced the ITER design.

Neural network: A computer algorithm that uses incoming data to derive plasma parameters, having previously been "trained" on a series of examples of a non-linear input-output mapping.

Neutrons: Neutral particles in the nucleus. Products of Deuterium-Tritium and other fusion reactions.

Neutral beams: Since charged particles cannot easily penetrate the magnetic confinement fields of the plasma, high energy beams of neutral atoms are injected into the plasma for fuelling, heating and current drive. Within the plasma, the atoms of the beam are ionized and are then confined.

Neutron multiplier: The fusion of deuterium and tritium consumes one tritium nucleus per reaction, producing one neutron. Since in the blanket of a power station not every neutron reacts with lithium to produce a new tritium atom, a neutron multiplying element may be used in the blanket to enhance the tritium production so as to make the power station self-sufficient in tritium supply.

Next Step: The next experimental device in the strategy of the European Fusion Programme. Presently pursued via the ITER EDA, with a European activity as a fall-back option. The generic name for an experimental reactor with a long pulse burning plasma at high fusion gain.

NFR: Naturvetenskapliga Forskningsrädet (Natural Science Council), Sweden. Partner in the Association EURATOM-NFR.

NIFS: National Institute for Fusion Science, Nagoya, Japan.

NRIM: National Research Institute for Metals, Sakura-mura, Japan.

Non-inductive heating and current drive: See additional heating and current drive.

NSTX: Spherical tokamak at Princeton, USA. A similar size to MAST, but of different design. Started operation in 1999.

Ohmic heating (OH): The resistive heating resulting from a current flowing within the plasma corresponding to the heating of a wire by a current flowing through it. Ohmic heating in a tokamak is insufficient to reach thermonuclear temperatures since, contrary to a wire, the resistance of a plasma decreases strongly with increasing temperature, thus making Ohmic heating weak at high temperatures.

ORNL: Oak Ridge National Laboratory, USA.

Operating limits: See tokamak operating boundaries.

Optimised shear: Adjusting the current profile to optimise tokamak.

PbLi: Eutectic lithium-lead alloy considered for use as blanket breeding material.

Peeling mode: An edge MHD instability which exists when the current density at the plasma edge is non-zero. It may be associated with ELMs.

Pellet: In inertial confinement concepts, the fuel is contained in tiny spheres, called pellets, which are compressed by laser or particle beams. In magnetic fusion, pellets of frozen hydrogen, deuterium, tritium, accelerated up to several kilometres per second, are used to refuel the plasma and to obtain very high densities.

PIREX: Proton Irradiation Experiment, material test facility (Association Euratom-Switzerland, CRPP-FT, PSI, Villigen, CH).

Plasma: State of matter above a few thousand degrees where atoms are broken into their constituents, ions and electrons, thereby creating an electrically conducting medium. Plasmas can therefore interact strongly with electric and magnetic fields.

Plasma confinement: Retention of plasma energy or particles within a given region, including the heat and particle losses from the plasma.

Plasma parameters: Physical quantities which characterise the plasma and which must be measured experimentally, such as current, density, temperature, confinement time, β.

Plasma pressure: Proportional to the product of plasma density and temperature. There is an electron and an ion pressure and the plasma pressure is the sum of the two. In magnetic

confinement devices, this pressure is counterbalanced by magnetic pressure.

Plasma shape: Describes the plasma vertical cross-section, circular, elongated, D-shape, diverted, single null, double null.

Polarimetry: Measurement of the rotation of the plane of polarisation of light passing through a magnetically confined plasma; used to measure the local magnetic field and thus the safety factor (see Faraday rotation).

Poloidal field: Component of the magnetic field perpendicular to the toroidal direction and the major radius. The poloidal field is essential for confinement and is generated in a tokamak by the plasma current and the external coils.

Power threshold: The L-H transition and improved performance regimes related to reversed shear occur when the power exceeds a certain threshold value - the power threshold.

PPPL: Princeton Plasma Physics Laboratory, New Jersey, USA.

Preliminary Tritium Experiment (PTE): Three plasma discharges on JET, November 1991, into which a significant amount of tritium was injected for the first time in a tokamak. The power liberated from fusion reactions (~ 2MW for ~ 2 seconds) was in accordance with expectations. Followed by the more ambitious DTE in 1997.

Profile: Variation of plasma parameters with minor radius.

Profile control: Controlling the profiles of pressure, density or current, in order to control instabilities.

PSI: Paul-Scherrer-Institut, Villigen, Switzerland, active, in muon physics among others fields. The Association EURATOM-Swiss Confederation has their fusion technology activities working in superconductor and materials technology located at Villigen.

Pumped divertor: Divertor field lines directed into a pumped chamber surrounding the target plate.

q, q_{95}: See Safety factor.

Q: Ratio of fusion power to total additional heating power. At $Q=\infty$, no external power is required and the plasma is said to be ignited. A power station should operate with $Q \sim 50$ to be economical.

Radial electric field: Arises when there is a charge imbalance in the plasma.

Radio frequency (RF) heating: Heating with waves in the radiofrequency range at resonance frequencies of the plasma (see ECH, ICRH, LHH).

Reflectometry: Use of reflected microwaves to measure plasma density.

Relaxation: The evolution of a plasma to a lower energy state.

Resistive ballooning modes: A class of ballooning mode which would be stable in the absence of resistivity, but can be unstable in its presence. Related to tearing modes, but topologically different.

Resistive instability: Instability due to diffusion and rearrangement of magnetic field lines. When the plasma resistivity is small, these instabilities have a slow growth rate.

Resistivity: The tendency to resist the flow of electric current, thereby dissipating energy. Plasmas are very good conductors of electric current, so that their resistivity can often be neglected. In this case, 'ideal' magnetohydrodynamics may be applied.

Resonant ions/electrons: Resonance occurs when one of the characteristic frequencies of particle motion in the plasma (for example, the cyclotron frequency) matches the frequency of some applied perturbation (for example, an RF wave).

Resonant magnetic perturbation (RMP): An externally applied magnetic perturbation matched to the spatial structure and optionally the frequency and phase of an instability.

Reverse Field Pinch (RFP): A toroidal magnetic confinement device, similar to a tokamak, in which the poloidal and toroidal fields are of comparable magnitude. Capable of higher plasma current and pressure for a given external magnetic field. They require a conducting shell close to the plasma for stabilisation.

Reverse (magnetic) shear: In a tokamak the current density is usually greatest at the magnetic axis, in which case the safety factor increases from the centre to the edge of the plasma. Using non-inductive current drive and/or the bootstrap current the current density can be made to increase away from the centre. In this "reverse shear" case, the safety factor has a minimum away from the plasma centre.

Using reverse or low shear ("optimised shear") some tokamaks, notably DIII-D and TFTR in the US and more recently JT-60U in Japan and JET, have shown greatly improved plasma performance. Reverse shear is an attractive option for advanced tokamak scenarios.

RF: Radio-Frequency.

RFX: Reversed Field pinch Experiment at CNR-Padova, Italy (Association EURATOM-ENEA).

RISØ: Forskningscenter Risø, Denmark. Partner in the Association EURATOM-RISØ.

Rotational transform: Measure of the ratio of poloidal to toroidal flux defining the pitch of the helical field lines. The q-value of the tokamak is proportional to the reciprocal of the rotational transform.

RTP: Rijnhuizen Tokamak PETULA, for study of transport in a plasma, at Nieuwegein (Rijnhuizen), the Netherlands (Association EURATOM-FOM). Ceased operation in 1998, the activities of the Association being transferred to TEXTOR, as part of the Tri-lateral Euregio Cluster.

Runaway electron: An electron with a very high energy has a decreasing probability of colliding with another charged particle and of losing its energy. Such a particle then gains more and more energy in the electric field of a tokamak, reaching 10's of MeV.

Safety factor: Number of turns the helical magnetic field lines in a tokamak make round the major circumference for each turn round the minor circumference, denoted q. Has no connection with the ordinary sense of "safety" other than q=1 surfaces are ideally unstable. For diverted plasmas q goes to infinity at the separatrix, so instead q_{95} is used to describe the safety factor near the edge, which is the safety factor of the plasma surface which contains 95% of the poloidal flux.

Sawtooth: A cyclically recurring instability which causes an energy loss from the central region of tokamak discharges. The temperature periodically falls abruptly, then slowly recovers. The jagged trace produced by plotting temperature against time gives the instability its name.

Sawtooth crash: The rapid collapse of the central temperature in a tokamak during a sawtooth cycle.

Scaling laws: Empirical or theoretical expressions for how various plasma phenomena (eg confinement, power threshold, etc) vary with tokamak parameters. They are particularly used for predicting the performance of future tokamaks.

Scrape-off-layer (SOL): The residual plasma between the "edge" of the plasma (defined by the limiter radius or the separatrix) and the tokamak vessel wall.

Semi-empirical: A theoretical approach in which the behaviour of some key quantities is deduced from experiment, rather than a priori.

SEAFP: The Safety and Environmental Assessment of Fusion Power is an extensive study conducted by several teams in the associated laboratories, NET, industry and the JRC, published in June 1995.

SEAL: The Safety and Environmental Assessment of Fusion Power Long-term is a programme, launched in 1995, being undertaken for the European Commission in the framework of the Fusion Programme.

Separatrix: Magnetic surface at which the rotational transform vanishes and the safety factor becomes infinite.

Shear: The safety factor usually varies from magnetic surface to magnetic surface across the plasma cross-section; this variation is measured by the non-dimensional quantity called "shear". Also refers to the variation of plasma flow (flow shear). If the type of shear is not specified, it usually means magnetic shear.

Single/double null: Points of zero poloidal magnetic field where the separatrix crosses itself are the X-points or nulls. Usually sited above and/or below the plasma. Tokamak divertor configurations have either one or two nulls.

Single fluid model: The set of equations which represent a plasma as a magnetised, electrically conducting fluid with the usual fluid properties of viscosity, thermal conductivity, etc. The possibility of distinct behaviour of electrons and ions (i.e. 2 "fluids") is excluded.

Small aspect ratio: Same as Low aspect ratio.

Spectroscopy: The detection and analysis of the spectrum of radiation emitted by a plasma. This can yield information about temperatures, impurities, rotation, using different parts of the electromagnetic spectrum (IR, visible, VUV, XUV, etc.)

Spherical tokamak (ST): A very low aspect ratio tokamak - it appears almost spherical, though topologically it remains a torus with a centre column. The spherical tokamak is being further investigated, with larger experiments, MAST and NSTX.

Spheromak: A spherical plasma in which comparable toroidal and poloidal currents flow. The toroidal current is not driven by transformer action.

Stability theory: The theory of how small perturbations to a system evolve in time. Spontaneous growth is due to instability. Instabilities can saturate at some small amplitude, in which case they may degrade confinement, or grow uncontrollably, in which case the equilibrium is lost leading to a disruption.

START: Small Tight Aspect Ratio Tokamak, a "spherical" tokamak with a very small aspect ratio at the Association EURATOM-UKAEA (Culham). This very fat ring-shaped configuration showed experimentally a lesser tendency to disruptions and is efficient in its use of magnetic energy. Ceased operation in 1998, replaced by MAST.

Start-up assist: Assisting plasma formation to cross a range of plasma temperature at which impurities radiate strongly, with the aim of minimising the start-up delay and transformer requirements, usually using ECH.

STAC: Scientific and Technical Advisory Committee set up by EURATOM.

Steady state power plant: A continuously (as opposed to cyclically) operated power plant.

Stellarator: Closed configuration having the shape of a three-dimensionally distorted ring in which the plasma is confined principally by an externally generated magnetic field (produced by non-planar coils outside the plasma vessel). The coils can be arranged in a modular fashion. Stellarators do not need a transformer; they need an additional heating system for the plasma start-up. Due to the fact that no toroidal plasma current is needed to maintain the confinement configuration, they naturally provide steady state operation.

SULTAN: Supra Leiter Test ANlage. Large Superconductor Test Facility, CRPP at PSI Villigen, Switzerland (Association EURATOM-Swiss Confederation).

Super Alfvénic velocity: A velocity greater than the Alfvén velocity. In a tokamak, only energetic particles have super Alfvénic velocities; because they satisfy this condition, they may resonantly transfer their energy to magnetohydrodynamic modes, which may grow as a result (eg TAE modes).

Superthermal radiation: Electromagnetic radiation produced by energetic particles, as opposed to thermal particles.

Survey spectrometer: An instrument which gives information concerning the radiated spectrum over a large range of frequencies.

TAE modes: Toroidal Alfvén Eigenmodes. One class of Alfvén gap modes.

Target plates: See Divertor.

TCV: "Tokamak à Configuration Variable", for study of elongated and strongly shaped plasmas, at Lausanne, Switzerland (Association EURATOM-Swiss Confédération).

TEKES: Technology Centre Finland. Partner in the Association EURATOM-TEKES.

Tearing magnetic islands: The disturbance caused by a tearing mode which alters the topology of the confining magnetic field and causes transfer of heat across the affected region.

Tearing mode: A class of resistive MHD instability which has been predicted theoretically in tokamaks and positively identified in experiments.

Temperature pedestal: In an H-mode discharge there is a region of steep temperature gradient at the plasma edge. The temperature at the top of this steep gradient region is the temperature pedestal.

Tesla: Unit of magnetic field strength (more exactly the magnetic induction). $1T = 1Vs/m^2 = 10,000Gauss$.

TEXTOR: Torus Experiment for Technology Oriented Research. Tokamak at Jülich, Germany (Association EURATOM-FZJ). Refurbished and upgraded, in 1994, as TEXTOR-94.

TFTR: "Tokamak Fusion Test Reactor" at Princeton, the largest US device with a major campaign using deuterium-tritium fuel from 1993 - 1997. Ceased operation in March 1997.

Thermal cycling: Successive heating and cooling of materials can lead to cracks or

rupture, particularly at boundaries between materials that expand at different rates.

Thermal particles: As a result of collisional energy exchange, the energy of most plasma particles falls within a Maxwellian distribution which is described by a single temperature (typically 1-30keV for tokamaks). These are the thermal particles, as distinct from energetic particles which lie outside the thermal distribution.

Thomson scattering diagnostic: Diagnostic to measure temperature and density by detecting laser light scattered and Doppler shifted by the thermal plasma electrons.

Tight aspect ratio: Same as Low aspect ratio.

TJ-II: A heliac stellarator at Madrid, Spain (Association EURATOM-CIEMAT). (TJ-IU was a torsatron at CIEMAT, built and operated in preparation for TJ-II).

Tokamak: Magnetic configuration with the shape of a torus. The plasma is stabilised by a strong toroidal magnetic field. The poloidal component of the magnetic field is produced by an electrical current flowing toroidally in the plasma. This current is induced via transformer action and, for steady state, must be maintained by non-inductive current drive and by self-generation of bootstrap current inside the plasma.

Tokamak operating boundaries: The set of plasma parameters, beyond which it is impossible to operate a tokamak. Careful choice of plasma cross-sectional shapes and current and pressure profiles can increase the operating regime.

TORE SUPRA: Large tokamak with superconducting toroidal magnetic field coils and a circular plasma cross-section at the Association EURATOM-CEA in Cadarache, France. It features long high total energy plasmas.

Toroidal Alfvén Eigenmodes: See TAE modes.

Toroidal field: The component of the magnetic field along the major circumference of the torus. The largest magnetic field component in a tokamak.

Toroidal stability: Stability analysis taking account of effects due to the toroidal geometry. These are sometimes neglected to identify possible instabilities, but must usually be included for accurate predictions of stability boundaries.

Toroidal turbulence code: A turbulence code which includes effects due to the toroidal geometry.

T O S K A: Large testing facility for superconductors (Association EURATOM-FZK, Karlsruhe, Germany).

Transformer drive: The use of a transformer action to induce plasma current.

Transport: The processes by which particles and energy move across magnetic surfaces.

Transport barrier: In certain operational scenarios (e.g. the H-mode or ITB-mode) a region of low transport exists giving rise to a steep local pressure gradient. Such a region is referred to as a transport barrier.

Transport scaling: The magnitude of heat transport may be expressed, empirically or theoretically, in terms of a simple functional dependence on a few plasma parameters. This allows us to model how the heat transport varies (scales) in response to changes in the value of these parameters.

Trapped particles: The outside (large major radius) of a tokamak plasma has a lower magnetic field than the inside. Particles with low velocity parallel to the magnetic field compared with the velocity perpendicular to the magnetic field may not enter the higher field (inside) region and become trapped on the outside. They are not free to circulate toroidally but instead bounce back and forth, performing so-called banana orbits.

Tri-lateral Euregio Cluster (TEC): A collaboration between the Associations Euratom-FZJ, -FOM and –Etat Belge, to exploit the TEXTOR tokamak at FZJ, Julich, Germany.

Tritium: An isotope of hydrogen, whose nucleus consists of one proton and two neutrons. Tritium is unstable to radioactive decay with a half-life of 12.3 years. Due to its rapid decay, tritium is almost absent on earth. For a fusion reactor, tritium will be produced in the breeding blanket surrounding the core of a fusion power station. Special tritium-handling technology is required whenever the use of deuterium-tritium plasmas is contemplated and has been developed on TFTR and JET.

Tritium inventory: The amount of tritium contained in a fusion power station or in a specified part of it.

Turbulence: Randomly fluctuating, as opposed to coherent, wave action. For example, the turbulent water beneath a waterfall can only be described in terms of its averaged properties, such as the scale and duration of fluctuations; whereas a more systematic description can be given to waves on the surface of a still pond.

Turbulent transport: Anomalous heat transport associated with plasma turbulence.

Two-fluid model and multi-fluid model: The extended set of equations which represent a plasma as interpenetrating and interacting fluids of electrons and ions, impurity ions etc.

UKAEA: United Kingdom Atomic Energy Authority. Partner in the Association EURATOM-UKAEA which operates the tokamak COMPASS-D and the spherical tokamak MAST. Also charged with the operation of the JET facilities under EFDA.

Vertical Displacement Event (VDE): An event which arises when control of the plasma is lost and the plasma moves vertically. It can lead to a "halo current" in components which surround the plasma resulting in large, potentially damaging, forces on these components. The forces are much larger in larger tokamaks and are therefore of particular concern for JET and ITER.

VUV: The "Vacuum Ultra Violet" range of the electromagnetic spectrum.

Warm plasma refuelling: Fuelling of plasma using medium energy particles or particle clusters.

WEC: World Energy Council.

WENDELSTEIN VII-AS: Advanced stellarator, at Garching, Germany (Association EURATOM-IPP).

WENDELSTEIN VII-X: Large advanced superconducting stellarator, optimised to produce a reactor-relevant plasma configuration, designed at Garching. Construction is in progress at Greifswald, Germany (Association EURATOM-IPP).

X-point: See single/double null.

XUV: The "Extreme Ultra Violet" range of the electromagnetic spectrum. Shorter wavelengths than VUV.

APPENDIX G   Sources of Financial Support

The work carried out at the CRPP and presented in this annual report was financed from several sources. The major financial support is derived from the Ecole Polytechnique Fédérale de Lausanne (EPFL), EURATOM, the Paul Scherrer Institute (PSI), which hosts the supraconductivity and materials science activities, and the Swiss National Science Foundation. Other public and private organisations which contributed funding for our research in 2005 include, in alphabetical order: Allper, Balzers Tribology, Charmilles SA, the Swiss Commission pour la Technologie et l'Innovation (CTI), the Secrétariat d'Etat à l'Education et à la Recherche (SER), Sulzer Metco AG, Tetra Pak SA and Unaxis Balzers.

The CRPP is the Host of a Euratom Fellow, Dr. A. Mueck, who's fellowship is entitled *"Electron Bernstein wave studies in TCV"*.

The Fonds National Suisse de la Recherche Scientifique provided a grant during this period for *"Basic plasma physics for fusion energy research"*, which partly financed TORPEX and the CRPP-JET collaboration on Alfven waves and fast particles. Prof. A. Fasoli was supported by this grant as "Professeur Boursier du Fonds National".